

PhD Thesis – Duncan J. Findlay McMaster – School of Geography and Earth Science

**THE INTERNAL SKELETAL GEOCHEMISTRY OF  
SOME MODERN AND ANCIENT CEPHALOPODS**

PhD Thesis – Duncan J. Findlay McMaster – School of Geography and Earth Science

**THE INTERNAL SKELETAL GEOCHEMISTRY OF  
SOME MODERN AND ANCIENT CEPHALOPODS**

By

DUNCAN JOHN FINDLAY, B.Sc (Hons), M.Sc

A Thesis

Submitted to the School of Graduate Studies

in Partial Fulfilment of the Requirements

for the Degree

Doctor of Philosophy

**McMaster University**

**© Copyright by Duncan John Findlay, August 2008**

PhD Thesis – Duncan J. Findlay McMaster – School of Geography and Earth Science

Doctor of Philosophy (2009)  
(Geography and Earth Science)

McMaster University  
Hamilton, Ontario, Canada

TITLE: The Internal Skeletal Geochemistry of Some Modern and  
Ancient Cephalopods

AUTHOR: Duncan J. Findlay B.Sc (Hons)  
(University of Aberdeen, Aberdeen,  
Scotland, 2001)

M.Sc  
(Brock University, St. Catharines,  
Ontario, Canada, 2004)

SUPERVISOR: Dr D. Gröcke

NUMBER OF PAGES: xxiii, 268

## ABSTRACT

This dissertation explores the internal geochemistry of *Sepia officinalis* cuttlebones and the rostra of several genera of extinct Belemnnoidea with the aim of improving our ability to reconstruct the palaeoclimatic record. *Sepia* share several unique morphological features with Belemnnoidea and may be their most suitable modern analogue. Consequently, a geochemical comparison between the internal skeleton of *Sepia* and Belemnnoidea may help improve the understanding of the geochemistry of Belemnnoidea rostra, which are often used to investigate Mesozoic palaeoenvironmental conditions.

High resolution sampling of oxygen isotope values from five *S. officinalis* cuttlebones from the English Channel confirmed that *S. officinalis* cuttlebones provide an accurate record of water temperature that preserves seasonal temperature variation consistent with sea surface temperature records. Carbon isotope values show increasing values with growth until a sharp decline late in life, documenting a decrease in metabolism with ontogeny, followed by a late life increase. Trace element concentrations measured from two of these cuttlebones document a small but statistically significant correlation between oxygen isotope values and both Sr and Mn concentration, suggesting some degree of temperature control on their rate of incorporation. Mg concentration exhibits a small but statistically significant correlation with carbon isotope values, suggesting metabolism may exert some control on the rate of Mg incorporation.

Due to the process of fossilisation, diagenesis may alter the geochemistry of Belemnnoidea rostra, which is difficult to detect using stable isotope values alone. It is necessary to detect samples that have diagenetic overprinting of the original environmental signal so that past geochemical relationships may be accurately reconstructed. As Mn and Sr are enriched and depleted (respectively) in diagenetic fluids, they may be used as indicators of alteration. Following the removal of diagenetically altered samples, the carbon isotope values of Belemnnoidea rostra sampled from the Green Beds at Carbondale River, Alberta, Canada document a statistically significant increase with ontogeny, suggesting a decrease in metabolic rate similar to *S. officinalis*. Contrasting with *S. officinalis*, oxygen isotope values do not show seasonal palaeotemperature cycles, possibly the result of latitudinal migration with favourable water temperatures. Trace element concentrations of Mg exhibit a small but statistically significant correlation with Belemnnoidea oxygen isotope values, contrasting with Sr and Mn in *S. officinalis*, suggesting some temperature control on the incorporation rate of Mg in belemnnoidea calcite. The

ranges in oxygen isotope and Mg values were used to investigate changes in surface and deeper water palaeotemperatures during the deposition of the Green Beds. Similarly, the range in carbon isotope values within individual Green Bed *Belemnoidea* rostra documented a positive isotope excursion in the Green Bed section, which may become a useful geochemical marker for the region.

In most previous studies, palaeoenvironmental conditions have been reconstructed using a single sample from unspecified locations within *Belemnoidea* rostra. A high resolution sampling approach is necessary to capture the range of geochemical values preserved in individual rostra and may help to minimise the effects of sample bias in the geochemical record. Sampling radially from the apical line to the outside edge of an individual *Belemnoidea* rostrum is permitted the collection of geochemical information spanning the organism's lifespan, and will improve the interpretation of the biology and environment while minimising sample bias.

## ACKNOWLEDGMENTS

I would primarily like to thank my family for providing unerring support, both emotionally and financially, during my four year tenure at McMaster. You kept me on track when I could very easily have given up and quit. I hope I have made you proud. I couldn't have done it without you. Now, hopefully it is time for me to give back.

I sincerely thank my committee for their support, advice and encouragement, particularly near the end of the process when I felt like I had lost my way. Thank you for giving me a dose of confidence and/or a kick in the backside when I needed it.

The National Science and Engineering Research Council is acknowledged for providing funding for the analyses required for this project through grants to Dr Darren Gröcke. I would also like to take this opportunity to thank McMaster University for the opportunity to teach two full time courses during my studies. Lecturing these courses required me to really hone my knowledge, and made me a better scientist.

The government of Alberta is thanked greatly for granting me a fossil collection permit. It goes without saying that much of this thesis would have been impossible without this, so thank you for allowing me to collect some of the wonderful fossils I found while wandering through your lovely province.

I would also like to thank Dr Hilary Stuart-Williams for collecting the cuttlebones for me while on holiday on Jersey, and then being kind enough to post them to me. As above, this thesis would look much different without his help.

I would sincerely like to thank Martin Knyf, whose laboratory genius made life with a mass spectrometer possible. Regardless of what was happening, Martin remained collected and personable, and he really helped me out on numerous occasions. He is not just a commuter hero, but a hero of mine in general.

Dr Henry Schwarz deserves thanks for taking me aside for the occasional brief discussion. His knowledge of the discipline is unrivalled, and I am pleased to have benefited from his experience.

I would like to thank Dr Hernan Ugalde and Dr William Morris for their help with three dimensional modelling.

My time at McMaster would have been significantly less enjoyable without the presence of several close friends, these follow in no particular order. Dr April Hayward deserves many thanks for bigging me up, providing a much needed musical outlet, but most, most importantly, for spending a

gruelling week with me going over and over this manuscript, ensuring that what I thought I wrote, was actually what I had written. You showed me the way! Much love. I thank Andrew Benson for his technical wizardry in recovering my back up hard drive after a bout of extreme bad luck. My good man, I could have quit right there, thanks for bailing me out. Miss Stephanie Erickson deserves thanks for being lovely in every way, but primarily for keeping me grounded and calm during the writing up process. It would have sucked a lot more without you gorgeous. I greatly thank Andrew Kingston for his willingness to have a beer and get out of town, as well as provide a sympathetic ear to listen to my complaints. Steven Farber deserves thanks for the crash course in statistics he provided for me, which raised the bar both in my papers and in the statistics applied to belemnite geochemistry in general. Good work fella.

Even though these people were a continent away, they were instrumental in giving me motivation in the “Doctor Race”, in which I hope to come in third by a whisker. Dr Barry Schyma, thanks for constantly visiting and falling seriously ill giving me something else to worry about. Hope that repaired sternum works out for you. Thanks to Dr Steven Andrews for being the keenest geologist I know, as well as being the possessor of fantastic bass stylings. You give me something to strive for my good man. Also, I would like to thank Ian “Rambo” Johnston for allowing me to not come last in the Doctor Race. Nice try.

## TABLE OF CONTENTS

ABSTRACT	iv
ACKNOWLEDGEMENTS	vi
TABLE OF CONTENTS	vii
LIST OF FIGURES	x
LIST OF TABLES	xiii
PREFACE	xiv
Chapter 1	1
Introduction	2
<i>Sepia</i> as a Modern Analogue	5
Research Objectives	6
Thesis Structure	7
Chapter 2	10
High-resolution carbon and oxygen isotope analyses of <i>Sepia officinalis</i> from Jersey, UK	
Rationale and Objectives	11
Abstract	12
Introduction	13
Material and Methods	15
Results	16
Discussion	17
Conclusions	21
Figures and Tables	23
Chapter 3	39
Cuttlebone trace elements of two wild specimens of <i>Sepia officinalis</i> collected from the shores of Jersey, English Channel	
Rationale and Objectives	40
Abstract	41
Introduction	41
Methods	44
Results	45
Discussion	46
Conclusion	48
Figures and Tables	50

Chapter 4	60
Internal stable isotope and trace element variability in belemnite rostra: comparison with a modern analogue and some suggested sampling strategies	
Rationale and Objectives	61
Abstract	62
Introduction	62
Objectives	63
Background	64
Sample Locations	68
Methods	69
Results and Discussion	70
Conclusions	80
Figures and Tables	81
 Chapter 5	 108
High resolution intra-rostral belemnite geochemistry from the Green Beds of southern Alberta, Canada: a possible North American record of an Oxfordian positive carbon isotope excursion	
Abstract	109
Introduction	110
Geologic Setting	112
Methods	113
Results and Discussion	114
Conclusions	124
Figures and Tables	126
 Chapter 6	 152
General Conclusions and Future Research	
Specific Conclusions	153
Future Research	154
 References	 158

## **LIST OF FIGURES**

All figures are located in a consecutive manner at the end of each chapter, as per the general style required for submission of manuscripts to peer-reviewed journals.

### **Chapter 2**

Figure 2.1 A scanning electron microscope study of the internal structure of the cuttlebone.

Figure 2.2 Map of Jersey, English Channel, and surrounding bathymetry showing cuttlebone collection locations.

Figure 2.3 A graph of the sea surface temperature variation around Jersey between Early 2001 and early 2006

Figure 2.4 The oxygen isotope variation in the five cuttlebone collected from Jersey, English Channel. Oxygen isotope axis is inverted to show increases in temperature.

Figure 2.5 The carbon isotope variation in the five cuttlebone collected from Jersey, English Channel.

Figure 2.6 A bulk cross plot of carbon and oxygen isotopes from the sampled cuttlebones.

Figure 2.7 Oxygen isotope profiles calibrated using SST data. Oxygen isotope axis is inverted to show increases in temperature.

Figure 2.8 Carbon isotope profiles correlated using the close match of SST variation and cuttlebone oxygen isotopes.

### **Chapter 3**

Figure 3.1 Map of Jersey, English Channel, showing cuttlebone collection sites.

Figure 3.2 The geochemical trends observed in CF5 correlated using the close fit between oxygen isotope values and sea surface temperature.

Figure 3.3 The geochemical trends observed in CF8 correlated using the close fit between oxygen isotope values and sea surface temperature.

Figure 3.4 A cross plot of oxygen isotope values vs. Sr abundance.

Figure 3.5 A cross plot of carbon isotope values vs. Mg abundance.

### **Chapter 4**

Figure 4.1 The phylogenetic family tree of known Coleoidea.

Figure 4.2 Idealised morphology of belemnite and cuttlefish skeleton

Figure 4.3 Simplified geologic map of the Isle of Skye, Scotland, showing the collection site.

Figure 4.4 Simplified geologic map of southern Alberta, Canada, showing the collection sites.

Figure 4.5 Belemnite sample patterns. a) a 2mm grid pattern centred on the apical line b) a high resolution radial sampling profile.

Figure 4.6 Carbon and oxygen isotope cross plots. a) The slice cut from the Scottish belemnite b) Slice 1 from the Albertan belemnite rostrum c) Slice 2 from the Albertan Belemnite c) Slice 3 from the Albertan Belemnite.

Figure 4.7 Stable isotope maps from the Scottish belemnite, with carbon isotope values to the left, oxygen isotope values to the right.

Figure 4.8 Stable isotope maps from the Albertan belemnite, with carbon isotope values to the left and oxygen isotope values to the right. Slice 1 is top, slice 2 is middle, and slice 3 is bottom.

Figure 4.9 Three dimensional model of interior  $\delta^{18}\text{O}$  and  $\delta^{13}\text{C}$  variation within a single Bighorn Creek belemnite rostra.

Figure 4.10 Stable isotope and trace element profiles from belemnites collected from the 15cm horizon of the Green Beds section, Southern Alberta, Canada. The oxygen isotope axis is inverted to facilitate the intuitive interpretation of temperature change.

Figure 4.11 Stable isotope and trace element profiles from belemnites collected from the 750cm horizon of the Green Beds section, Southern Alberta, Canada. The oxygen isotope axis is inverted to facilitate the intuitive interpretation of temperature change.

Figure 4.12 Stable isotope and trace element profiles from belemnites collected from the 1100cm horizon of the Green Beds section, Southern Alberta, Canada. The oxygen isotope axis is inverted to facilitate the intuitive interpretation of temperature change.

Figure 4.13  $\delta^{13}\text{C}$  vs  $\delta^{18}\text{O}$  for the Carbondale River Belemnites

Figure 4.14 Stable isotope and trace element profiles from belemnites collected from the 15cm horizon of the Green Beds section, Southern Alberta, Canada with diagenetic samples removed. The oxygen isotope axis is inverted to facilitate the intuitive interpretation of temperature change.

Figure 4.15 Stable isotope and trace element profiles from belemnites collected from the 750cm horizon of the Green Beds section, Southern Alberta, Canada with diagenetic samples removed. The oxygen isotope axis is inverted to facilitate the intuitive interpretation of temperature change.

Figure 4.16 Stable isotope and trace element profiles from belemnites collected from the 1100cm horizon of the Green Beds section, Southern Alberta, Canada with diagenetic samples removed. The oxygen isotope axis is inverted to facilitate the intuitive interpretation of temperature change.

## Chapter 5

Figure 5.1 A simplified geologic map of southern Alberta showing the location of the Carbondale River collection site.

Figure 5.2 The stratigraphy of the Fernie Formation.

Figure 5.3 An idealised representation of the sampling strategy utilised for belemnite rostra in this study (after Findlay and Gröcke).

Figure 5.4 Cross plots of  $\delta^{13}\text{C}$  and  $\delta^{18}\text{O}$ . a) Pre diagenetic screening b) post diagenetic screening

Figure 5.5 The geochemistry of the belemnite samples that survived diagenetic screening, including sample number and stratigraphic height. The  $\delta^{18}\text{O}$  scale is inverted to intuitively show temperature change.

Figure 5.6 Cross plots of *Cylindroteuthis* geochemistry vs. normalised distance from the apical line to the outer edge of the rostrum.

Figure 5.7 Cross plots of *Pachyteuthis* geochemistry vs. normalised distance from the apical line to the outer edge of the rostrum.

Figure 5.8 Stratigraphic profiles of the geochemistry of the Green Bed belemnites. Stratigraphic positions are presented as centimetres from the contact between the overlying Passage Beds and the Green Beds.

Figure 5.9 Schematic summarising belemnite life history.

Figure 5.10 Cross plots of stable isotopes and trace elements analysed from the same sample.

## **LIST OF TABLES**

### Chapter 2

Table 2.1 Stable isotope data from five English Channel cuttlebones.

Table 2.2 Growth Rate Statistics

### Chapter 3

Table 3.1 Trace element data from two English Channel cuttlebones.

### Chapter 4

Table 4.1 Stable isotope data from the belemnite stable isotope maps.

Table 4.2 Stable isotope and trace element data of belemnite rostra collected from discrete horizons of the Green Beds, Carbondale River, southern Alberta, Canada.

### Chapter 5

Table 5.1 Stable isotope and trace element data of belemnites collected from the Green Beds, Carbondale River, southern Alberta, Canada.

## **PREFACE**

This thesis is the compilation of several research papers that are prepared for publication in peer reviewed academic journals. At the time of thesis submission, none have been accepted, but all are formatted for the journal of choice. The relationships of these papers to a general research theme are described in chapter one. The final chapter summarises the contributions of these papers to science and contains suggestions as to further research.

Each of these papers is co-authored, but the first author in each case is the doctoral candidate, who conducted the vast majority of the investigation, literature review, analyses, interpretation and illustration. Dr Darren Gröcke and Dr Alan Dickin, Dr Carolyn Eyles and Dr John Drake provided guidance as to the direction of research. Funding for sample collection and analysis was provided by NSERC Grants to Dr Darren Gröcke. Martin Knyf, co-author of chapter two, is the lab technician in the stable isotope lab at McMaster University. He aided in the development of lab methods, and provided valuable insights in aspects of marine ecology.

This is a sandwich thesis, and as such, each chapter displays formatting appropriate to the targeted journal. Because these papers are targeted at different journals and have been structured as isolated pieces of work, the reader may encounter some minor repetition in terms of background and methods between chapters.

**Chapter 1**  
**Introduction**

## Chapter 1

### Introduction

Belemnnoidea is an extinct super-order of marine cephalopods (Doyle et al. 1994), commonly referred to as belemnites, which were abundant in Mesozoic oceans and are commonly used for palaeoclimatic reconstruction. Having evolved in the Jurassic, these organisms largely went extinct at the end of the Cretaceous, with a few survivors disappearing in the early Tertiary (Murray 1985). One of the features of Belemnnoidea that separates them from coeval shelled cephalopods such as ammonites and nautiloids, is that their skeleton was internal. The rostrum, a dense bullet or cigar shaped calcitic structure, acted as a counter balance for the phragmocone which served to regulate buoyancy for the organism (Ellis 2001). The phragmocone was composed of aragonite, and is rarely geochemically preserved in its original form, however the rostrum was composed of low Mg calcite, which is resistant to post-burial alteration (Spaeth et al. 1971). The preservation potential of Belemnnoidea rostra has led to their widespread use in Mesozoic geochemical studies.

In the 1940s, it was discovered that measurements of the ratio of  $^{18}\text{O}$  to  $^{16}\text{O}$  in biologic carbonate and the precipitating water may be used to reconstruct ambient water temperatures with a reasonable degree of accuracy (Epstein et al. 1951, Urey et al. 1951, Epstein et al. 1953). As sea surface temperature exerts a large control on global climatic patterns, this discovery had great potential for palaeoclimatic investigation, and as a result, Belemnnoidea rostra became popular tools for investigating climatic change during the Mesozoic. More recently, it has been recognised that the elemental composition of carbonate ( $\text{CaCO}_3$ ) also allows for investigations of ancient carbon isotope ratios, which have been used to investigate changes in the carbon isotope value of ancient seawater, which may be useful for stratigraphic purposes, as well as understanding changes in palaeoproductivity (Bailey et al. 2003, McArthur et al. 2004, Pirrie et al. 2004, Price and Mutterlose 2004, Rosales et al. 2004a, Wierzbowski 2004, van de Schootbrugge, B. et al. 2005). However, the geochemical record constructed from the Belemnnoidea rostra shows several per mil variability in both oxygen and carbon isotope values, with coeval rostra from the same region displaying different values (Podlaha 1998, Veizer et al. 1999, McArthur et al. 2007). The source of this variability within the population, which does not seem to reflect short-term climatic fluctuations (McArthur et al. 2007), must be understood in order to ensure sound interpretation of any palaeoenvironmental information that might be preserved in the rostra.

Many early studies demonstrated that individual belemnite rostra contain substantial internal variation in stable isotopes (on the order of several per mil), which is likely controlled by environmental, behavioural and biological factors (Urey et al. 1951, Lowenstam and Epstein 1954, Bowen 1961a, Bowen 1961b, Spaeth et al. 1971). However, despite recognition that individual rostra contain environmental, physiological, and behavioural signals, most recent geochemical studies analyse only one sample per rostrum (Bailey et al. 2003, Voigt et al. 2003, McArthur et al. 2004, Pirrie et al. 2004, Rosales et al. 2004a, van de Schootbrugge, B. et al. 2005, Wierzbowski and Joachimski 2007, Gomez et al. 2008). Such a coarse sampling methodology does not account for any internal geochemical variability, and may have contributed to the wide range in geochemical values observed in coeval rostra. As such, high-resolution sampling may aid in understanding the paleoclimatic record preserved in belemnite rostra.

Higher-resolution sampling may also help to better address complications arising from diagenetic alteration. Although belemnite rostra may be generally better preserved than other coeval genera, diagenesis can still overprint pristine geochemical signals (Tan and Hudson 1974, Veizer 1983, Saelen 1989, McArthur et al. 2007). While early belemnite geochemical studies documented variation in oxygen isotope values within the rostrum, the chemistry of post-burial alteration was less well developed and few precautions were taken to screen for diagenesis. Given our modern understanding of the chemical effects of carbonate diagenesis (Veizer 1983), the results of these early studies may be questioned. More recent studies have included stringent diagenetic screening processes, but these almost exclusively analyse one sample per rostrum, which will not account for internal variability: A reinvestigation of the internal geochemistry of Belemnoida rostra using a sensitive diagenetic screening process is clearly required.

The geochemistry of Belemnoida rostra is likely influenced by many environmental parameters. The oxygen isotope palaeothermometer is well established, but it has shortcomings (Epstein et al. 1951, Urey et al. 1951, Epstein et al. 1953, Anderson and Arthur 1983). A limitation of oxygen isotope temperature calculation is that the oxygen isotope value of both biogenic and inorganic calcite is influenced by both the temperature and oxygen isotope value of ambient water. As the isotopic composition of Mesozoic ocean waters can not easily be measured in the geologic record, assumptions must be made. The foraminifera oxygen isotope record of the last 150 kyr has documented large (~2 ‰) variations as a result of  $^{16}\text{O}$  being preferentially evaporated and stored in continental ice. It has been estimated that the ocean water oxygen isotope value during the last glacial maximum was ~1 ‰ (VSMOW) higher than modern ocean water (Schrag and DePaolo 1993, Adkins et al. 1998). Conversely, when there is

little or no land ice, the world ocean oxygen isotope value has been calculated to be approximately  $-1 \text{ ‰}$  (SMOW) (Shackleton and Kennett 1975, Billups and Schrag 2002). In this way, the volume of continental ice controls the oxygen isotope value of ocean water. In addition to this, local exposure to meteoric water, estuaries, deltas etc. and local evaporative regimes will also influence the isotope value of seawater, and may lead to spurious palaeotemperature values from even pristine fossil carbonate (Sharp 2007, Anderson and Arthur 1983).

Estimates of the oxygen isotope value of the ancient oceans are based on estimates of continental ice volume. As much of the Mesozoic is thought to be free of continental ice, it is usually assumed that ocean water was approximately  $-1 \text{ ‰}$  VSMOW (Vienna Standard Mean Ocean Water) (Rosales et al. 2004b). However, as investigations of the last hundred thousand years have demonstrated, the isotopic composition of the oceans can change over the course of decades. In addition, any oceanic sediments found on land where the vast majority of macro fossils are collected, were likely deposited in a restricted inland sea. Where similar situations exist today, oxygen isotope values can deviate widely from VSMOW because of local evaporative regimes and runoff. Hence, some indication of local ancient seawater composition would be valuable.

There may be a method of circumventing the problem of measuring the isotopic composition of ancient seawater: If an independent palaeothermometer were developed that could be used alongside stable isotope analysis, the calcite oxygen isotope palaeotemperature equation may be used to calculate the oxygen isotope value of ancient seawater (Lea et al. 2000, Klein et al 1996). As discussed above, knowledge of the isotopic composition of ancient seawater would allow inferences to be made regarding local precipitation patterns, movement of migratory species, and possibly the extent of continental ice cover. Magnesium is readily incorporated into calcite, and in many modern calcite secreting organisms the incorporation rate of Mg in shell material has been observed in some cases to be directly proportional to temperature (Mitsuguchi et al. 1997, Steuber 1999, Hendry et al. 2001, Palacios-Fest and Dettman 2001, McArthur et al. 2004, McArthur et al. 2007, Shen et al. 2007). While Mg levels in seawater do effect the quantity of Mg incorporated into shell carbonate, the quantity of Mg in seawater is relatively uniform over a wide range of salinities, unlike oxygen isotope values (Klein et al. 1996). Mg concentration has therefore been investigated as a salinity independent palaeothermometer in foraminifera (Nurnberg 2000, Lea et al. 2000), and should be investigated in *Belemnoides* rostra.

In addition, other trace elements have been used to extract environmental and/or biological information from biogenic calcite. Barium is highly abundant in upwelling water and continental runoff, and has been used successfully to

reconstruct upwelling, palaeo-flood events and seasonal increases in runoff (Vander Putten et al. 1999, Putten et al. 2000, Hendry et al. 2001, Gillikin et al. 2006). This may be a valuable tool in detecting the influence of meteoric water in biogenic calcite, and its applicability should be investigated in belemnite rostra.

### *Sepia* as a Modern Analogue

The use of geochemical tools like those described above may provide valuable insights into the biology, behaviour and ecology of extinct Belemnoidea which can only improve our ability to make inferences about the paleoclimatic record from the geochemistry of belemnite rostra. Since rostra record behavioural and physiological signals in addition to environmental ones, our understanding of how environmental and behavioural factors influence the internal geochemistry of rostra may be enhanced through the examination of a modern analogue whose behaviour can be observed.

Although the modern squid (*Loligo*) is commonly cited as the best extant analogue for Belemnoidea, this comparison is inappropriate as the squid lacks a calcitic buoyancy regulating internal skeleton and are therefore virtually unrestricted in terms of depth of habitat. A more appropriate modern analogue is the cuttlefish (*Sepia*), which is the only known extant cephalopod to secrete an internal skeleton (Boyle 1983, Boyle and Rodhouse 2005). Buoyancy regulation in the cuttlefish is controlled by the phragmocone (commonly referred to as the cuttlebone), which is composed of aragonitic lamella and pillars which form discrete layers, making it analogous to the phragmocone observed in Belemnoidea (Richard 1969, Bettencourt and Guerra 1999, Sherrard 2000, Rexfort and Mutterlose 2006). The *Sepia* cuttlebone has several inherent physical limitations that are applicable to Belemnoidea studies.

Firstly, gas exchange regulates the buoyancy of the cuttlefish, meaning vertical migration through the water column is relatively slow (Boyle 1983, Boyle and Rodhouse 2005). This suggests that Belemnoidea, like *Sepia*, are nekto-benthic, likely spending most of their time at or around the sea floor. Secondly, the structure of the cuttlebone fails beyond a critical pressure threshold (Sherrard 2000), limiting *Sepia* to maximum depths of ~200m. Belemnoidea phragmocones were similar in structure to modern cuttlebones, and belemnites were probably subject to similar bathymetric limitations. For these reasons, Belemnoidea probably occupied a similar ecological niche to modern *Sepia*. Thus, the nature of the phragmocone in *Sepia* make cuttlefish a more appropriate modern analogue for belemnites than squid, despite the fact that *Sepia* lack the large rostrum observed in belemnites. The similarity between the cuttlefish and

Belemnite phragmacones suggests that improving our understanding of the internal geochemistry of the modern cuttlefish and using it as a modern analogue may aid the interpretation of Belemnoida geochemical signals.

To date, the geochemistry of the cuttlebone has been investigated by only a handful of studies that have primarily focused on laboratory-raised *Sepia* specimens (Bettencourt and Guerra 1999, Rexfort and Mutterlose 2006). Since the analysis of cuttlefish geochemistry is intended to provide a better understanding of the ecology and behaviour of an extinct *wild* organism, the analysis of cuttlebones from free-living, naturally deceased cuttlefish would likely improve our understanding of the geochemistry of the belemnite rostra distributed in the fossil record. In addition, while the concentration of key trace elements in biogenic carbonate are increasingly investigated as potential records of environmental information, the trace element composition of *Sepia* cuttlebones has yet to be explored, making it an important area of research.

#### Research objectives

The goal of this thesis is to advance the understanding of ancient Belemnoida, both in terms of their behaviour, biology, and ecology as well as their utility as environmental proxies, while improving upon the techniques used to sample rostra. Achieving this goal involves several steps.

Firstly, the *Sepia* cuttlebones are examined for both stable isotopes and trace elements. Such an analysis allows the geochemical interpretation of the cuttlebone to be compared with and contrasted against the rostra of ancient Belemnoida. Since the behaviour and ecology of *Sepia* affect the geochemistry of the cuttlebone (Bettencourt and Guerra 1999), understanding these geochemical signals better may aid in our interpretation of the geochemical signals preserved in Belemnoida rostra.

Secondly, the geochemistry of Belemnoida rostra are investigated using high-resolution sampling techniques and results are interpreted in terms of what was learned about *Sepia*. Such analyses are intended to provide context for the interpretation of climate over geological time. For example, if a specific genus of Belemnoida did not occupy very shallow water, palaeotemperatures calculated from rostral calcite of this genus should not be interpreted as sea surface temperatures. Consequently, understanding the behaviour of Belemnoida, which may be recorded in signals that can only be detected at relatively high sampling resolutions, may be valuable when interpreting palaeoclimatic data.

Thirdly, a standardised sampling and data handling strategy is devised for belemnite rostra. The standardised regime accounts for any intra-rostrum

variability such that future Belemnoida geochemical studies may maximise the amount of palaeoenvironmental data extracted and minimise the sample bias which may introduce variability between coeval specimens of the same genus. The sampling strategy is then applied to a geologic section to test its effectiveness.

### Thesis Structure

The research objectives outlined above are addressed over the course of four papers intended for publication in scientific journals. The four papers are included in this thesis as individual chapters, which are presented complete with figures and tables as they are intended to eventually appear in publication. This has led to some unavoidable duplication of material throughout these papers, such as the description of analytical methodologies, collection sites, and relevant background information about the problems addressed. A brief summary of the findings of each of the chapters is presented below..

#### Chapter 2

*“High-resolution carbon and oxygen isotope analyses of Sepia officinalis from Jersey, UK”*

This chapter is formatted for submission to *Chemical Geology*.

This is the first study to investigate the stable isotope values of several wild cuttlebones. Five cuttlebones of *Sepia officinalis* collected from the shores of Jersey, on the English Channel were analysed for stable isotope values. Analyses revealed an excellent record of seawater temperature over the lifespan of each cuttlebone that was largely consistent between specimens collected from the same area. An increase in carbon isotope values with ontogeny was observed, suggesting a gradual slowing of metabolic rate with age. Carbon isotope values were also consistent between specimens collected from the same area. The annual migration of English Channel *S. officinalis* to deep water is also visible in stable isotope values.

#### Chapter 3

*“Cuttlebone trace elements of two wild specimens of Sepia officinalis collected from the shores of Jersey, English Channel”*

This chapter is formatted for submission to *Chemical Geology*

This is the first study to examine trace element abundances in cuttlebone aragonite. Trace element concentrations are compared to the previously measured stable isotope values from Chapter 2. Sr and Mn concentrations display statistically significant correlations with oxygen isotope values, implying that temperature may in some way control the incorporation of Sr and Mn in cuttlebone aragonite. In one cuttlebone, Mg concentration displays a low, but statistically significant correlation with carbon isotope values, implying that the incorporation of Mg may be partially controlled by metabolic rate in *Sepia*. However, the same correlation between carbon and Mg is not apparent in the second cuttlebone. Ba levels are low with occasional spikes, consistent with previous research on related species, but specific controls on the incorporation of Ba remain unclear at this time.

#### Chapter 4

*“Stable isotope and trace element variability in belemnite rostra: comparisons with a modern analogue and suggested sampling strategies”*

This chapter is formatted for submission to *The International Journal of Earth Science*.

Several belemnite rostra were sampled at high resolution to investigate their internal geochemical variability. A diagenetically altered Belemnitida *Passaloteuthis* rostrum was shown to exhibit a wide range in stable isotope values arranged in a generally radial pattern around the apical line, as would be expected in well preserved samples. Symmetry in 2 stable isotope profiles, or concentricity around the apical line, is therefore not necessarily an indicator that pristine geochemical values have been preserved. Further analyses were carried out on diagenetically screened samples. Mg abundances were correlated with oxygen isotope values, suggesting that Mg incorporation may relate to temperature in belemnites. This contrasts the apparent temperature-dependence of Sr (and not Mg) incorporation in cuttlebones. Patterns in oxygen isotopes and Mg concentrations hint that sampled organisms may start life in shallow water and migrate to deeper waters with maturity. Such ontogenetic behavioural patterns have been observed in related species and have been shown to be reflected in the geochemical analysis of rostra. As in *Sepia*, carbon isotope values were observed to increase with ontogeny, suggesting that metabolic rate slows with ontogeny in belemnites. Ba values were generally low, but exhibited occasional peaks, similar to those observed in modern carbonate. The cause of the peaks has yet to be

adequately understood. Two possible standardised high-resolution sampling strategies are discussed.

#### Chapter 5

*“High resolution intra-rostral belemnite geochemistry from the Green Beds of southern Alberta, Canada: a possible North American record of an Oxfordian positive carbon isotope excursion”*

This chapter is formatted for submission to *The Canadian Journal of Earth Science*.

A total of 44 rostra from the Green Beds of the Fernie Formation were analysed for stable isotope values and trace element concentration following one of the sampling methods developed and recommended in Chapter 4. Individuals from both of the Belemnnoidea genera that were identified in the section were found to show increasing carbon isotope values with ontogeny. When examined in stratigraphic position, a positive carbon isotope excursion was identified, which may be a valuable age marker for the region. Both oxygen isotope values and Mg concentrations show a general trend towards lower temperatures with ontogeny in *Cylindroteuthis*. Such a pattern could be explained by migration from warmer, shallower water to cooler, deeper water through ontogeny. If migration through ontogeny is the underlying cause of the patterns in oxygen isotopes and Mg concentrations, it may be possible to investigate the evolution of both surface and deeper water temperatures over geologic time using the information recorded in the geochemistry of belemnite rostra. Ranges in carbon isotope values suggest that there is a positive ~2 ‰ isotope excursion within the Green Beds which may be a valuable geochemical age marker for the region.

## **Chapter 2**

**High-resolution carbon and oxygen isotope analyses of**

***Sepia officinalis* from Jersey, UK**

## Rationale and Objectives

The main goal of this thesis is to better understand and interpret the geochemical signals preserved in belemnite rostra. To this end, examining a modern analogue may provide valuable insight into the behaviour and biology of the extinct belemnite. As the presence of a phragmocone will limit the depth of habitat, an extant cephalopod which utilises a phragmocone for buoyancy regulation would be the best choice. Therefore, as the first data chapter of this thesis, the initial step was to investigate the internal stable isotope variability of *Sepia* cuttlebones. For reasons outlined in chapter 1, it was expected that oxygen isotopes would provide some record of temperature variation over the lifespan of the organism, and the reliability of this as a temperature proxy should be examined. In addition, carbon isotopes were investigated in the hope that they would provide some information as to diet, metabolism and/or other aspects of their biology.

Stable isotope investigations were conducted on 5 cuttlebones collected from the shores of Jersey in the English Channel, and these were found to contain an excellent record of ocean temperatures over the lifespan of the organism. The record was of sufficient quality to allow the time of hatching and death to be inferred, and to identify annual migrations to colder, deeper water nearer the centre of the English Channel. Carbon isotopes appear to vary with ontogeny, documenting a declining metabolic rate with growth, followed by an increase in metabolism late in life, which may be a result of a spawning forcing an increase in metabolism and/or a reallocation of carbon to facilitate egg growth.

# High-resolution carbon and oxygen isotope analyses of *Sepia officinalis* from Jersey, UK

Duncan J. Findlay<sup>1</sup>, Darren R. Gröcke<sup>2</sup>, Martin C. Knyf<sup>1</sup>

1. School of Geography and Earth Sciences, McMaster University, 1280 Main Street W, Hamilton, Ontario L8S 4K1 Canada, (emails: findlad@mcmaster.ca, knyf@mcmaster.ca)

2. Department of Earth Sciences, Durham University, Science Laboratories, Durham DH1 3LE, UK (email: d.r.grocke@durham.ac.uk)

**Abstract** Stable isotope analysis of biological carbonate can provide important information regarding temperature of secretion and metabolic processes.  $\delta^{13}\text{C}$  and  $\delta^{18}\text{O}$  values were determined for 5 *Sepia officinalis* cuttlebones, collected autumn 2005, Jersey, U.K.  $\delta^{18}\text{O}_{\text{arag}}$  values from sequentially sampled aragonite layers within the cuttlebones reveal cyclic variability, the peaks and troughs of which allow inter-cuttlebone correlation. Temperatures calculated from  $\delta^{18}\text{O}_{\text{arag}}$  values exhibit excellent agreement with the sea surface temperatures of the collection area between February 2003 and February 2005, suggesting the cuttlefish secreting these cuttlebones were alive between ~October 2003 and ~August 2005. This strong temperature correlation suggests that cuttlebone  $\delta^{18}\text{O}_{\text{arag}}$  values may be used to reliably reconstruct environmental information. While there is some variation in spring, summer and autumn  $\delta^{18}\text{O}_{\text{arag}}$  values, winter values tend to be similar in all cuttlebones, supporting field observation of migration to the Hurd Deep during the winter months.  $\delta^{13}\text{C}_{\text{arag}}$  values display an increase from hatching until late middle life, interpreted as a decrease in metabolic rate with ontogeny. Once correlated using the  $\delta^{18}\text{O}_{\text{arag}}$  value dates,  $\delta^{13}\text{C}_{\text{arag}}$  values from all cuttlebones are observed to converge in the winter. This also supports field evidence of cuttlefish from different areas migrating to deeper waters during the winter months.

The excellent temperature record acquired from these cuttlebones implies that ancient, well preserved belemnite phragmocones, and even perhaps the corresponding rostra, may accurately preserve sea water temperatures from the Mesozoic. As the cuttlefish is the only other known cephalopod with an internal skeleton, better understanding the geochemistry of the cuttlebone may be beneficial in interpreting the belemnite geochemical record.

**Key Words** *Sepia officinalis*, stable isotopes, environmental proxy, belemnite

## Introduction

Cuttlefish (*Sepia sp.*) are shallow living (<120m) nektobenthic marine cephalopods that prey on an array of marine organisms including crustaceans and fish. Separating from what would evolve into octopi (Octopoda) and squid (Teuthida) in the late Triassic (Doyle et al. 1994), *Sepia* contains over 100 species and, like squid, have eight arms, two tentacles and often exhibit the ability to actively camouflage themselves (Hanlon and Messenger 1996). *Sepia* spend much of their lives around sandy substrate either buried in the sand or moving just above the sea floor hunting small fish and crabs (Boyle, 1983). *Sepia* differs from other extant cephalopods in their internal aragonitic phragmocone, or cuttlebone, which contains numerous gas filled chambers that are used to regulate buoyancy (Fig 1; Boyle 1983). Most cuttlefish species have a lifespan of ~2 years (Boyle 1983; Hanlon and Messenger 1996; Rexfort and Mutterlose, 2006) and can achieve mantle lengths in excess of 50cm (Giant Cuttlefish, *Sepia apama*; Hall and Hanlon 2002). While the biology of Cuttlefish is well understood, relatively little is known about the ecology and habit of *Sepia* beyond broad habitat and migratory information (Bouchard-Camou and Boismery 1991, Gabr et al. 1998; Minton et al. 2001; Minton 2004). In the English Channel, *Sepia officinalis* have been observed to live in near shore environments between April and October, migrating to the deeper waters of the Hurd Deep, approximately 70km to the north west of Jersey over the winter months. The following spring there is a rapid inshore migration, usually to the original hatching ground. Adults appear to expire soon after spawning which usually occurs between April and October (Boucaud-Camou and Boismery 1991). Since cuttlebone aragonite is rapidly and sequentially secreted throughout ontogeny, cuttlebones may provide a record of the environmental and metabolic conditions experienced over each individual's lifespan. Indeed, it has been shown that environmental information can be obtained using cuttlebone morphology alone: For example, deeper dwelling species exhibit much thicker lamellae with more densely spaced pillars than shallower dwelling species (Sherrard 2000).

In fact, stable isotope values of many carbonate secreting marine species have been used to investigate biologic and environmental information of the habitat in which they live (Carpenter and Lohmann 1995; Curry and Fallick 2002; Høie et al. 2004; Mulitza et al. 1998 and many others). However, only a few studies have been published on the stable isotope geochemistry of *Sepia* cuttlebones (Hewitt and Strait 1988; Bettencourt and Guerra 1999; Rexfort and Mutterlose, 2006). Initial work (Hewitt and Strait 1988; Bettencourt and Guerra 1999) utilized low-resolution sampling (homogenizing ~10 lamellae per sample for isotope analysis) of both wild and cultivated specimens of the common European cuttlefish, *S. officinalis*. More recently, Rexfort and Mutterlose (2006) provided high-resolution sampling (sampling each

individual lamella for isotope analysis) on one wild and one cultured *S. officinalis* specimen that yielded a far more detailed record.

Bettencourt and Guerra (1999) showed that the  $\delta^{18}\text{O}_{\text{arag}}$  of the laboratory-reared *S. officinalis* cuttlebone specimens are secreted in isotopic equilibrium with seawater, later confirmed by Rexfort and Mutterlose (2006), suggesting that  $\delta^{18}\text{O}_{\text{arag}}$  in *S. officinalis* could be used as a proxy for environmental and climatic studies. In a study of the relationship between seawater temperature and  $\delta^{18}\text{O}_{\text{arag}}$ , Grossman and Ku (1986) established a temperature equation for molluscs, which was subsequently updated and modified by Goodwin et al. (2003):

$$T = 20.6 - 4.34(\delta^{18}\text{O}_{\text{arag}} - (\delta^{18}\text{O}_{\text{w}} - 0.2)) \quad [2.1]$$

where T is temperature in degrees Celsius,  $\delta^{18}\text{O}_{\text{arag}}$  is the  $\delta^{18}\text{O}$  value (VPDB) of mollusc aragonite, and  $\delta^{18}\text{O}_{\text{w}}$  is the  $\delta^{18}\text{O}$  value (VSMOW: Vienna Standard Mean Ocean Water) of ambient water. This was shown to be appropriate for *S. officinalis* by Rexfort and Mutterlose (2006). Therefore, reliable water temperatures may be calculated from cuttlefish  $\delta^{18}\text{O}_{\text{arag}}$  values, assuming that the  $\delta^{18}\text{O}$  value of ambient seawater ( $\delta^{18}\text{O}_{\text{w}}$ ) is known.

In contrast to  $\delta^{18}\text{O}$  isotopes, cuttlebone  $\delta^{13}\text{C}_{\text{arag}}$  values have been shown to vary independently from ambient water  $\delta^{13}\text{C}_{\text{DIC}}$  (Dissolved Inorganic Carbon) suggesting that  $\delta^{13}\text{C}_{\text{arag}}$  is not precipitated in equilibrium with seawater (Bettencourt and Guerra 1999, Guerra et al. 1998).  $\delta^{13}\text{C}_{\text{arag}}$  values in *Sepia* cuttlebones are therefore likely controlled primarily by factors other than DIC, and may reflect a combination of factors such as diet, perhaps associated with migration (food sources may vary with location), ontogeny (larger animals being able to consume larger prey as observed in squid (Cherel and Hobson 2005; Takai et al. 2000)), or metabolic changes with ontogeny (Rexfort and Mutterlose 2006).

This study presents high-resolution stable isotope records sampled from the cuttlebones of five wild specimens of *S. officinalis*, collected from the shores of Jersey in the English Channel (Fig. 2). Palaeotemperatures calculated from the  $\delta^{18}\text{O}_{\text{arag}}$  values of these samples are compared to satellite-derived sea surface temperatures from 2001 to 2006, averaged over a 2° latitude and longitude square encompassing the collection area (Fig. 3).  $\delta^{13}\text{C}_{\text{arag}}$  records are also examined in order to examine ontogenetic changes. The interpretation of these stable isotope records is important for the geochemical study of extinct belemnites, a closely related extinct cephalopod that also had an internal buoyancy regulating skeleton. Wild, flotsam cuttlebone specimens were selected over laboratory or fishery specimens in order to provide the strongest possible analogy to the distribution of belemnite rostra in the fossil record, which were commonly concentrated spatially by wave action. A better understanding of the modern analogue may improve palaeoenvironmental reconstructions using belemnite rostra.

## Materials and Methods

All five cuttlebones (CF4, CF5, CF6, CF7, and CF8) were collected from beaches along the Jersey coastline in the English Channel during 2005, and are thus considered geochemically pristine. Since the cuttlebone is a fragile structure, it would be unlikely to survive wave action and/or bird feeding for more than a few weeks. It is therefore likely that these specimens died only a short time before collection. Birds commonly consume cuttlebones as a source of  $\text{CaCO}_3$ , and CF4 exhibits indentations consistent with bird feeding.

CF4 and CF7 were collected from the north west coast, CF5 and CF8 from the north east coast, and CF6 from the south east coast (Fig. 2). The cuttlebones ranged from 11 to 16cm in length (CF4: 12cm, CF5: 15cm, CF6: 14cm, CF7: 11cm, CF8: 16cm), and were identified as *S. officinalis* (Norman 2000). Each cuttlebone was split longitudinally down the midline, cutting an additional slit parallel to the cut edge at ~5mm to facilitate the removal of individual layers using a scalpel (Fig. 1). Sequential samples of ~10 mg from each layer of lamella and underlying pillar were obtained for chemical treatment to remove organic debris (see below) prior to isotopic analysis. Following the removal of a lamella and most of the underlying pillar for analysis, the remaining debris was removed using compressed air to prevent cross-contamination between layers. Due to its relatively small size, it was necessary to completely remove the most recently secreted lamella of the cuttlebone in order to provide adequate mass for analysis. Similarly, a few of the oldest lamellae of a cuttlebone are also very small and several layers and had to be completely removed to provide adequate mass for analysis.

Preliminary analysis of a *S. pharaonis* specimen indicated that organic matter within the cuttlebone shifted both  $\delta^{13}\text{C}_{\text{arag}}$  and  $\delta^{18}\text{O}_{\text{arag}}$  values by +1.0-2.5‰ and +0.10-0.35‰ respectively: a similar enrichment was noted by Hewitt and Stait (1988). In an attempt to remove the organic content, Bettencourt and Guerra (1999) heated powdered samples to ~350 °C in air for ~45 minutes. Hewitt and Stait (1988) also roasted their powdered samples, but only to 50°C with some samples treated with bleach. In this study, each sample was soaked in 30% peroxide for ~1 hour before being rinsed 3 times with deionised water and dried over night in an oven at 60°C.

Isotopic analyses of *S. officinalis* samples were carried out using a Fison Optima isotope-ratio mass-spectrometer, coupled to an on-line common acid bath, at McMaster University. Samples were reacted with 100% phosphoric acid at 90°C.  $\delta^{13}\text{C}_{\text{arag}}$  and  $\delta^{18}\text{O}_{\text{arag}}$  values are reported in standard delta ( $\delta$ ) notation expressed as per mil (‰):

$$\delta = \left( \frac{R_{\text{sample}}}{R_{\text{standard}}} - 1 \right) \times 1000 \quad [2.2]$$

where R is the ratio between the isotopes of interest ( $^{13}\text{C}/^{12}\text{C}$  and  $^{18}\text{O}/^{16}\text{O}$ ). All isotopic values are reported relative to Vienna Pee Dee Belemnite (VPDB) calibrated using the NBS 19 limestone. The reproducibility for both  $\delta^{13}\text{C}$  and  $\delta^{18}\text{O}$  values is better than  $\pm 0.1\text{‰}$  on replicate analyses.

Sea surface temperatures (SST) were acquired from the NOMAD satellite Optimal Interpolation v2 data set (Fig. 3; [http://nomad3.ncep.noaa.gov/cgi-bin/pdisp\\_sst.sh](http://nomad3.ncep.noaa.gov/cgi-bin/pdisp_sst.sh)) in order to enable comparison between temperatures calculated from cuttlebone geochemistry and actual sea surface temperatures. Sea surface temperatures ranged from  $6.2^{\circ}\text{C}$  to  $18.9^{\circ}\text{C}$ , averaging  $12.7^{\circ}\text{C}$ . As no water samples were collected with the cuttlebones,  $\delta^{18}\text{O}_w$  values for cuttlebone temperature calculations made using equation 2.1 were estimated using salinity data from the area. Ocean salinity correlates well with  $\delta^{18}\text{O}_w$  value, allowing a close approximation of  $\delta^{18}\text{O}$  value to be calculated from psu data. Based on an average salinity of 35 psu for this area (Laane et al 1996), and the relationship between salinity and oxygen isotope value of seawater from the nearby North Sea (Harwood et al. 2008), a  $\delta^{18}\text{O}_w$  of  $0.3\text{‰}$  was selected for temperature calculation.

Calculating water temperatures from  $\delta^{18}\text{O}_{\text{arag}}$  values according to equation 2.1 (Goodwin et al. 2003) allows seasonal highs and lows to be correlated across the records preserved in each cuttlebone in order to correct  $\delta^{18}\text{O}$  records for differences in growth rate and hatching time among individuals (Fig. 7).  $\delta^{18}\text{O}$  records were superimposed by matching maximum and minimum seasonal values across cuttlebones and the distance between maximum and minimum values averaged over the intervening lamellae to determine the date of secretion for each lamellae in each individual.

## Results

A total of 443 samples were processed for stable isotopes, with each cuttlebone averaging 89 lamellae of sufficient size for analysis. Cuttlebone  $\delta^{18}\text{O}_{\text{arag}}$  (VPDB) values (Fig. 4) range between  $+0.4\text{‰}$  and  $+3.5\text{‰}$ , with a mean value of  $+1.8\text{‰}$  ( $\sigma = 0.7$ ) (Table 1).  $\delta^{18}\text{O}_{\text{arag}}$  values cycle throughout ontogeny, appearing as broad troughs interrupted by peaks of short duration (Fig. 4). Specimens from the same areas (CF4 and CF7 were collected from the same beach, as were CF5 and CF8; Fig 2), show similar ranges in  $\delta^{18}\text{O}_{\text{arag}}$  values, with CF4 and CF7 ranging between  $+0.6\text{‰}$  and  $+3.3\text{‰}$ , and  $+0.6\text{‰}$  and  $+2.7\text{‰}$  respectively; CF5 and CF8 range between  $+0.8\text{‰}$  and  $3.4\text{‰}$ , and  $+1.2\text{‰}$  and  $+3.4\text{‰}$  respectively; while CF6 ranges between  $+0.4\text{‰}$  and  $+3.4\text{‰}$ .

$\delta^{13}\text{C}_{\text{arag}}$  trends display a general increase through ontogeny before a rapid fall near the end of each specimen's life, except for specimen CF6 (Fig. 5).  $\delta^{13}\text{C}_{\text{arag}}$  values range between  $-6.6\text{‰}$  and  $+1.4\text{‰}$ , with a mean value of  $-1.6\text{‰}$  ( $\sigma = 1.2$ ) (Table 1). Although the inter-cuttlebone similarity observed

in  $\delta^{18}\text{O}_{\text{arag}}$  values is also apparent in  $\delta^{13}\text{C}_{\text{arag}}$ , some variability is exhibited among individuals late in life, with some individuals showing a more pronounced decline than others (Fig. 5). A cross plot reveals that  $\delta^{13}\text{C}_{\text{arag}}$  and  $\delta^{18}\text{O}_{\text{arag}}$  values exhibit no linear correlation (Fig. 6;  $r^2$  of 0.02), indicating that they vary independently.

## Discussion

### Cuttlefish $\delta^{18}\text{O}_{\text{arag}}$ values

The cycles observed in cuttlebone  $\delta^{18}\text{O}_{\text{arag}}$  values consist of broad troughs and sharp peaks (Fig. 4), which likely reflect seasonal temperature cycles. Since there is an inverse correlation between aragonite  $\delta^{18}\text{O}$  values and water temperature (Grossman and Ku 1986), similar to that observed in calcite (Urey et al. 1947), the sharp peaks are interpreted to represent a reduced growth rate associated with winter minimum temperatures. In fact, the number of cycles in  $\delta^{18}\text{O}_{\text{arag}}$  values suggests that these specimens were alive for  $\sim 1.75$  years, which is consistent with the observed lifespan of this species (Boyle 1983, Boyle and Rodhouse 2005).

The  $\delta^{18}\text{O}_{\text{arag}}$ -derived temperatures are generally in good agreement with the satellite sea surface temperature (SST) record between 2001 and 2006, which allows dating of the cuttlebones. The calculated cuttlebone temperature profiles are best correlated with the SST from February 2004, August 2004, and February 2005 (Fig. 3, Fig. 7). During this time, between February 2004 and 2005, a relatively mild winter was followed by a relatively severe winter, which provides a clear marker with which to date individual cuttlebones. Low winter temperatures fall from  $\sim 7^\circ\text{C}$  for both SST and  $\delta^{18}\text{O}_{\text{arag}}$  derived temperatures during the winter of 2003/2004, to  $\sim 6^\circ\text{C}$  SST and  $\sim 5^\circ\text{C}$   $\delta^{18}\text{O}_{\text{arag}}$  for the winter of 2004/2005.

It is well known that *S. officinalis* migrate to the deeper, more stable waters of the Hurd Deep (maximum depth  $\sim 150\text{m}$ ) with the onset of winter (Boyle 1983; Hewitt and Strait 1988; Boyle and Rodhouse 2005; Boyle and Boletzky 1996; Boucaud-Camou and Boismery 1991). Similar values in low winter temperatures are observed in all cuttlebones, suggesting that all specimens migrated to waters of a common temperature during cold periods. Winter mixing of ocean water will homogenise temperatures over the top 100-200m, which may explain the similarity of the calculated temperatures and measured sea surface temperatures.

Growth rates were assessed by dividing the number of lamella secreted between the correlative points, described above, by elapsed time between points. These suggest that more lamellae were secreted in the autumn than the spring: Whereas CF4 accumulated new lamellae every 4.5 days on average in late 2003, and every 4.2 days on average in late 2004 (Table 2), spring growth rates were estimated as  $\sim 9$  and  $\sim 12$  days per lamella in early 2004 and early

2005 respectively. Thus, at these localities in Jersey, *S. officinalis* appears to grow more rapidly in the autumn than the spring.

The structure of the  $\delta^{18}\text{O}_{\text{arag}}$  cycles also indicate that fewer lamellae are secreted during the winter months than during the summer, which initially gives the impression of a disproportionately short winter (Fig. 7). Since low temperatures reduce growth rates in cephalopods (Richard 1969), the number of lamellae secreted is reduced in winter, resulting in a reduction in sampling resolution. As such, the apparent brevity of winter is likely an artefact of reduced growth rates associated with lower temperatures. The fact that the maximum and minimum temperatures calculated from cuttlebone  $\delta^{18}\text{O}_{\text{arag}}$  are in good agreement with the satellite measured SST (Fig. 8), suggests that these cuttlefish grew all year, with rapid growth in the warm shallow water inhabited during the spring, summer and early autumn, and slower growth during the winter when inhabiting deep water. The continuous record of growth also implies that the cuttlefish did not exceed a lower or upper temperature tolerance level for growth (which has been observed in clams; Goodwin et al. 2001).

The strong correlation between  $\delta^{18}\text{O}_{\text{arag}}$  derived temperatures and SST allowed the determination of approximate hatching season, provided there are no lamellae missing, there are no major changes in growth rate between the maxima and minima correlation points, and that the organisms all come from the same location. Results suggest that specimens hatched at different times during the late summer and autumn. These data suggest that CF4 hatched at the latest November 2003, CF5 hatched at the latest October 2003, CF6 at the latest July 2004, CF7 hatched at the latest February 2004 and CF8 hatched at the latest November 2003 (Fig 7). This is largely incompatible with the commonly cited hatching period between May and August (Boyle and Rodhouse 2005, Nixon and Mangold, 1998). One possible explanation for the disagreement between our data and prior research is that the cuttlebones were insufficiently sampled: Septa become smaller towards the outer cone and spine, and the last several septa were sampled together to ensure an adequate sample size. However, it is unlikely that such sampling issues resulted in a margin of error greater than about one month, since *Sepia* hatch looking like small adults (Boyle 1983), and have eight or nine cuttlebone chambers secreted at this time (Nixon and Mangold 1998). Our specimens are, therefore, unlikely to be more than one month older than the profiles would suggest and, given the excellent correlation between SST and  $\delta^{18}\text{O}_{\text{arag}}$  based temperatures; it seems unlikely that the hatching season is wildly inaccurate. This may indicate that previously established hatching periods for *S. officinalis* require re-examining.

Specimens were collected from different beaches on Jersey (Fig 2) and, apart from winter temperature minima, contain subtly different stable isotope records. The lower calculated temperatures of CF5 and CF8 from spring to

autumn may be explained by these specimens living in deeper and colder water than CF4 or CF7. This hypothesis is consistent with the bathymetry around the collection sites (Fig. 2): The site at which CF5 and CF8 were collected exhibits deeper water than the other collection sites, providing these individuals with access to a deeper and therefore cooler, habitat. In this way vertical migration through the water column will influence the  $\delta^{18}\text{O}_{\text{arag}}$  values preserved in the cuttlebone during the summer months. As noted for the winter migration, winter mixing of ocean waters results in relatively uniform temperature depth profiles, and so vertical migration is more of a problem in summer months. It may be possible to use the temperatures calculated from  $\delta^{18}\text{O}_{\text{arag}}$  to reconstruct depth migration in *S. officinalis* with adequate knowledge of water temperature changes with depth.

It is possible that the springtime increase in calculated temperatures recorded in all cuttlebones in the spring of 2004 (Fig. 7) may be the result of meteoric water input since the temperatures calculated from  $\delta^{18}\text{O}_{\text{arag}}$  values are higher than the satellite measures SST for this periods. Since meteoric water has a lower  $\delta^{18}\text{O}$  value than sea water, the increase in meteoric runoff into the system during spring may lower the  $\delta^{18}\text{O}$  value of the seawater. If unaccounted for, such an effect will lead to the calculation of anomalously high, inaccurate temperatures. Interpreted in this manner, the apparently warmer spring conditions recorded in these cuttlebones may be attributable to increased spring runoff in this area.

#### Cuttlefish $\delta^{13}\text{C}_{\text{arag}}$ values

The similarity in  $\delta^{18}\text{O}_{\text{arag}}$  observed in cuttlebones from the same beach is also apparent in early life history  $\delta^{13}\text{C}_{\text{arag}}$  values, with some differences emerging towards the end of life. The ranges in  $\delta^{13}\text{C}_{\text{arag}}$  values of *S. officinalis* from this study (Fig. 5) are similar to the cultured specimens of Rexfort and Mutterlose (2003) (but larger than their wild specimen) and display a greater range than those reported by Bettencourt and Guerra (1999), which were reported to vary by  $\sim 1.5\%$  within an individual cuttlebone.

$\delta^{13}\text{C}_{\text{arag}}$  values increase with ontogeny before a rapid decrease near the end of each specimen's life, with the exception of CF6 (Fig. 5). Similar trends were observed in *Sepia* by Rexfort and Mutterlose (2006), and proposed for well preserved ammonites by Lécuyer and Bucher (2006). A general decrease in metabolic rate with ontogeny is likely a primary control on  $\delta^{13}\text{C}_{\text{arag}}$  values in biogenic carbonate (Klein et al. 1996). Small changes in growth rate, metabolism or dietary changes, either by migration or through changes in prey preference with maturity, may account for the small perturbations and deviations from the described trend. This would imply that the  $\delta^{13}\text{C}_{\text{arag}}$  value of cuttlebone aragonite is a function of changes in metabolic rate superimposed on an environmental DIC signal, similar to that which is observed in salmonids (Wurster et al. 2005; Romanuk and Levings 2005;

Sherwood and Rose 2003; Schwarcz et al. 1998; and Zazzo et al. 2006). This interpretation of the increasing  $\delta^{13}\text{C}_{\text{arag}}$  values with ontogeny is also supported by the work of Rexfort and Mutterlose (2006) who found similar  $\delta^{13}\text{C}_{\text{arag}}$  trends for laboratory reared specimens of *S. officinalis* which did not migrate and which were raised with a controlled dietary regime. In fact, DIC likely controls the background  $\delta^{13}\text{C}_{\text{arag}}$  value in *S. officinalis*, while metabolism controls the variation in  $\delta^{13}\text{C}_{\text{arag}}$  from or around this background value: As DIC is utilised by primary producers, the initial  $\delta^{13}\text{C}$  value of the seawater from a given area is passed on through the food chain because there is minimal trophic level alteration. Notably, the increasing trend in  $\delta^{13}\text{C}$  values contrasts that observed in scallops, where it has been proposed that  $\delta^{13}\text{C}_{\text{arag}}$  decreases through ontogeny as a consequence of an increase in the respiratory carbon component with ontogeny (Lorrain et al. 2004). This suggests that respiratory carbon is not a dominant source of carbon in *S. officinalis* cuttlebones.

When the date calculated using the  $\delta^{18}\text{O}_{\text{arag}}$  value from the appropriate lamella are related to the  $\delta^{13}\text{C}_{\text{arag}}$  values from each cuttlebone, it becomes apparent that  $\delta^{13}\text{C}_{\text{arag}}$  values converge on a value of approximately -2.5 ‰ over the winter of 2003/4 and to approximately -1 ‰ over the winter of 2004/5 (Fig. 8). Such a convergence in values across individuals may be explained by migration to deeper waters during winter, during which time individuals would acquire the  $\delta^{13}\text{C}$  values inherent to that area via the food chain. This interpretation is supported by both the similar winter  $\delta^{18}\text{O}_{\text{arag}}$  values discussed above and by field observation of migrations to deeper waters during the winter (Boyle 1983; Hewitt and Strait 1988; Boyle and Rodhouse 2005; Boyle and Boletzky 1996; Boucaud-Camou and Boismery 1991). During the rest of the year, these individuals would live in a variety of shallow locations, as *S. officinalis* have been observed to migrate inshore between the winter solstice and spring equinox (Boyle and Boletzky 1996; Boucaud-Camou and Boismery 1991), which would explain the divergence in  $\delta^{13}\text{C}$  values among individuals from spring to autumn.

$\delta^{13}\text{C}_{\text{arag}}$  values fall rapidly near the end of these specimens' lives, a trend that is most pronounced in CF5 and CF7. Three possible explanations for this trend are considered here. Firstly, lowered  $\delta^{13}\text{C}_{\text{arag}}$  values near the end of these specimens' lives may reflect the fact that *Sepia* migrate to near shore environments to spawn near the end of their life cycle: Terrestrial organic matter (and consequently freshwater DIC) generally displays lower  $\delta^{13}\text{C}$  values than those of marine environments and may be incorporated into the cuttlebone via the food chain during spawning. Interpreted in this manner, the cuttlefish must remain at a sufficient distance from any terrestrial water source so as to influence the  $\delta^{13}\text{C}_{\text{arag}}$  but not the  $\delta^{18}\text{O}_{\text{arag}}$ , as the  $\delta^{18}\text{O}_{\text{arag}}$  values do not indicate a terrestrial signal at these times of low  $\delta^{13}\text{C}_{\text{arag}}$  values.

Secondly, the  $\delta^{13}\text{C}_{\text{arag}}$  value preserved in the cuttlebone may change toward the end of individuals' life spans if they refrain from eating while

spawning, or as they near the end of their life cycle in general. However, as starvation inhibits cuttlebone growth in *S. officinalis* (Richard 1969), and there is no evidence for a cessation in cuttlebone growth in the  $\delta^{18}\text{O}_{\text{arag}}$  values, it is considered unlikely that starvation has influenced the  $\delta^{13}\text{C}_{\text{arag}}$  in this case.

Thirdly, the rapid fall in late life  $\delta^{13}\text{C}_{\text{arag}}$  values may also be related to spawning stresses such as egg production, and may highlight an interesting sexual isotopic difference between *S. officinalis* specimens. The production of eggs requires a change in metabolic rate and/or carbon reallocation, which may influence the  $\delta^{13}\text{C}_{\text{arag}}$  value preserved in the cuttlebone. The larger decrease in  $\delta^{13}\text{C}_{\text{arag}}$  observed in CF5 and CF7 may be the result of egg production, and therefore may provide an indication of sex, suggesting in this case that CF5 and CF7 are female. A similar decrease in  $\delta^{13}\text{C}$  value has been noted in breeding birds (Hobson et al. 2000), and possibly land snails (Leng et al. 1998). CF4, CF6 and CF8 may therefore be male *S. officinalis* with the minor drop in  $\delta^{13}\text{C}_{\text{arag}}$  values possibly representing inshore migration as above. This hypothesis cannot be tested using current data, as there is as yet no way to discern cuttlefish sex from cuttlebone morphology.

## Conclusions

1.  $\delta^{18}\text{O}_{\text{arag}}$  values of *Sepia officinalis* cuttlebones are consistent with both sea surface temperatures and field observations of *Sepia* behaviour, indicating that the  $\delta^{18}\text{O}_{\text{arag}}$  values of these cuttlebones accurately record variations in water temperature through seasonal variation and migration.
2. Similar values for both  $\delta^{18}\text{O}_{\text{arag}}$  and  $\delta^{13}\text{C}_{\text{arag}}$  in each cuttlebone during the winter months strongly suggest that these specimens migrated to common waters, supported by field observations of *S. officinalis* migrating to the Hurd Deep during the winter.
3. The  $\delta^{13}\text{C}_{\text{arag}}$  of *S. officinalis* document a general decline in metabolic rate with ontogeny, superimposed on an environmental DIC signal. The sharp decline in  $\delta^{13}\text{C}_{\text{arag}}$  towards the end of individuals' life cycle in some specimens may be the result of sex-specific carbon reallocation and/or metabolic change for breeding.
4. A high resolution sampling approach is essential to extrapolate the full ontogenetic and seasonal changes preserved in *S. officinalis* cuttlebones.

**Acknowledgements** *Sepia officinalis* samples were kindly provided by Dr H Stuart-Williams, who collected them while on holiday in Jersey. We greatly appreciate his efforts. This project was funded by an NSERC Discovery Grant to Dr Gröcke.

## Figure Captions

- Fig. 1. Morphology of a modern cuttlebone. a) Sectioned cuttlebone showing the removal of lamella for stable isotope analysis. b) SEM micrograph showing the lamellae and pillar couplets. c) Close-up of two lamellae and the dividing pillars, supporting a single chamber. d) Close-up of a single pillar, showing fine laminations.
- Fig. 2. Map of Jersey, U.K. showing collection sites of the cuttlebones. Bathymetry is presented in meters.
- Fig. 3. NOMAD satellite sea surface temperature (SST) variation for the Jersey area between 2001 and 2006. Note the unique shape of the curve as well as the values between late 2003 and late 2005 (highlighted).
- Fig. 4.  $\delta^{18}\text{O}_{\text{arag}}$  values over the length of the cuttlebone. Temperatures are calculated using the equation of Goodwin et al. (2003). a) CF4 and CF7 b) CF5 and CF8 c) CF6.
- Fig. 5.  $\delta^{13}\text{C}_{\text{arag}}$  value variation over the length of the cuttlebone. a) CF4 and CF7 b) CF5 and CF8 c) CF6.
- Fig. 6. Cross plot of  $\delta^{13}\text{C}_{\text{arag}}$  and  $\delta^{18}\text{O}_{\text{arag}}$  values exhibiting no statistically significant linear trend.
- Fig. 7. Correlated temperatures calculated from  $\delta^{18}\text{O}_{\text{arag}}$  values of CF4, CF5, CF6, CF7 and CF8 superimposed on NOMAD SST data for between September 2003 and July 2005. The close match of the three records to the nomad dataset allowed the dating of the cuttlebones.
- Fig. 8.  $\delta^{13}\text{C}_{\text{arag}}$  values for CF4 and CF5 correlated using the dates established for the  $\delta^{18}\text{O}_{\text{arag}}$  value record. Note convergence between specimens in winter, and the drop in  $\delta^{13}\text{C}_{\text{arag}}$  near death. The convergence is the result of movement to common waters during winter.
- Table 1. Complete dataset for CF4, CF5, CF6, CF7 and CF8
- Table 2. Growth rates calculated from oxygen isotopes.

Findlay, Gröcke, Knyf  
Figure 1

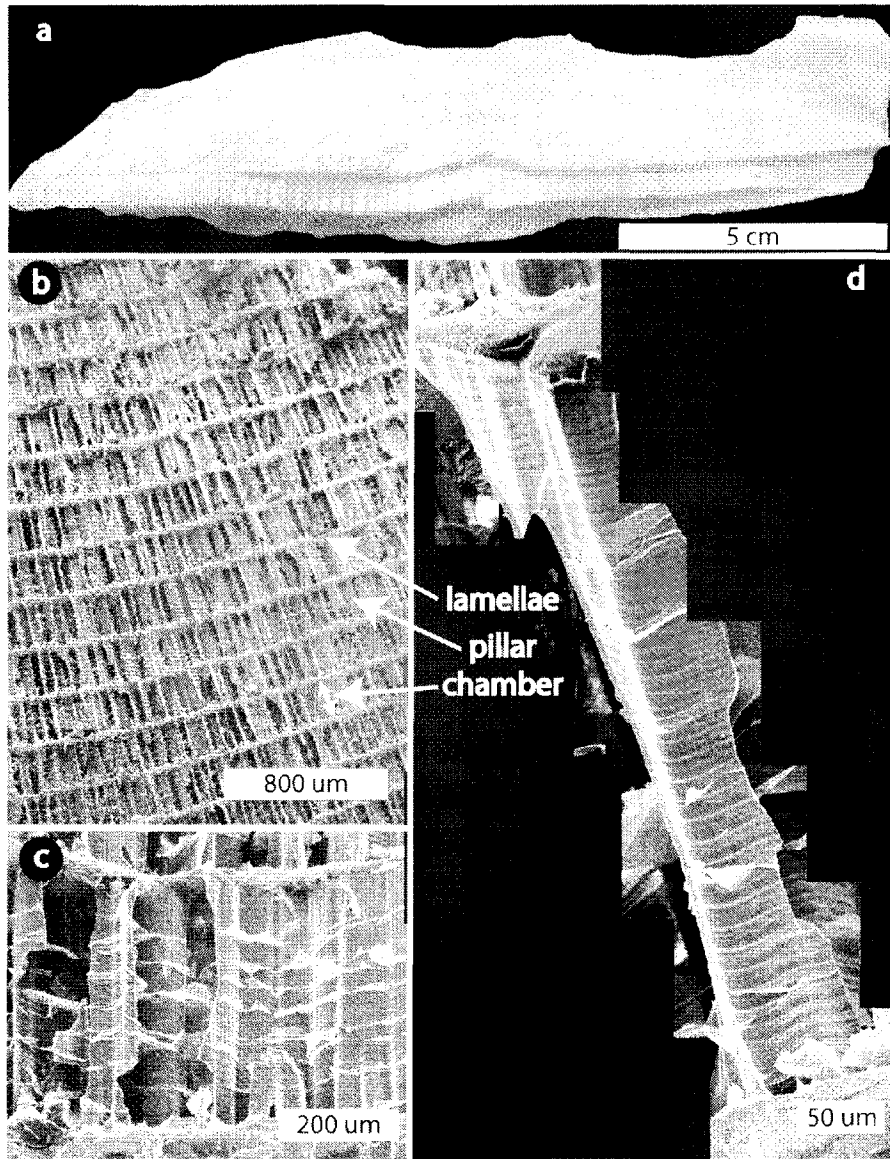


Fig. 1. Morphology of a modern cuttlebone. a) Sectioned cuttlebone showing the removal of lamella for stable isotope analysis. b) SEM micrograph showing the lamellae and pillar couplets. c) Close-up of two lamellae and the dividing pillars, supporting a single chamber. d) Close-up of a single pillar, showing fine laminations.

Findlay, Gröcke, Knyf  
Figure 2

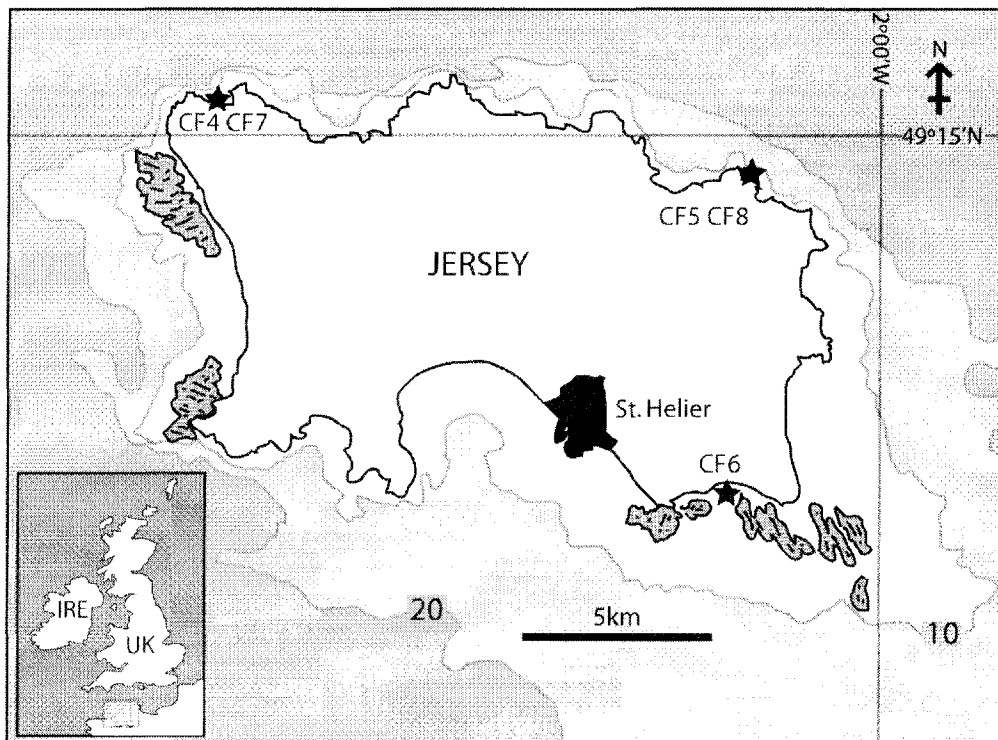


Fig. 2. Map of Jersey, U.K. showing collection sites of the cuttlebones. Bathymetry is presented in meters.

Findlay, Gröcke, Knyf  
Figure 3

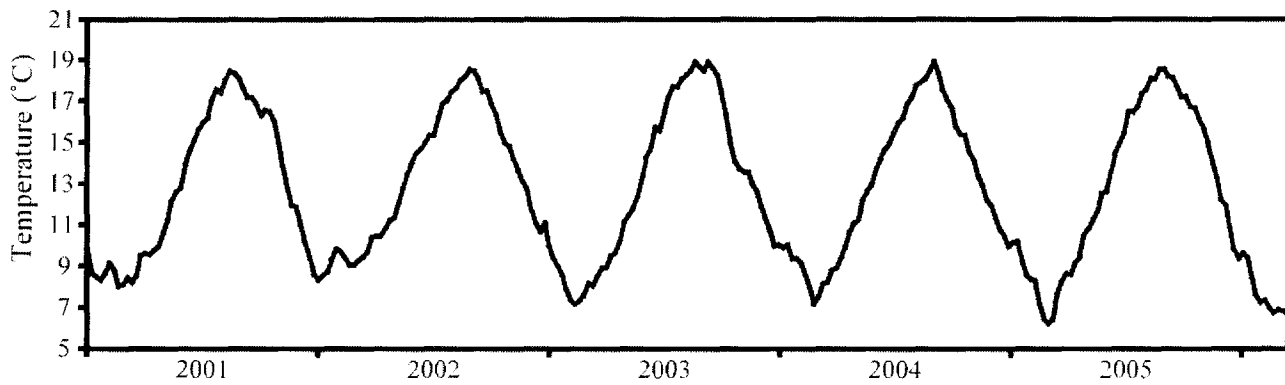


Fig. 3. NOMAD satellite sea surface temperature (SST) variation for the Jersey area between 2001 and 2006. Note the unique shape of the curve as well as the values between late 2003 and late 2005 (highlighted).

Findlay, Gröcke, Knyf  
Figure 4

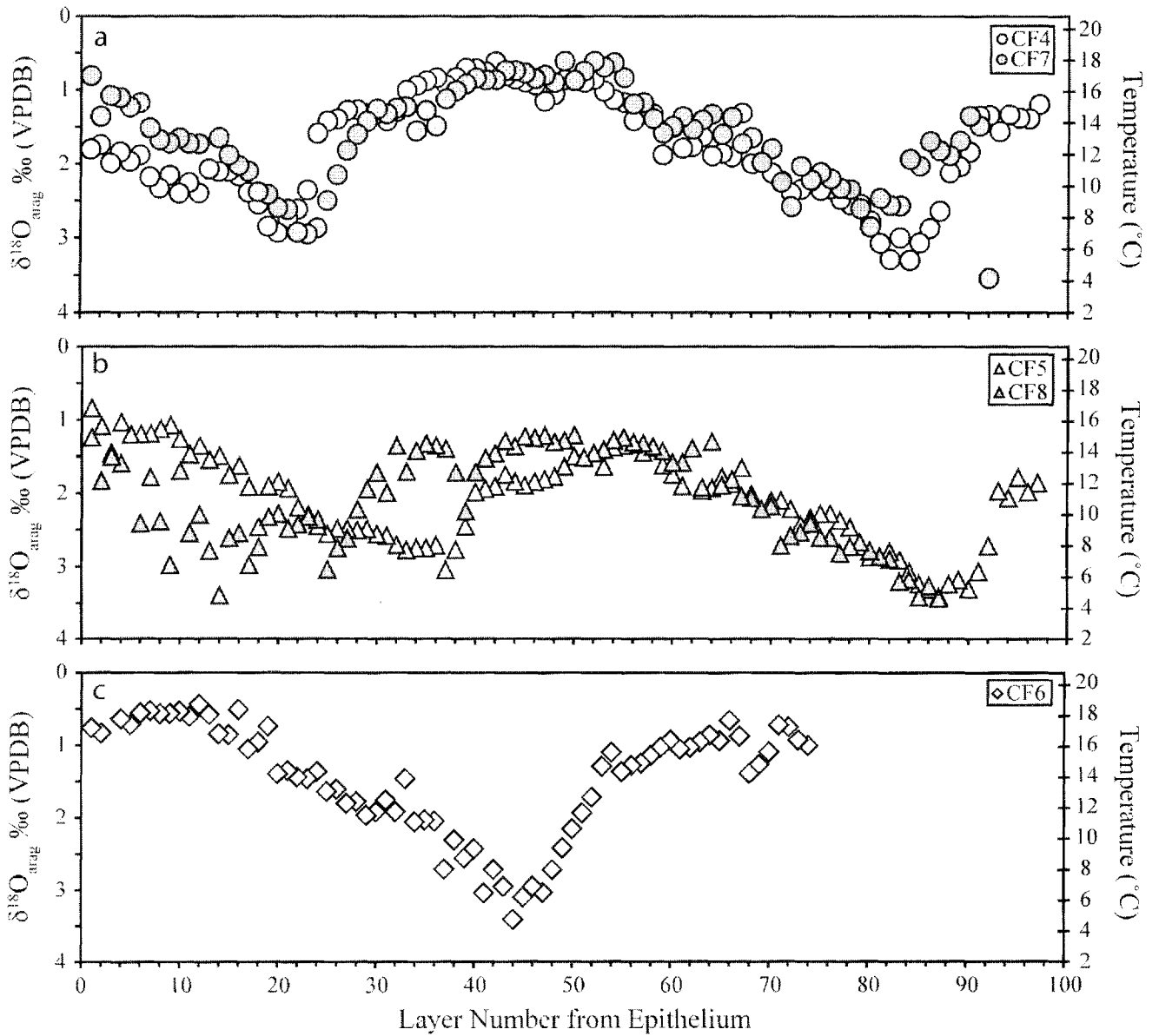


Fig. 4.  $\delta^{18}\text{O}_{\text{arag}}$  value variation over the length of the cuttlebone. Temperatures calculated using the equation of Goodwin et al. (2003). a) CF4 and CF7 b) CF5 and CF8 c) CF6.

Findlay, Grocke, Knyf  
Figure 5

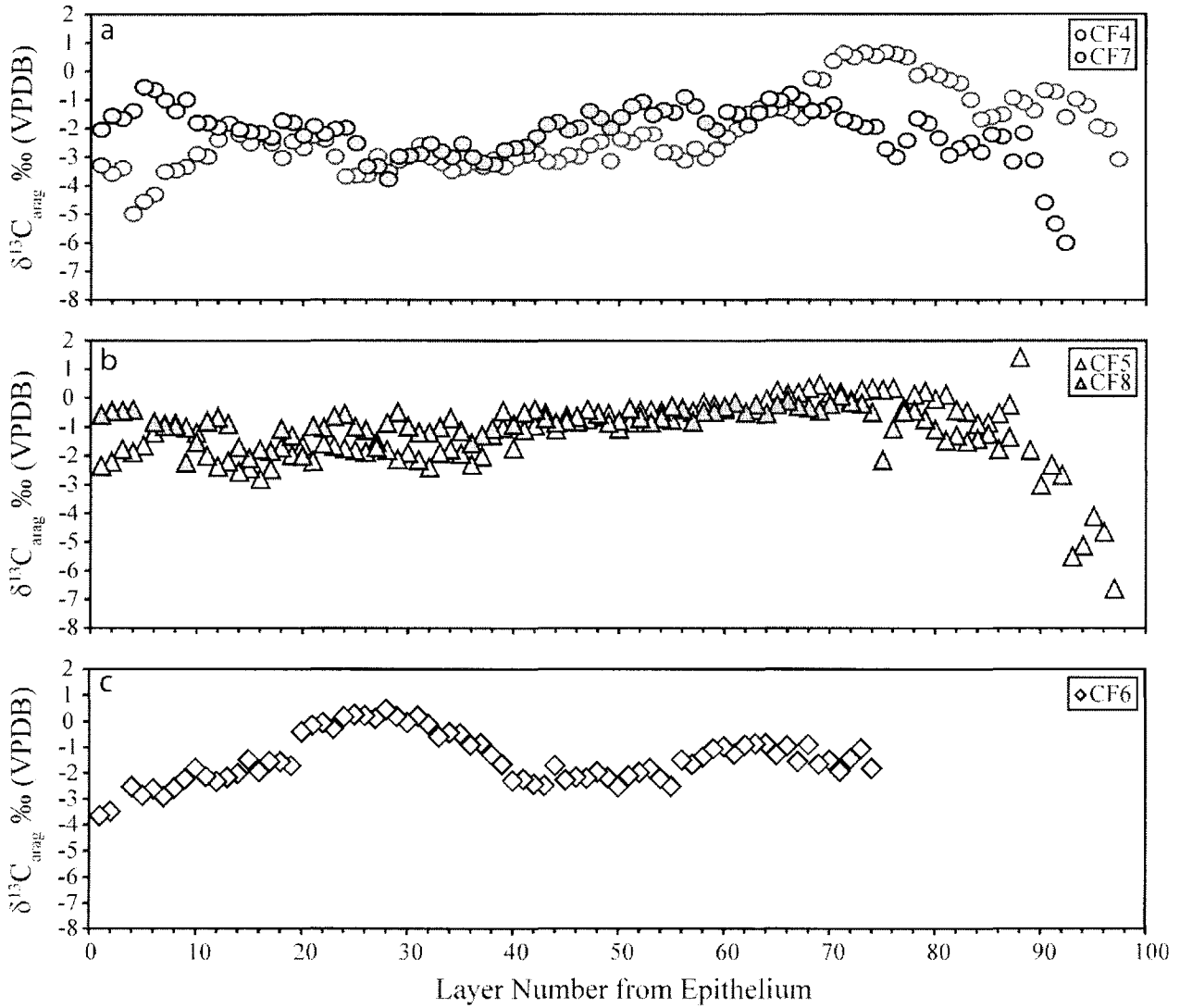


Fig. 5.  $\delta^{13}\text{C}_{\text{arag}}$  value variation over the length of the cuttlebone. a) CF4 and CF7 b) CF5 and CF8 c) CF6.

Findlay, Gröcke, Knyf  
Figure 6

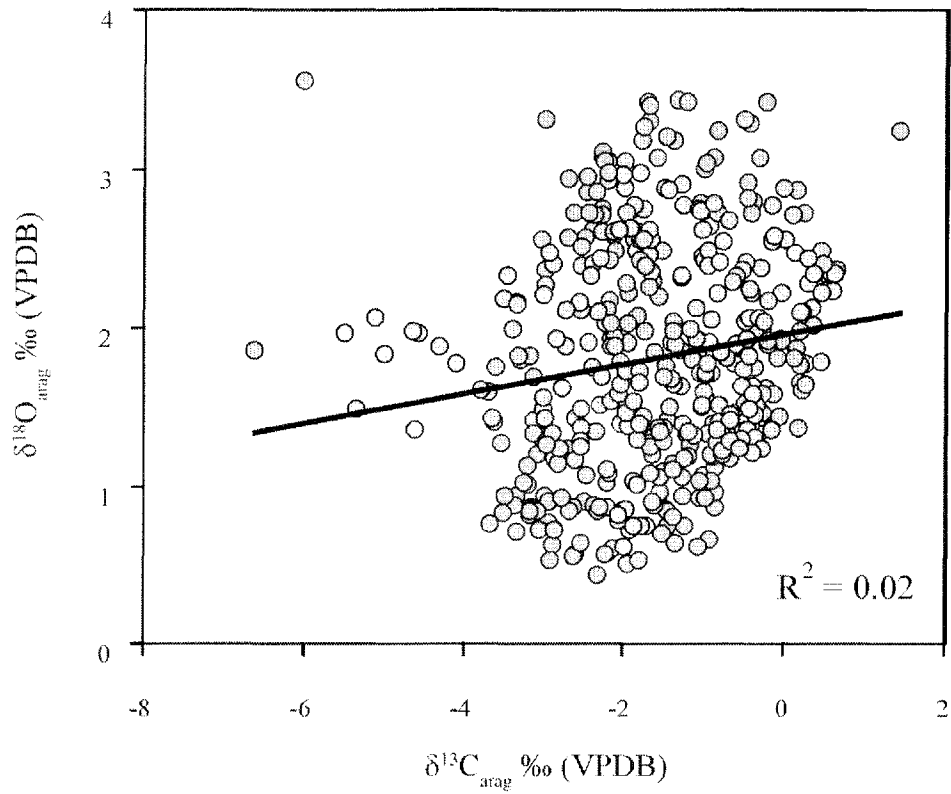


Fig. 6. Cross plot of  $\delta^{13}\text{C}_{\text{arag}}$  and  $\delta^{18}\text{O}_{\text{arag}}$  values exhibiting no statistically significant linear trend.

Findlay, Gröcke, Knyf  
Figure 7

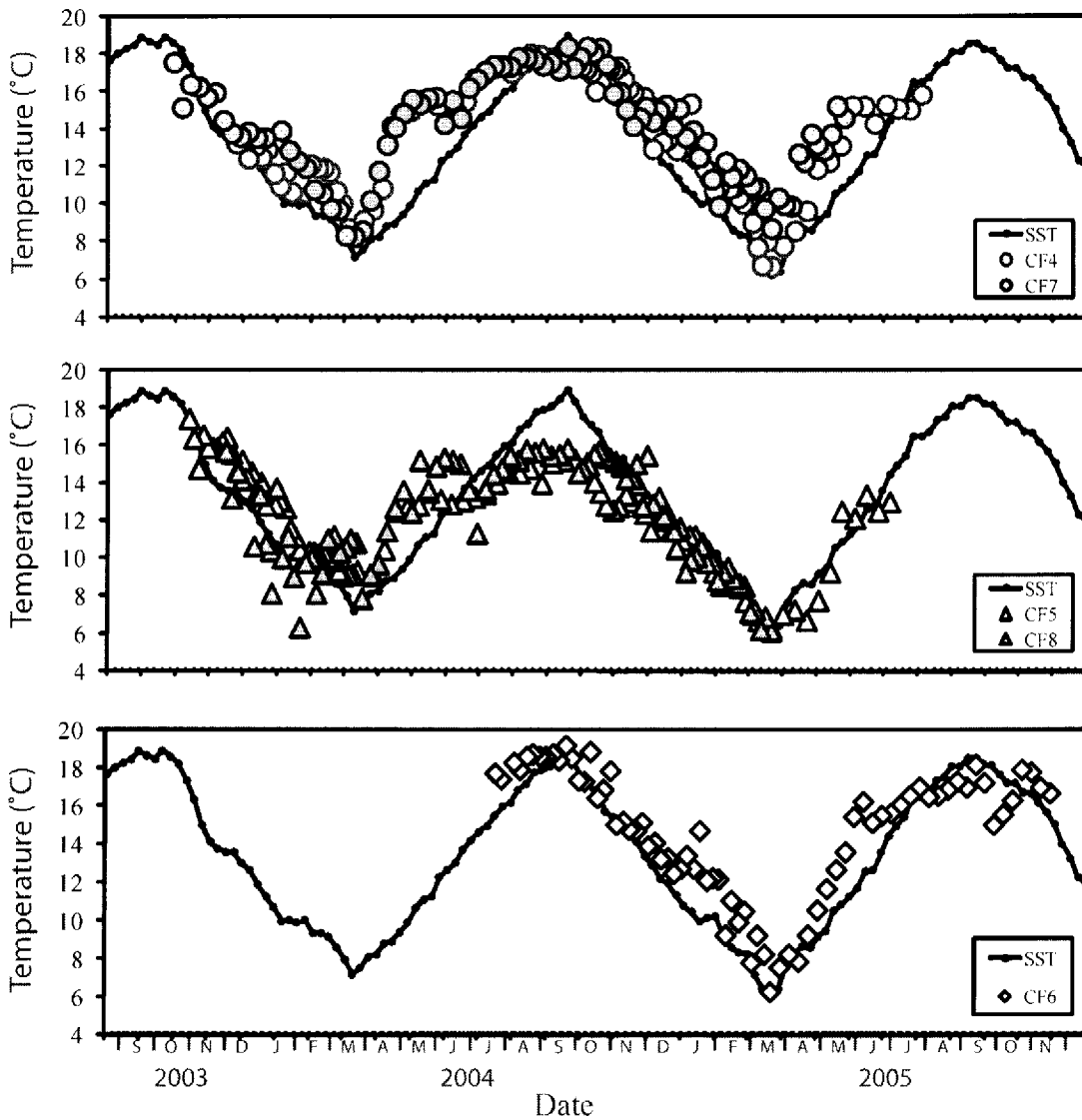


Fig. 7. Correlated temperatures calculated from  $\delta^{18}\text{O}_{\text{arag}}$  values of CF4, CF5, CF6, CF7 and CF8 superimposed on NOMAD SST data for between September 2003 and July 2005. The close match of the three records to the nomad dataset allowed the dating of the cuttlebones.

Findlay, Gröcke, Knyf  
Figure 8

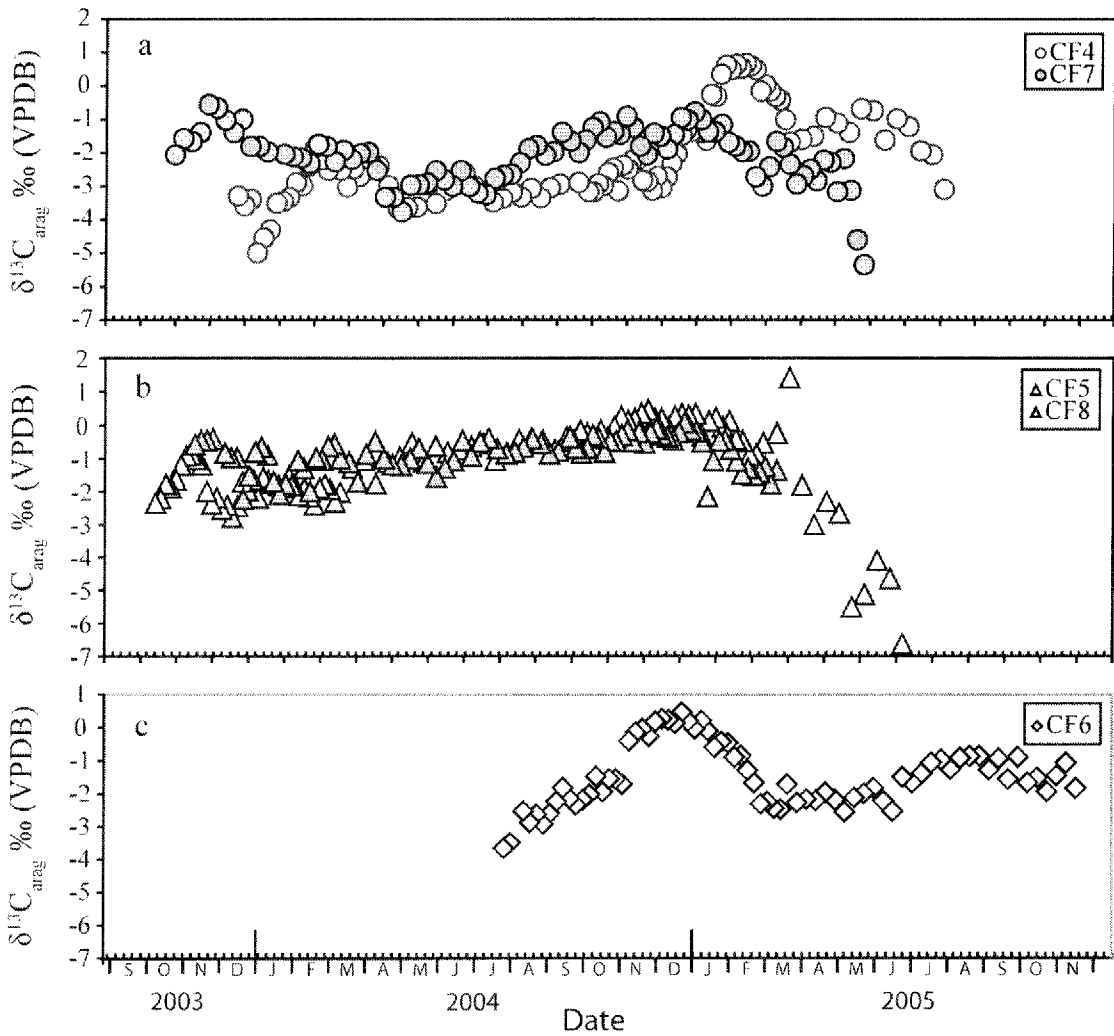


Fig. 8.  $\delta^{13}\text{C}_{\text{arag}}$  values for CF4 and CF5 correlated using the dates established for the  $\delta^{18}\text{O}_{\text{arag}}$  value record. Note convergence between specimens in winter, and the drop in  $\delta^{13}\text{C}_{\text{arag}}$  near death. The convergence is the result of movement to common waters during winter.

**Table 1**

CF4					CF5					CF6				
Sample	Layer	$\delta^{13}\text{C}$	$\delta^{18}\text{O}$	Temp ( $^{\circ}\text{C}$ )	Sample	Layer	$\delta^{13}\text{C}$	$\delta^{18}\text{O}$	Temp ( $^{\circ}\text{C}$ )	Sample	Layer	$\delta^{13}\text{C}$	$\delta^{18}\text{O}$	Temp ( $^{\circ}\text{C}$ )
cf4-1	97	-3.1	1.2	15.8	cf5-1	97	-6.6	1.9	13.0	cf6-1	79	-1.8	1.0	16.7
cf4-2	96	-2.0	1.4	15.0	cf5-2	96	-4.6	2.0	12.4	cf6-2	78	-1.0	0.9	17.0
cf4-3	95	-1.9	1.4	15.1	cf5-3	95	-4.1	1.8	13.3	cf6-3	77	-1.4	0.7	17.8
cf4-4	94	-1.2	1.3	15.3	cf5-4	94	-5.1	2.1	12.1	cf6-4	76	-1.9	0.7	17.9
cf4-5	93	-1.0	1.6	14.3	cf5-5	93	-5.5	2.0	12.5	cf6-5	75	-1.5	1.1	16.3
cf4-6	92	-1.6	1.3	15.2	cf5-6	92	-2.6	2.7	9.2	cf6-6	74	-1.6	1.3	15.5
cf4-7	91	-0.7	1.4	15.2	cf5-7	91	-2.3	3.1	7.7	cf6-7	73	-0.9	1.4	15.0
cf4-8	90	-0.7	1.8	13.1	cf5-8	90	-3.0	3.3	6.7	cf6-8	72	-1.5	0.9	17.2
cf4-9	89	-1.4	2.0	12.2	cf5-9	89	-1.8	3.2	7.2	cf6-10	71	-0.9	0.7	18.2
cf4-10	88	-1.1	2.1	11.8	cf5-10	88	1.4	3.2	7.0	cf6-11	70	-1.3	0.9	17.0
cf4-11	87	-0.9	2.6	9.6	cf5-11	87	-0.2	3.4	6.2	cf6-12	69	-0.8	0.9	17.3
cf4-12	86	-1.5	2.9	8.6	cf5-12	86	-0.5	3.3	6.7	cf6-13	68	-0.9	1.0	16.9
cf4-13	85	-1.6	3.1	7.7	cf5-13	85	-0.8	3.2	7.0	cf6-14	67	-0.9	1.0	16.6
cf4-14	84	-1.7	3.3	6.7	cf5-14	84	-0.9	3.1	7.7	cf6-15	65	-1.2	1.1	16.5
cf4-15	83	-1.0	3.0	8.0	cf5-15	83	-0.5	2.9	8.4	cf6-16	64	-1.0	0.9	17.0
cf4-16	82	-0.4	3.3	6.8	cf5-16	82	-0.4	2.8	8.9	cf6-17	63	-1.0	1.0	16.5
cf4-17	81	-0.3	3.1	7.7	cf5-17	81	0.1	2.9	8.6	cf6-18	62	-1.4	1.1	16.1
cf4-18	80	-0.1	2.8	9.0	cf5-18	80	0.0	2.9	8.6	cf6-19	61	-1.7	1.2	15.6
cf4-19	79	0.0	2.5	10.0	cf5-19	79	0.2	2.7	9.2	cf6-20	60	-1.5	1.3	15.5
cf4-20	78	-0.2	2.6	10.0	cf5-20	78	0.1	2.5	10.3	cf6-21	59	-2.5	1.4	15.1
cf4-21	77	0.5	2.5	10.3	cf5-21	77	-0.3	2.4	10.8	cf6-22	58	-2.2	1.1	16.3
cf4-22	76	0.6	2.3	10.9	cf5-22	76	0.4	2.3	11.1	cf6-23	57	-1.8	1.3	15.4
cf4-23	75	0.7	2.4	10.8	cf5-23	75	0.3	2.3	11.1	cf6-24	56	-2.0	1.7	13.6
cf4-24	74	0.5	2.2	11.4	cf5-24	74	0.4	2.3	10.9	cf6-25	54	-2.1	1.9	12.6
cf4-25	73	0.6	2.3	10.9	cf5-25	73	0.3	2.4	10.5	cf6-26	53	-2.5	2.2	11.7
cf4-26	72	0.5	2.4	10.7	cf5-26	72	0.0	2.2	11.4	cf6-27	52	-2.2	2.4	10.5
cf4-27	71	0.6	2.2	11.4	cf5-27	71	0.2	2.1	11.9	cf6-28	51	-2.0	2.7	9.2
cf4-28	70	0.3	2.1	11.8	cf5-28	70	0.2	2.1	11.9	cf6-29	50	-2.2	3.0	7.8
cf4-29	69	-0.3	2.0	12.5	cf5-29	69	0.5	2.2	11.4	cf6-30	49	-2.2	3.0	8.2
cf4-30	68	-0.3	2.0	12.4	cf5-30	68	0.4	2.0	12.3	cf6-31	48	-2.3	3.1	7.6
cf4-31	67	-1.6	1.3	15.3	cf5-31	67	0.2	1.7	13.9	cf6-32	47	-1.7	3.4	6.2
cf4-32	66	-1.4	1.9	12.8	cf5-32	66	0.2	1.9	12.9	cf6-33	45	-2.5	2.9	8.2
cf4-33	65	-1.3	1.9	13.0	cf5-33	65	0.3	1.8	13.3	cf6-34	44	-2.4	2.7	9.2
cf4-34	64	-1.3	1.9	12.8	cf5-34	64	0.0	1.9	12.7	cf6-35	43	-2.2	3.0	7.8
cf4-35	63	-1.3	1.6	14.0	cf5-35	63	-0.4	2.0	12.5	cf6-36	42	-2.3	2.4	10.5
cf4-36	62	-1.5	1.8	13.4	cf5-37	62	-0.1	1.9	12.8	cf6-37	41	-1.7	2.6	9.9
cf4-37	61	-2.0	1.8	13.3	cf5-38	61	-0.3	1.7	13.5	cf6-38	39	-1.3	2.3	11.0
cf4-38	60	-2.3	1.5	14.5	cf5-39	60	-0.2	1.6	14.0	cf6-39	38	-0.8	2.7	9.3
cf4-39	59	-2.7	1.9	12.9	cf5-40	59	-0.1	1.4	15.1	cf6-41	37	-0.9	2.1	12.1
cf4-40	58	-3.0	1.3	15.3	cf5-41	58	-0.4	1.4	14.8	cf6-42	36	-0.5	2.0	12.2
cf4-41	57	-2.7	1.2	15.7	cf5-42	57	-0.3	1.3	15.3	cf6-43	35	-0.4	2.1	12.1

**Table 1**

CF4					CF5					CF6				
Sample	Layer	$\delta^{13}\text{C}$	$\delta^{18}\text{O}$	Temp ( $^{\circ}\text{C}$ )	Sample	Layer	$\delta^{13}\text{C}$	$\delta^{18}\text{O}$	Temp ( $^{\circ}\text{C}$ )	Sample	Layer	$\delta^{13}\text{C}$	$\delta^{18}\text{O}$	Temp ( $^{\circ}\text{C}$ )
cf4-42	56	-3.1	1.4	14.9	cf5-43	56	-0.7	1.3	15.2	cf6-44	34	-0.6	1.5	14.7
cf4-43	55	-2.9	1.2	16.0	cf5-44	55	-0.4	1.4	15.1	cf6-45	33	-0.1	1.9	12.7
cf4-44	54	-2.8	1.1	16.1	cf5-45	54	-0.4	1.6	14.0	cf6-47	32	0.2	1.8	13.4
cf4-45	53	-2.2	1.0	16.6	cf5-46	53	-0.4	1.4	14.8	cf6-48	31	0.0	1.9	12.7
cf4-46	52	-2.2	0.9	17.3	cf5-47	52	-0.8	1.5	14.5	cf6-49	30	0.2	2.0	12.5
cf4-47	51	-2.5	0.9	17.1	cf5-48	51	-1.0	1.5	14.6	cf6-50	29	0.5	1.8	13.3
cf4-48	50	-2.4	0.9	17.2	cf5-49	50	-0.5	1.6	14.0	cf6-51	28	0.1	1.8	13.2
cf4-49	49	-3.1	0.9	17.3	cf5-50	49	-0.6	1.8	13.4	cf6-52	27	0.2	1.6	14.1
cf4-50	48	-2.4	1.1	16.4	cf5-51	48	-0.7	1.8	13.2	cf6-53	26	0.3	1.6	13.9
cf4-51	47	-2.6	1.2	16.0	cf5-52	47	-0.8	1.8	13.0	cf6-54	25	0.2	1.4	15.1
cf4-52	46	-3.0	0.9	17.0	cf5-53	46	-0.6	1.9	12.8	cf6-56	24	-0.3	1.5	14.7
cf4-53	45	-2.9	0.9	17.1	cf5-54	45	-1.1	1.8	13.1	cf6-57	23	0.0	1.4	14.8
cf4-54	44	-3.2	0.9	17.3	cf5-55	44	-0.5	1.7	13.5	cf6-58	22	-0.1	1.3	15.2
cf4-55	43	-3.2	0.8	17.5	cf5-56	43	-0.9	1.9	12.8	cf6-59	21	-0.4	1.4	15.0
cf4-57	42	-2.9	0.6	18.3	cf5-57	42	-1.1	1.9	12.6	cf6-60	20	-1.7	0.7	17.8
cf4-56	41	-2.9	0.8	17.7	cf5-58	41	-1.7	2.0	12.4	cf6-61	19	-1.5	1.0	16.9
cf4-58	40	-3.0	0.7	17.9	cf5-59	40	-1.0	2.4	10.4	cf6-62	18	-1.5	1.1	16.4
cf4-59	39	-3.3	0.7	18.0	cf5-60	39	-1.2	2.8	9.0	cf6-63	17	-1.9	0.5	18.8
cf4-60	38	-3.1	0.8	17.4	cf5-61	38	-2.0	3.0	7.8	cf6-64	16	-1.5	0.9	17.3
cf4-61	37	-3.3	0.9	17.0	cf5-62	37	-2.3	2.7	9.3	cf6-65	15	-2.0	0.8	17.4
cf4-62	36	-3.2	0.8	17.4	cf5-63	35	-1.9	2.7	9.1	cf6-67	14	-2.2	0.6	18.5
cf4-63	35	-3.4	0.9	17.2	cf5-64	34	-1.8	2.7	9.1	cf6-68	13	-2.3	0.4	19.1
cf4-64	34	-3.5	0.9	17.0	cf5-65	33	-1.9	2.8	9.0	cf6-69	12	-2.1	0.6	18.4
cf4-65	33	-3.2	1.0	16.7	cf5-66	32	-2.4	2.7	9.3	cf6-70	11	-1.8	0.5	18.7
cf4-66	32	-3.0	1.3	15.4	cf5-67	31	-2.1	2.6	9.9	cf6-71	10	-2.2	0.6	18.6
cf4-67	31	-2.6	1.4	14.9	cf5-68	30	-1.9	2.6	10.0	cf6-72	8	-2.6	0.6	18.6
cf4-68	30	-3.0	1.3	15.3	cf5-69	29	-2.1	2.5	10.3	cf6-73	7	-2.9	0.5	18.8
cf4-69	29	-3.1	1.3	15.3	cf5-70	28	-1.8	2.5	10.2	cf6-74	6	-2.6	0.6	18.6
cf4-70	28	-3.5	1.3	15.5	cf5-71	27	-1.5	2.5	10.3	cf6-75	5	-2.9	0.7	17.9
cf4-71	27	-3.0	1.3	15.5	cf5-72	26	-1.8	2.5	10.3	cf6-76	4	-2.5	0.6	18.3
cf4-72	26	-3.6	1.4	15.0	cf5-73	25	-1.8	2.6	10.0	cf6-77	3			
cf4-73	25	-3.6	1.4	14.8	cf5-74	24	-1.7	2.4	10.4	cf6-78	2	-3.5	0.8	17.4
cf4-74	24	-3.7	1.6	14.1	cf5-75	23	-1.6	2.3	11.1	cf6-79	1	-3.7	0.8	17.7
cf4-75	23	-3.0	2.4	10.8	cf5-76	22	-1.6	2.2	11.5					
cf4-76	22	-2.4	2.6	9.7	cf5-77	21	-2.2	1.9	12.7					
cf4-77	21	-2.3	2.7	9.1	cf5-78	20	-1.6	1.8	13.0					
cf4-78	20	-2.7	2.9	8.3	cf5-79	19	-1.9	1.9	12.8					
cf4-79	19	-2.5	2.8	8.7	cf5-80	18	-1.7	2.5	10.4					
cf4-80	18	-3.0	2.5	10.0	cf5-81	17	-2.4	1.9	12.8					
cf4-81	17	-2.5	2.4	10.7	cf5-82	16	-2.8	1.6	14.0					
cf4-82	16	-2.2	2.2	11.6	cf5-83	15	-2.4	1.7	13.5					

**Table 1**

CF4					CF5					CF6				
Sample	Layer	$\delta^{13}\text{C}$	$\delta^{18}\text{O}$	Temp (°C)	Sample	Layer	$\delta^{13}\text{C}$	$\delta^{18}\text{O}$	Temp (°C)	Sample	Layer	$\delta^{13}\text{C}$	$\delta^{18}\text{O}$	Temp (°C)
cf4-83	15	-2.5	2.1	11.9	cf5-84	14	-2.5	1.5	14.6					
cf4-84	14	-2.2	2.1	11.9	cf5-85	13	-2.2	1.5	14.4					
cf4-85	13	-1.8	2.1	12.1	cf5-86	12	-2.3	1.3	15.2					
cf4-86	12	-2.4	2.4	10.6	cf5-87	11	-2.0	1.5	14.7					
cf4-87	11	-3.0	2.3	11.2	cf5-88	10	-1.2	1.3	15.6					
cf4-88	10	-2.9	2.4	10.6	cf5-89	9	-1.0	1.1	16.4					
cf4-89	9	-3.3	2.2	11.7	cf5-90	8	-0.9	1.1	16.2					
cf4-90	8	-3.5	2.3	10.9	cf5-91	7	-0.9	1.2	15.9					
cf4-91	7	-3.5	2.2	11.6	cf5-92	6	-1.2	1.2	15.9					
cf4-92	6	-4.3	1.9	12.9	cf5-93	5	-1.6	1.2	15.9					
cf4-93	5	-4.6	2.0	12.5	cf5-94	4	-1.9	1.0	16.6					
cf4-94	4	-5.0	1.8	13.1	cf5-95	3	-1.8	1.4	14.8					
cf4-95	3	-3.4	2.0	12.4	cf5-96	2	-2.2	1.1	16.4					
cf4-96	2	-3.6	1.7	13.5	cf5-97	1	-2.3	0.8	17.4					
cf4-97	1	-3.3	1.8	13.2										
<b>Max</b>		0.7	3.3	18.3	<b>Max</b>		1.4	3.4	17.4	<b>Max</b>		0.5	3.4	19.1
<b>Min</b>		-5.0	0.6	6.7	<b>Min</b>		-6.6	0.8	6.2	<b>Min</b>		-3.7	0.4	6.2
<b>Ave</b>		-2.2	1.8	13.4	<b>Ave</b>		-1.2	2.1	12.0	<b>Ave</b>		-1.5	1.5	14.7
<b>Std Dev</b>		1.3	0.7	3.0	<b>Std Dev</b>		1.3	0.6	2.7	<b>Std Dev</b>		1.0	0.8	3.4

**Table 1**

CF7				CF8					
Sample	Layer	$\delta^{13}\text{C}$	$\delta^{18}\text{O}$	Temp (°C)	Sample	Layer	$\delta^{13}\text{C}$	$\delta^{18}\text{O}$	Temp (°C)
cf7-1	94				cf8-1	87	-1.3	3.4	6.1
cf7-2	93				cf8-2	86	-1.7	3.3	6.9
cf7-3	92	-6.0	3.5	5.7	cf8-3	85	-1.2	3.4	6.2
cf7-4	91	-5.3	1.5	14.6	cf8-4	84	-1.4	3.2	7.2
cf7-5	90	-4.6	1.4	15.2	cf8-5	83	-1.5	3.2	7.1
cf7-6	89	-3.1	1.7	13.7	cf8-6	82	-1.3	2.9	8.5
cf7-7	88	-2.2	1.9	12.9	cf8-7	81	-1.4	2.9	8.6
cf7-8	87	-3.2	1.8	13.1	cf8-8	80	-1.1	2.8	9.0
cf7-9	86	-2.3	1.7	13.7	cf8-9	79	-0.7	2.7	9.5
cf7-10	85	-2.2	2.0	12.2	cf8-10	78	-0.4	2.7	9.2
cf7-11	84	-2.8	1.9	12.6	cf8-11	77	-0.4	2.8	8.8
cf7-12	83	-2.5	2.6	9.9	cf8-12	76	-1.0	2.6	9.7
cf7-13	82	-2.7	2.6	9.9	cf8-13	75	-2.1	2.6	9.7
cf7-14	81	-2.9	2.5	10.3	cf8-14	74	-0.5	2.4	10.6
cf7-15	80	-2.3	2.9	8.7	cf8-15	73	-0.2	2.5	10.0
cf7-16	79	-1.8	2.6	9.7	cf8-16	72	-0.1	2.6	9.8
cf7-17	78	-1.6	2.3	10.8	cf8-17	71	0.1	2.7	9.3
cf7-18	77	-2.4	2.3	10.9	cf8-18	70	-0.2	2.2	11.6
cf7-20	76	-3.0	2.2	11.5	cf8-19	69	-0.4	2.2	11.4
cf7-21	75	-2.7	2.1	11.9	cf8-20	68	-0.3	2.1	12.1
cf7-22	74	-1.9	2.2	11.4	cf8-21	67	-0.3	2.0	12.2
cf7-23	73	-2.0	2.0	12.2	cf8-22	66	-0.1	1.8	13.2
cf7-24	72	-1.8	2.6	9.8	cf8-23	65	-0.2	1.9	12.8
cf7-25	71	-1.7	2.2	11.3	cf8-24	64	-0.5	1.3	15.4
cf7-26	70	-1.1	1.8	13.3	cf8-25	63	-0.2	1.9	12.7
cf7-27	69	-1.4	2.0	12.4	cf8-26	62	-0.5	1.4	15.0
cf7-28	68	-1.4	1.6	13.9	cf8-27	61	-0.1	1.6	14.2
cf7-29	67	-1.0	1.7	13.5	cf8-28	60	-0.3	1.6	14.2
cf7-30	66	-0.8	1.4	15.1	cf8-29	59	-0.4	1.4	14.9
cf7-31	65	-1.0	1.6	14.1	cf8-30	58	-0.4	1.4	15.1
cf7-32	64	-0.9	1.3	15.3	cf8-31	57	-0.8	1.3	15.3
cf7-33	63	-1.4	1.4	14.9	cf8-32	56	-0.4	1.3	15.4
cf7-34	62	-1.9	1.5	14.4	cf8-33	55	-0.3	1.2	15.7
cf7-35	61	-1.5	1.4	15.1	cf8-34	54	-0.7	1.3	15.5
cf7-36	60	-1.4	1.5	14.5	cf8-35	53	-0.8	1.4	15.0
cf7-37	59	-2.1	1.6	14.2	cf8-36	52	-0.7	1.4	14.7
cf7-38	58	-1.8	1.4	15.0	cf8-37	51	-0.3	1.5	14.5
cf7-39	57	-1.2	1.2	15.9	cf8-38	50	-0.8	1.2	15.8
cf7-49	56	-0.9	1.2	15.9	cf8-39	49	-0.8	1.3	15.5
cf7-50	55	-1.4	0.8	17.4	cf8-40	48	-0.5	1.3	15.4
cf7-51	54	-1.4	0.6	18.3	cf8-41	47	-0.4	1.2	15.8

**Table 1**

CF7					CF8				
Sample	Layer	$\delta^{13}\text{C}$	$\delta^{18}\text{O}$	Temp (°C)	Sample	Layer	$\delta^{13}\text{C}$	$\delta^{18}\text{O}$	Temp (°C)
cf7-52	53	-1.5	0.7	18.0	cf8-42	46	-0.6	1.2	15.6
cf7-53	52	-1.1	0.6	18.4	cf8-43	45	-0.8	1.2	15.7
cf7-54	51	-1.2	0.7	17.8	cf8-44	44	-0.8	1.4	15.2
cf7-55	50	-1.6	0.9	17.2	cf8-45	43	-0.7	1.3	15.5
cf7-56	49	-2.0	0.6	18.4	cf8-46	42	-0.4	1.4	14.7
cf7-57	48	-1.6	0.9	17.1	cf8-47	41	-0.5	1.5	14.4
cf7-58	47	-1.4	0.8	17.5	cf8-48	40	-0.9	1.7	13.6
cf7-59	46	-2.0	0.9	17.3	cf8-49	39	-0.4	2.2	11.3
cf7-60	45	-2.1	0.8	17.7	cf8-50	38	-1.0	1.7	13.6
cf7-61	44	-1.8	0.7	17.8	cf8-51	37	-1.3	1.4	15.0
cf7-62	43	-1.9	0.7	17.8	cf8-52	36	-1.5	1.3	15.2
cf7-63	42	-2.3	0.9	17.3	cf8-53	35	-1.1	1.3	15.3
cf7-64	41	-2.6	0.9	17.3	cf8-54	34	-0.7	1.4	14.9
cf7-65	40	-2.7	0.8	17.4	cf8-55	33	-1.0	1.7	13.7
cf7-66	39	-2.8	0.9	17.0	cf8-56	32	-1.2	1.3	15.2
cf7-67	38	-3.2	1.0	16.6	cf8-57	31	-1.2	2.0	12.4
cf7-68	37	-3.2	1.1	16.2	cf8-58	30	-1.0	1.7	13.6
cf7-69	36	-3.0	1.5	14.6	cf8-59	29	-0.5	1.9	12.6
cf7-70	35	-2.5	1.3	15.5	cf8-60	28	-0.8	2.2	11.4
cf7-71	34	-3.0	1.6	14.3	cf8-61	27	-1.7	2.6	9.7
cf7-72	33	-2.8	1.2	15.7	cf8-62	26	-1.1	2.7	9.1
cf7-73	32	-2.5	1.2	15.6	cf8-63	25	-1.0	3.0	7.9
cf7-74	31	-2.9	1.3	15.3	cf8-64	24	-0.5	2.4	10.8
cf7-75	30	-2.9	1.3	15.6	cf8-65	23	-0.6	2.3	11.0
cf7-76	29	-3.0	1.4	14.8	cf8-66	22	-1.0	2.4	10.5
cf7-77	28	-3.8	1.6	14.1	cf8-67	21	-0.9	2.5	10.3
cf7-78	27	-3.3	1.8	13.1	cf8-68	20	-2.0	2.3	11.2
cf7-79	26	-3.3	2.1	11.7	cf8-69	19	-1.3	2.3	11.0
cf7-80	25	-2.5	2.5	10.2	cf8-70	18	-1.0	2.7	9.2
cf7-81	24	-2.0	2.9	8.6	cf8-71	17	-1.8	3.0	8.1
cf7-82	23	-2.0	3.0	8.2	cf8-72	16	-1.7	2.5	10.0
cf7-83	22	-2.2	2.9	8.3	cf8-73	15	-2.0	2.6	9.7
cf7-84	21	-1.9	2.6	9.7	cf8-74	14	-1.7	3.4	6.3
cf7-85	20	-2.3	2.6	9.8	cf8-75	13	-0.9	2.8	9.0
cf7-86	19	-1.8	2.4	10.5	cf8-76	12	-0.6	2.3	11.1
cf7-87	18	-1.7	2.4	10.7	cf8-77	11	-0.8	2.5	10.0
cf7-88	17	-2.3	2.1	11.9	cf8-78	10	-1.5	1.7	13.7
cf7-89	16	-2.1	2.0	12.3	cf8-79	9	-2.2	3.0	8.2
cf7-90	15	-2.1	1.9	12.9	cf8-80	8	-0.9	2.4	10.7
cf7-91	14	-2.0	1.6	13.9	cf8-81	7	-0.9	1.8	13.3
cf7-92	13				cf8-82	6	-0.8	2.4	10.6

**Table 1**

CF7					CF8				
Sample	Layer	$\delta^{13}\text{C}$	$\delta^{18}\text{O}$	Temp (°C)	Sample	Layer	$\delta^{13}\text{C}$	$\delta^{18}\text{O}$	Temp (°C)
cf7-93	12	-2.0	1.7	13.5	cf8-83	5			
cf7-94	11	-1.8	1.7	13.5	cf8-84	4	-0.4	1.6	14.2
cf7-95	10	-1.8	1.7	13.9	cf8-85	3	-0.4	1.5	14.6
cf7-96	9	-1.0	1.7	13.6	cf8-86	2	-0.4	1.8	13.1
cf7-97	8	-1.4	1.7	13.8	cf8-87	1	-0.6	1.2	15.7
cf7-98	7	-1.0	1.5	14.5					
cf7-99	6	-0.7	1.2	15.9					
cf7-100	5	-0.6	1.2	15.7					
cf7-101	4	-1.4	1.1	16.2					
cf7-102	3	-1.7	1.1	16.4					
cf7-103	2	-1.6	1.4	15.1					
cf7-104	1	-2.0	0.8	17.5					
<hr/>					<hr/>				
<b>Max</b>		-0.6	3.5	18.4	<b>Max</b>		0.1	3.4	15.8
<b>Min</b>		-6.0	0.6	5.7	<b>Min</b>		-2.2	1.2	6.1
<b>Ave</b>		-2.1	1.6	13.9	<b>Ave</b>		-0.8	2.1	12.1
<b>Std Dev</b>		0.9	0.7	2.8	<b>Std Dev</b>		0.5	0.7	2.9

**Table 2****Growth Rates (days per layer)**

<b>Period</b>	<b>CF4</b>	<b>CF5</b>	<b>CF6</b>	<b>CF7</b>	<b>CF8</b>
Winter 2003/4	5.5	4.3		7.3	5.1
Spring-Summer 2004	8.2	9.9		7.3	7.3
Summer-Autumn 2004	4.2	5.6	5.7	5.9	4.8
Winter 2004/5	10.2	10.5	5.7	5.9	4.8
Spring-Summer 2005			8.3		
Summer-Autumn 2005			8.3		

**Table 2**  
**Growth Rates (days per layer)**

Period	CF4	CF5	CF6	CF7	CF8
Winter 2003/4	5.5	4.3		7.3	5.1
Spring-Summer 2004	8.2	9.9		7.3	7.3
Summer-Autumn 2004	4.2	5.6	5.7	5.9	4.8
Winter 2004/5	10.2	10.5	5.7	5.9	4.8
Spring-Summer 2005			8.3		
Summer-Autumn 2005			8.3		

## **Chapter 3**

### **Trace element chemistry of *Sepia officinalis* cuttlebones from Jersey, Channel Islands**

## **Rationale and Objectives**

In chapter 2, the stable isotope values of *Sepia* cuttlebones from the English Channel were shown to contain detailed water temperature records over the lifetime of the organism, in concert with a record of declining metabolic rates with ontogeny. In addition to this, trace element concentrations within the cuttlebone may also record environmental and/or biological information. Therefore, in this second data chapter, the concentrations of Sr, Mn, Mg and Ba were measured, and compared to their coeval stable isotope values in an effort to better understand their relationships to environmental and/or biological factors.

The concentrations of these trace elements were not proportional to any single factor. Instead, concentrations of Sr and Mn appeared to be ~25% controlled by temperature, and Mg was shown to have a small yet statistically significant correlation with carbon isotope values, suggesting some degree of metabolic control. Ba however showed no correlation with any of the other measured variables, and other than it must initially reflect the Ba concentration of water in some way, the controls on Ba incorporation in cuttlebones are not understood.

## Trace element chemistry of *Sepia officinalis* cuttlebones from Jersey, Channel Islands

Duncan J. Findlay<sup>1</sup>, Darren R. Gröcke<sup>2</sup>

1. School of Geography and Earth Sciences, McMaster University, 1280 Main Street W, Hamilton, Ontario L8S 4K1 Canada, (emails: findlad@mcmaster.ca, knyf@mcmaster.ca)

2. Department of Earth Sciences, Durham University, Science Laboratories, Durham DH1 3LE, UK (email: d.r.grocke@durham.ac.uk)

### Abstract

Concentrations of the trace elements Sr, Mn, Mg, and Ba were measured for two modern *Sepia officinalis* cuttlebones collected from the shores of Jersey, Channel Islands, and compared to their corresponding  $\delta^{18}\text{O}$  and  $\delta^{13}\text{C}$  values. The concentrations of Sr and Mn display a statistically significant inverse relationship with coeval  $\delta^{18}\text{O}$  values, suggesting some temperature dependence. However, the correlation between either element and coeval  $\delta^{18}\text{O}$  values is too low to construct a useful temperature equation. There are no statistically significant relationships between  $\delta^{18}\text{O}$  values and either Mg or Ba concentrations. However, Mg concentration exhibits a statistically significant correlation to  $\delta^{13}\text{C}$  values in CF5.  $\delta^{13}\text{C}$  values and Mg concentration exhibit increasing values between hatching and late middle age, followed by both variables exhibiting a decline in late life, suggesting an increase in metabolic rate prior to death. There is no statistically significant relationship between  $\delta^{13}\text{C}$  value and Mg or Ba concentration. Ba concentrations exhibit low background concentrations punctuated by occasional spikes in one cuttlebone, consistent with the literature for Ba concentration in other mollusc shell material.

### Introduction

The common cuttlefish (*Sepia officinalis*) is a cephalopod mollusc that lives in shallow water, exhibits high intelligence, active mobility, and can rapidly vary skin colour through manipulation of chromatophores (Boyle 1983; Hanlon and Messenger 1996; Norman and Reid 2000). The cuttlefish is also the only known extant cephalopod that secretes an internal carbonate skeleton, which is termed the cuttlebone and is composed of many aragonitic lamella separated by pillars. The cuttlebone is utilised as a support structure for gas exchange in order to regulate the buoyancy of the organism. The cuttlebone structure has been observed to mechanically fail beyond a critical hydrostatic pressure, thereby limiting the ecological range of *S. officinalis* to a depth of only a few hundred

meters (Sherrard 2000). Therefore, the trace element and stable isotope chemistry of the cuttlebone may provide valuable information regarding the shallow water environment.

The oxygen isotope ratios in modern biogenic and inorganically precipitated carbonate are strongly correlated with ambient water temperature. This permits the calculation of water temperature from shell carbonate oxygen isotope values, assuming knowledge of the  $\delta^{18}\text{O}$  value of the ambient water and isotopic equilibrium precipitation of the shell material (Anderson and Arthur 1983; Ditchfield 1997; Emiliani 1966; Epstein et al. 1951; Epstein et al. 1953; Grossman and Ku 1986; McArthur et al. 2007). Many modern molluscs (including *S. officinalis*) and brachiopods do secrete calcium carbonate in oxygen isotopic equilibrium with ambient water, permitting the use of their shells for temperature studies (Bettencourt and Guerra 1999; Brand et al. 2003; Carpenter and Lohmann 1995 and many others). However, the field of cuttlebone geochemistry is in its infancy, with only a handful of published studies (Bettencourt and Guerra 1999; Rexfort and Mutterlose 2006). Cuttlebone  $\delta^{18}\text{O}$  values have been demonstrated to vary inversely to water temperature, with laboratory reared specimens exhibiting  $\delta^{18}\text{O}$  values that provide an accurate record of water temperature and fluctuations due to periodic changes of water in the tank (Bettencourt and Guerra 1999; Rexfort and Mutterlose 2006). In the wild, cuttlebone  $\delta^{18}\text{O}$  values show a clear seasonal variation. Temperatures calculated from these  $\delta^{18}\text{O}$  values very closely match sea surface temperatures measured by satellite for the collection area (see Chapter 2).

The  $\delta^{13}\text{C}$  value of secreted carbonate is partially controlled by metabolic rate in many species, including *S. officinalis*; displaying low  $\delta^{13}\text{C}$  values when metabolic activity is high (see Chapter 2; Putten et al. 1999; Putten et al. 2000; Dehairs et al. 1999; Rosenberg and Hughes 1991). As there is little trophic level influence on carbon isotope values along the food chain, the baseline  $\delta^{13}\text{C}$  value for cuttlebone aragonite must be proportional to the  $\delta^{13}\text{C}$  value of the food consumed. The  $\delta^{13}\text{C}$  value of cuttlebone aragonite should therefore contain information of metabolic rate, superimposed on an environmental dissolved inorganic carbon (DIC) signal (see Chapter 2). Indeed, laboratory studies of *S. officinalis* have demonstrated that the  $\delta^{13}\text{C}$  value of cuttlebone carbonate is in disequilibrium with the  $\delta^{13}\text{C}$  value of DIC (Bettencourt and Guerra 1999), exhibiting an increasing trend with ontogeny that is generally interpreted as a decrease in metabolic rate with age (Findlay et al. previous chapter, Rexfort and Mutterlose 2006). However, the exact relationship between diet, DIC and the  $\delta^{13}\text{C}$  value of carbonate is currently undetermined for *S. officinalis*.

As stable isotope values will vary with location as a consequence of differences in the background DIC signal and ambient temperature, migration is visible in the cuttlebone stable isotope record. As illustrated in Chapter 2, comparisons of the winter portions of several cuttlebones from Jersey showed convergence on similar values for both  $\delta^{13}\text{C}$  and  $\delta^{18}\text{O}$ , suggesting that each specimen migrated to similar water conditions over this time period, which is consistent with field observations of winter migration to deep water (Boucaud-Camou and Boismery 1991).

In addition to well established stable isotope techniques, valuable environmental information may be recorded by the trace element chemistry of shell material, with many recent studies exploring the internal trace element variability of single organisms (Carpenter and Lohmann 1995; Hendry et al. 2001; Lee et al. 2004; McArthur et al. 2007; Putten et al. 2000; Sinclair et al. 1998). The crystal lattice of aragonite permits the incorporation of larger cations, such that Sr abundance is usually temperature dependant in aragonitic species, though the underlying cause of this relationship is unclear (Schrag 1999; Shen et al. 2007; Sinclair et al. 1998). In some species, the incorporation of Sr into shell material has correlated well with growth rate (Carre et al. 2006), which may explain some of the temperature dependence, as temperature is a control on growth rate in molluscs. The concentration of Sr may therefore provide an additional temperature proxy that is independent from  $\delta^{18}\text{O}$  values. In contrast to the temperature-dependence of Sr accumulation in aragonite shells, organisms that rely on low Mg calcite for shell construction, have been observed to incorporate Mg in proportion to temperature (rather than Sr). These differences in temperature-dependence of trace element accumulation result from differences in the crystal lattice structure of low Mg calcite and aragonite shells. The role of Mg in aragonitic species is less clear. Some mollusc studies indicate that the incorporation of Mg is controlled by growth rate, and should therefore be related in some way to  $\delta^{13}\text{C}$  values, which appears to be related to metabolism in cuttlefish (see chapter 2). Sr and Mg will be compared to  $\delta^{18}\text{O}$  and  $\delta^{13}\text{C}$  to assess any temperature or metabolic control on their incorporation into cuttlebone aragonite.

Mn concentration has been used as an indicator of diagenesis in fossil carbonate, as diagenetic fluids and therefore secondary carbonate are enriched in Mn relative to unaltered carbonate. It would be useful to measure the Mn concentration of modern cuttlebone aragonite to allow some assessment to the level of preservation for both ancient cuttlebones and belemnite phragmocones that may be used for palaeoenvironmental reconstruction. In addition, the level of Mn in modern carbonate has been related to metabolism and growth rate, and may

become a useful proxy for metabolic or environmental changes with further development.

Concentrations of Ba in biogenic calcite have also been investigated as an environmental proxy. As the main sources of Ba in surface waters are upwelling and continental runoff, it is possible that the quantity of Ba in biogenic carbonate may be a useful indicator of upwelling, changes in runoff, or migration between open ocean and brackish areas. (Hendry et al. 2001, Putten et al. 2000). Background cuttlebone Ba concentrations should be proportional to the Ba concentration of seawater (Gillikin et al. 2006). However, most modern molluscs display a low background Ba concentration punctuated by large peaks, which are yet to be adequately explained (Gillikin et al. 2006). As such, the utility of Ba as an environmental proxy remains an important area of research.

This study presents high resolution geochemical data (Ba, Mg, Mn and Sr concentrations) acquired from two *S. officinalis* cuttlebones collected from the shores of Jersey in the English Channel. This is the first study to explore trace element chemistry in *S. officinalis* cuttlebones, which will be compared to stable isotope values presented in Chapter 2.

## Methods

Five wild *Sepia officinalis* cuttlebones were collected from the Jersey coastline in the English Channel during autumn 2005. Cuttlebones CF5 and CF8, which were examined for trace element chemistry, were collected from Jersey's north east coast (Fig. 1), Soft tissues adhering to these cuttlebones suggest that they were fresh and thus are considered geochemically pristine.

CF5 and CF8 were split longitudinally, with successive lamella and supporting pillars sampled along the length of the cuttlebone using a scalpel. Compressed air was used to remove debris prior to collecting subsequent lamella to avoid cross contamination. Since initial analysis of a *Sepia pharaonis* cuttlebone aragonite indicated the organic matter within the sample altered the stable isotope values preserved (see Chapter 2), organic matter was removed by soaking the collected lamella in 30% peroxide for 1 hour. Samples were then rinsed 3 times with deionised water and dried overnight in a 60°C oven. The remaining powders were analysed for stable isotope values and trace element chemistry. To evaluate any isotopic fractionation introduced by this method, these processes were also applied to several NBS 19 standards. The stable isotope values of the treated standards were within analytical error of untreated standards, suggesting the process does not significantly alter the preserved carbonate stable isotope values.

For stable isotope analysis, samples of ~0.3mg were reacted with 100% phosphoric acid using a common acid bath system, with the resulting CO<sub>2</sub> analyzed in a VG Optima Isotope Ratio Mass Spectrometer. Stable-isotope ratios are expressed in per mil (‰) and are calculated according to

$$\delta = \left( \frac{R_{sample}}{R_{standard}} - 1 \right) \times 1000, \quad [3.1]$$

where R is the ratio between <sup>13</sup>C and <sup>12</sup>C for carbon and the ratio <sup>18</sup>O and <sup>16</sup>O for oxygen, relative to Vienna Pee Dee Belemnite (VPDB) standard. Reproducibility for both δ<sup>13</sup>C and the δ<sup>18</sup>O is better than ±0.1‰ on replicate analyses.

In this study, temperatures are calculated from cuttlebone oxygen isotope values using the equation of Grossman and Ku (1986) which was subsequently updated and modified by Goodwin et al. 2001, as

$$T = 20.6 - 4.34(\delta_{arag} - (\delta_w - 0.2)), \quad [3.2]$$

where T is temperature in degrees Celsius, δ<sub>arag</sub> is the δ<sup>18</sup>O value of cuttlebone aragonite, and δ<sub>w</sub> is the δ<sup>18</sup>O VSMOW of seawater. In the absence of δ<sup>18</sup>O<sub>w</sub> values for this region, δ<sup>18</sup>O value may be estimated from salinity data. Based on an average salinity of 35 psu for this area (Laane et al 1996), and the relationship between salinity and oxygen isotope value of seawater from the nearby North Sea (Harwood et al. 2008), a δ<sup>18</sup>O<sub>w</sub> of 0.3 ‰ was selected for temperature calculation.

For trace element analysis, samples of ~3mg were weighed before dissolution in 10ml of 2% trace-metal grade nitric acid. These solutions were then analysed using an ELAN 6100 quadrupole inductively coupled plasma mass spectrometer for Ba, Mg, Mn and Sr. Results are presented in parts per million (ppm). Reproducibility is better than ±15% on replicate analysis, with regression statistics calculated using Microsoft Excel 2003. Adjusted r<sup>2</sup> values are presented over r<sup>2</sup> as a large number of data points may artificially inflate the r<sup>2</sup> value. The adjusted r<sup>2</sup> value is corrected for the number of data points used in the regression analysis.

## Results

The stable isotope values of *S. officinalis* cuttlebones CF5 and CF8 were described and discussed at length in Chapter 2. In summary, δ<sup>18</sup>O values range between +1.1 and +3.4 ‰, with a mean value of +2.1 ‰ and exhibit strong seasonal cycles. Temperatures calculated from these δ<sup>18</sup>O values range between 5

and 15 °C, with a mean value of 11 °C.  $\delta^{13}\text{C}$  values range between -6.6 and +1.4‰, with a mean value of -1.0‰. These exhibit a general increase between hatching and late middle life, followed by a decrease in later life. Data presented in Table 1.

Sr values for CF8 range between 615 and 4487 ppm with a mean value of 2880 ppm (Fig. 3, Table 1). No Sr data is available for CF5 due to a machine breakdown. Mg values vary between 33 and 966ppm with a mean value of 313ppm, displaying a general increase from hatching to late middle life, followed by a decline late in life in CF5 (Fig. 2 and 3, Table 1). Mn values vary between 0 and 12ppm, with a mean value of 3ppm (Fig. 2 and 3, Table 1). Ba values range between 0 and 17ppm with a mean value of 6ppm (Fig. 2 and 3, Table 1).

## Discussion

In Chapter 2 it was shown that the temperature record preserved in the  $\delta^{18}\text{O}$  values of the cuttlebone allowed a date to be estimated for the precipitation of each lamella. Consequently, since aragonite preferentially incorporates larger cations into the crystal lattice, it was expected that the incorporation of Sr would be temperature dependant in cuttlebone aragonite, which proves to be the case according to the Sr values obtained for CF8 (Fig. 3). Although there is more variability observed in the Sr record, the general trend is similar to that observed for  $\delta^{18}\text{O}$  values (Fig. 3). A five point moving average was applied to the Sr data in order to better illustrate trends within the variability in Sr concentration with ontogeny (Fig. 3). A cross plot of the complete data set of  $\delta^{18}\text{O}$ -derived temperatures and the Sr values showed a linear correlation with an  $r^2_{\text{adj}}$  of 0.21 and p-value <0.001 for CF8 (Fig. 4), suggesting that temperature is responsible for about 21% of the variation in Sr. While the trend is statistically significant, it is not sufficiently strong to construct a robust equation predicting the temperature-dependence of Sr. Indeed, it would be premature to draw conclusions from the analysis of a single cuttlebone, and future work should involve the expansion of Sr dataset.

Mn has been used as an indicator for diagenesis in shell material preserved in the fossil record (Veizer 1983). It is useful therefore to establish the Mn concentration of modern biogenic carbonate such that it might be used to better understand relationships in the fossil record (e.g. in Belemnites, which are commonly used to reconstruct palaeoclimatic data). This is the first study to examine Mn concentration in *S. officinalis* cuttlebones. Mn concentrations are low, and vary little with ontogeny. Since Cuttlefish are the best modern analogues for belemnites and because belemnite phragmocones are also composed of

aragonite, well-preserved belemnite phragmocones might be expected to exhibit similar trends in Mn concentrations through ontogeny as those observed here. However, using the upper limit of the observed Mn values for the cuttlebones (12ppm) as an indicator of diagenesis in belemnite rostra, which are composed of low Mg calcite, is probably not appropriate, since the differences in crystal lattice structure between aragonite and low Mg calcite will result in different rates of Mn incorporation.

Mn concentrations show a statistically significant linear correlation with coeval  $\delta^{18}\text{O}$  values for CF5 ( $r^2_{\text{adj}} = 0.38$ ,  $p < 0.0001$ ) and CF8 ( $r^2_{\text{adj}} = 0.25$ ,  $p < 0.0001$ ) (Fig. 5). Since Mn concentration exhibits no correlation with  $\delta^{13}\text{C}$  value (CF5:  $r^2_{\text{adj}} = 0.001$ ,  $p = 0.33$ ; CF8:  $r^2_{\text{adj}} = 0.017$ ,  $p = 0.12$ ) these results suggest that the incorporation Mn is more likely related to temperature than metabolism as previously suggested (Putten et al. 2000). However, the correlation coefficients between Mn concentration and  $\delta^{18}\text{O}$  value or the concentration of Sr (CF8:  $r^2_{\text{adj}} = 0.04$ ,  $p = 0.03$ ) are too low for the construction of a reliable temperature equation.

Mg concentrations co varied with  $\delta^{13}\text{C}$  values for CF5 (Fig. 2), a trend which was accentuated with the use of a five point moving average on the Mg transect. Such covariance was not apparent in CF8, however, which may result in part, from the relatively low slope of the increasing trend in  $\delta^{13}\text{C}$  values (Fig. 3). Covariance between  $\delta^{13}\text{C}$  and Mg concentration may mean that the rate of Mg incorporation into cuttlebone aragonite is controlled by metabolic rate, as with  $\delta^{13}\text{C}$  values (Putten et al. 2000). This being the case, one would expect a significant correlation between  $\delta^{13}\text{C}$  values and Mg concentration. A cross plot of Mg and  $\delta^{13}\text{C}$  exhibits an  $r^2_{\text{adj}}$  of 0.23 ( $p < 0.001$ ) for CF5 and an  $r^2_{\text{adj}}$  of 0.01 ( $p = 0.384$ ) for CF8 (Fig. 6). While statistically significant, a linear relationship accurately describes only 23% of the data in CF5 and does not explain a significant portion of the explained variation of Mg in CF8 at all. Compared to CF5, the range in  $\delta^{13}\text{C}$  values, and the slope of ontogenetic increase, is much lower in CF8. The greater variability exhibited by Mg concentration in concert with the low slope of the  $\delta^{13}\text{C}$  value trend may mask any covariance that may be present. This in turn may suggest that CF8 exhibited a slower metabolic decline with ontogeny than CF5. While metabolism is likely a control on both the  $\delta^{13}\text{C}$  value and the concentration of Mg in cuttlebone aragonite, our results suggest that other factors influence  $\delta^{13}\text{C}$  and Mg incorporation in different ways, resulting in poor correlation between the two. Perhaps more importantly, the lack of correlation between  $\delta^{13}\text{C}$  and Mg may suggest that metabolism and/or growth rate is not the primary determinants of Mg accumulation in aragonite cuttlebones. However, the relatively small sample size (two cuttlebones) is insufficient to

identify subtle trends that might exist between  $\delta^{13}\text{C}$  and Mg, and further work is required to improve our understanding of Mg incorporation in cuttlebone aragonite. There was no significant correlation between  $\delta^{18}\text{O}$  and Mg values, implying temperature is not a control on the incorporation of Mg in cuttlebone aragonite.

This is the first study to examine the concentration of Ba in cuttlebone aragonite. Cuttlebone Ba concentrations tend to be uniform (Fig. 2 and Fig. 3), with the occasional peak on CF5, which is in consistent with similar, as yet unexplained peaks in Ba concentrations that have been observed in mussel calcite (Gillikin et al. 2006) and other bivalves (Carre et al. 2006). Following the work of Gillikin et al. (2006), who suggested that background level of Ba in the cuttlebone should be proportional to the Ba concentration of seawater, the data presented here suggest a background Ba value for the northeast coast of Jersey of ~6ppm. However, the mineralogical difference between mussel calcite and cuttlebone aragonite will affect the rate of Ba uptake, and thus our estimation of the background Ba value for the northeast coast of Jersey should be interpreted with some caution. In addition, the work of Gillikin et al. (2006) was focused in an estuary, so the relationships established between calcite and water Ba concentrations may not be applicable to the more open ocean conditions observed at Jersey. In fact, the Ba values observed here are relatively low, implying that there were no major river systems supplying fresh water into the habitat and no planktonic blooms (Hendry et al. 2001). Clearly, more research is required to better understand the factors that determine the incorporation of Ba in cuttlebones if Ba is to be successfully developed as an environmental proxy.

### Conclusion

Sr concentration exhibits a low but statistically significant correlation with coeval  $\delta^{18}\text{O}$  values. Unfortunately, the amount of variability in the concentration of Sr means that the construction of a Sr-based temperature equation is not possible at this time. Mn concentrations also exhibit low values and inverse covariance with  $\delta^{18}\text{O}$  values, suggesting Mn incorporation in cuttlebone aragonite is temperature controlled to some degree. Mg concentration exhibits a weak correlation with  $\delta^{13}\text{C}$  values implying that while metabolism may exert some control on the rate of Mg incorporation in cuttlebone aragonite, it may be relatively minor compared to other factors that introduce variability. Ba concentration profiles are consistent with previous bivalve literature, periodically exhibiting sharp, unexplained spikes.

In summary, this study is the first to explore the trace element composition of cuttlebone aragonite, and has illustrated weak, yet statistically significant relationships between several potential proxies. This may be valuable for future palaeoclimate studies. An important conclusion is that the relationships between stable isotope values and coeval trace element concentrations are complicated. While there may be some temperature control on the incorporation of Sr and Mn, temperature accounts for only ~25% of the variability. Similarly, Mg concentration may only partially be explained by metabolic changes, and thus is heavily influenced by other, as yet undiscovered, causes in cuttlebone aragonite. The incorporation of Ba is unrelated to any of the other variables, and while Ba must be extracted from the ambient water, the controls on this in *Sepia* are not understood.

## Figure Captions

- Fig 1. Map of Jersey, U.K. Cuttlebone collection site represented by the black star (modified from Findlay et al. previous chapter). Bathymetry presented in metres.
- Fig 2. Stable isotope values and trace element concentrations for CF5. Stable isotope values from Findlay et al. (previous chapter). Bold line in the Mg profile is a 5 point moving average to better illustrate trends.
- Fig 3. Stable isotope values and trace element concentrations for CF8. Stable isotope values from Findlay et al. (previous chapter). Bold line in Sr and Mg profiles is a 5 point moving average to better illustrate trends.
- Fig 4. Cross plot and regression statistics of  $\delta^{18}\text{O}$  derived temperatures vs. Sr concentration sampled from CF8. CF5 Sr values not measured due to machine breakdown.
- Fig 5. Cross plot and regression statistics of  $\delta^{18}\text{O}$  derived temperatures vs. Mn concentration from CF5 and CF8.
- Fig 6. Cross plot and regression statistics of  $\delta^{13}\text{C}$  value vs. Mg concentration from CF5 and CF8.

# Findlay and Gröcke Figure 1

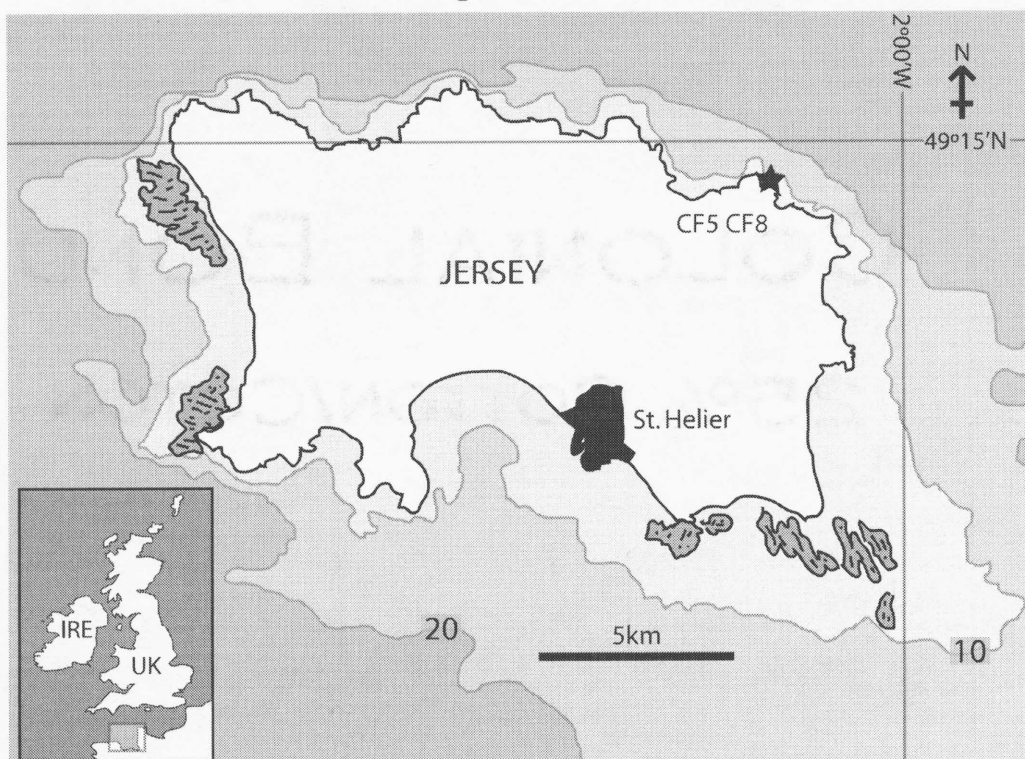


Fig 1. Map of Jersey, U.K. Cuttlebone collection site represented by the black star (modified from Findlay et al. previous chapter). Bathymetry presented in metres.

Findlay and Gröcke  
Fig 2

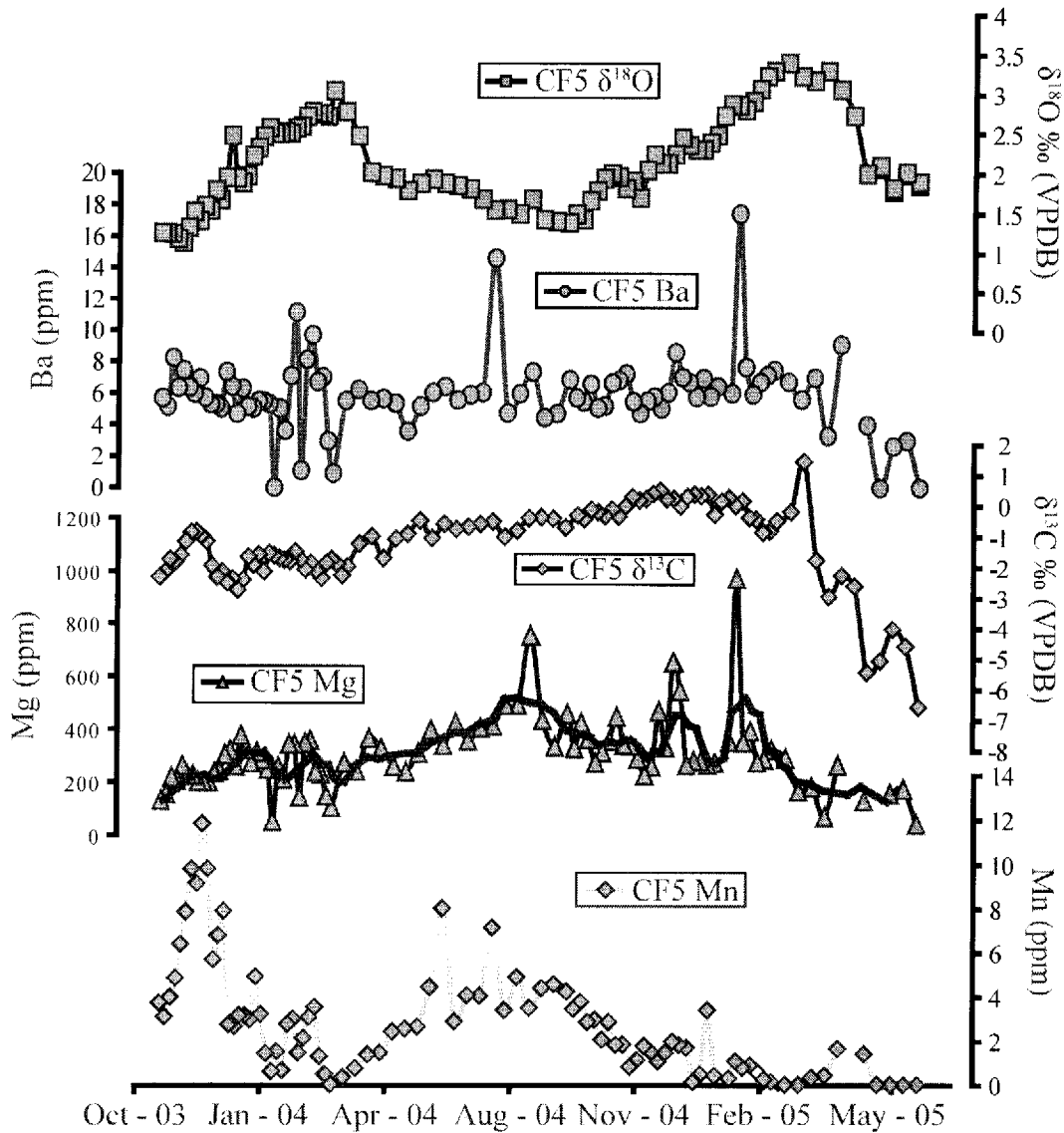


Fig 2. Stable isotope values and trace element concentrations for CF5. Stable isotope values from Findlay et al. (previous chapter). Bold line in the Mg profile is a 5 point moving average to better illustrate trends in noisy data.

Findlay and Gröcke  
Fig 3

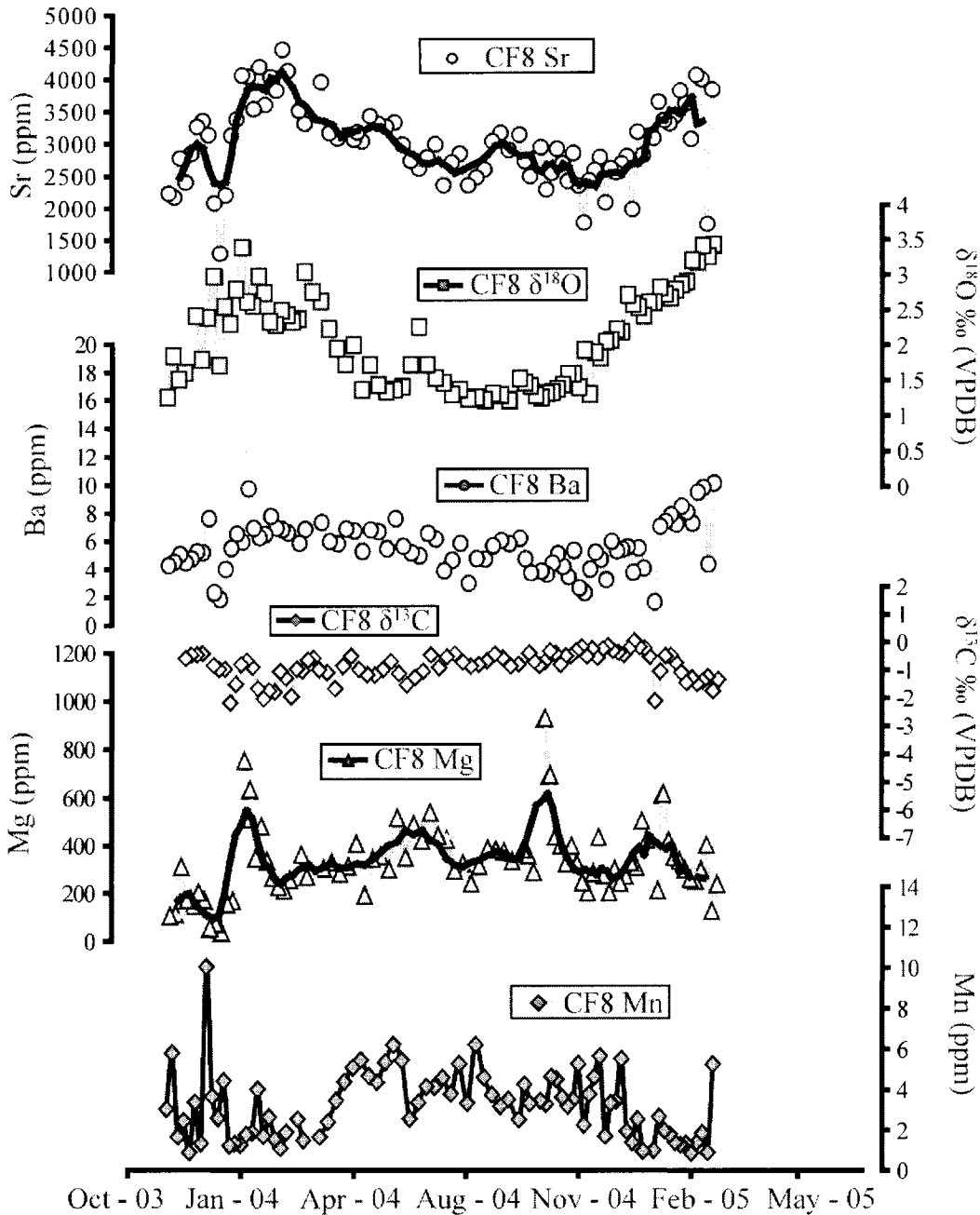


Fig 3. Stable isotope values and trace element concentrations for CF8. Stable isotope values from Findlay et al. (previous chapter). Bold line in Sr and Mg profiles is a 5 point moving average to better illustrate trends in noisy data.

Findlay and Gröcke  
Fig 4

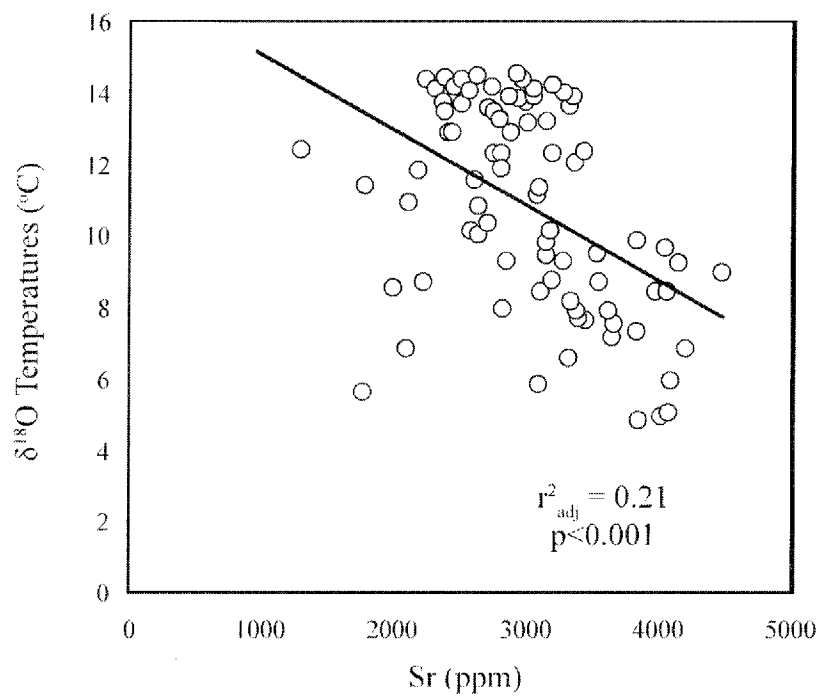


Fig 4. Cross plot and regression statistics of  $\delta^{18}\text{O}$  derived temperatures vs. Sr concentration sampled from CF8. CF5 Sr values not measured due to machine breakdown.

Findlay and Gröcke  
Fig 5

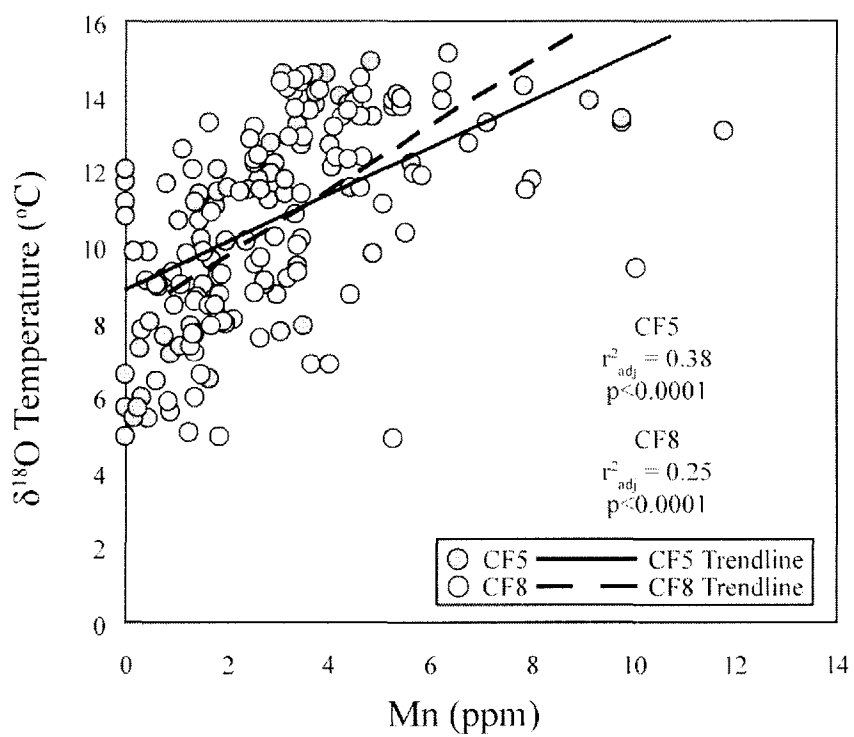


Fig 5 Cross plot and regression statistics of  $\delta^{18}\text{O}$  derived temperatures vs. Mn concentration from CF5 and CF8.

Findlay and Gröcke  
Fig 6

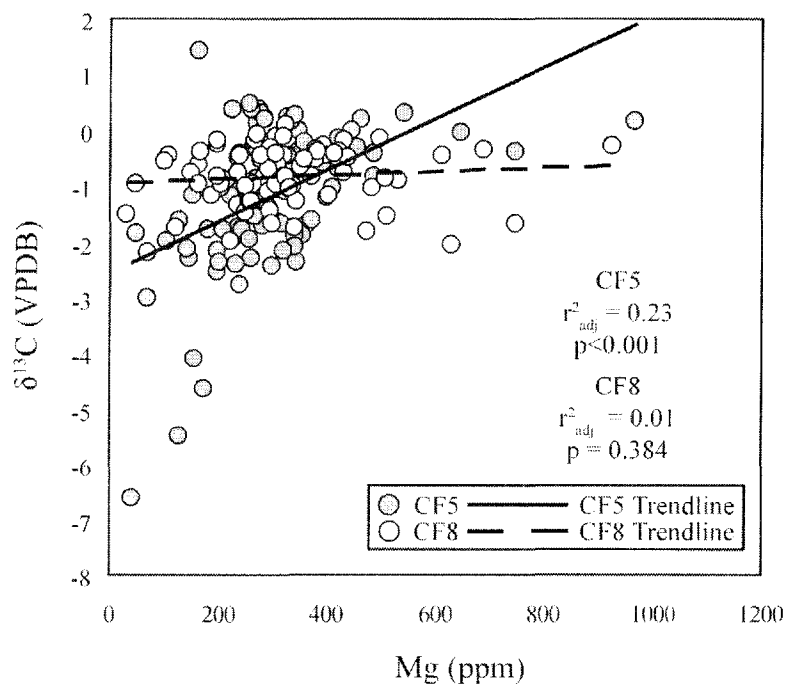


Fig 6. Cross plot and regression statistics of  $\delta^{13}\text{C}$  value vs. Mg concentration from CF5 and CF8.

**Table 1**

CF5								CF8								
Sample	Date	$\delta^{13}\text{C}$ (PDB)	$\delta^{18}\text{O}$ (PDB)	Temp (°C)	Ba	Mg	Mn	Sample	Date	$\delta^{13}\text{C}$ (PDB)	$\delta^{18}\text{O}$ (PDB)	Temp (°C)	Ba	Mg	Mn	Sr
cf5-1	22/06/05	-6.61	1.86	11.7	0	41	0	cf8-1	09/03/05	-1.32	3.43	4.8	10	235	5	3853
cf5-2	11/06/05	-4.63	1.98	11.1	3	172	0	cf8-2	04/03/05	-1.74	3.26	5.6	4	122	1	1766
cf5-3	01/06/05	-4.08	1.78	12.0	3	155	0	cf8-3	27/02/05	-1.21	3.42	4.9	10	399	2	4013
cf5-4	21/05/05	-5.10	2.06	10.8	0		0	cf8-4	22/02/05	-1.38	3.18	5.9	10	294	1	4082
cf5-5	11/05/05	-5.49	1.97	11.2	4	128	1	cf8-5	17/02/05	-1.48	3.20	5.8	7	249	1	3089
cf5-6	30/04/05	-2.63	2.72	7.9				cf8-6	13/02/05	-1.27	2.90	7.2	8	256	1	3640
cf5-7	20/04/05	-2.28	3.06	6.4	9	262	2	cf8-7	08/02/05	-1.44	2.86	7.3	9	296	1	3837
cf5-8	09/04/05	-2.98	3.30	5.4	3	68	0	cf8-8	03/02/05	-1.05	2.78	7.7	7	332	1	3446
cf5-9	30/03/05	-1.78	3.18	5.9	7	180	0	cf8-9	29/01/05	-0.69	2.67	8.2	8	348	2	3329
cf5-10	19/03/05	1.44	3.24	5.7	6	165	0	cf8-10	24/01/05	-0.41	2.72	7.9	7	416	2	3376
cf5-11	09/03/05	-0.21	3.41	4.9	7	288	0	cf8-11	20/01/05	-0.44	2.82	7.5	7	612	3	3666
cf5-12	25/02/05	-0.50	3.30	5.4	8	319	0	cf8-12	15/01/05	-1.03	2.61	8.4	2	207	1	3101
cf5-13	20/02/05	-0.83	3.24	5.7	7	284	0	cf8-13	10/01/05	-2.13	2.60	8.4				
cf5-14	14/02/05	-0.87	3.07	6.4	7	273	1	cf8-14	05/01/05	-0.47	2.41	9.3	4	419	1	2842
cf5-15	08/02/05	-0.45	2.91	7.1	6	389	1	cf8-15	31/12/04	-0.16	2.53	8.7	5	499	3	3197
cf5-16	03/02/05	-0.39	2.79	7.6	8	348	1	cf8-16	27/12/04	-0.11	2.58	8.5	4	305	1	1995
cf5-17	28/01/05	0.15	2.86	7.3	18	966	1	cf8-17	22/12/04	0.10	2.71	8.0	6	324	2	2822
cf5-18	22/01/05	-0.01	2.87	7.3	6	349	0	cf8-18	17/12/04	-0.18	2.17	10.3	5	269	6	2710
cf5-19	17/01/05	0.24	2.72	7.9				cf8-19	12/12/04	-0.41	2.21	10.1	5	239	3	2571
cf5-20	11/01/05	0.14	2.46	9.0	6	271	0	cf8-20	08/12/04	-0.31	2.06	10.8	6	296	3	2636
cf5-21	05/01/05	-0.30	2.37	9.5	6	263	3	cf8-21	03/12/04	-0.25	2.04	10.9	3	198	2	2106
cf5-22	31/12/04	0.37	2.28	9.8	7	275	0	cf8-22	28/11/04	-0.07	1.81	11.9	5	272	6	2810
cf5-23	25/12/04	0.31	2.28	9.8	6	278	0	cf8-23	23/11/04	-0.19	1.89	11.5	5	430	5	2608
cf5-24	19/12/04	0.36	2.33	9.6	7	261	2	cf8-24	18/11/04	-0.50	1.29	14.1	4	280	4	2451
cf5-25	14/12/04	0.29	2.43	9.2	7	541	2	cf8-25	14/11/04	-0.18	1.92	11.4	2	199	2	1785
cf5-26	08/12/04	-0.03	2.21	10.1	9	649	2	cf8-26	09/11/04	-0.46	1.38	13.7	3	241	5	2367
cf5-27	03/12/04	0.22	2.10	10.6	6	328	1	cf8-27	04/11/04	-0.12	1.58	12.9	5	320	4	2873
cf5-28	27/11/04	0.21	2.10	10.6	5	464	1	cf8-28	30/10/04	-0.27	1.58	12.9	3	394	3	2435
cf5-29	21/11/04	0.48	2.21	10.1	6	257	1	cf8-29	25/10/04	-0.45	1.42	13.6	4	322	4	2713
cf5-30	16/11/04	0.38	2.01	11.0	6	225	2	cf8-30	21/10/04	-0.44	1.36	13.8	5	397	5	2937
cf5-31	10/11/04	0.21	1.65	12.6	5	286	1	cf8-31	16/10/04	-0.77	1.31	14.0	4	433	5	2567
cf5-32	04/11/04	0.16	1.87	11.6	6	335	1	cf8-32	11/10/04	-0.35	1.30	14.1	4	690	3	2309
cf5-33	30/10/04	0.28	1.77	12.0	7	340	2	cf8-33	06/10/04	-0.26	1.23	14.4	4	926	3	2964
cf5-34	24/10/04	-0.02	1.92	11.4	7	444	2	cf8-34	01/10/04	-0.65	1.27	14.2				
cf5-35	18/10/04	-0.37	1.96	11.2	7	353	3	cf8-35	27/09/04	-0.81	1.40	13.7	4	285	3	2513
cf5-37	13/10/04	-0.13	1.90	11.5	5	309	2	cf8-36	22/09/04	-0.65	1.45	13.4	5	355	4	2749
cf5-38	07/10/04	-0.35	1.74	12.2	5	271	3	cf8-37	17/09/04	-0.34	1.51	13.2	6	379	3	3154
cf5-39	01/10/04	-0.21	1.61	12.7	7	360	3	cf8-38	08/09/04	-0.75	1.20	14.5	6	331	4	2923
cf5-40	26/09/04	-0.14	1.37	13.8	5	421	4	cf8-39	31/08/04	-0.83	1.28	14.2	6	371	3	3185
cf5-41	20/09/04	-0.45	1.44	13.5	6	326	3	cf8-40	24/08/04	-0.52	1.29	14.1	6	379	4	3055
cf5-42	15/09/04	-0.32	1.33	14.0	7	454	4	cf8-41	17/08/04	-0.37	1.21	14.5	5	382	5	2622

**Table 1**

CF5								CF8								
Sample	Date	$\delta^{13}\text{C}$ (PDB)	$\delta^{18}\text{O}$ (PDB)	Temp (°C)	Ba	Mg	Mn	Sample	Date	$\delta^{13}\text{C}$ (PDB)	$\delta^{18}\text{O}$ (PDB)	Temp (°C)	Ba	Mg	Mn	Sr
cf5-43	05/09/04	-0.72	1.34	13.9	5	332	5	cf8-42	09/08/04	-0.62	1.24	14.3	5	310	6	2500
cf5-44	26/08/04	-0.43	1.37	13.8	4	432	4	cf8-43	02/08/04	-0.77	1.22	14.4	3	237	3	2375
cf5-45	16/08/04	-0.39	1.63	12.6	7	748	3	cf8-44	26/07/04	-0.83	1.35	13.9	6	320	5	2866
cf5-46	06/08/04	-0.42	1.45	13.5	6	488	5	cf8-45	19/07/04	-0.67	1.28	14.2	5	292	4	2732
cf5-47	27/07/04	-0.82	1.51	13.2	5	488	3	cf8-46	11/07/04	-0.37	1.45	13.4	4	420	5	2378
cf5-48	17/07/04	-1.02	1.49	13.3	15	410	7	cf8-47	04/07/04	-0.47	1.52	13.1	6	437	4	3006
cf5-49	07/07/04	-0.52	1.63	12.6	6	403	4	cf8-48	27/06/04	-0.89	1.71	12.3	7	533	4	2805
cf5-50	27/06/04	-0.61	1.77	12.1	6	353	4	cf8-49	19/06/04	-0.43	2.24	10.0	5	415	3	2629
cf5-51	17/06/04	-0.70	1.80	11.9	6	420	3	cf8-50	12/06/04	-1.03	1.71	12.3	5	483	3	2752
cf5-52	07/06/04	-0.78	1.84	11.7	6	336	8	cf8-51	05/06/04	-1.26	1.39	13.7	6	344	5	2996
cf5-53	28/05/04	-0.60	1.89	11.5	6	395	4	cf8-52	29/05/04	-1.53	1.35	13.9	8	510	6	3342
cf5-54	18/05/04	-1.06	1.84	11.8	5	307	3	cf8-53	21/05/04	-1.11	1.32	14.0	5	294	5	3272
cf5-55	08/05/04	-0.50	1.74	12.2	4	237	3	cf8-54	14/05/04	-0.67	1.41	13.6	7	351	4	3323
cf5-56	28/04/04	-0.93	1.90	11.5	5	257	2	cf8-55	07/05/04	-0.98	1.70	12.4	7	339	5	3439
cf5-57	18/04/04	-1.08	1.93	11.3	6	324	1	cf8-56	29/04/04	-1.17	1.34	13.9	5	187	5	3049
cf5-58	08/04/04	-1.72	1.98	11.1	6	361	1	cf8-57	22/04/04	-1.16	1.99	11.1	7	403	5	3078
cf5-59	29/03/04	-1.01	2.45	9.1	6	239	1	cf8-58	15/04/04	-0.96	1.71	12.3	7	308	4	3191
cf5-60	19/03/04	-1.25	2.76	7.7	6	269	0	cf8-59	08/04/04	-0.46	1.93	11.3	6	277	3	3093
cf5-61	10/03/04	-1.99	3.04	6.5	1	103	0	cf8-60	31/03/04	-0.84	2.22	10.1	6	324	2	3179
cf5-62	05/03/04	-2.28	2.71	8.0	3	146	0	cf8-61	24/03/04	-1.68	2.61	8.4	7	299	2	3973
cf5-63	01/03/04	-1.90	2.74	7.8	7	228	1	cf8-62	17/03/04	-1.08	2.74	7.8				
cf5-64	26/02/04	-1.75	2.74	7.8	7	236	4	cf8-63	10/03/04	-0.97	3.03	6.6	7	264	1	3323
cf5-65	21/02/04	-1.88	2.77	7.7	10	355	3	cf8-64	04/03/04	-0.53	2.36	9.5	6	357	3	3526
cf5-66	17/02/04	-2.37	2.70	8.0	8	345	2	cf8-65	28/02/04	-0.61	2.32	9.7				
cf5-67	13/02/04	-2.12	2.58	8.6	1	141	1	cf8-66	23/02/04	-1.00	2.42	9.2	7	252	2	4141
cf5-68	09/02/04	-1.88	2.55	8.7	11	340	3	cf8-67	18/02/04	-0.95	2.48	9.0	7	207	1	4478
cf5-69	04/02/04	-2.10	2.48	9.0	7	341	3	cf8-68	13/02/04	-1.97	2.28	9.9	7	223	2	3837
cf5-70	31/01/04	-1.77	2.50	8.9	4	208	1	cf8-69	08/02/04	-1.27	2.32	9.7	8	261	3	4049
cf5-71	27/01/04	-1.51	2.48	9.0	5	254	2	cf8-70	03/02/04	-1.03	2.73	7.9	6	330	2	3616
cf5-72	22/01/04	-1.84	2.48	9.0	0	50	1	cf8-71	29/01/04	-1.80	2.97	6.8	6	475	4	4204
cf5-73	18/01/04	-1.79	2.55	8.7	5	245	1	cf8-72	24/01/04	-1.75	2.54	8.7	7	341	2	3550
cf5-74	14/01/04	-1.72	2.44	9.1	6	282	3	cf8-73	19/01/04	-2.05	2.61	8.4	10	630	2	4055
cf5-75	10/01/04	-1.64	2.29	9.8	6	308	5	cf8-74	14/01/04	-1.67	3.39	5.0	6	749	1	4078
cf5-76	05/01/04	-1.55	2.19	10.2	5	269	3	cf8-75	09/01/04	-0.87	2.78	7.7	7	507	1	3395
cf5-77	01/01/04	-2.16	1.93	11.4	5	320	3	cf8-76	04/01/04	-0.64	2.29	9.8	5	163	1	3144
cf5-78	28/12/03	-1.60	1.84	11.7	6	373	3	cf8-77	30/12/03	-0.77	2.54	8.7	4	151	4	2220
cf5-79	24/12/03	-1.94	1.90	11.5	5	259	3	cf8-78	25/12/03	-1.50	1.69	12.4	2	33	3	1301
cf5-80	19/12/03	-1.68	2.46	9.1	6	316	3	cf8-79	20/12/03	-2.20	2.97	6.9	2	69	4	2093
cf5-81	15/12/03	-2.43	1.90	11.5	7	300	8	cf8-80	15/12/03	-0.95	2.38	9.4	8	50	10	3144
cf5-82	11/12/03	-2.76	1.62	12.7	5	241	7	cf8-81	10/12/03	-0.95	1.77	12.0	5	165	1	3365
cf5-83	06/12/03	-2.39	1.74	12.2	5	232	6	cf8-82	04/12/03	-0.81	2.41	9.3	5	197	3	3273

**Table 1**

CF5								CF8								
Sample	Date	$\delta^{13}\text{C}$ (PDB)	$\delta^{18}\text{O}$ (PDB)	Temp (°C)	Ba	Mg	Mn	Sample	Date	$\delta^{13}\text{C}$ (PDB)	$\delta^{18}\text{O}$ (PDB)	Temp (°C)	Ba	Mg	Mn	Sr
cf5-84	02/12/03	-2.52	1.48	13.3	5	197	10	cf8-83	29/11/03				5	142	1	2857
cf5-85	28/11/03	-2.16	1.54	13.1	6	198	12	cf8-84	24/11/03	-0.38	1.59	12.9	4	165	2	2414
cf5-86	24/11/03	-2.34	1.35	13.9	7	200	9	cf8-85	19/11/03	-0.42	1.49	13.3	5	305	2	2787
cf5-87	19/11/03	-1.97	1.47	13.4	6	222	10	cf8-86	14/11/03	-0.43	1.82	11.8	4	108	6	2181
cf5-88	15/11/03	-1.17	1.26	14.3	6	223	8	cf8-87	09/11/03	-0.56	1.23	14.4	4	100	3	2242
cf5-89	11/11/03	-0.99	1.07	15.1	8	259	6									
cf5-90	06/11/03	-0.86	1.11	14.9	6	204	5									
cf5-91	02/11/03	-0.88	1.18	14.6	8	215	4									
cf5-92	29/10/03	-1.18	1.19	14.6	5	154	3									
cf5-93	25/10/03	-1.62	1.19	14.6	6	129	4									
cf5-94	20/10/03	-1.86	1.03	15.3												
cf5-95	16/10/03	-1.75	1.44	13.5												
cf5-96	12/10/03	-2.18	1.08	15.1												
cf5-97	08/10/03	-2.33	0.83	16.1												

## **Chapter 4**

### **Stable isotope and trace element variability in belemnite rostra: comparisons with a modern analogue and suggested sampling strategies**

## Rationale and Objectives

The previous chapters investigated the stable isotope and trace element geochemistry of several *Sepia* cuttlebones. These showed that:

1. Oxygen isotope values accurately record water temperature with ontogeny.
2. Carbon isotope values document changes in metabolism with ontogeny.
3. Sr and Mn are ~25% controlled by temperature.
4. Mg is ~10% controlled by metabolism.
5. The controls on Ba are not understood.

Following this, the next step is to reinvestigate the internal geochemical variability within belemnite rostra.

This third data chapter initially establishes that it is difficult to visually assess the influence of diagenesis on belemnite calcite stable isotope values. Rostra were then sampled for stable isotopes and trace elements so as to remove any diagenetic calcite while examining belemnite life history. Belemnites collected from the same bed record similar geochemical signals. Where different genera were collected from the same bed, the amount of variability between individuals was similar to the variability between genera, indicating that while there may be habitat preferences, each genus records the same signal when these habitats overlap.

Unlike modern *Sepia*, belemnites do not record a seasonal temperature cycle, suggesting a migration with favourable water conditions. Belemnite rostra exhibit an ontogenetic increase in carbon isotope values, suggesting that like *Sepia*, their metabolism slows with age. Belemnite Mg concentrations tend to co vary with oxygen isotope values, contrasting with Sr concentrations in *Sepia*, suggesting Mg is partially temperature dependant in belemnite rostra.

The results of this research suggest that problems such as variability within the belemnite geochemical record over geologic time may be artefacts of sampling techniques which inadequately sample the geochemical variability inherent to the rostrum. The belemnite may still be a valuable proxy for palaeoclimatic change, and a source of palaeoecological information, providing that a high resolution sampling practice is employed.

## Chapter 4

### Stable isotope and trace element variability in belemnite rostra: comparisons with a modern analogue and suggested sampling strategies

Duncan J. Findlay<sup>1</sup>, Darren R. Gröcke<sup>2</sup>

1. School of Geography and Earth Sciences, McMaster University, 1280 Main Street W, Hamilton, Ontario L8S 4K1 Canada, (emails: findlad@mcmaster.ca, knyjf@mcmaster.ca)

2. Department of Earth Sciences, Durham University, Science Laboratories, Durham DH1 3LE, UK (email: d.r.grocke@durham.ac.uk)

#### Abstract

The low Mg calcite rostra of extinct Belemnoida are commonly used in Mesozoic palaeoenvironmental reconstructions as they often exhibit excellent preservation. However, current studies show that there can be substantial variability (on the order of 3 ‰) in both oxygen and carbon isotope values in the belemnite geochemical record. This variability must be better understood if belemnites are to be used as a reliable record of the palaeoenvironmental record. To this end, high resolution trace element and stable isotope analysis of belemnite rostra were performed along a radial profile and confirm prior suggestions that belemnite rostra are not geochemically homogenous. Such heterogeneity may account for some of the variability observed in the geochemical record. However, rostra collected from the same horizon show similar values, implying that coeval belemnites record the same signals. More specifically,  $\delta^{18}\text{O}$  values do not display obvious seasonal cyclicality, contrasting with *Sepia*, suggesting the occurrence of seasonal migration in these organisms. Mg abundance and  $\delta^{18}\text{O}$  values tend to co-vary along the growth profile, which may indicate that the rate of Mg precipitation is temperature-dependant, contrasting with Sr and Mn in *S. officinalis* cuttlebones. The general trends observed in Mg and  $\delta^{18}\text{O}$  may imply that these belemnites migrated from shallow to deep water with maturity. Similar *S. officinalis* cuttlebones,  $\delta^{13}\text{C}$  values increase with ontogeny indicating a decrease in metabolic rate with age. As these fossils display a wide array of geochemical values across their lifespan, a single sample from within the rostra is inadequate for palaeoclimate reconstruction: While a bulk sample drilled along the growth axis may approximate an average value for an individual's lifetime, it will also contain some sample bias due to the geochemical variability associated with an individual's life history. High resolution sampling along the growth axis should attain an ontogenetic record of environmental and metabolic change.

#### Introduction

Belemnnoidea are extinct Mesozoic marine cephalopods that evolved during the Jurassic (Fig. 1) and are characterised by the secretion of a low Mg calcite rostrum towards their posterior end, which is thought to act as a counterweight to the aragonite phragmocone, adding stability for movement through water (Ellis 2001, Jeletzki 1966). The structure and chemical composition of belemnite rostra render them resistant to post-burial alteration: The rostrum is densely secreted and contains large crystals, low porosity, and low permeability. This overarching structure of the rostrum restricts reaction area and fluid flow in the rostrum, which in turn restricts diagenetic dissolution and/or replacement (Urey 1948, Urey et al. 1951). As pore waters are usually saturated with low Mg calcite, other carbonate polymorphs (e.g. aragonite, high Mg calcite) are preferentially dissolved and replaced, often leaving low Mg calcite unaltered (Veizer 1983). Consequently, the preservation potential of belemnite rostra is higher than many other coeval fossils making them particularly useful in Mesozoic palaeoclimate reconstruction (Veizer et al. 1999, McArthur et al. 2007, Price and Mutterlose 2004 and many others). However, significant variance has been observed in the belemnite geochemical record, with variability on the order of 3 ‰ superimposed on a background trend (Veizer et al. 1999). This geochemical variation does not result from short term environmental change (McArthur et al. 2007), but may instead result from heterogeneity in the internal geochemistry of the rostra that stems from metabolic or behavioural changes through ontogeny. As such, the adoption of a standard sampling procedure that accounts for any such within-individual variation is needed if we are to compare geochemical records in a meaningful manner.

### Objectives

In this chapter, high resolution geochemical data are measured from eleven belemnite rostra (collected from the west coast of Scotland and two localities in the Albertan foothills of the Canadian Rockies) and compared to cuttlefish geochemistry (see chapters 2 and 3). This study has several goals, all of which are intended to enhance our understanding of both the ecology of Belemnnoidea and their utility as an environmental proxy.

1. Re-evaluate the isotopic variability within belemnite rostra, and compare visibly well preserved to visibly diagenetic specimens, and based on this, sample individual rostra at high resolution for stable isotopes and trace elements, so as to permit the examination of life history, following the exclusion of a diagenetic signal.
2. Assess inter-bed variability within individuals and genera.
3. Compare the geochemistry of the belemnite to that of the modern analogue.

4. Outline sampling strategies to maximise the information extracted from a rostrum, and minimise the sample bias in the long term geochemical record.

### Background

Oxygen isotope ratios in modern biological and inorganically precipitated carbonate are strongly correlated with ambient water temperature. This allows for the calculation of ambient water temperature from the isotopic composition of shell material assuming adequate knowledge of the oxygen isotope ratio of the ambient water (Epstein et al. 1951, Epstein et al. 1953, Emiliani 1966, Anderson and Arthur 1983, Grossman and Ku 1986, Ditchfield 1997, McArthur et al. 2007). Many modern molluscs (including *Sepia*) and brachiopods secrete calcium carbonate with oxygen isotope values in isotopic equilibrium with ambient water (Carpenter and Lohmann 1995, Bettencourt and Guerra 1999, Brand et al. 2003). The oxygen isotope values of belemnite rostra are mostly in good agreement with coeval brachiopods. Many modern brachiopods generally exhibit little or no vital effect, suggesting the oxygen isotope ratios within belemnite rostra were also secreted in equilibrium with ambient seawater (Veizer et al. 1999, McArthur et al. 2000, van de Schootbrugge et al. 2000, Voigt et al. 2003).

While there is good evidence that belemnite oxygen isotope values are precipitated in equilibrium with ambient water, the same is not true for belemnite carbon isotope values. Many species, including *S. officinalis*, display an inverse correlation between carbon isotope values and metabolic rate (Putten et al. 1999, Vander Putten et al. 1999, Putten et al. 2000, Findlay et al. previous chapter). Since Belemnoida, were probably active carnivores (like modern *Sepia* and squid), the carbon isotope values of their calcified structures will likely reflect a combination of metabolism, diet, and the background dissolved inorganic carbon (DIC) isotope values.

In addition to the palaeoenvironmental information that can be obtained from the well established oxygen and carbon stable isotope techniques, valuable environmental information may also be recorded by the incorporation of certain key trace elements like Mg, Sr, and Ba into biological carbonate. For example, the precipitation rate of Mg in calcite is primarily temperature dependant (Klien et al 1996, Nurnberg 2000, Lea et al. 2000), so the use of Mg is being explored actively as a temperature proxy (Mitsuguchi et al. 1997, Steuber 1999, Lea et al. 2000, Hendry et al. 2001, Palacios-Fest and Dettman 2001, McArthur et al. 2004, McArthur et al. 2007, Shen et al. 2007). This may be useful as Mg concentration is relatively uniform across a wide range of salinities, compared to  $\delta^{18}\text{O}$  values (Klein et al. 1996) and so may provide a salinity independent temperature proxy, which when used in combination with oxygen isotope values and a relevant oxygen isotope

temperature equation, may be used to calculate the oxygen isotope value of ambient water (Rosenthal and Lohmann 2002). The oxygen isotope value of ancient seawater is important for assessing palaeoglacial levels, which are much debated for the Mesozoic.

Sr abundance in biogenic calcite has been used to reconstruct metabolic changes with ontogeny (Rosenberg and Hughes 1991, Hendry et al. 2001). As carbon isotope values have been shown to vary with metabolism, the concentration of Sr and the  $\delta^{13}\text{C}$  value of calcite should co-vary (Klein et al. 1996, Putten et al. 2000, Stoll and Schrag 2001) and would be expected to vary with ontogeny, with younger faster-growing shelled organisms having higher metabolic rates (Rosenberg and Hughes 1991). Sr abundance may also be used for diagenetic screening in fossil calcite. As meteoric water contains only very small quantities of Sr, secondary replaced calcite will also be low in Sr (Veizer 1983). The modern range of Sr in calcite is ~800 to ~2000 ppm (Steuber 1999), so anything below this range may be disregarded from further analysis. Furthermore, the abundance of Mn may be useful in identifying diagenetic alteration. While Sr is present in lower quantities in meteoric water, Mn is relatively concentrated (Veizer 1983). Modern calcite secreting marine organisms show very low concentrations of Mn (Steuber 1999). Samples containing more than 150ppm of Mn or less than 800ppm of Sr should be excluded from analyses, which should eliminate most diagenetic calcite.

Ba abundance has been used to reconstruct flooding events in a Jurassic lagoon (Hendry et al. 2001) and detect blooms in bivalve shells (Putten et al. 2000). The main sources of Ba at the ocean surface are rivers and upwelling events, which may stimulate blooms (Gillikin et al. 2006). Ba is rapidly removed from surface waters by primary producers which fall to the sea floor, decompose, and release Ba and other nutrients into the surrounding water (Bruland and Lohan 2004). Ba may therefore be useful as an indicator of upwelling, increased precipitation, changes in runoff, or migration to shallow areas, where there is adequate ecological knowledge for the biological proxy (Putten et al. 2000). This may also be useful to determine if carbonate samples should be removed from  $\delta^{18}\text{O}$  palaeotemperature analysis due to the influence of meteoric derived runoff.

Although trace element analysis may provide useful insights into the palaeoenvironmental record, many trace element studies show high internal variability in carbonate trace element composition within a single individual (Carpenter and Lohmann 1995, Sinclair et al. 1998, Putten et al. 2000, Hendry et al. 2001, Lee et al. 2004, McArthur et al. 2007). In fact, both  $\delta^{18}\text{O}$  and  $\delta^{13}\text{C}$  values show variation in every study that has investigated the internal geochemistry of the rostrum (Lowenstam and Epstein 1954, Bowen 1961, Longinelli 1969, Spaeth et al 1971, McArthur et al. 2007).

Some of the within-individual variability in stable isotopes and trace elements is probably the result of belemnites being mobile organisms.

Activities like seasonal migration would complicate the geochemical record as environmental information from the migration route is recorded in the carbonate. If ignored, such behavioural signals could lead to spurious palaeoenvironmental interpretations. In fact *S. officinalis*, a modern analogue for Belemnnoidea, is known to migrate inshore to breed and to deeper waters over winter, both of which influence the geochemistry of the cuttlebone (see Chapter 3; Boucaud-Camou and Boismery 1991, Nixon and Mangold 1998). Such behaviour in belemnites should be understood if accurate palaeoenvironmental interpretations are to be constructed using their geochemistry.

Despite the evidence that there is geochemical heterogeneity within single organisms which may be correlated to seasonality and organism ecology, such variation is generally ignored when belemnites are sampled for isotopic and trace element analysis (McArthur et al. 2004, Pirrie et al. 2004, Price and Mutterlose 2004, Rosales et al. 2004a, Wierzbowski 2004, van de Schootbrugge, B. et al. 2005).

#### *Sepia officinalis* as a modern analogue

The belemnite phragmocone is analogous to the *Sepia* cuttlebone as both structures are composed of aragonite and probably fail beyond a critical hydrostatic pressure (Sherrard 2000). In fact, the geochemical nature of these structures would limit the depth of habitat for each of these organisms to 100-200m and it has been shown that both the functional morphology and distribution of belemnites in sediments suggests that they inhabited cool, shallow waters despite their nektonic nature (Urey et al. 1951). This common feature of belemnite and *Sepia* morphology make *Sepia* one of the closest modern analogues to Belemnnoidea, since other close relatives that are often used as analogues have no morphological limit on habitat depth (e.g. squid). As such, comparisons between belemnites and modern *Sepia* may provide insights into the geochemistry of the extinct belemnite, since the presence of aragonite phragmocones impose similar bathymetric restrictions on the life-histories of both taxa.

However, while modern *Sepia* are similar to the belemnite in many respects (Murray 1985, Moore et al. 1952; Fig. 2), there are also several important differences between them. The most notable of these differences is the fact that *Sepia* lacks the rostrum so prevalent in the belemnite record. Since belemnite phragmocones are poorly preserved in the fossil record, the aragonite phragmocone of *S. officinalis* must be compared to the low Mg calcite rostrum of the belemnite. While the underlying differences in the geochemical nature of the belemnite rostra and *Sepia* cuttlebone introduce fundamental chemical differences among the structures, it is relatively easy to account for differences in the underlying geochemical nature of the two

structures using established temperature equations for low Mg calcite and aragonite respectively (Anderson and Arthur 1983, Grossman and Ku 1986). Thus, the geochemical trends associated with changes in both environmental conditions and behaviour through ontogeny recorded in the two structures remains comparable. However, a better understanding of the internal geochemistry of both structures is required to improve the interpretation of temporal geochemical curves constructed from belemnite analyses.

#### Previous studies of geochemical variability within belemnite rostra

The work of Urey et al. (1951) was the first to establish that the chemistry of belemnite rostra varies internally, and that they are more likely to preserve the original lifetime geochemical values than many other coeval fossils. Both  $\delta^{18}\text{O}$  and  $\delta^{13}\text{C}$  values show variation in every study that has investigated the internal geochemistry of the rostrum (Lowenstam and Epstein 1954, Bowen 1961, Longinelli 1969, Spaeth et al 1971, McArthur et al. 2007). After establishing that the rostra varies internally, Urey et al. (1951) ground samples across the entire rostral growth axis to achieve a lifetime average, which were then used to investigate Upper Cretaceous palaeotemperatures. They suggested that symmetry in isotopic signals preserved on separate transects across the rostra may be used as a preservation indicator, an idea later exploited for brachiopods (Lee et al. 2004).

Apparent seasonal variability was observed in the oxygen isotope values of several belemnite rostra (Lowenstam and Epstein 1954, Bowen 1961). However, radial variation of belemnite oxygen isotopes from both well and poorly preserved specimens was examined by Longinelli (1969) who found that all specimens exhibited several per mil cyclic variation in  $\delta^{18}\text{O}$  values, with poorly preserved rostra documenting lower mean values. The concentric “growth lines” preserved in these rostra did not consistently correlate with  $\delta^{18}\text{O}$  values, suggesting that “growth line” formation is not controlled by annual growth. The calcite forming these “growth lines” was identified as opaque and therefore likely diagenetic. All the belemnite profiles presented by Longinelli exhibited approximately 5 ‰ variation in  $\delta^{18}\text{O}$  values, with low values near the apical line that increase outwards. As these “growth lines” are likely radially consistent zones of diagenetic alteration, symmetry or apparently seasonal stable isotope values may not therefore be used as an indicator of preservation, as radial alteration of the rostra may have a similar isotopic signature to what would be expected from a pristine specimen.

After collecting some very well preserved belemnites that still contain the rarely-preserved aragonite phragmocone, Spaeth et al (1971) investigated the isotopic composition of both the rostra and the phragmocone. As aragonite was still present in these fossils, their preservation was judged to be excellent. They found several per mil variation in the  $\delta^{13}\text{C}$  and  $\delta^{18}\text{O}$  values of single

belemnite rostra with  $\delta^{18}\text{O}$  values showing some cyclicity, although following the work of Longinelli (1969), they argued that the presence of cyclic variability in  $\delta^{18}\text{O}$  values can not be used as an indicator of preservation. However, Spaeth et al were unable to give a satisfactory explanation for the higher stable isotope values of the phragmocone, which when used for palaeotemperature analysis, yielded values incompatible with those of the rostrum. The phragmocone also displayed a strong linear relationship between  $\delta^{18}\text{O}$  and  $\delta^{13}\text{C}$  values. Retrospectively, the difference between  $\delta^{18}\text{O}$  values of the phragmocone and the rostrum may be resolved by the use of the appropriate temperature equation. Spaeth et al used the calcite temperature equation for both structures, which is not appropriate in light of later work establishing a distinct aragonite temperature equation (Grossman and Ku 1986).

More recently, the internal geochemical variability of belemnite rostra has been reinvestigated by McArthur et al. (2007). In addition to stable isotope analyses, they investigated the internal variability of belemnites with regards to Mg, Sr and Na with a view to testing whether the variability in the belemnite geochemical signal over geologic time was the result of short term environmental change. The rostra they examined were extracted from a fossilised regurgitation deposited by a large Jurassic predator, and therefore all were probably alive at the same time allowing for a strong comparison of within- and between-rostra geochemical patterns and variability. Interestingly, McArthur et al. (2007) observed internal geochemical variability within individual rostra, as well as significant geochemical differences between species and possibly gender. It was concluded that the variability in the long term belemnite record is not the result of short term environmental change as belemnites of the same species contained near identical geochemical values.

### Sample Locations

Belemnite rostra were collected from three locations. (1) A large, unfractured rostrum was collected from the middle Jurassic strata of Bearreraig Bay, Isle of Skye, Scotland (Fig. 3). These shallow sea siliciclastic sediments belong to the Staffin Shale Formation, and were deposited below fair weather wave base, at a depth of between 100-150m (Wierzbowski 2004). (2) A large, relatively undamaged belemnite was collected from the ammonite rich Bajocian shales of the Bighorn Creek section, near the Yaha Tinda Ranch in central Alberta, Canada (Fig. 4). During the Bajocian, this area was part of a shallow, epicontinental sea to the east of the emerging Rocky Mountains (Marion 1984). (3) Many rostra were collected from the Oxfordian Green Bed sediments exposed along Carbondale River, southern Alberta, Canada (Fig. 4). This unit overlies the Ribbon Creek Member, and is overlain by the Passage Beds. These sediments are part of the middle Jurassic Fernie Formation, and

represent the same shallow epicontinental sea that covered much of Alberta during the Mesozoic (McLearn 1927, Stronach 1984). The characteristic green colour of this unit is the result of diagenetic berthierine (Hall 1984).

## Methods

This study examines a total of 11 rostra, 9 of which were collected from 3 stratigraphic horizons within the Green Beds in order to assess the geochemical variability preserved in belemnites from a single layer. As organic matter may influence the geochemistry of modern biological carbonate, the presence of any residual organic matter in these belemnite rostra needed to be assessed. A stable isotope transect of a previously analysed belemnite rostra was split in two. One half was treated with 30% peroxide to remove any organic matter that may have survived fossilisation while the other half was left untreated. Peroxide was also applied to several NBS19 calcite standards. Upon comparison, the peroxide treated standards and belemnite samples were within analytical error of the untreated samples, suggesting that the treatment does little to alter the carbon and oxygen isotope values of calcite, and that little organic matter survived fossilisation. Further belemnite samples were not treated chemically prior to analysis.

In order to assess the spatial variability of stable isotope values in belemnite rostra, discs were cut perpendicular to the long axis of the Bearreraig Bay, Scotland and Bighorn Creek, Canada rostra and then sub-sampled with a micro drill using a 2mm grid centred on the apical line (Fig 5a). The Bearreraig Bay belemnite disc was 2mm thick and cut 5mm from the aviolis. This yielded 74 stable isotope samples. The Bighorn Creek belemnite was cut into three 2mm thick discs at spaced intervals along the rostrum: Disc 1 was cut 22mm from the tip of the aviolis and contained 49 samples; disc 2 at 36mm with 44 samples; and disc 3 at 52mm near the tip of the rostrum containing 40 samples. As disc 3 was smaller than the other discs, a 1mm sampling grid was used. A total of 133 analyses were performed for the Bighorn Creek belemnite.

Belemnite rostra from the Carbondale River Green Bed section were cut longitudinally, and two profiles were drilled radially from the apical line to the outer edge of the rostra. One of the profiles was used for stable isotope analysis and the other was used for the analysis of trace elements. (Fig 5b). As trace element analysis required more material than stable isotope analysis, trace element transects were completed at a slightly lower resolution.

Stable isotope samples of ~0.3mg were reacted with 100% phosphoric acid using a common acid bath system, with the resulting CO<sub>2</sub> analyzed in a VG Optima Isotope Ratio Mass Spectrometer. Stable-isotope ratios are expressed in per mil (‰) and are calculated as

$$\delta = \left( \frac{R_{sample}}{R_{standard}} - 1 \right) \times 1000 \quad [4.1]$$

where R is the ratio between  $^{13}\text{C}$  and  $^{12}\text{C}$  in the case of carbon, and  $^{18}\text{O}$  and  $^{16}\text{O}$  for oxygen, relative to Vienna Pee Dee Belemnite (VPDB) standard. Reproducibility for both  $\delta^{13}\text{C}$  and the  $\delta^{18}\text{O}$  is better than  $\pm 0.1\%$  on replicate analyses.

Trace element samples of  $\sim 3\text{mg}$  were weighed before dissolution in 10ml of 2% trace-metal grade nitric acid. These solutions were then analysed in an ELAN 6100 quadrupole ICP MS for Ba, Mg, Mn and Sr with a suite of standards at the beginning, middle and end of each run. An individual standard was also analysed after every 10 samples to further check consistency. Each sample was analysed twice, with reproducibility better than 15% on replicate analysis. Results are presented in parts per million (ppm).

Belemnite palaeotemperatures were calculated using the equation of Anderson and Arthur (1983),

$$T = 16.0 - 4.14(\delta^{18}\text{O}_{cal} - \delta^{18}\text{O}_w) + 0.13(\delta^{18}\text{O}_{cal} - \delta^{18}\text{O}_w)^2, \quad [4.2]$$

where T is temperature in Celsius,  $\delta^{18}\text{O}_{cal}$  is the  $\delta^{18}\text{O}$  (VPDB) of belemnite calcite and  $\delta^{18}\text{O}_w$  is the oxygen isotope value (VSMOW) of ambient water. For practical purposes, this equation produces the same results as equations established for inorganically precipitated calcite over the normal range of oceanic temperatures (Sharp 2007), so assuming equilibrium precipitation of oxygen isotope values, should be appropriate for belemnite analyses.  $\delta^{18}\text{O}_w$  was assumed to be  $-1\%$ , consistent with the general lack of continental ice during the Jurassic (Rosales et al. 2004b). For details of temperatures calculated from cuttlebone aragonite, see chapter 2.

Regression statistics were calculated using Microsoft Excel. Adjusted  $r^2$  values are reported, as opposed to  $r^2$ , as large numbers of data points used lead to an artificially inflated  $r^2$ . The adjusted  $r^2$  value is automatically corrected for the number of data points used in the regression analysis.

## Results and Discussion

### Belemnite Disc Stable Isotope Distribution

The Berreraig Bay belemnite was identified as *Belemnitida Passaloteuthis* (Lissajous 1925) and has well defined “growth bands” consisting of diagenetic opaque calcite, and pyrite formation around the apical line, providing ample evidence of post burial alteration. The distribution of

stable isotope values in this sample will therefore be considered diagenetically altered.  $\delta^{13}\text{C}$  values ranged between  $-3.3$  and  $+5.9\text{‰}$  with a mean of  $1.5\text{‰}$ , with  $\delta^{18}\text{O}$  ranging between  $-13.8$  and  $+7.2\text{‰}$ , with a mean of  $-2.0\text{‰}$  (Table 1). A cross-plot revealed no significant relationship between  $\delta^{18}\text{O}$  and  $\delta^{13}\text{C}$  ( $r^2_{\text{adj}} = 0.006$ ,  $p = 0.46$ ; Fig. 6a). Although  $\delta^{18}\text{O}$  and  $\delta^{13}\text{C}$  values do not covary, there are some extremely negative  $\delta^{18}\text{O}$  values, as well as many outliers in both positive and negative directions which may be suggestive of diagenetic alteration. With the exception of the upper left corner of the isotope map, which is coincident with a small fracture, there is a generally concentric distribution of both  $\delta^{18}\text{O}$  and  $\delta^{13}\text{C}$  values (Fig. 7).  $\delta^{18}\text{O}$  values tend to vary in a radial pattern around the apical line and  $\delta^{13}\text{C}$  values tend to vary in a radial pattern around the spatial centre of the disc (Fig. 7).  $\delta^{18}\text{O}$  values are extreme near the apical line, where pyrite was observed, and progress from negative to positive with increasing distance from the centre. In contrast,  $\delta^{13}\text{C}$  values show a positive-negative-positive cycle from the centre outwards, which may be explained by differential diagenesis of the rostrum, with dissolution and replacement occurring preferentially in zones of increased permeability. These zones may have originally been related to ontogeny, with changing growth rates influencing the permeability of the secreted calcite, and hence varying the preservation potential within the rostrum. Diagenetic fluids may have permeated the rostrum from the outside edge and/or apical line. Such replacement and/or alteration processes would result in a broadly concentric pattern of stable isotope values in belemnite calcite. This rostrum (Fig. 7) demonstrates that concentricity and apparently cyclic variability in stable isotope values can be preserved in heavily altered belemnite rostra, and should not be used as an indicator of preservation, supporting Longinelli's assertions (1969).

The Albertan Bighorn Creek rostra was identified as Belemnitida *Belemnopsis* (Lissajous 1925) and contains no pronounced "growth line" pattern. It appears to be composed solely of calcite and, as such, is visually better preserved than the *Passaloteuthis* from Berreraig Bay.  $\delta^{13}\text{C}$  values range between  $+0.6$  and  $+2.3\text{‰}$ , with a mean of  $+1.9\text{‰}$ .  $\delta^{18}\text{O}$  values range between  $-1.9$  and  $-8.5\text{‰}$ , with a mean of  $-4.9\text{‰}$  (Table 1). A cross-plot showed no significant correlation between  $\delta^{13}\text{C}$  and  $\delta^{18}\text{O}$  in disc 1, with 4 samples plotting outside a central cluster ( $r^2_{\text{adj}} = 0.076$ ,  $p = 0.034$ ; Fig. 6b). Disc 2 also shows no significant correlation ( $r^2_{\text{adj}} = 0.01$ ,  $p = 0.517$ ; Fig. 6c) with only one outlier. In contrast, Disc 3 exhibits a significant correlation between  $\delta^{13}\text{C}$  and  $\delta^{18}\text{O}$  ( $r^2_{\text{adj}} = 0.40$ ,  $p < 0.001$ ; Fig. 6d) with no discernable central cluster. Disc 3 also contains the most extreme values, which may indicate that this sample has experienced the greatest amount of diagenetic alteration of any of the discs. Each of the three discs exhibits some degree of concentricity in  $\delta^{18}\text{O}$ , but less concentricity in  $\delta^{13}\text{C}$ , with disc 2 exhibiting almost no central pattern at all (Fig. 8). As with the Berreraig Bay belemnite,

$\delta^{18}\text{O}$  values tend to vary in a radial pattern around the apical line, with the exception of disc 2. Concentricity is observed in disc 2, but it varies around the spatial centre of the disc, not the apical line.

The three Bighorn Creek *Belemnopsis* discs (Fig. 8) generally show more positive  $\delta^{18}\text{O}$  and  $\delta^{13}\text{C}$  values in the centre, and more negative values near the outer rim. As we have information as to the location within the rostrum from which each disc was taken, these discs were modelled in three dimensions to examine the longitudinal continuity of the patterns, with the modelling software displaying stable isotope values along the z-axis (Fig. 9). The fit between each disc revealed that the isotopic variability observed in each disc was continuous along the length of the belemnite.

While the concentric manner in which the isotope values of these belemnites vary is interesting, this sampling technique provides inadequate resolution to obtain a detailed record of geochemical variation with growth. In addition, the lack of diagenetic screening means that it is not possible to discuss the meaning of these stable isotope distributions with any certainty. For example, the Bearreraig Bay belemnite, which is diagenetically altered, demonstrates that symmetry in two stable isotope profiles and/or concentricity are not necessarily indicators that pristine geochemical values have been preserved, as similar effects may be produced by differential diagenesis. Thus, if undetected, diagenesis will render apparently “reasonable” average values for  $\delta^{13}\text{C}$  and  $\delta^{18}\text{O}$  meaningless, as shown in the above rostra discs. The Bighorn Creek rostrum demonstrates that the same might also be true of longitudinal geochemical trends.

#### Carbondale River Belemnites

Following examination of the previously discussed rostrum discs, it was decided that ontogenetic information could be extracted more economically by sampling for stable isotope and trace element analysis at high resolution along a radial profile from the apical line to the outer edge (Fig. 5b), sampling the entire lifespan of the organism. Isotopic profiles are presented for nine Carbondale River belemnites. Stratigraphic heights are presented as centimetres below the contact between the Green Beds and the overlying Passage Beds. Belemnites CRB1 and CRB2 were collected 15cm below the contact (Fig. 10), CRB 26, CRB 29 and CRB 31 from 750cm below the contact (Fig. 11), and finally CRB 40, CRB 48, CRB 51 and CRB 57 from 1100 cm below the contact (Fig. 12). CRB 2, CRB 40, CRB 51 and CRB 57 were identified as the genus *Belemnitida Pachyteuthis* with CRB 1, CRB 26, CRB 29, CRB 31 and CRB 48 identified as *Belemnitida Cyllindroteuthis* (Doyle 2008, personal communication; Lissajous 1925). As several belemnites were collected from each of the discrete horizons, inter bed variability may be assessed.

As previously illustrated, diagenesis is not easily detected by stable isotope distribution and may bias environmental interpretations of the geochemistry of preserved structures. Prior to diagenetic screening, stable isotope values for these belemnites range between +1.0 and +4.3‰ for all  $\delta^{13}\text{C}$  values, with a mean of +3.1‰, with all  $\delta^{18}\text{O}$  values ranging between -5.4 and +2.0‰ with a mean of -0.3‰. Carbon and oxygen isotope values exhibit an increasing trend from apical line to the outer edge in every Carbondale River rostrum presented. There is a small, statistically significant correlation between  $\delta^{13}\text{C}$  and  $\delta^{18}\text{O}$  ( $r^2_{\text{adj}} = 0.11$ ,  $p < 0.0001$ ). When plotted according to individual beds, a cross plot between  $\delta^{18}\text{O}$  and  $\delta^{13}\text{C}$  from the 15cm horizon exhibits a statistically significant positive correlation between  $\delta^{13}\text{C}$  and  $\delta^{18}\text{O}$  ( $r^2_{\text{adj}} = 0.32$ ,  $p < 0.0001$ ; Fig. 11a). The 750cm horizon also showed a statistically significant positive correlation ( $r^2_{\text{adj}} = 0.22$ ,  $p < 0.001$ ; Fig. 11b). The 1100cm horizon displays no statistically significant correlation between  $\delta^{13}\text{C}$  and  $\delta^{18}\text{O}$  ( $r^2_{\text{adj}} = 0.02$ ,  $p = 0.914$ ; Fig. 13c).

Trace element abundances for these belemnites show significant variation. For all Carbondale River belemnites, Ba values vary between 2 and 3210ppm, with a mean of 134 ppm, with most of the variation in the form of isolated peaks on otherwise low values. Mg values vary between 213 and 5239ppm, averaging 1181 ppm and, with the exception of CRB 29, generally show reduced values with ontogeny. Mn concentration varies between 5 and 541ppm, with a mean of 108 ppm. Like Ba values, Mn concentrations tend to be low with occasional peaks, with the exception of CRB 57, CRB51 and CRB 48, which are all more elevated. Finally, Sr values range between 173 and 3330ppm, with a mean of 927 ppm, and with the exception of CRB 29 are almost unchanged with ontogeny.

### Diagenetic Screening

As diagenetic fluids tend to have high concentrations of Fe and Mn and low concentrations of Sr (Veizer 1983), previous literature has used various concentrations of these elements to detect, and eliminate, diagenesis. In the current study, Fe was not measured as the samples were drilled using a carbide steel bit which may have contaminated the rostrum carbonate through bit wear. In addition argon-argon compounds in the plasma have the same mass as Fe, adding further uncertainty. Samples with Mn >150ppm and/or Sr <800, which are the upper and lower values in modern bivalves observed respectively (Steuber 1999), will be regarded as recrystallised, and not reflecting primary environmental or biological conditions. Consequently, Samples that fail these standards were excluded from environmental interpretation.

Based on the trace element screening process, some sections of CRB1 and the first 2 samples of CRB2 from the 15cm horizon have been removed

from discussion, which eliminated some high Ba and negative  $\delta^{18}\text{O}$  values. The left most portion of CRB29, from 750cm horizon, is either markedly above 150ppm Mn or below 800ppm Sr. CRB48, CRB51, and CRB57 from the 1100cm horizon are almost exclusively diagenetic, along with one sample from CRB40, which does not appear to correlate with any extreme values (Fig. 12). The peaks in Mn observed in CRB48, CRB51, and CRB57 tend to correlate with negative  $\delta^{13}\text{C}$  values, but not with negative  $\delta^{18}\text{O}$  values (Fig. 12). This is unusual as  $\delta^{18}\text{O}$  values are typically considered more susceptible to diagenesis than  $\delta^{13}\text{C}$  values because oxygen is more readily exchanged with any fluids present and because there is much less carbon in diagenetic fluids for exchange (Veizer 1983).

In total, of the 155 stable isotope and 122 trace element measurements originally taken, only 81 and 60 measurements respectively survive the trace element screening (Table 2). Revised profiles for these rostra are presented in Fig. 14, 15 and 16.  $\delta^{18}\text{O}$  values now range between -6.9 and 1.2‰, with a mean of -1.1 ‰, with calculated palaeotemperature ranging between 7 and 45°C, with a mean temperature of 17 °C.  $\delta^{13}\text{C}$  values range between -1.3 and 4.6‰, with a mean of 2.3‰. Further discussion is based on this diagenetically-screened data only.

#### Oxygen Isotope Values

Oxygen isotope values typically increase with ontogeny (Fig. 14, 15 and 15). Although undulations in the geochemical profiles exist, no clear seasonal pattern in  $\delta^{18}\text{O}$  values can be discerned. This was unexpected as the seasonal cycle was so prevalent in cuttlebone  $\delta^{18}\text{O}$  values (see chapter 2). The absence of the pattern may stem from a resolution problem (as noted in several older studies (Urey et al. 1951, Lowenstam and Epstein 1954, Bowen 1961a, Bowen 1961b). These belemnites have <30mm between the apical line and the outer edge of the rostrum, compared with the 80+ lamellae within single cuttlebone. As most cephalopods live ~ 2 years (Boyle 1983), the sample resolution is necessarily much lower in the belemnite rostra. Thus the detail lost as a consequence of sampling resolution in the belemnite rostra may mask part of a seasonal signal, as a single belemnite sample has been averaged over a longer time than a single cuttlebone lamella. However, assuming a 2 year belemnite lifespan, the temporal resolution documented here would consist of several samples per annum (the exact number would vary with the diameter of the rostrum), so some seasonality would be expected, unless these sediments represent a tropical climate, where seasonal temperature variability would be limited or nonexistent. However, this is inconsistent with the palaeolatitude of southern Alberta, and so may be excluded as a possibility (Gradstein et al. 2004, Scotese 1997).

Assuming that the lack of seasonal patterns is a real phenomenon rather than an artefact of sampling or lifespan the general rise in  $\delta^{18}\text{O}$  values may be explained by a short life span: If these belemnites hatched in summer and only lived to be 6 months old, this would show a seasonal decrease in temperature before death.

An alternative explanation for a lack of preserved seasonality in individual rostra could involve species ecology: migration away from cooler waters in the winter (or warmer waters in the summer) would result in a roughly constant record of temperatures being preserved in the geochemical profiles of the rostra. Indeed, if migration was seasonal and of sufficient scale, a seasonal temperature signal would be virtually lost by an organism following favourable water conditions. In fact, migration, albeit on a smaller scale than than envisaged here, has been observed in the stable isotope values of cuttlefish, the best modern analogue of belemnites, in English Channel (see Chapter 2), with individuals migrating to deeper common waters for the winter months (Boucaud-Camou and Boismery 1991).

#### Carbon Isotope Values

Carbon isotope values also vary within the rostrum, with low values early in life gradually increasing through ontogeny (Fig. 14, 15 and 16). This likely reflects changes in metabolism as belemnites age. Such a trend is also observed in *S. officinalis* (see Chapter 3) and in another internal belemnite stable isotope study (Urey et al. 1951). Models of bivalve  $\delta^{13}\text{C}$  values indicate that carbon isotope values vary with metabolic rate, with high values associated with low metabolism and vice versa (Rosenberg and Hughes 1991). Interpreted in this manner, *Pachyteuthis* and *Cylindroteuthis*, like *S. officinalis*, have high metabolic rates while juvenile, which gradually decrease. CRB1 (*Cylindroteuthis*) displays a sharp decrease in  $\delta^{13}\text{C}$  values towards the end of life (Fig 12) as is also observed in some cuttlebones. This trend in *S. officinalis* has been explained by carbon isotope discrimination resulting from a spawning related increase in metabolic rate in females (Findlay et al. previous chapter). With future work and increased resolution, it may be possible to determine the sex of a reproductively mature belemnite.

#### Relationship between $\delta^{13}\text{C}$ and $\delta^{18}\text{O}$

As previously identified, a cross plot of all the diagenetically-corrected  $\delta^{13}\text{C}$  and  $\delta^{18}\text{O}$  values showed a statistically significant positive correlation ( $r^2_{\text{adj}}$  = of 0.31,  $p < 0.0001$ ). A cross plot of  $\delta^{13}\text{C}$  and  $\delta^{18}\text{O}$  from the 15cm and 750cm horizons showed a statistically significant positive correlation (15cm:  $r^2_{\text{adj}}$  = 0.29,  $p < 0.005$ , Fig. 13d; (750cm:  $r^2_{\text{adj}}$  = 0.16,  $p < 0.007$ , Fig. 13e). The 1100cm horizons showed no statistically significant correlation between  $\delta^{13}\text{C}$

and  $\delta^{18}\text{O}$  ( $r^2_{\text{adj}} = -0.01$ ,  $p = 0.381$ , Fig. 13f). Positive correlations between  $\delta^{13}\text{C}$  and  $\delta^{18}\text{O}$  values in pristine calcite are characteristic of brackish conditions, as meteoric water  $\delta^{13}\text{C}$  and  $\delta^{18}\text{O}$  values are low due to evaporation and the influence of terrestrial plants on DIC  $\delta^{13}\text{C}$  values. As the trace element concentrations of these specimens show no detectable signs of diagenesis, these data suggest that these specimens occupied areas which were significantly influenced by meteoric runoff during the deposition of the 15 and 750 cm horizons. The presence of meteoric water may explain the anomalously high (45 °C) palaeotemperature values.

### Trace Element Concentrations

As more material was required for trace element analysis these profiles are lower resolution than the accompanying stable isotope profiles. This is problematic as it permits only visual comparison and no reliable means for statistically comparing trace element concentrations with coeval stable isotope values. As a result, no correlation coefficients or other statistical measures will be quoted for belemnite trace element values. For all of the screened data, Mg concentrations range between 5239 and 390 ppm, with a mean value of 1252 ppm, with Ba concentrations ranging between 3210 and 2 ppm, with a mean value of 146 ppm.

As with Sr concentrations in *S. officinalis*, Mg concentrations in the belemnites generally show similar trends to those observed for the associated  $\delta^{18}\text{O}$  values (with the exception of CRB29, which shows a Mg peak midlife). This implies that in belemnite rostra, Mg concentrations are in some way influenced by temperature, as temperature is the primary control on  $\delta^{18}\text{O}$  composition (Anderson and Arthur 1983, McArthur et al. 2007, Hendry et al. 2001 and many others). Assuming that temperature is the underlying cause of the analogous parallel trends in  $\delta^{18}\text{O}$  and Mg, a divergence in  $\delta^{18}\text{O}$  value from Mg concentration could be interpreted as the increased influence of meteoric water, since Mg varies little with salinity compared to  $\delta^{18}\text{O}$  under normal marine and estuarine conditions (Klein et al. 1996). This being the case, CRB26, CRB29 and CRB40 likely hatched in meteorically influenced water, before moving to more open sea conditions, consistent with the positive correlation between  $\delta^{18}\text{O}$  and  $\delta^{13}\text{C}$  values. Notably, there is no discernable seasonal cycle in Mg, which may be explained by migratory behaviour or short lifespan, as discussed for  $\delta^{18}\text{O}$ , above. A more detailed analysis of the correlation between Mg and  $\delta^{18}\text{O}$  will be carried out in Chapter 5, when  $\delta^{18}\text{O}$  values and Mg abundance from the same sample are analysed.

Ba values are generally low, with occasional peaks in individual profiles. Background Ba values should be proportional to seawater Ba levels (Gillikin et al. 2006). Putten et al. (2000) noted that Ba concentration

increased during algal blooms in mussel shells, which was associated with a decrease in  $\delta^{13}\text{C}$  value. Since no analogous relationship between Ba and  $\delta^{13}\text{C}$  was observed in the belemnites analysed here, Ba concentrations are unlikely to be related to upwelling and any consequent algal bloom. An alternate source of Ba is runoff (Hendry et al. 2001, Gillikin et al. 2006), suggesting that these belemnites may have swam into an estuary or otherwise restricted basin for a short period of time during their lives. Such a migration into fresh water would result in a meteoric water signal in coeval  $\delta^{18}\text{O}$  and Mg values. However, an increase in background Ba coincident with a meteoric Mg/ $\delta^{18}\text{O}$  signal is not observed in these specimens. Peaks in Ba values have also been observed in modern mussel calcite (Gillikin et al. 2006) and, to some extent, in cuttlebone aragonite (see Chapter 3). Notably, the Ba peaks in belemnite calcite are also far higher than those observed in modern carbonate. The origin of these peaks is poorly understood as their magnitude far exceeds what may reasonably be expected in seawater (Bruland and Lohan 2004). It has been suggested that these peaks are related the filter feeding mussel ingesting the occasional suspended barite grain, but the sudden ingestion of large amounts of barite seems unlikely in an active carnivore, as they are unlikely to take Ba directly from seawater as in mussels (Gillikin et al. 2006). Alternatively, the peaks may stem from laboratory contamination. However, the peaks are present upon replicate analyses and in diverse specimens from different taxa analysed by many different laboratories (Gillikin et al. 2006, Carre et al. 2006). Consequently, the peaks are unlikely to result from analytical errors and the underlying cause of the Ba peaks remains elusive at this time.

#### Inter bed variability

Every rostrum sampled from Carbondale River shows gradual changes in stable isotope values with ontogeny. The 15 and 750cm horizons (Fig. 14 and 15 respectively) show similar values and trends in both  $\delta^{18}\text{O}$  and  $\delta^{13}\text{C}$  for each belemnite. The geochemical similarity between individual belemnites, all of which were well-preserved, suggests that they record similar information about the environmental conditions during their life span. The similarity in values within the individual beds is consistent with that observed in wild examples of modern *S. officinalis* (see Chapter 2) and, as with modern *S. officinalis*, well-preserved belemnites appear to record environmental geochemical signals. In addition, the geochemical variability exhibited between genera (i.e. CRB 1 *Cylindroteuthis* and CRB 2. *Pachyteuthis*, Fig. 14) appears to be similar to the geochemical variability within the same genus. Although the admittedly limited nature of the dataset comparing the geochemistry of the two genera does not allow firm conclusions to be drawn, the similarity in within- and between-genera variability suggests that the two genera may have exhibited similar behaviour when occupying the same

environment. It would be interesting to examine this further using a larger data set.

### Belemnite Sampling Strategy

The belemnite geochemical record displays ~3 ‰ variability in both the carbon and oxygen isotope signals through geologic time (Veizer et al. 1999, McArthur et al. 2007), which is similar in magnitude to the variation observed in the individual rostra discussed here. This variability across the geological record, which has been shown not to result from short-term environmental variability (McArthur et al. 2007), may obscure the interpretation of palaeoenvironmental trends and demands resolution. One possible explanation is that the variability observed in geological record results from variability in the internal geochemistry of individuals, in combination with inadequate sampling of such internal variability. Indeed, this paper shows that  $\delta^{13}\text{C}$ ,  $\delta^{18}\text{O}$  and trace element values can vary with ontogeny, perhaps reflecting changes with environment and biology. Consequently, it would be prudent to explicitly account for such variation while sampling. Therefore two sampling techniques are evaluated to account for the internal variability in rostra geochemistry, depending on the nature and goals of the study at hand.

First, if the aim of the study is to extract ontogenetic variation, then high resolution sampling radially from the apical line to the outer edge of a longitudinally section of a well preserved rostra will provide the required data (Fig. 5b). A diagenetic screening process applied to such a sampling strategy would allow the exclusion of small scale alteration in an otherwise well preserved rostrum. In principle, and with improved understanding of their incorporation into belemnite calcite, high resolution sampling of biogenic carbonate may allow the extraction of information about the biology of the organism (through the metabolic effect on  $\delta^{13}\text{C}$  values with ontogeny), water temperature (through the examination of  $\delta^{18}\text{O}$  values), migration (through trends in  $\delta^{18}\text{O}$  values and possibly Mg concentration with ontogeny), the relative influence of meteoric water input into seawater (through a decoupling of the  $\delta^{18}\text{O}$  value and Mg concentration signals) and possibly the individual's sex (decrease in  $\delta^{13}\text{C}$  values towards the end of life). However, such high resolution sampling is both expensive and time consuming and may not always be feasible. In such cases, the second method may be more practical.

The second method, which was first employed by Urey et al (1951), involves grinding powder evenly across the growth axis, avoiding problem areas such as the apical line and the outer rim which commonly contain secondary calcite. This method has the advantage of requiring only one sample per belemnite, while achieving a close approximation of a lifetime average. This method is preferable to crushing the entire rostrum and sampling the

resulting powder for geochemical investigation, as this would be biased towards late life values, as the outer layers of the rostrum contain more calcite. In addition, isotopic values and trace element concentrations obtained by crushing an entire rostrum are more likely to be contaminated by diagenesis as small problem areas can not be identified. Thus when only one sample can be obtained from an individual, as is common in the literature (Bailey et al. 2003, McArthur et al. 2004, Pirrie et al. 2004, Price and Mutterlose 2004, Rosales et al. 2004a, Wierzbowski 2004, van de Schootbrugge, B. et al. 2005), the method employed by Urey et al. (1951) is preferable.

However, although this method is certainly better than crushing the rostrum as a whole or conducting random sampling within a rostrum, it will still result in some sample bias in the belemnite geochemical signal over geologic time due to differences in hatching times and life span between individuals. For example, the geochemical information obtained from a belemnite hatching in early summer and dying the following summer will be skewed towards summer values. Similarly, a longer lived belemnite may record two winter periods, and may exhibit values skewed in that direction as a result. The high resolution method circumvents this problem and is preferred as it provides much more information and reduces sample bias.

## Conclusions

1. Similar to *Sepia officinalis* cuttlebones, belemnite rostra show chemical inhomogeneity, with variation on the order of several per mill observed in belemnite  $\delta^{13}\text{C}$  and  $\delta^{18}\text{O}$  values and wide variations in the concentrations of Ba and Mg.
2. Belemnites do not show obvious seasonality in  $\delta^{18}\text{O}$  values, contrasting with *S. officinalis*, which may result from migration masking a seasonal signal, or short lifespan.
3.  $\delta^{13}\text{C}$  values increase with ontogeny, suggesting a decrease in metabolic rate with age. This parallels observations from *S. officinalis*, suggesting similar biology
4. Despite the internal variability observed within individual rostra, there is limited intra-bed variation among belemnites collected from the same horizon, implying that coeval belemnites record the same geochemical signals. Such correlation among individuals provides evidence that belemnites are useful tools for the reconstruction of palaeoenvironmental information.
5. The variability in the geochemical signal previously evident in the belemnite record may be influenced by inadequate sampling of belemnite calcite. To minimise the effect of this internal inhomogeneity on the geochemical record, future analysis should either sample at high resolution from the apical line to the outer edge of the rostrum, or grind sample powder evenly along the growth axis. The high resolution approach is preferred under most circumstances.

## Figure Captions

Fig. 1. The phylogenetic family tree of known Coleoidea. Of special note in this paper are Belemnitida and Diplobella, which are members of Belemnoidea, and Sepiida which contains the modern cuttlefish. Modified from Doyle et al. (1994).

Fig. 2. Morphology of the hard parts commonly preserved for a) an idealised belemnite specimen and b) a typical *Sepia* specimen. The rostrum of belemnite may have been condensed into the spine of modern *Sepia*. Note common chambered phragmocone which are both composed of layered aragonite structures.

Fig. 3. Simplified geologic map of the Isle of Skye, U.K. showing the collection site of one of the analysed rostra.

Fig. 4. Simplified geologic map of southern Alberta, Canada, showing the location of the Bighorn Creek and Carbondale River collection sites.

Fig. 5. a) The grid sampling strategy used when collecting samples on each of the belemnite discs. b) Longitudinal sampling strategy along the axis of maximum growth in a belemnite rostrum.

Fig. 6.  $\delta^{13}\text{C}$  vs  $\delta^{18}\text{O}$  cross plots from belemnite discs. a) Scottish belemnite cut 5mm from the aviolis b) Disc 1 of a Belemnite collected from Big Horn Creek, Alberta, Canada cut 22mm from aviolis c) disc 2, cut at 36mm from the aviolis, and d) disc 3 cut at 52mm from the aviolis.

Fig. 7. Stable isotope maps of a disc cut from a diagenetically altered belemnite rostrum collected from Bay, Isle of Skye, Scotland. This rostrum is characterised by well refined bands of opaque calcite and pyrite precipitated at the apical line. This shows that diagenetically altered belemnites may still show several per mil variation and concentric stable isotope values.

Fig. 8. Stable isotope maps of sections from a Bajocian Wilson Creek belemnite from Alberta, Canada showing  $\delta^{13}\text{C}$  value variation (left) and  $\delta^{18}\text{O}$  value variation (right) a) and b) are from near the phragmocone; c) and d) from near the middle of the rostrum; and e) and f) near the apex. Note the offsets in the concentric pattern between  $\delta^{13}\text{C}$  and  $\delta^{18}\text{O}$  values. This belemnite did not exhibit the signs of alteration identified in the Scottish belemnite, but still may be altered. A more stringent screening process for diagenesis is required.

Fig. 9. Three dimensional model of interior  $\delta^{18}\text{O}$  and  $\delta^{13}\text{C}$  value variation within a single Bighorn Creek belemnite rostra.

Fig. 10. All stable isotope and trace element profiles from belemnites collected from the 15cm horizon of the Green Beds section, Southern Alberta, Canada. The oxygen isotope axis is inverted for the interpretation of temperature change.

Fig. 11. All stable isotope and trace element profiles from belemnites collected from the 750cm horizon of the Green Beds section, Southern Alberta, Canada. The oxygen isotope axis is inverted for the interpretation of temperature change.

Fig. 12. All stable isotope and trace element profiles from belemnites collected from the 1100cm horizon of the Green Beds section, Southern Alberta, Canada. The oxygen isotope axis is inverted for the interpretation of temperature change.

Fig. 13.  $\delta^{13}\text{C}$  vs.  $\delta^{18}\text{O}$  values of the Carbondale River Belemnites. a) 15cm horizon pre diagenetic screening. b) 750cm horizon pre diagenetic screening. c) 1100cm horizon pre diagenetic screening. d) 15cm horizon post diagenetic screening. e) 750 cm horizon post diagenetic screening. f) 1100cm horizon post diagenetic screening.

Fig. 14. Stable isotope and trace element profiles from belemnites collected from the 15cm horizon of the Green Beds section, Southern Alberta, Canada with diagenetic samples removed. The oxygen isotope axis is inverted for the interpretation of temperature change.

Fig. 15. Stable isotope and trace element profiles from belemnites collected from the 750cm horizon of the Green Beds section, Southern Alberta, Canada with diagenetic samples removed. The oxygen isotope axis is inverted to for the interpretation of temperature change.

Fig. 16. Stable isotope and trace element profiles from belemnites collected from the 1100cm horizon of the Green Beds section, Southern Alberta, Canada with diagenetic samples removed. The oxygen isotope axis is inverted for the interpretation of temperature change.



Findlay and Gröcke  
Fig 2

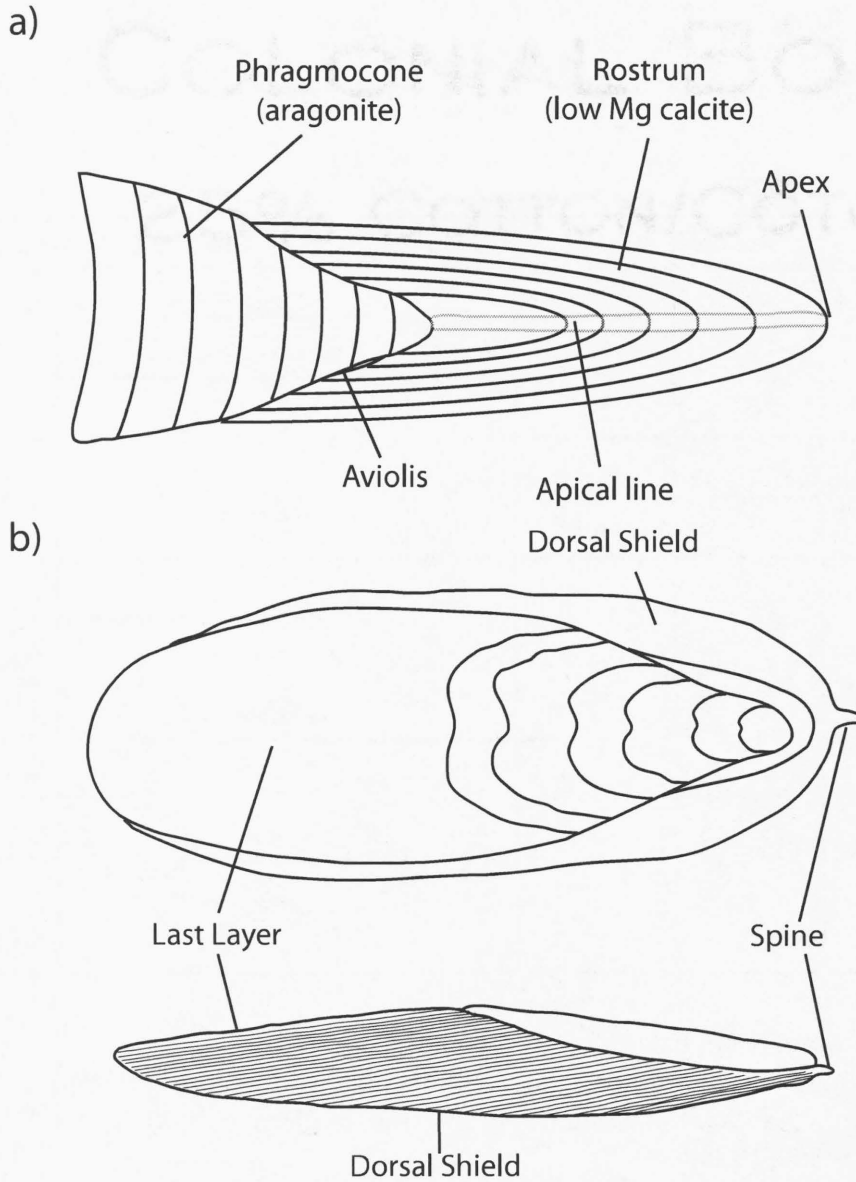


Fig. 2. Morphology of the hard parts commonly preserved for a) an idealised belemnite specimen and b) a typical *Sepia* specimen. The rostrum of belemnite may have been condensed into the spine of modern *Sepia*. Note common chambered phragmocone which are both composed of layered aragonite structures.

Findlay and Gröcke  
Fig. 3

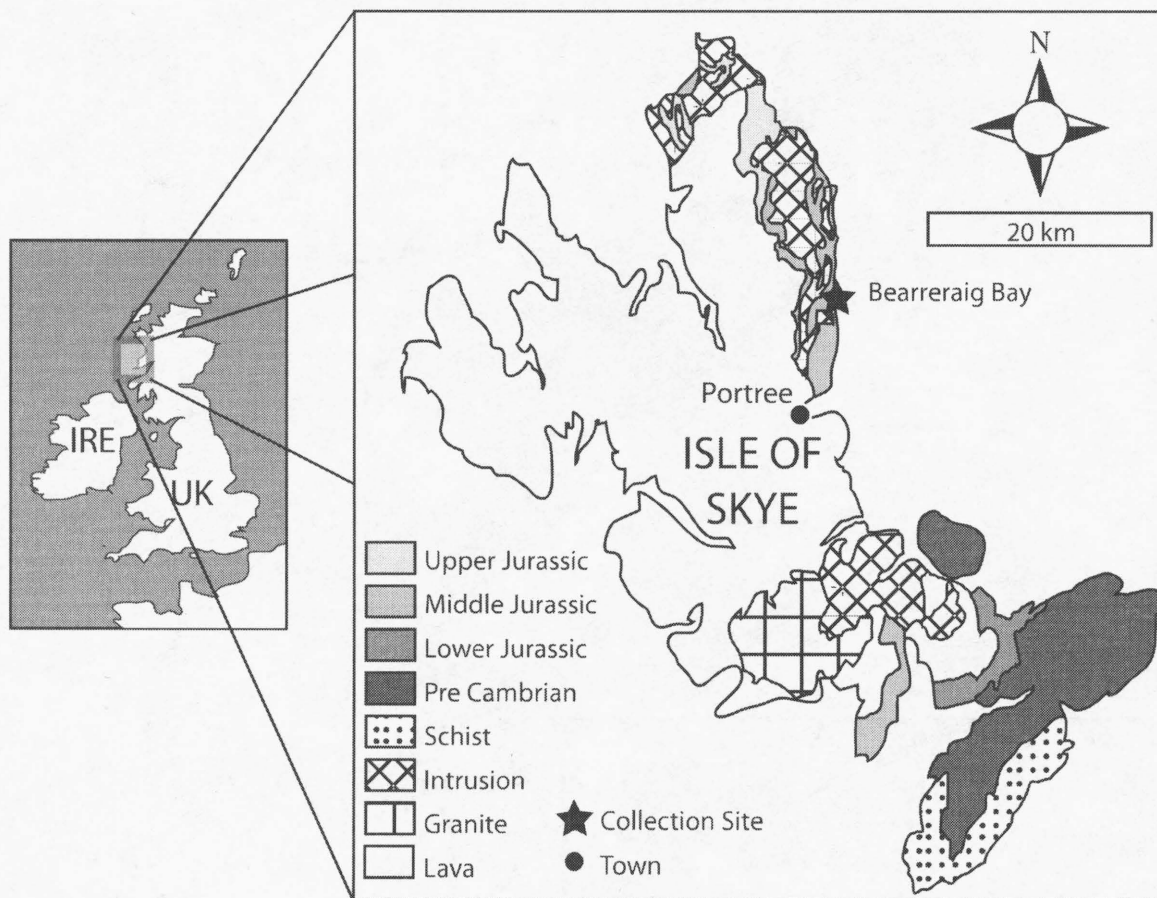


Fig. 3. Simplified geologic map of the Isle of Skye, U.K. showing the collection site of one of the analysed rostra.

Findlay and Gröcke

Fig. 4

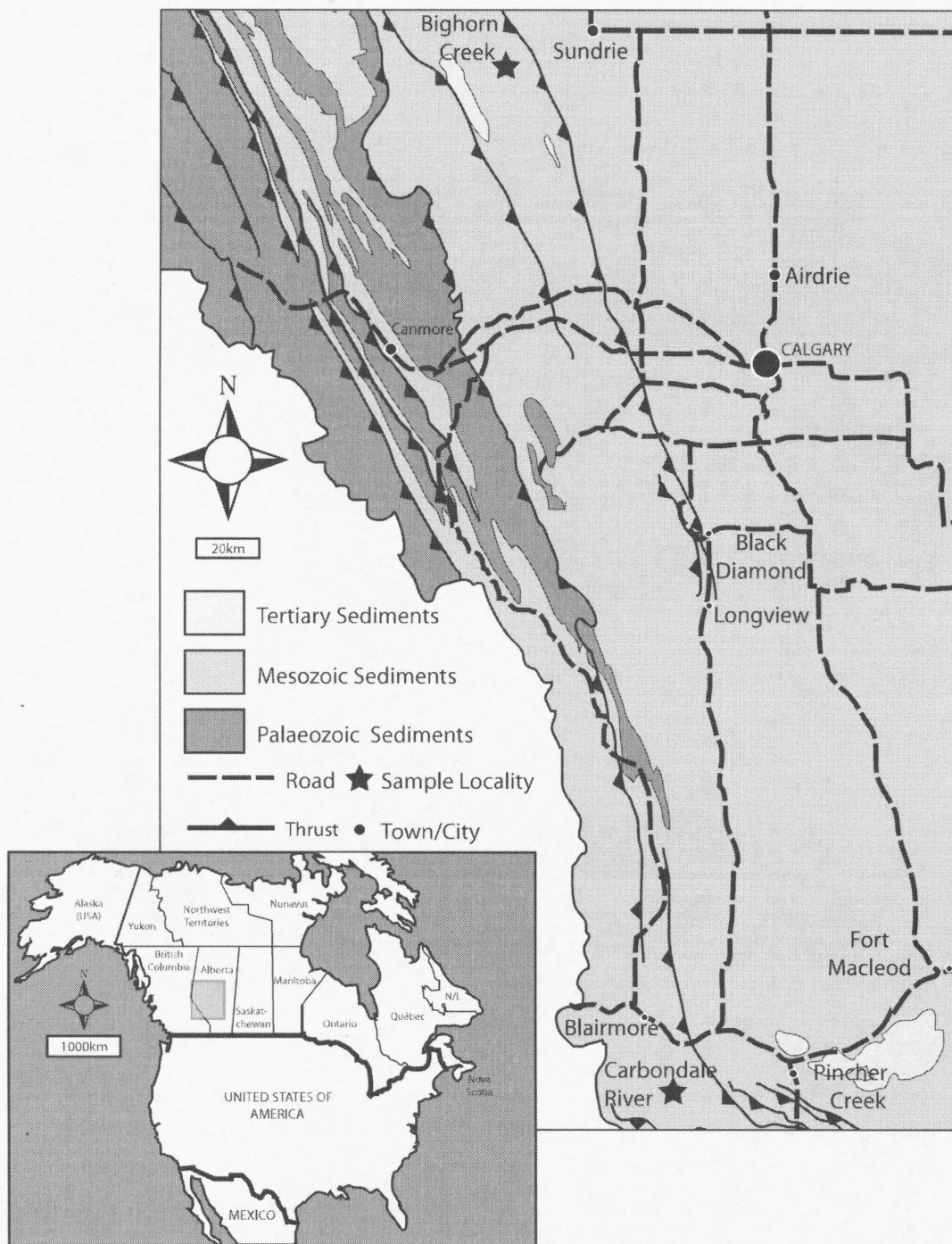


Fig. 4. Simplified geologic map of southern Alberta, Canada, showing the location of the Bighorn Creek and Carbondale River collection sites.

Findlay and Gröcke  
Fig 5

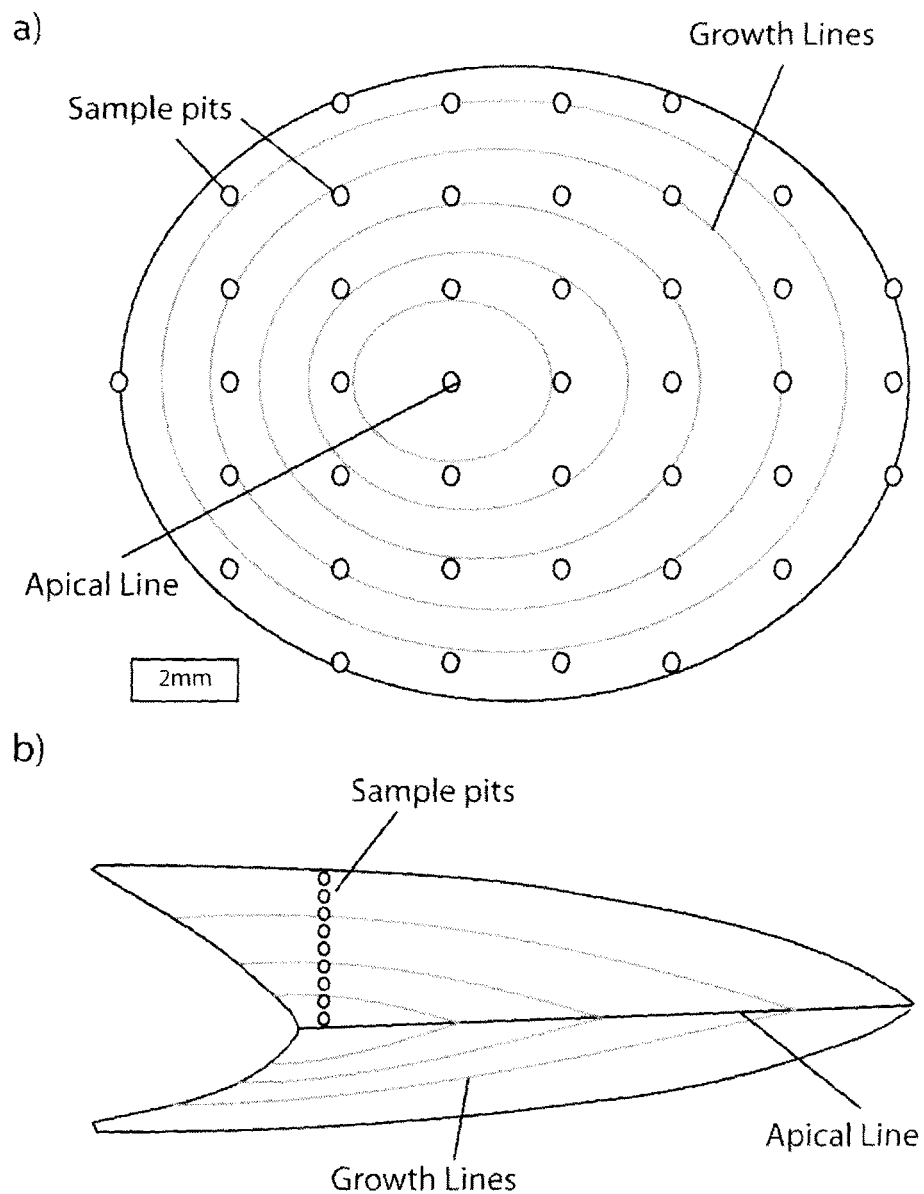


Fig 5. a) The grid sampling strategy used when collecting samples on each of the belemnite discs. b) Longitudinal sampling strategy along the axis of maximum growth in a belemnite rostrum.

Findlay and Gröcke  
Fig 6

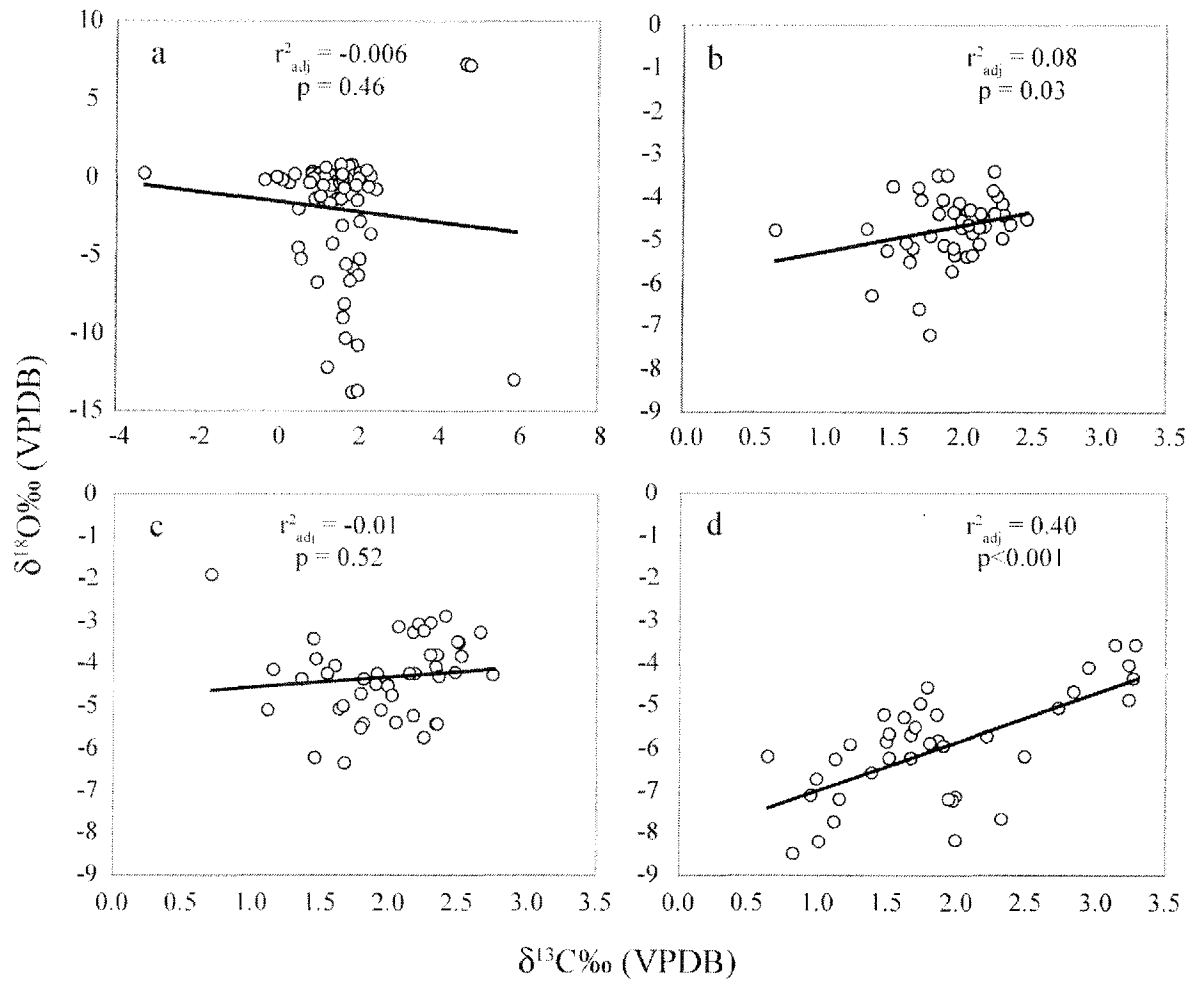


Fig 6.  $\delta^{13}\text{C}$  vs  $\delta^{18}\text{O}$  cross plots from belemnite discs. a) Scottish belemnite cut 5mm from the aviolis b) Disc 1 of a Belemnite collected from Big Horn Creek, Alberta, Canada cut 22mm from aviolis b) disc 2, cut at 36mm from the aviolis, and c) disc 3 cut at 52mm from the aviolis.

Findlay and Gröcke  
Fig 7

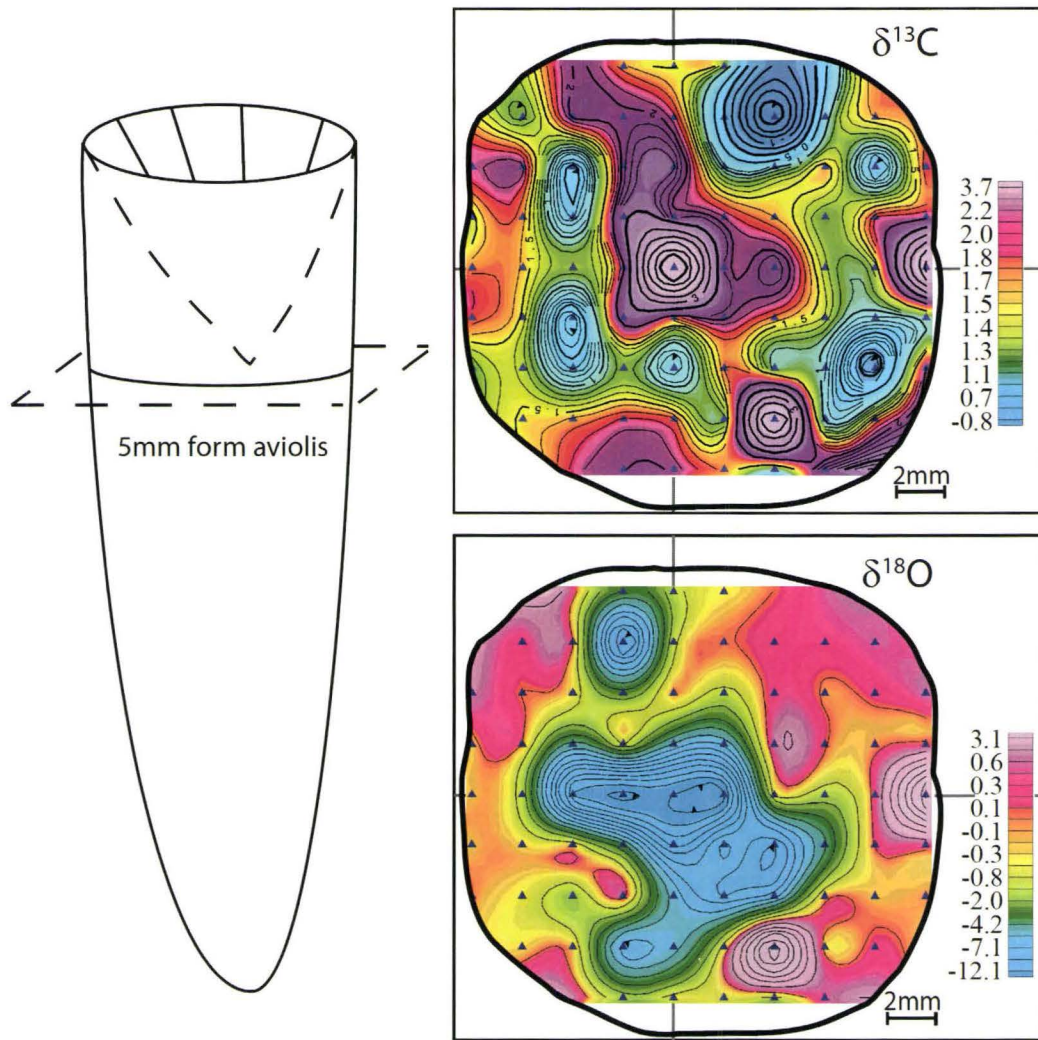


Fig. 7. Stable isotope maps of a disc cut from a diagenetically altered belemnite rostrum collected from Bay, Isle of Skye, Scotland. This rostrum is characterised by well refined bands of opaque calcite and pyrite precipitated at the apical line. This shows that diagenetically altered belemnites may still show several per mil variation and concentric stable isotope values.

Findlay and Gröcke  
Fig 8

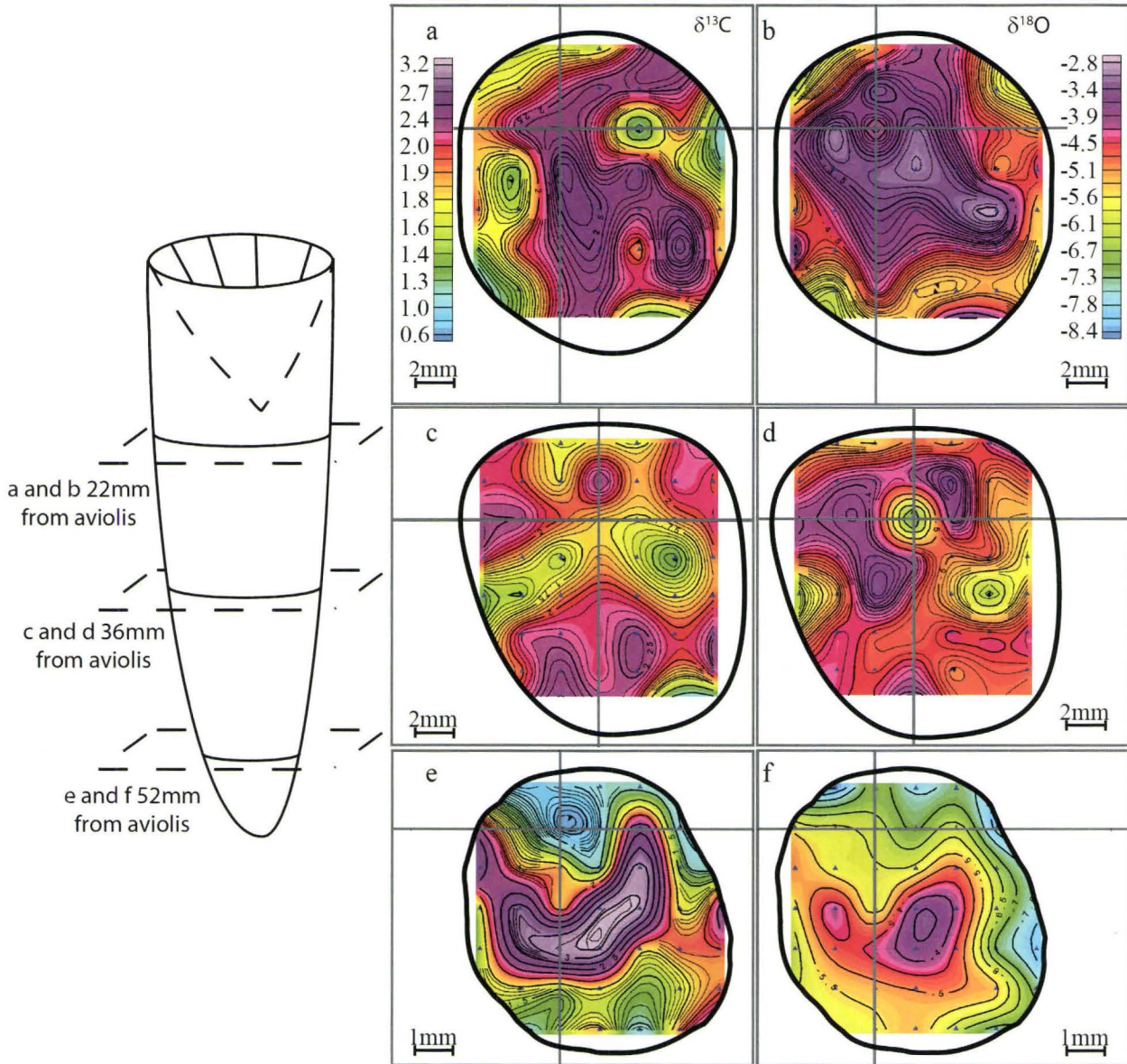


Fig. 8. Stable isotope maps of sections from a Bajocian Wilson Creek belemnite from Alberta, Canada showing  $\delta^{13}\text{C}$  value variation (left) and  $\delta^{18}\text{O}$  value variation (right) a) and b) are from near the phragmocone; c) and d) from near the middle of the rostrum; and e) and f) near the apex. Note the offsets in the concentric pattern between  $\delta^{13}\text{C}$  and  $\delta^{18}\text{O}$  values. This belemnite did not exhibit the signs of alteration identified in the Scottish belemnite, but still may be altered. A more stringent screening process for diagenesis is required.

Findlay and Gröcke  
Fig 9

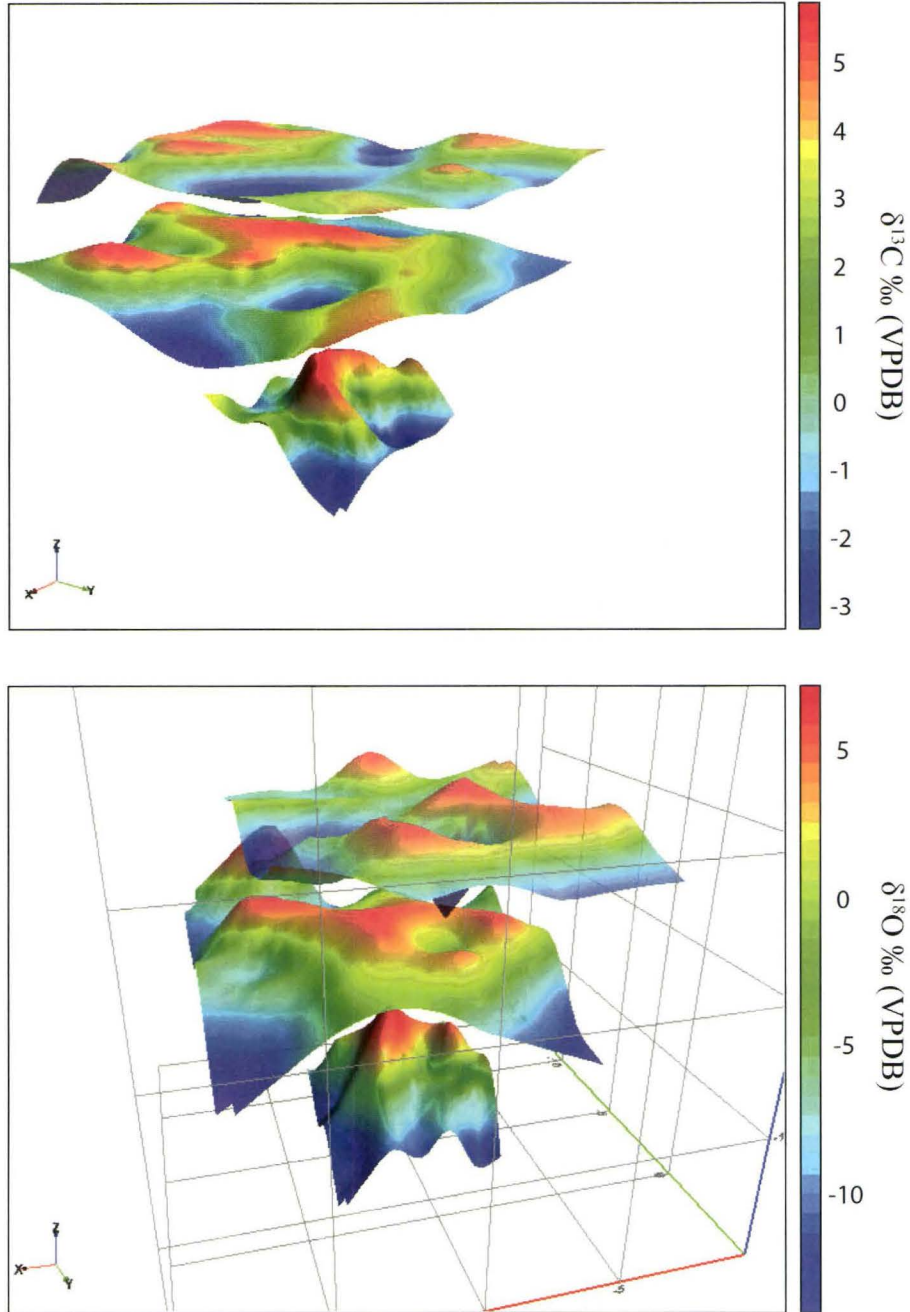


Fig. 9. Three dimensional model of interior  $\delta^{18}\text{O}$  and  $\delta^{13}\text{C}$  value variation within a single Bighorn Creek belemnite rostra.

Findlay and Gröcke  
Fig 9

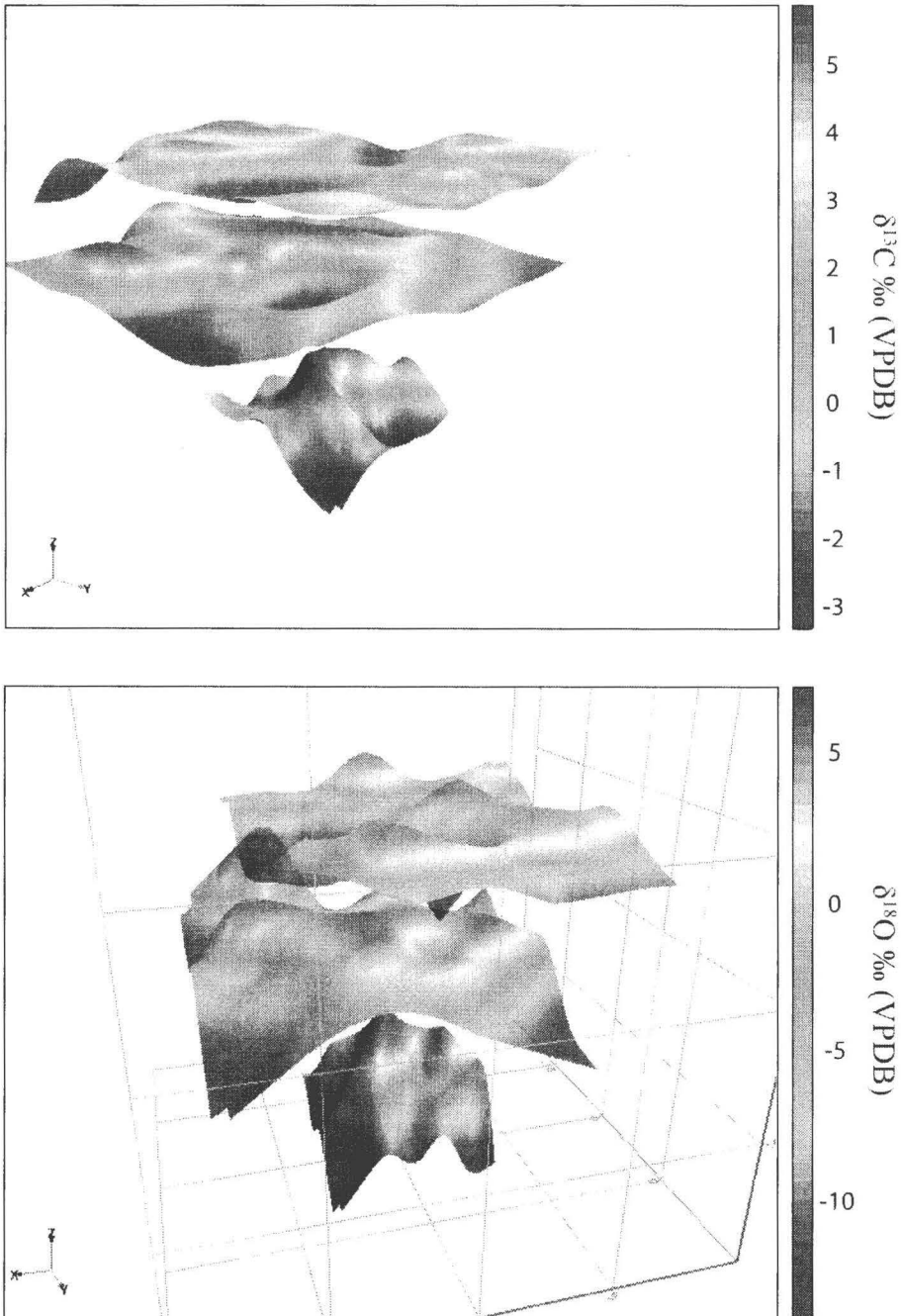


Fig. 9. Three dimensional model of interior  $\delta^{18}\text{O}$  and  $\delta^{13}\text{C}$  value variation within a single Bighorn Creek belemnite rostra.

Findlay and Gröcke  
 Fig 10

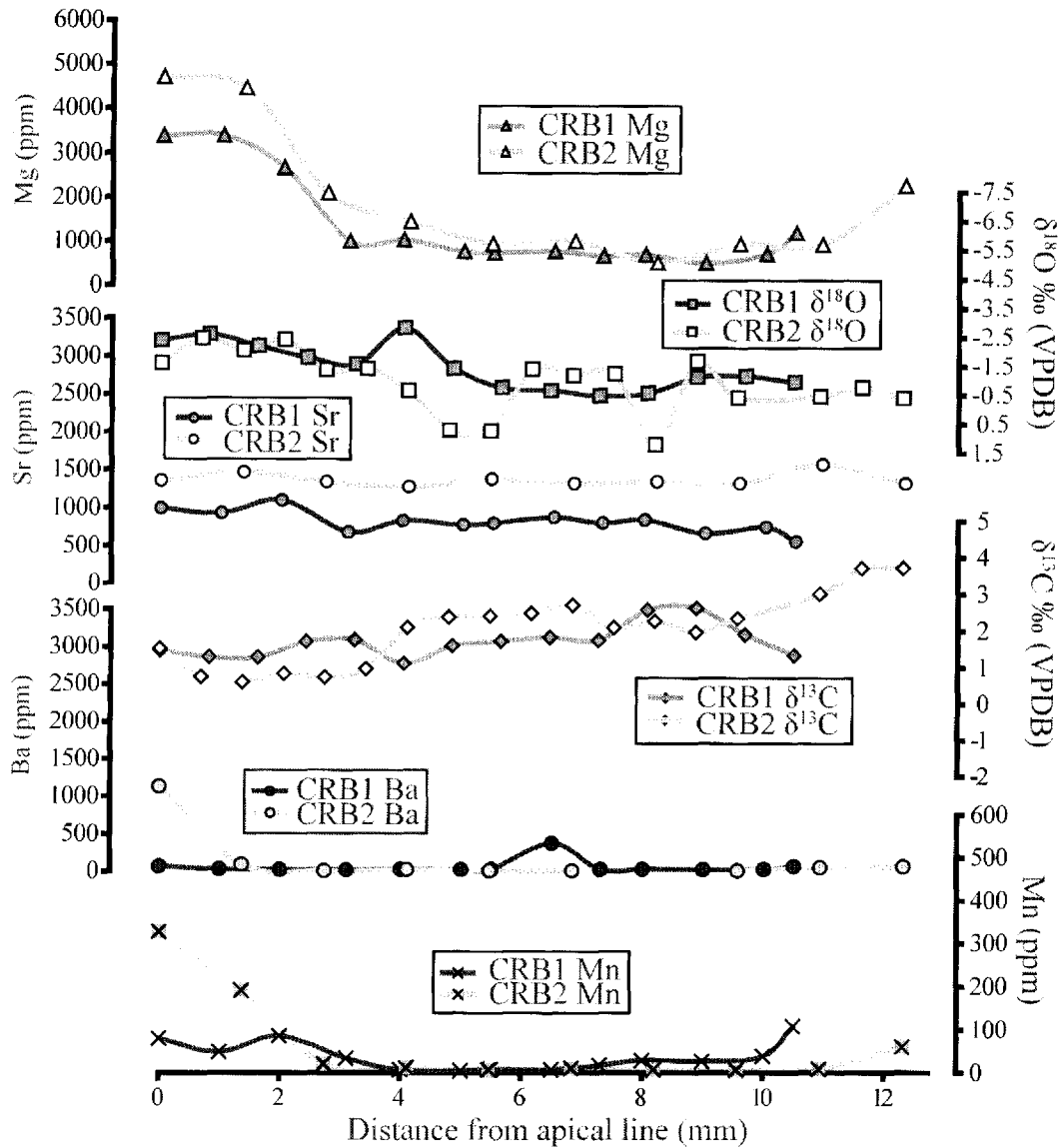


Fig. 10 All stable isotope and trace element profiles from belemnites collected from the 15cm horizon of the Green Beds section, Southern Alberta, Canada. The oxygen isotope axis is inverted for the interpretation of temperature change.

Findlay and Gröcke  
Fig 11

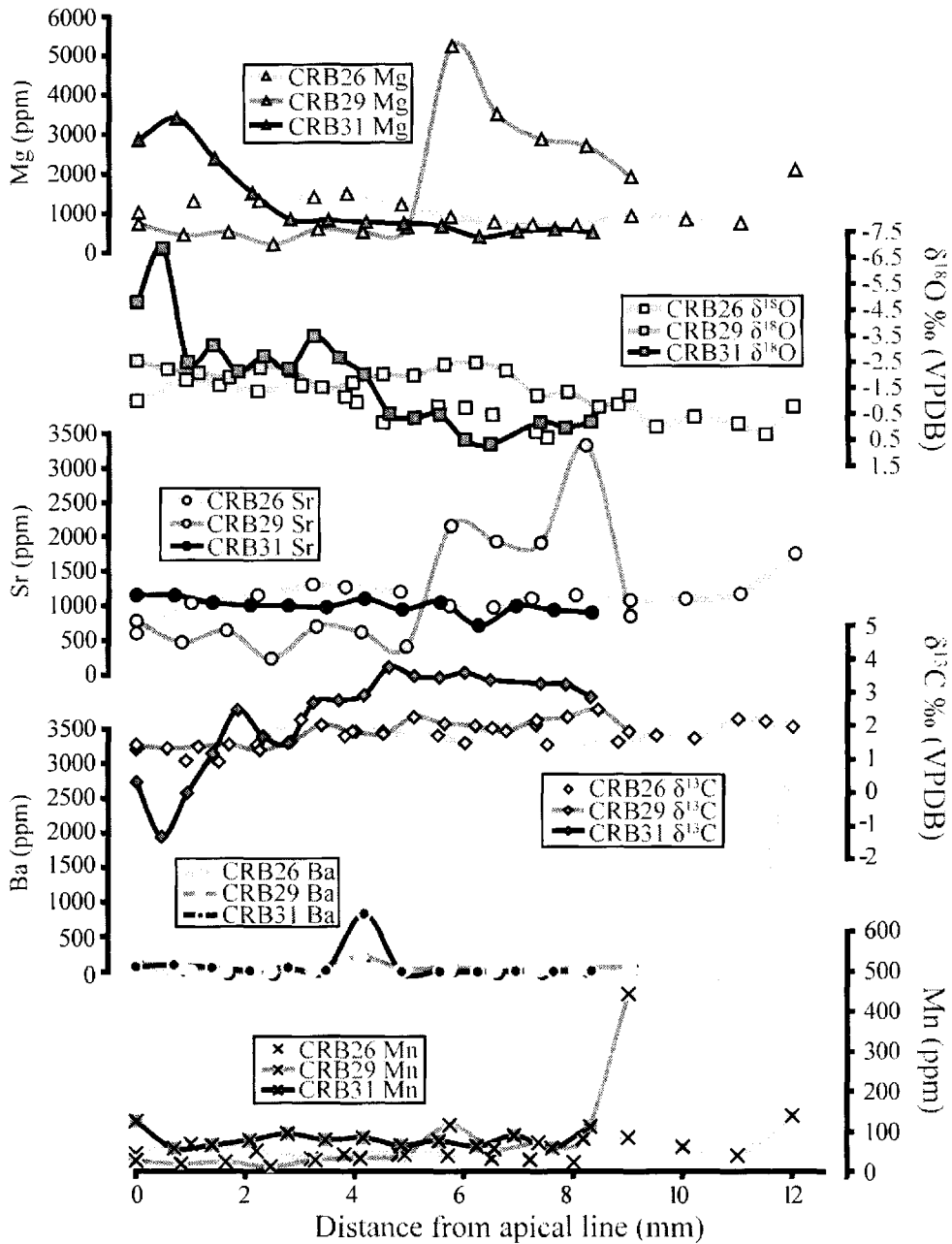


Fig. 11 All stable isotope and trace element profiles from belemnites collected from the 750cm horizon of the Green Beds section, Southern Alberta, Canada. The oxygen isotope axis is inverted for the interpretation of temperature change.

Findlay and Gröcke

Fig 12

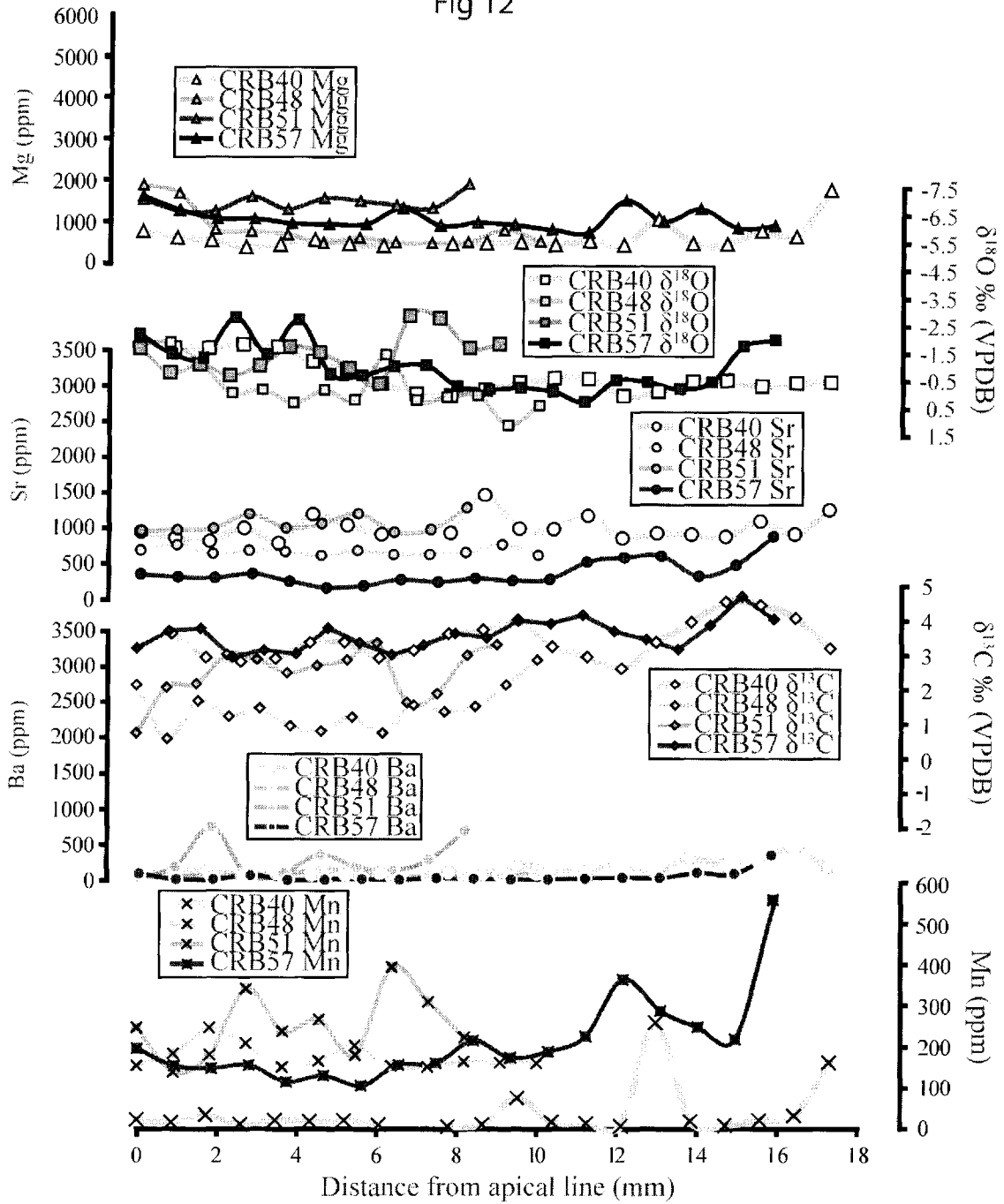


Fig. 12. All stable isotope and trace element profiles from belemnites collected from the 1100cm horizon of the Green Beds section, Southern Alberta, Canada. The oxygen isotope axis is inverted for the interpretation of temperature change.

Findlay and Gröcke  
Fig 13

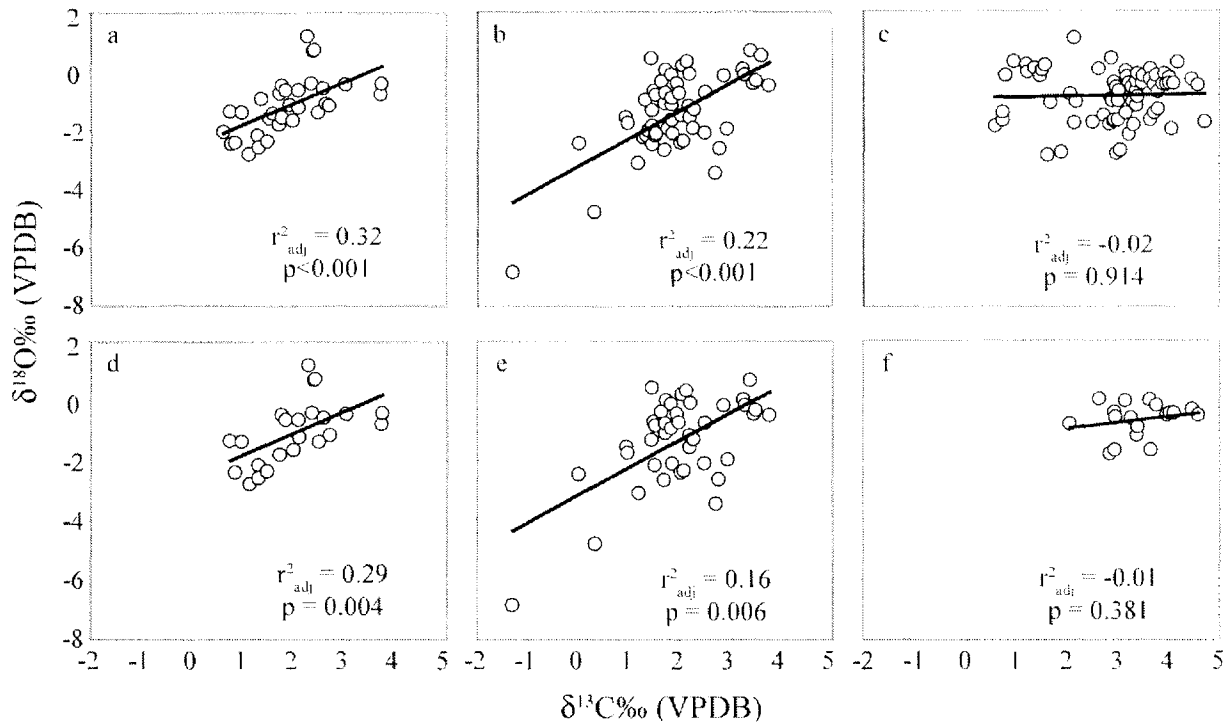


Fig. 13.  $\delta^{13}\text{C}$  vs.  $\delta^{18}\text{O}$  values of the Carbondale River Belemnites. a) 15cm horizon pre diagenetic screening. b) 750cm horizon pre diagenetic screening. c) 1100cm horizon pre diagenetic screening. d) 15cm horizon post diagenetic screening. e) 750 cm horizon post diagenetic screening. f) 1100cm horizon post diagenetic screening.

Findlay and Gröcke  
 Fig 14

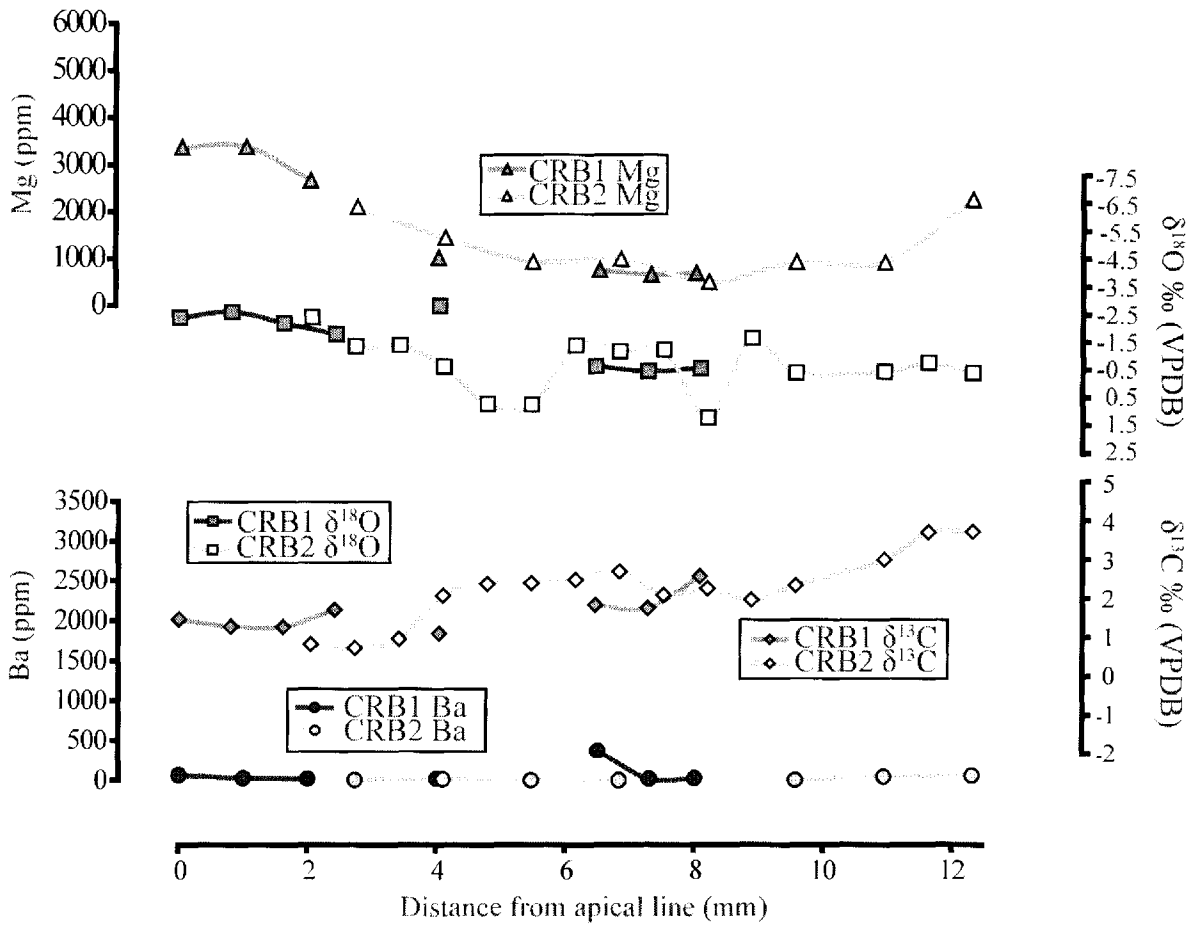


Fig. 14. Stable isotope and trace element profiles from belemnites collected from the 15cm horizon of the Green Beds section, Southern Alberta, Canada with diagenetic samples removed. The oxygen isotope axis is inverted for the interpretation of temperature change.

Findlay and Gröcke  
Fig 15

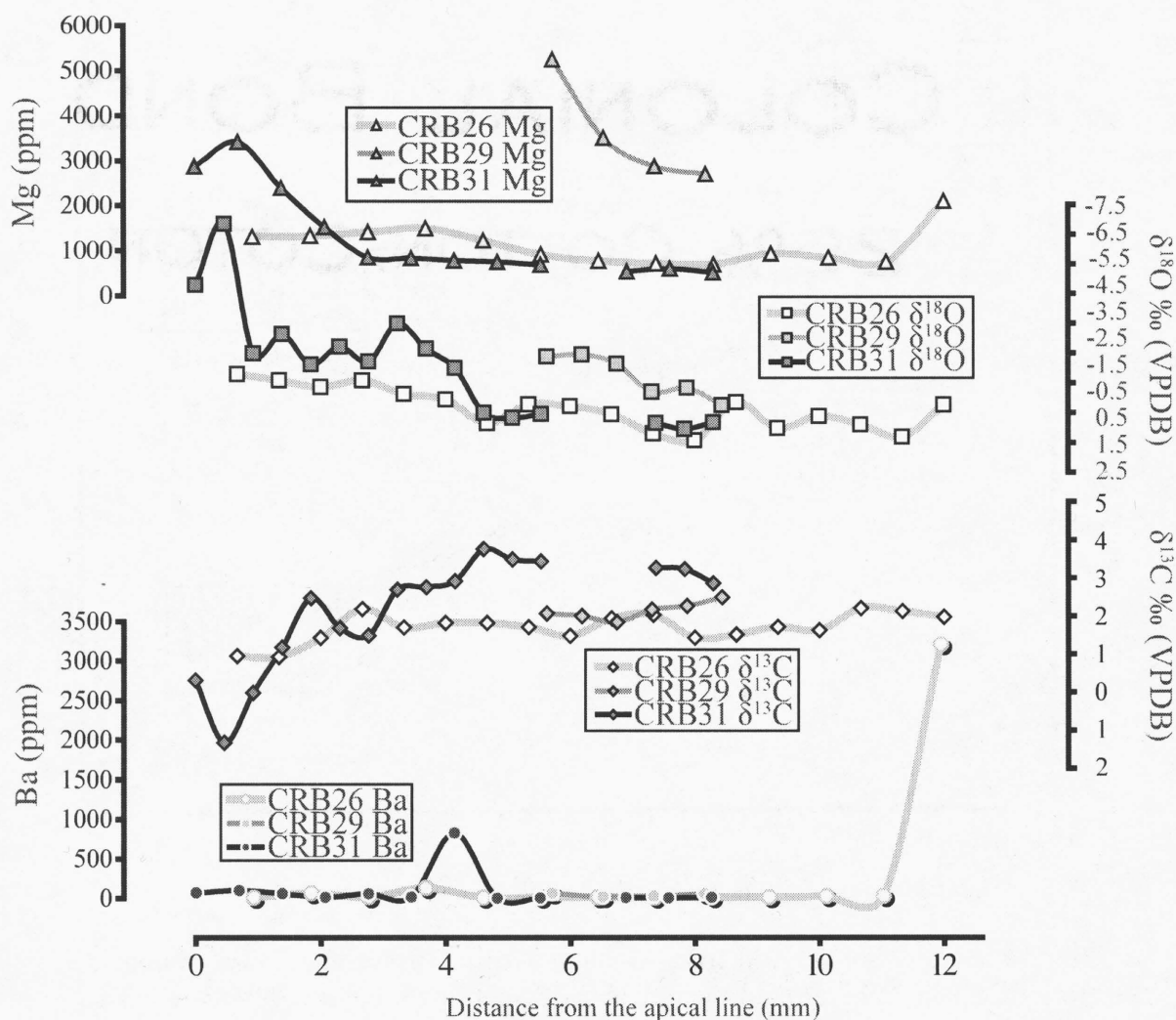


Fig. 15. Stable isotope and trace element profiles from belemnites collected from the 750cm horizon of the Green Beds section, Southern Alberta, Canada with diagenetic samples removed. The oxygen isotope axis is inverted to for the interpretation of temperature change.

Findlay and Gröcke  
Fig 16

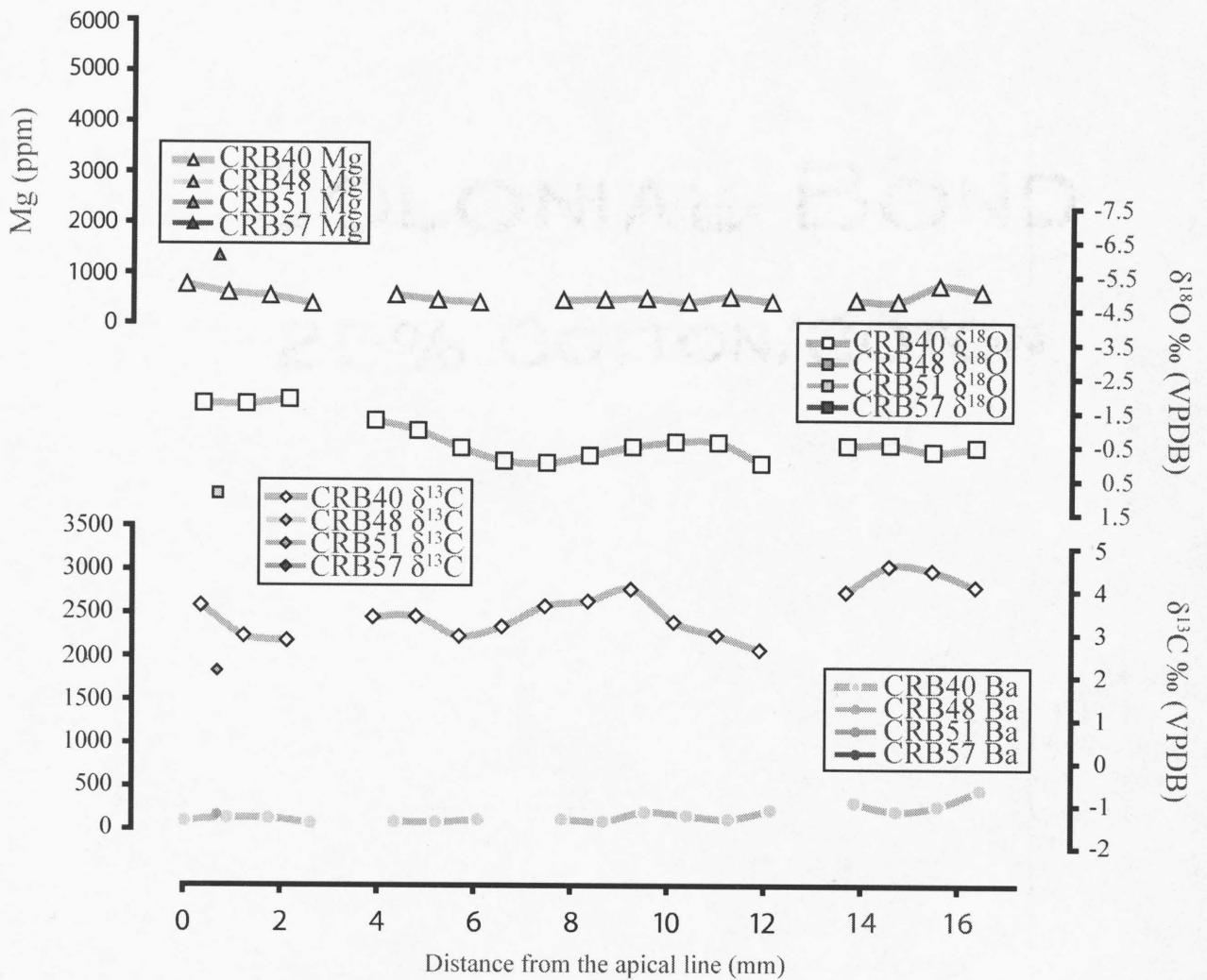


Fig. 16. Stable isotope and trace element profiles from belemnites collected from the 1100cm horizon of the Green Beds section, Southern Alberta, Canada with diagenetic samples removed. The oxygen isotope axis is inverted for the interpretation of temperature change.

**Table 1**

<b>Scottish Passaloteuthis</b>					<b>Albertan Cylindroteuthis</b>				
<b>5mm from Aviolis</b>					<b>Disc 1: 11mm from Aviolis</b>				
<b>Sample</b>	<b>X (mm)</b>	<b>Y(mm)</b>	<b><math>\delta^{13}\text{C}</math> (VPDB)</b>	<b><math>\delta^{18}\text{O}</math> (VPDB)</b>	<b>Sample</b>	<b>X (mm)</b>	<b>Y(mm)</b>	<b><math>\delta^{13}\text{C}</math> (VPDB)</b>	<b><math>\delta^{18}\text{O}</math> (VPDB)</b>
B2S1-1	-2	8	1.6	-3.1	B1S11-1	-4	4	2.1	-5.4
B2S1-10	6	6	0.9	0.3	B1S11-2	-2	4	1.7	-5.5
B2S1-11	8	6	1.6	0.5	B1S11-3	0	4	1.8	-4.9
B2S1-12	-8	4	1.9	0.8	B1S11-4	2	4	1.7	-5.2
B2S1-13	-6	4	2.0	0.0	B1S11-5	4	4	2.1	-4.3
B2S1-14	-4	4	0.3	-0.4	B1S11-6	-6	2	2.1	-4.7
B2S1-15	-2	4	2.1	-2.8	B1S11-7	-4	2	2.0	-4.2
B2S1-16	0	4	2.3	0.0	B1S11-8	-2	2	1.7	-4.1
B2S1-17	2	4	0.9	-1.4	B1S11-9	0	2	2.3	-4.2
B2S1-18	4	4	1.0	0.3	B1S11-10	2	2	1.8	-3.5
B2S1-19	6	4	1.7	-0.1	B1S11-11	4	2	2.1	-5.1
B2S1-2	0	8	1.5	-1.5	B1S11-12	6	2	2.0	-4.7
B2S1-20	8	4	0.4	0.2	B1S11-13	-6	0	2.3	-4.0
B2S1-21	10	4	1.8	0.7	B1S11-14	-4	0	2.2	-3.9
B2S1-22	-8	2	1.4	-0.2	B1S11-15	-2	0	2.0	-4.1
B2S1-23	-6	2	1.6	0.0	B1S11-16	0	0	1.8	-7.2
B2S1-24	-4	2	0.6	-4.5	B1S11-17	2	0	1.7	-3.8
B2S1-25	-2	2	2.5	-0.8	B1S11-18	4	0	1.9	-5.1
B2S1-26	0	2	2.1	-5.2	B1S11-19	6	0	2.1	-5.4
B2S1-27	2	2	1.9	-5.9	B1S11-20	-6	-2	2.1	-4.6
B2S1-28	4	2	1.6	0.8	B1S11-21	-4	-2	1.9	-4.4
B2S1-29	6	2	1.2	0.1	B1S11-22	-2	-2	1.5	-3.7
B2S1-3	2	8	1.3	-0.5	B1S11-23	0	-2	1.9	-4.1
B2S1-30	8	2	1.8	-0.1	B1S11-24	2	-2	1.6	-5.0
B2S1-31	10	2	1.9	0.1	B1S11-25	4	-2	1.3	-4.7
B2S1-32	-8	0	1.7	-0.2	B1S11-26	6	-2	2.0	-5.7
B2S1-33	-6	0	1.6	-1.5	B1S11-27	-6	-4	1.4	-6.3
B2S1-34	-4	0	1.3	-12.2	B1S11-28	-4	-4	1.5	-5.3
B2S1-35	-2	0	1.9	-13.8	B1S11-29	-2	-4	1.9	-3.5
B2S1-36	0	0	5.9	-13.0	B1S11-30	0	-4	2.1	-4.5
B2S1-37	2	0	2.0	-13.8	B1S11-31	2	-4	2.0	-5.4
B2S1-38	4	0	2.3	-0.7	B1S11-32	4	-4	1.7	-6.6
B2S1-39	6	0	1.3	-1.7	B1S11-33	6	-4	2.0	-5.2
B2S1-4	-6	6	1.1	0.2	B1S11-34	-4	-6	2.2	-4.4
B2S1-40	8	0	1.3	0.2	B1S11-35	-2	-6	2.2	-4.7
B2S1-41	10	0	4.7	7.3	B1S11-36	0	-6	2.1	-4.8
B2S1-42	-8	-2	1.8	-0.2	B1S11-37	2	-6	2.3	-4.4
B2S1-43	-6	-2	1.5	-0.3	B1S11-38	4	-6	2.0	-4.5
B2S1-44	-4	-2	0.1	-0.2	B1S11-39	6	-6	2.3	-4.4
B2S1-45	-2	-2	2.3	-3.6	B1S11-40	-4	-8	2.0	-4.4
B2S1-46	0	-2	1.7	-10.4	B1S11-41	-2	-8	2.4	-4.7

**Table 1**

<b>Scottish Passaloteuthis</b>					<b>Albertan Cylindroteuthis</b>				
<b>5mm from Aviolis</b>					<b>Disc 1: 11mm from Aviolis</b>				
<b>Sample</b>	<b>X (mm)</b>	<b>Y(mm)</b>	<b><math>\delta^{13}\text{C}</math> (VPDB)</b>	<b><math>\delta^{18}\text{O}</math> (VPDB)</b>	<b>Sample</b>	<b>X (mm)</b>	<b>Y(mm)</b>	<b><math>\delta^{13}\text{C}</math> (VPDB)</b>	<b><math>\delta^{18}\text{O}</math> (VPDB)</b>
B2S1-47	2	-2	2.0	-6.3	B1S11-42	0	-8	2.1	-4.3
B2S1-48	4	-2	1.7	-9.1	B1S11-43	2	-8	2.3	-5.0
B2S1-49	6	-2	1.4	-4.3	B1S11-44	4	-8		
B2S1-5	-4	6	2.1	0.3	B1S11-45	6	-8	2.2	-4.7
B2S1-50	8	-2	0.9	0.1	B1S11-46	-2	-10	2.5	-4.5
B2S1-51	10	-2	1.0	0.2	B1S11-47	0	-10	2.3	-3.4
B2S1-52	-8	-4	1.2	0.0	B1S11-48	2	-10	2.1	-4.7
B2S1-53	-6	-4	1.4	-0.6	B1S11-49	4	-10	0.7	-4.8
B2S1-54	-4	-4	0.6	-2.0					
B2S1-55	-2	-4	1.2	0.6					
B2S1-56	0	-4	0.6	-5.3					
B2S1-57	2	-4	1.7	-8.2					
B2S1-58	4	-4	1.0	-6.8					
B2S1-59	6	-4	0.9	-0.1					
B2S1-6	-2	6	2.0	-10.9					
B2S1-60	8	-4	-0.3	-0.2					
B2S1-61	10	-4	2.0	-0.1					
B2S1-62	-6	-6	1.5	-0.4					
B2S1-63	-4	-6	1.6	-0.2					
B2S1-64	-2	-6	1.8	-6.7					
B2S1-65	0	-6	1.7	-5.6					
B2S1-66	2	-6	1.2	-0.6					
B2S1-67	4	-6	4.8	7.2					
B2S1-68	6	-6	0.8	-0.4					
B2S1-69	8	-6	1.6	0.2					
B2S1-7	0	6	1.9	-1.2					
B2S1-70	-2	-8	2.0	-1.6					
B2S1-71	0	-8	1.9	-0.5					
B2S1-72	2	-8	1.7	-0.7					
B2S1-73	4	-8	1.1	-1.3					
B2S1-74	6	-8	2.2	0.5					
B2S1-8	2	6	0.0	0.0					
B2S1-9	4	6	-3.3	0.3					

**Table 1**

<b>Albertan <i>Cylindroteuthis</i></b>					<b>Albertan <i>Cylindroteuthis</i></b>				
<b>Disc 2: 18mm from Aviolis</b>					<b>Disc 3: 26mm from Aviolis</b>				
<b>Sample</b>	<b>X (mm)</b>	<b>Y (mm)</b>	<b><math>\delta^{13}\text{C}</math></b>	<b><math>\delta^{18}\text{O}</math></b>	<b>Sample</b>	<b>X (mm)</b>	<b>Y (mm)</b>	<b><math>\delta^{13}\text{C}</math></b>	<b><math>\delta^{18}\text{O}</math></b>
			<b>(VPDB)</b>	<b>(VPDB)</b>				<b>(VPDB)</b>	<b>(VPDB)</b>
B1S18-1	0	4	1.6	-5.1	B1S26-1	-1	1	0.8	-8.5
B1S18-2	2	4	1.6	-4.0	B1S26-2	0	1	1.0	-6.7
B1S18-3	4	4	2.2	-4.2	B1S26-3	1	1	1.1	-7.7
B1S18-4	-4	2	1.7	-6.3	B1S26-4	2	1	1.2	-7.2
B1S18-5	-2	2	1.8	-4.7	B1S26-5	-2	0	2.2	-5.7
B1S18-6	0	2	2.2	-3.3	B1S26-6	-1	0	1.5	-5.9
B1S18-7	2	2	2.3	-3.8	B1S26-7	0	0	0.6	-6.2
B1S18-8	4	2	2.3	-4.1	B1S26-8	1	0	1.0	-7.1
B1S18-9	6	2	2.3	-5.8	B1S26-9	2	0	2.5	-6.2
B1S18-10	-4	0	1.9	-4.2	B1S26-10	3	0	1.0	-8.2
B1S18-11	-2	0	2.3	-3.1	B1S26-11	-2	-1	2.7	-5.1
B1S18-12	0	0	2.4	-4.3	B1S26-12	-1	-1	1.9	-5.8
B1S18-13	2	0	2.1	-3.1	B1S26-13	0	-1	1.9	-5.9
B1S18-14	4	0	1.2	-4.2	B1S26-14	1	-1	1.2	-5.9
B1S18-15	6	0	2.0	-4.5	B1S26-15	2	-1	3.2	-4.8
B1S18-16	8	0	1.1	-5.1	B1S26-16	3	-1	1.4	-6.6
B1S18-17	-4	-2	1.8	-4.4	B1S26-17	-2	-2	1.7	-5.7
B1S18-18	-2	-2	1.5	-3.4	B1S26-18	-1	-2	2.9	-4.1
B1S18-19	0	-2	2.7	-3.3	B1S26-19	0	-2	1.8	-5.9
B1S18-20	2	-2	2.2	-3.1	B1S26-20	1	-2	3.1	-3.6
B1S18-21	4	-2	2.5	-3.5	B1S26-21	2	-2	3.2	-4.0
B1S18-22	6	-2	1.7	-5.0	B1S26-22	3	-2	1.7	-6.2
B1S18-23	8	-2	1.4	-4.4	B1S26-23	4	-2	2.3	-7.7
B1S18-24	-4	-4	1.9	-5.1	B1S26-24	-2	-3	1.5	-6.2
B1S18-25	-2	-4	1.6	-4.2	B1S26-25	-1	-3	2.8	-4.7
B1S18-26	0	-4	2.5	-3.5	B1S26-26	0	-3	3.3	-4.3
B1S18-27	2	-4	2.5	-3.8	B1S26-27	1	-3	3.3	-3.6
B1S18-28	4	-4	2.3	-3.2	B1S26-28	2	-3	1.8	-4.6
B1S18-29	6	-4	2.4	-2.9	B1S26-29	3	-3	2.0	-7.2
B1S18-30	8	-4	1.8	-5.4	B1S26-30	4	-3	2.0	-8.2
B1S18-31	-4	-6	1.5	-3.9	B1S26-31	-1	-4	1.7	-5.5
B1S18-32	-2	-6	2.0	-4.7	B1S26-32	0	-4	1.5	-5.2
B1S18-33	0	-6	2.3	-3.8	B1S26-33	1	-4	1.7	-5.0
B1S18-34	2	-6	2.5	-4.2	B1S26-34	3	-4	1.6	-5.3
B1S18-35	4	-6	1.9	-4.5	B1S26-36	4	-4	2.0	-7.2
B1S18-36	6	-6	2.8	-4.3	B1S26-37	0	-5	1.5	-5.6
B1S18-37	8	-6	1.8	-5.5	B1S26-38	1	-5	1.9	-5.2
B1S18-38	-2	-8	1.5	-6.2	B1S26-39	2	-5	1.1	-6.3
B1S18-39	0	-8	2.1	-4.2	B1S26-40	3	-5	1.9	-7.2
B1S18-40	2	-8	2.3	-5.4					
B1S18-41	4	-8	2.1	-5.4					

**Table 1**

<b>Albertan Cylindroteuthis</b>					<b>Albertan Cylindroteuthis</b>				
<b>Disc 2: 18mm from Aviolis</b>					<b>Disc 3: 26mm from Aviolis</b>				
<b>Sample</b>	<b>X (mm)</b>	<b>Y(mm)</b>	<b><math>\delta^{13}\text{C}</math></b>	<b><math>\delta^{18}\text{O}</math></b>	<b>Sample</b>	<b>X (mm)</b>	<b>Y(mm)</b>	<b><math>\delta^{13}\text{C}</math></b>	<b><math>\delta^{18}\text{O}</math></b>
			<b>(VPDB)</b>	<b>(VPDB)</b>				<b>(VPDB)</b>	<b>(VPDB)</b>
BIS18-42	6	-8	2.2	-5.2					
BIS18-43	2	-10	2.3	-5.4					
BIS18-44	4	-10	0.7	-1.9					

**Table 2**  
**15cm bellow Passage Beds**

Stable Isotopes				Trace Elements					
Sample	cm from Apical Line	$\delta^{13}\text{C}$ (VPDB)	$\delta^{18}\text{O}$ (VPDB)	Sample	cm from Apical Line	Ba	Mg	Mn	Sr
crb-1-1	10.5	1.3	-1.0	crb1-1	10.5	66	1184	108	556
crb-1-2	9.7	1.9	-1.2	crb1-2	10.0	22	709	38	745
crb-1-3	8.9	2.6	-1.1	crb1-3	9.0	20	506	27	665
crb-1-4	8.1	2.6	-0.6	crb1-4	8.0	25	689	29	842
crb-1-5	7.3	1.8	-0.5	crb1-5	7.3	22	660	17	801
crb-1-6	6.5	1.8	-0.7	crb1-6	6.5	371	763	7	874
crb-1-7	5.7	1.7	-0.8	crb1-7	5.5	21	734	8	798
crb-1-8	4.8	1.6	-1.4	crb1-8	5.0	19	763	5	775
crb-1-9	4.0	1.1	-2.8	crb1-9	4.0	21	1027	7	832
crb-1-10	3.2	1.8	-1.6	crb1-10	3.1	19	1000	34	681
crb-1-11	2.4	1.7	-1.8	crb1-11	2.0	21	2676	86	1101
crb-1-12	1.6	1.3	-2.2	crb1-12	1.0	29	3389	49	931
crb-1-13	0.8	1.3	-2.6	crb1-13	0.0	67	3380	80	994
crb-1-14	0.0	1.5	-2.4						
crb2-1	12.3	3.7	-0.4	crb2-1	12.3	59	2267	61	1325
crb2-2	11.6	3.7	-0.8	crb2-2	10.9	48	925	8	1572
crb2-3	10.9	3.0	-0.5	crb2-3	9.6	4	935	7	1323
crb2-5	9.6	2.3	-0.4	crb2-4	8.2		508	7	1343
crb2-6	8.9	2.0	-1.7	crb2-5	6.8	2	994	10	1320
crb2-7	8.2	2.3	1.2	crb2-6	5.5	5	942	7	1380
crb2-8	7.5	2.1	-1.2	crb2-7	4.1	20	1448	11	1277
crb2-9	6.8	2.7	-1.2	crb2-8	2.7	5	2104	21	1345
crb2-10	6.2	2.5	-1.4	crb2-9	1.4	92	4463	191	1469
crb2-11	5.5	2.4	0.7	crb2-10	0.0	1130	4709	327	1358
crb2-12	4.8	2.4	0.7						
crb2-13	4.1	2.1	-0.6						
crb2-14	3.4	1.0	-1.4						
crb2-15	2.7	0.7	-1.4						
crb2-16	2.1	0.8	-2.4						
crb2-17	1.4	0.6	-2.1						
crb2-18	0.7	0.8	-2.5						
crb2-19	0.0	1.5	-1.6						

**Table 2**  
**750cm below Passage Beds**

Stable Isotopes				Trace Elements					
Sample	cm	$\delta^{13}\text{C}$ (VPDB)	$\delta^{18}\text{O}$ (VPDB)	Sample	cm from	Ba	Mg	Mn	Sr
	from				Apical				
	Apical				Line				
	Line								
crb26-1	12.0	2.0	-0.8	crb26-1	12.0	3210	2103	141	1762
crb26-2	11.5	2.1	0.3	crb26-2	11.0	31	752	41	1175
crb26-3	11.0	2.2	-0.1	crb26-3	10.0	29	842	63	1103
crb26-4	10.2	1.6	-0.4	crb26-4	9.0	17	935	86	1080
crb26-5	9.5	1.7	0.0	crb26-5	8.0	18	692	23	1151
crb26-6	8.8	1.5	-0.9	crb26-6	7.2	15	717	31	1105
crb26-7	7.5	1.4	0.4	crb26-7	6.5	17	777	33	979
crb26-8	7.3	2.0	0.2	crb26-8	5.7	15	913	40	998
crb26-9	6.5	1.9	-0.5	crb26-9	4.8	14	1224	43	1203
crb26-10	6.0	1.5	-0.7	crb26-10	3.8	136	1500	42	1273
crb26-11	5.5	1.7	-0.8	crb26-11	3.2	19	1415	32	1307
crb26-12	4.5	1.8	-0.2	crb26-12	2.2	68	1331	52	1153
crb26-13	4.0	1.8	-0.9	crb26-13	1.0	11	1307	69	1040
crb26-14	3.8	1.7	-1.1	crb26-14	0.0	10	1026	45	602
crb26-15	3.0	2.2	-1.6						
crb26-16	2.2	1.4	-1.4						
crb26-17	1.5	0.9	-1.6						
crb26-18	0.9	1.0	-1.8						
crb26-19	0.0	1.3	-1.0						
crb29-1	9.0	1.8	-1.2	crb29-1	9.0	76	1925	445	851
crb29-2	8.4	2.5	-0.8	crb29-2	8.2	61	2700	83	3330
crb29-3	7.9	2.3	-1.3	crb29-3	7.4	30	2875	74	1915
crb29-4	7.3	2.2	-1.2	crb29-4	6.5	21	3505	58	1934
crb29-5	6.8	1.8	-2.2	crb29-5	5.7	67	5239	117	2161
crb29-6	6.2	2.0	-2.5	crb29-6	4.9	42	648	42	410
crb29-7	5.6	2.1	-2.4	crb29-7	4.1	224	530	33	621
crb29-8	5.1	2.3	-2.0	crb29-8	3.3	58	609	29	702
crb29-9	4.5	1.8	-2.0	crb29-9	2.5	10	213	13	236
crb29-10	3.9	1.8	-1.7	crb29-10	1.6	15	523	25	647
crb29-11	3.4	2.0	-1.5	crb29-11	0.8	86	454	20	474
crb29-12	2.8	1.5	-2.1	crb29-12	0.0	122	734	28	779
crb29-13	2.3	1.3	-2.3						
crb29-14	1.7	1.4	-1.9						
crb29-15	1.1	1.4	-2.1						
crb29-16	0.6	1.3	-2.2						
crb29-17	0.0	1.4	-2.5						
crb31-1	8.3	2.9	-0.2	crb31-1	8.3	16	518	114	905
crb31-2	7.8	3.2	0.0	crb31-2	7.6	6	601	60	939

**Table 2**  
**750cm below Passage Beds**

Stable Isotopes				Trace Elements					
Sample	cm	$\delta^{13}\text{C}$ (VPDB)	$\delta^{18}\text{O}$ (VPDB)	Sample	cm from	Ba	Mg	Mn	Sr
	from				Apical				
	Apical				Line				
	Line								
crb31-3	7.4	3.3	-0.2	crb31-3	6.9	13	538	91	993
crb31-5	6.5	3.4	0.7	crb31-4	6.2	3	405	64	717
crb31-6	6.0	3.6	0.5	crb31-5	5.5	6	686	77	1051
crb31-7	5.5	3.4	-0.5	crb31-6	4.8	4	750	66	948
crb31-8	5.1	3.5	-0.3	crb31-7	4.2	832	785	85	1103
crb31-9	4.6	3.8	-0.5	crb31-8	3.5	18	836	80	979
crb31-10	4.2	2.9	-2.0	crb31-9	2.8	62	852	95	1000
crb31-11	3.7	2.8	-2.7	crb31-10	2.1	17	1524	79	1009
crb31-12	3.2	2.7	-3.5	crb31-11	1.4	65	2394	66	1045
crb31-13	2.8	1.5	-2.2	crb31-12	0.7	102	3417	59	1153
crb31-14	2.3	1.7	-2.7	crb31-13	0.0	74	2872	126	1154
crb31-15	1.8	2.5	-2.1						
crb31-16	1.4	1.2	-3.1						
crb31-17	0.9	0.0	-2.5						
crb31-18	0.5	-1.3	-6.9						
crb31-19	0.0	0.3	-4.8						

**Table 2**  
**1100cm below Passage Beds**

Stable Isotopes				Trace Elements					
Sample	cm from Apical Line	$\delta^{13}\text{C}$ (VPDB)	$\delta^{18}\text{O}$ (VPDB)	Sample	cm from Apical Line	Ba	Mg	Mn	Sr
crb40-1	17.3	3.2	-0.5	crb40-1	17.3	203	1771	162	1270
crb40-2	16.4	4.1	-0.5	crb40-2	16.4	471	650	33	931
crb40-3	15.6	4.5	-0.3	crb40-3	15.6	286	780	22	1110
crb40-4	14.7	4.6	-0.5	crb40-4	14.7	225	462	9	897
crb40-5	13.8	4.0	-0.5	crb40-5	13.8	322	479	19	924
crb40-6	13.0	3.4	-0.1	crb40-6	13.0	138	1060	259	938
crb40-7	12.1	2.6	0.0	crb40-7	12.1	232	445	8	869
crb40-8	11.2	3.0	-0.6	crb40-8	11.2	130	542	14	1182
crb40-9	10.4	3.3	-0.6	crb40-9	10.4	170	448	17	991
crb40-10	9.5	4.0	-0.5	crb40-10	9.5	212	508	76	1002
crb40-11	8.7	3.8	-0.2	crb40-11	8.7	101	488	11	1472
crb40-12	7.8	3.6	0.0	crb40-12	7.8	128	476	6	940
crb40-13	6.9	3.2	0.0	crb40-14	6.9				
crb40-14	6.1	2.9	-0.4	crb40-15	6.1	120	417	10	916
crb40-15	5.2	3.4	-0.9	crb40-16	5.2	91	470	21	1046
crb40-16	4.3	3.4	-1.2	crb40-17	4.3	91	567	19	1199
crb40-17	3.5	2.9	-1.8	crb40-18	3.5	112	451	22	796
crb40-18	2.6	2.8	-1.8	crb40-19	2.6	77	390	12	1007
crb40-19	1.7	2.9	-1.7	crb40-20	1.7	132	549	35	820
crb40-20	0.9	3.6	-1.7	crb40-21	0.9	137	614	17	866
crb40-21	0.0				0.0	101	765	24	951
crb48-1	10.0	2.9	0.4	crb48-1	10.0	113	527	161	627
crb48-2	9.2	2.1	1.1	crb48-2	9.1	84	797	162	777
crb48-3	8.5	1.5	0.0	crb48-3	8.2	74	508	166	661
crb48-4	7.7	1.4	0.1	crb48-4	7.3	61	484	152	633
crb48-5	6.9	1.6	0.2	crb48-5	6.4	70	496	155	634
crb48-6	6.2	0.7	-1.5	crb48-6	5.5	116	612	204	692
crb48-7	5.4	1.2	0.2	crb48-7	4.5	174	486	167	622
crb48-8	4.6	0.8	-0.2	crb48-8	3.6	74	693	152	674
crb48-9	3.8	1.0	0.3	crb48-9	2.7	89	761	210	688
crb48-10	3.1	1.5	-0.2	crb48-10	1.8	83	813	247	646
crb48-11	2.3	1.2	-0.1	crb48-11	0.9	66	1671	185	767
crb48-12	1.5	1.7	-1.1	crb48-12	0.0	50	1878	155	694
crb48-13	0.8	0.6	-1.9						
crb48-14	0.0	2.1	-1.8						
crb51-1	9.0	3.3	-1.9	crb51-1	8.2	697	1894	224	1290
crb51-2	8.3	3.0	-1.7	crb51-2	7.3	291	1313	309	983
crb51-3	7.5	1.9	-2.8	crb51-3	6.4	144	1388	394	949

**Table 2**  
**1100cm below Passage Beds**

Stable Isotopes				Trace Elements					
Sample	cm from Apical Line	$\delta^{13}\text{C}$ (VPDB)	$\delta^{18}\text{O}$ (VPDB)	Sample	cm from Apical Line	Ba	Mg	Mn	Sr
crb51-4	6.8	1.6	-2.9	crb51-4	5.5	191	1492	181	1208
crb51-5	6.0	3.4	-0.4	crb51-5	4.6	370	1558	266	1068
crb51-6	5.3	2.9	-1.0	crb51-6	3.6	104	1292	238	1010
crb51-7	4.5	2.7	-1.6	crb51-7	2.7	72	1594	342	1200
crb51-8	3.8	2.5	-1.8	crb51-8	1.8	756	1248	181	999
crb51-9	3.0	2.9	-1.1	crb51-9	0.9	193	1254	139	978
crb51-10	2.3	3.0	-0.7	crb51-10	0.0	51	1525	247	966
crb51-11	1.5	2.2	-1.1						
crb51-12	0.8	2.1	-0.8						
crb51-13	0.0	0.7	-1.7						
crb57-1	15.9	4.1	-2.0	crb57-1	15.9	362	901	541	894
crb57-2	15.1	4.7	-1.8	crb57-2	15.0	104	853	218	495
crb57-3	14.3	3.9	-0.5	crb57-3	14.0	119	1307	249	342
crb57-4	13.5	3.2	-0.2	crb57-4	13.1	48	1007	288	617
crb57-5	12.7	3.5	-0.5	crb57-5	12.2	49	1509	363	597
crb57-6	11.9	3.7	-0.5	crb57-6	11.2	38	745	226	535
crb57-7	11.1	4.2	0.2	crb57-5	10.3	26	806	189	293
crb57-8	10.3	3.9	-0.1	crb57-8	9.4	22	922	174	272
crb57-9	9.5	4.0	-0.3	crb57-9	8.4	31	970	216	303
crb57-10	8.7	3.5	-0.2	crb57-10	7.5	41	901	161	254
crb57-11	8.0	3.6	-0.3	crb57-11	6.5	20	1317	156	286
crb57-12	7.2	3.3	-1.1	crb57-12	5.6	28	936	106	201
crb57-13	6.4	3.0	-1.0	crb57-13	4.7	16	931	131	173
crb57-14	5.6	3.4	-0.7	crb57-14	3.7	14	953	116	265
crb57-15	4.8	3.8	-0.8	crb57-15	2.8	75	1062	156	370
crb57-16	4.0	3.0	-2.7	crb57-16	1.9	18	1067	148	311
crb57-17	3.2	3.2	-1.5	crb57-17	0.9	21	1271	155	320
crb57-18	2.4	3.0	-2.8	crb57-18	0.0	99	1616	197	360
crb57-19	1.6	3.8	-1.4						
crb57-20	0.8	3.7	-1.5						
crb57-21	0.0	3.2	-2.2						

## **Chapter 5**

**High resolution intra-rostral belemnite geochemistry  
from the Green Beds of southern Alberta, Canada: a  
possible North American record of an Oxfordian carbon  
isotope excursion**

High resolution intra-rostral belemnite geochemistry from the Green Beds of southern Alberta, Canada: a possible North American record of an Oxfordian carbon isotope excursion

Duncan J. Findlay<sup>1</sup>, Darren R. Gröcke<sup>2</sup>

1. School of Geography and Earth Sciences, McMaster University, 1280 Main Street W, Hamilton, Ontario L8S 4K1 Canada, (emails: findlad@mcmaster.ca)

2. Department of Earth Sciences, Durham University, Science Laboratories, Durham DH1 3LE, UK (email: d.r.grocke@durham.ac.uk)

Abstract

A total of 44 belemnite rostra containing two genera, *Cylindroteuthis* and *Pachyteuthis*, were collected from the Middle Jurassic (Oxfordian) Green Beds at Carbondale River, southern Alberta, Canada. These rostra were sampled at high resolution along a radial profile for  $\delta^{13}\text{C}$ ,  $\delta^{18}\text{O}$ , Ba, Mg, Mn, and Sr. Concentrations of Mn and Sr were used to eliminate diagenetic alteration.

A general trend of increasing  $\delta^{13}\text{C}$  values with ontogeny is observed in both genera, which is interpreted as metabolic slowdown with age superimposed on an environmental DIC signal. There is a difference in  $\delta^{13}\text{C}$  profiles between the two identified genera, suggesting differing metabolic rates in each. The internal range of  $\delta^{13}\text{C}$  values per rostra is relatively constant, and was used to investigate changes in DIC  $\delta^{13}\text{C}$  over geologic time. A positive  $\delta^{13}\text{C}$  excursion is observed at 1100cm, which may be a useful geochemical age marker for the region.

As with  $\delta^{13}\text{C}$  values, the two genera identified display slightly different  $\delta^{18}\text{O}$  values and Mg concentration profiles. *Cylindroteuthis* Mg concentration and  $\delta^{18}\text{O}$  value generally vary together along the growth profile and suggest high palaeotemperatures in early life that decrease with ontogeny. This temperature profile suggests that juveniles occupy warm, shallow water and migrate to cooler, deeper water with maturity. *Pachyteuthis* displays a trend of increasing Mg concentration with ontogeny, but no consistent trend in  $\delta^{18}\text{O}$  values. The correlation between Mg concentration and  $\delta^{18}\text{O}$  values in these data is currently too low to construct a Mg palaeothermometer, perhaps due to varying water  $\delta^{18}\text{O}$  values through time.

## Introduction

Belemnnoidea have a long history of use in Mesozoic palaeoenvironmental reconstruction. The low Mg calcite rostrum commonly preserved in Mesozoic sediments is thought to be a counterweight to the phragmocone (an internal structure used for buoyancy regulation) adding stability for movement through the water (Ellis 2001, Moore et al. 1952). The belemnite rostrum is also unusually resistant to diagenesis as it is composed of low Mg calcite, which is less prone to dissolution by meteoric water than other carbonate polymorphs (Veizer 1983). In addition, the rostrum is a dense, low porosity structure containing large crystals which limits the surface area available for chemical reaction (Urey et al. 1951). Because of these factors, belemnite rostra are generally better preserved than coeval brachiopods, ammonites and bivalves, and are commonly selected for geochemical investigations of Mesozoic environments.

The well-established inverse relationship between carbonate  $\delta^{18}\text{O}$  values and ambient water temperature is useful for reconstructing historical environments and has been exploited in many previous studies (for example Epstein et al. 1951, Epstein et al. 1953, Emiliani 1966, Anderson and Arthur 1983, Grossman and Ku 1986, Ditchfield 1997, McArthur et al. 2007). However the  $\delta^{18}\text{O}$  value of precipitated carbonate is also controlled by the  $\delta^{18}\text{O}$  value of ambient water, which may vary with meteoric runoff or evaporative conditions, complicating the use of  $\delta^{18}\text{O}$  values as a palaeothermometer.

$\delta^{13}\text{C}$  values of fossil carbonate have provided valuable information regarding the  $\delta^{13}\text{C}$  value of DIC (dissolved inorganic carbonate) of past oceans (Voigt and Hilbrecht 1997, Veizer et al. 1999, Jarvis et al. 2002, Brand et al. 2003, Wierzbowski and Joachimski 2007). However, belemnite  $\delta^{13}\text{C}$  values are likely controlled by metabolic changes superimposed on the environmental dissolved inorganic carbon signal, as observed in the modern mussel (Gillikin et al. 2006a) and cuttlefish (see Chapter 2). While this complicates the interpretation of belemnnoidea  $\delta^{13}\text{C}$  values, general trends may still be useful for carbon isotope stratigraphy and for investigating variations in ancient seawater DIC composition.

Strontium may be used to evaluate the extent of diagenesis in fossil biological calcite. Modern biological calcite is enriched with Sr, whereas diagenetic fluids, and therefore secondary calcite, tend to contain low concentrations of Sr (Veizer 1983). The modern range of Sr in biological calcite is between ~800 and ~2000ppm (Steuber 1999), therefore any sample falling below 800ppm may be removed from palaeoenvironmental consideration as it likely contains secondary calcite. Conversely, manganese is virtually absent in biogenic calcite yet relatively abundant in diagenetic fluids (Veizer 1983). As a result

samples with Mn concentrations in excess of 150ppm may be excluded as diagenetic. In this manner, a combination of Sr and Mn concentration may be used as a sensitive indicator of diagenetic alteration.

In addition to stable isotope analysis, the trace element concentrations of belemnite rostra are potentially useful palaeoenvironmental tools. For example, the concentration of magnesium in biological calcite is being developed as a palaeothermometer (Lea et al. 2000, Nurnberg 2000, Mitsuguchi et al. 1997, Steuber 1999, Hendry et al. 2001, Palacios-Fest and Dettman 2001, McArthur et al. 2004, McArthur et al. 2007, Shen et al. 2007). The use of Mg in belemnite rostra is in its infancy but may yield salinity-independent palaeotemperatures, as Mg varies little, in relation to  $\delta^{18}\text{O}$  values, over a wide range of seawater salinities, from normal seawater into the brackish range (Nurnberg 2000, Lea et al. 2000, Klein et al. 1996). One goal of establishing a salinity-independent palaeothermometer is that it could be used in conjunction with coeval  $\delta^{18}\text{O}$  values and the calcite temperature equation to give some indication of the oxygen isotope composition of ancient sea water. This may be useful for investigating global ice volume and local meteoric events over geologic time (Nurnberg 2000, Lea et al. 2000).

In carbonate remains, barium has been used to reconstruct palaeoflood information in a lagoonal setting (Hendry et al. 2001) and to reconstruct upwelling events (Putten et al. 2000). Ba in the ocean is mostly supplied by upwelling and continental runoff, but is rapidly consumed by primary production at the ocean surface (Bruland and Lohan 2004). The concentration of Ba in belemnite calcite may therefore be a useful indicator of upwelling, meteoric contamination or possibly papaeoprecipitation due to an associated increase in weathering and erosion transporting Ba into the ocean. However, analysis of Ba concentrations in both bivalves and corals has shown that while background levels of shell Ba are probably representative of seawater Ba concentrations, the Ba profile of a typical organism exhibits low background levels, followed by sharp, short-lived peaks, the origin of which has yet to be satisfactorily explained (Gillikin et al. 2006b).

The aim of this study is to explore the geochemical variability within individual belemnite rostra, and apply this to the study of longer term geochemical changes over geologic time. This paper presents stable isotope and trace element profiles of 44 rostra collected from the Green Beds of the Fernie formation exposed along the north bank of Carbondale River, south of Blairmore, southern Alberta, Canada (Fig. 1). These 44 rostra were analyzed for stable isotope values and trace element concentrations following the high resolution methodology described by Findlay and Gröcke (see Chapter 4) for excluding

diagenetic alteration while examining environmental and ontogenetic geochemical variation within individual rostra. The inter-rostra variability is interpreted in terms of general patterns of behaviour, with discussion of Mg as an additional palaeothermometer.

### Geological setting

The Mesozoic Fernie Formation consists largely of cyclic fossiliferous marine shales and sandstones, that filled a north south trending basin to the east of the Rocky Mountains (Stronach 1984). Ammonite stratigraphy identifies these rocks as Jurassic in age (Hall 1984), with the formation thinning eastwards, away from the orogenic belt and towards the Sweetgrass Arch (Stronach 1984). The Fernie Formation was deposited in the Logan Sea, a Jurassic marine water body covering much of western Canada and the United States, with the eastern shore running southeast in the Calgary area. Other than some uplift recorded by thick conglomerate sequences preserved in British Columbia, there is little evidence for major tectonic activity during the Calovian/Oxfordian (Freebold et al. 1959). The Logan Sea during the Oxfordian was a shallow epicontinental sea connected to the Pacific. There is some controversy regarding the possible presence of an island land mass to the west, which is apparent in some Palaeogeography reconstructions, but seems absent in others (Freebold et al. 1959).

Five regressive cycles of the Logan Sea are observed in the Fernie formation, taking the form of asymmetric shallowing upward depositional cycles (Fig. 2), controlled primarily by local subsidence not global eustacy (Stronach 1984). The Green Beds represent an early part of the 4<sup>th</sup> of these cycles, when the Logan Sea had flooded the low lying continent.

The Green Beds were first described as a ~15m thick unit of greenish sands and shales, overlying the Ribbon Creek Member and underlying the Passage Beds (McLearn 1927) (Fig. 2). The Green Beds appear to be limited in outcrop, but this is likely an artefact of erosion as these sediments appear to be laterally extensive in the subsurface, and have been used as a temporal marker unit (Freebold et al. 1959). The characteristic green colour of this unit is the result of diagenetic berthierine (Hall 1984), an early diagenetic alteration product of kaolinite, which may indicate low sedimentation rates. The Green Beds also contain terrestrial plant matter, a rich belemnite and brachiopod fauna, and rare ammonites (Freebold et al. 1959). The presence of cross-bedding and rolled belemnites concentrated by wave action in some areas in conjunction with the presence of terrestrial plant matter suggests that this deposit represents very shallow epicontinental sea conditions. Unfortunately, the Carbondale River

exposure of the Green Beds displays no visible sedimentary structures (Fig. 2). The colour of these sediments varies between green and purple as a result of differential weathering, not mineralogy (Hall 1984). Ammonite biostratigraphy suggests the Green Beds are early Oxfordian to Late Oxfordian/Early Kimmeridgian in age (Hall 1984), or 161-155 Ma (Gradstein et al. 2004), which in turn would suggest a palaeolatitude of  $\sim 50^\circ$  (Schettino and Scotese, 2005). As ammonites are rare, additional time markers would be valuable.

### Methods

A total of 44 belemnite rostra were analysed over the 12.3m of the Green Beds exposed at Carbondale River, Southern Alberta, Canada (Fig. 1). These were composed of two genera, Belemnoidea *Pachyteuthis* and Belemnoidea *Cylindroteuthis* (Doyle 2008, personal communication; Lissajous 1925), with *Cylindroteuthis* accounting for 32 of the sampled rostra and *Pachyteuthis* the remaining 12. The belemnite rostra were sectioned longitudinally, i.e. from apex to aviolis, using a low speed saw. Powder samples were then collected along a radial profile, from the apical line to the outer edge, using a dental drill (Fig. 3): one profile was collected for stable isotope analysis, with additional profiles collected for trace element analyses. Since trace element analyses required a larger sample size, radial trace element profiles are usually of slightly lower resolution than the corresponding stable isotope profiles. A total of 13 rostra sampled late in the study were radially sampled as above, but with each powder sample split for stable isotope and trace element analysis. A total of 540 stable isotope analyses and 486 trace element analyses were conducted.

Carbon and oxygen isotope ratios were measured using a Fison Optima isotope-ratio mass-spectrometer, coupled to an on-line common acid bath, at McMaster University. Samples of  $\sim 0.3\text{mg}$  were reacted with 100% phosphoric acid at  $90^\circ\text{C}$ . Carbon and oxygen isotope values are reported in standard delta ( $\delta$ ) notation, expressed as per mil (‰):

$$\delta = \left( \frac{R_{\text{sample}}}{R_{\text{standard}}} - 1 \right) \times 1000 \quad [5.1]$$

where R is the ratio between the isotopes of interest ( $^{13}\text{C}/^{12}\text{C}$  and  $^{18}\text{O}/^{16}\text{O}$ ). All isotopic values are reported relative to Vienna Pee Dee Belemnite (VPDB) standard calibrated using NBS 19 limestone. Reproducibility for both  $\delta^{13}\text{C}$  and the  $\delta^{18}\text{O}$  is better than  $\pm 0.1\text{‰}$  on replicate analyses.

This paper uses the calcite palaeotemperature equation of Anderson and Arthur (1983)

$$T = 16.0 - 4.14(\delta^{18}O_{cal} - \delta^{18}O_w) + 0.13(\delta^{18}O_{cal} - \delta^{18}O_w)^2 \quad [5.2]$$

where T is temperature in degrees Celsius,  $\delta^{18}O_{cal}$  is the  $\delta^{18}O$  VPDB value of the analysed belemnite calcite, and  $\delta^{18}O_w$  is the oxygen isotope value (VSMOW) of ambient water. For practical purposes, this equation gives almost identical results to temperature equations established for inorganically precipitated calcite (Sharp 2006). Therefore, assuming the equilibrium precipitation of belemnite calcite should be appropriate for this study. In this case,  $\delta^{18}O_w$  was assumed to be -1‰, a value commonly adopted for periods of limited continental ice such as the Jurassic (Rosales et al. 2004b).

Trace element samples of ~3mg were weighed before dissolution in 10ml of 2% trace-metal grade nitric acid. These solutions were then analysed using an ELAN 6100 quadrupole ICP MS for Ba, Mg, Mn and Sr with a suite of standards at the beginning, middle and end of each run. An individual standard was also analysed after every 10 samples to further check consistency. Many samples were analysed twice, with reproducibility better than 15% on replicate analysis (Table 1). Results are presented in parts per million (ppm).

Regression statistics were calculated using Microsoft Excel. Adjusted  $r^2$  values are reported as large numbers of data points used lead to an artificially inflated  $r^2$ . The adjusted  $r^2$  value is corrected for the number of data points used in the regression analysis.

## Results and Discussion

### Overview of analyses

$\delta^{13}C$  values varied between -7.8 and 7.5 ‰ (Table 1).  $\delta^{18}O$  values ranged between -17.8 and 7.8 ‰ (Table 1).  $\delta^{13}C$  and  $\delta^{18}O$  values were positively correlated ( $r^2_{adj} = 0.36$ ,  $p < 0.0001$ ; Fig. 4a). In terms of trace elements, the concentration of Ba ranged between 0 and 19 527 ppm, while Mg concentrations ranged between 6 and 7327 ppm. Mn was generally low and ranged between 0 and 1493 ppm. Sr concentration varied from 7 to 3642 ppm.

### Diagenetic Screening

The presence of berthierine in the Green Beds suggests that the sediments have been affected by diagenesis to some degree. As belemnites are composed of diagenetically resistant low Mg calcite, with low initial porosity and permeability, pristine geochemical signals may be preserved. Mn and Sr are often involved in post-burial alteration processes, and may be used to screen for diagenetic alteration. In this study, samples containing more than 150 ppm Mn and/or less than 800 ppm Sr were assumed diagenetic, and excluded from further consideration: 351/540 stable isotope and 317/475 trace element analyses passed the screening process. The post-diagenetic screening range for  $\delta^{13}\text{C}$  values was -1.3 to 4.6 ‰;  $\delta^{18}\text{O}$  values ranged between -6.9 and 1.2 ‰. The positive correlation between  $\delta^{18}\text{O}$  and  $\delta^{13}\text{C}$  remained following diagenetic screening ( $r^2_{\text{adj}} = 0.26$ ,  $p < 0.0001$ ; Fig. 4b). Ba concentration ranged between 0 and 19 527 ppm. Mg concentration varied between 13 and 5 239 ppm.

### Carbon Stable Isotopes

#### Variation with growth

As rostra of both genera vary in diameter and length, it was necessary to normalise the length of the radial sample transect to facilitate meaningful comparison between rostra. Sample position is therefore represented as percentage distance between the apical line (0%) and the outer edge of the rostra (100%). A weakness of this approach is that it assumes that each rostrum lived to approximately the same age, which is almost certainly not the case. However, it will cancel out the effect of differential growth rates between individuals, which is likely the greater source of error. Similarly, as these rostra were all collected from different horizons, they will be influenced by environmental variability over geologic time. As such, data for these rostra are presented as deviations from median geochemical values, which should remove the influence of varying background environmental values, and allow any general ontogenetic trends to be identified.

In individual rostra, there is a general trend towards higher  $\delta^{13}\text{C}$  values with ontogeny. 21 individuals (CRB1, CRB2, CRB3, CRB4, CRB6, CRB10, CRB12, CRB21, CRB26, CRB27, CRB28, CRB29, CRB30, CRB31, CRB32, CRB35, CRB36, CRB38, CRB40, CRB41, and CRB52) show clear trends toward positive  $\delta^{13}\text{C}$  values with time (Fig. 5). This has been attributed to a decrease in metabolic rate with ontogeny (see Chapter 4). The ontogenetic trend in  $\delta^{13}\text{C}$  values in *Cylindroteuthis* (Fig. 6) is best described by a second order polynomial

curve ( $r^2_{\text{adj}} = 0.41$ ,  $p < 0.0001$ ,  $n = 242$ ). *Pachyteuthis* (Fig. 7), also exhibits an ontogenetic trend best described by a second order polynomial curve, but is almost linear ( $r^2_{\text{adj}} = 0.11$ ,  $p < 0.001$ ,  $n = 107$ ). While both of these genera exhibit an increasing trend, it is more pronounced in *Cylindroteuthis* than *Pachyteuthis*, which may reflect different metabolic and/or behavioural regimes in these genera. Notably, the relatively higher significance level observed for the *Cylindroteuthis* curve may be a statistical artefact resulting from the fact that this genus comprised the majority of the rostra that were sampled.

As discussed above, the general trends in these genera are likely representative of behaviours and biology common to most individuals. It is therefore inappropriate to construct palaeoenvironmental interpretations using data points that likely represent aberrant behaviour, e.g. swimming into an estuary in search of food and incorporating a meteoric signal into secreted carbonate, or biology, e.g. repairing tissue and/or skeleton after injury. Data points deviating from the general trends identified in Fig. 6 and 7 will not be considered while interpreting changes in palaeoclimate over geologic time.

Reproduction has been observed to increase metabolic activity in modern mussels (Gillikin et al. 2006a), which should influence the quantity of metabolic carbon accumulating in the shell. In fact, many species display lower carbon isotope values when metabolism is highest (Putten et al. 1999, Vander Putten et al. 1999, Putten et al. 2000, Findlay et al. previous chapter). It has been suggested that the low  $\delta^{13}\text{C}$  values late in life documented in cuttlefish may be the result of a spawning-related increase in metabolism as females are required to increase their metabolic rate and/or reallocate carbon to facilitate egg production (see Chapter 4). If true, such a rapid late life decline in  $\delta^{13}\text{C}$  values may be useful for determining sex in belemnites, with low end life values indicating female specimens. CRB11, CRB19, CRB21, CRB28, CRB36, CRB40 and CRB45 all display a decrease in  $\delta^{13}\text{C}$  values late in life. These data would suggest a relatively small number of females (7 of 36) in this area resulting in a male to female ratio of ~4:1, which approximates the sex ratio observed in modern cuttlefish (Hall and Hanlon 2002, Naud et al. 2004).

### Stratigraphic $\delta^{13}\text{C}$ Evolution

As previously established, belemnoida likely do not secrete carbon isotope values in equilibrium with ambient seawater, which may negatively impact the use of belemnite rostra for carbon isotope stratigraphy. However, as the initial source of carbon in belemnoida is probably diet, and the base of the food chain must initially reflect the  $\delta^{13}\text{C}$  values of DIC, the internal variability

documented in these rostra may be the effects of metabolism superimposed on an environmental signal (see Chapter 4). As such, variations in DIC composition may be observed as shifts in the *range* of carbon isotope values preserved in the rostrum over geologic time.

In order to evaluate the temporal evolution of the range of  $\delta^{13}\text{C}$  values preserved in these rostra, the range in values for each rostra is presented at the stratigraphic height of collection, with two 3 point moving average curves, one through the maximum, and another through the minimum values of this suite of rostra (Fig. 8). Presented in this way, belemnite geochemistry may be used to investigate temporal variability in ancient DIC  $\delta^{13}\text{C}$  values. Moving averages show that the mean range of  $\delta^{13}\text{C}$  values remains fairly constant at  $\sim 2\text{‰}$ , but that the position of the range varies through time (Fig. 8). The lack of variability in the range of  $\delta^{13}\text{C}$  suggests that metabolic effects on  $\delta^{13}\text{C}$  are fairly constant in these genera over geologic time, while the shift in the range through time suggests variation in ambient DIC.

A positive excursion, a deviation of  $2.4\text{‰}$  from the mean value of the section, is observed in the  $\delta^{13}\text{C}$  values around 1100cm, reaching a height of  $4.6\text{‰}$ . This excursion may reflect local changes in primary productivity, perhaps as a result of increased nutrient availability, which would influence ambient DIC  $\delta^{13}\text{C}$ . A positive carbon isotope excursion has also been noted in European Oxfordian sediments (Weissert and Mohr 1996, Wierzbowski 2002, Wierzbowski 2004, Pearce et al. 2005, Glowniak and Wierzbowski 2007, Louis-Schmid et al. 2007b). The favoured explanation for the European excursion, which is not associated with an oceanic anoxic event, is an increase in global coastline due to the reorganisation of continents at this time, which would have increased the nutrients available for primary productivity (Louis-Schmid et al. 2007a, Louis-Schmid et al. 2007b). The Green Beds also show no evidence of anoxia, similar to the European carbon isotope excursion, suggesting that the increase in  $\delta^{13}\text{C}$  values is not related to the increased sequestration of organic matter during an ocean anoxic event. If the excursion in the Green Beds proves to be the same event observed in Europe, the peak observed here occurred  $\sim 158\text{Ma}$  (Gradstein et al. 2004), a value which is consistent with ammonite biostratigraphy for the area (Hall 1984). However, the values associated with each excursion differ: Whereas in Europe the background  $\delta^{13}\text{C}$  values are  $\sim 0\text{‰}$  with the excursion peaking at around  $2\text{‰}$ , in the Green Beds, the background maximum  $\delta^{13}\text{C}$  values are  $\sim 2.5\text{‰}$  with the excursion peaking at around  $\sim 4.5\text{‰}$ . While the magnitude of the excursion is similar, the  $\sim 2\text{‰}$  offset in  $\delta^{13}\text{C}$  values between the European and North American sections may be explained by the local geologic setting. For example, while this was a time of global marine transgression (Haq et al. 1987), it is

possible that Europe experienced more reworking of carbonate rocks, resulting in a low background DIC  $\delta^{13}\text{C}$  value compared to western North America, where local sea level was regressing slowly and carbonate deposition was limited (Freebold et al. 1959). Alternatively, the ~2% offset between the European and North American sections may be a “vital effect”, resulting from metabolic alteration of the DIC  $\delta^{13}\text{C}$  signal preserved in belemnite rostra, as previously discussed. As bulk rock carbon samples, and not belemnite rostra, were used when identifying the European excursion, this seems the most likely explanation for the difference in offset. Whether the excursion identified here and the European excursion have the same origin and represent a global carbon isotope event is an interesting question: Further studies involving other Oxfordian sequences in North America should explore this possibility. Regardless of its origin, the excursion identified here may be a valuable geological age marker for this region.

#### Palaeotemperature and the influence of meteoric water

##### Individual Rostra

Generally, trends of Mg concentration and  $\delta^{18}\text{O}$  value compare well on an individual rostra level. 20 rostra (CRB1, CRB3, CRB10, CRB12, CRB16, CRB26, CRB 27, CRB28, CRB29, CRB30, CRB31, CRB32, CRB35, CRB36, CRB37, CRB38, CRB44, CRB45, CRB52 and CRB56) show a strong inverse relationship between  $\delta^{18}\text{O}$  value and Mg concentration (Fig. 5).

When separated by genera, *Cylindroteuthis* Mg concentrations are best described by a second order polynomial curve ( $r^2_{\text{adj}} = 0.22$ ,  $p < 0.0001$ ,  $n = 217$ ; Fig. 6), which show a trend towards lower values with ontogeny. Similarly, *Cylindroteuthis*  $\delta^{18}\text{O}$  values are best described by a second order polynomial curve ( $r^2_{\text{adj}} = 0.42$ ,  $p < 0.0001$ ,  $n = 242$ ) which shows a trend towards higher values with ontogeny. The slope of both curves are similar, which may suggest that they are controlled, at least in part, by the same process (Lea et al. 2000, Nürnberg 2000, Mitsuguchi et al. 1997, Steuber 1999). For both groups, trends preserved in the  $\delta^{18}\text{O}$  and Mg values of the rostra could be explained by migratory behaviour, if juveniles inhabit warmer, shallow areas and then migrate to cooler, deeper waters as they mature and then migrating with favourable water temperatures (see Chapter 4).

*Pachyteuthis* Mg concentrations (Fig. 7) are also best described by a second order polynomial curve ( $r^2_{\text{adj}} = 0.20$ ,  $p < 0.0001$ ,  $n = 83$ ), and show a trend towards lower values with ontogeny which is less pronounced than the curve

documented for *Cylindroteuthis*.  $\delta^{18}\text{O}$  values show a weak ( $r^2_{\text{adj}} = 0.05$ ) but significant ( $p < 0.024$ ,  $n = 107$ ) trend towards higher values with ontogeny that is best described as a second order polynomial curve. There is little consistent ontogenetic trend for *Pachyteuthis*  $\delta^{18}\text{O}$  values. The lack of a trend in  $\delta^{18}\text{O}$  values may be the result of deep-water spawning, but such behaviour would be difficult to reconcile with the Mg concentration profiles. The number of data points is low as there were fewer *Pachyteuthis* rostra collected, however *Pachyteuthis* does tend to exhibit lower Mg concentrations and higher  $\delta^{18}\text{O}$  values than *Cylindroteuthis*, indicating it may be a colder- or deeper-water genera.

The lack of an obvious seasonal signature in both  $\delta^{18}\text{O}$  and Mg in either of these genera may be the result of migration. A seasonal migration of sufficient distance may completely mask a seasonal temperature signal by organisms following favourable water conditions as suggested in chapter 4. A large-scale latitudinal migration, analogous to the migratory behaviour observed in many modern cephalopods, is at least plausible since the Logan Sea, where these sediments were deposited, stretched as far south as the middle of the USA during the Oxfordian (Freebold et al, 1959, Boyle 1983).

A number of these rostra (CRB3, CRB6, CRB16, CRB19, CRB26, CRB32, CRB44, CRB45 and CRB56) also show a rise in palaeotemperature (according to  $\delta^{18}\text{O}$  values and/or Mg concentrations), toward the end of their lives. This pattern could be explained by the onset of spawning in shallow waters, followed by death. While spawning may require females to return to shallow waters to deposit eggs, the same may not be true for males, if mating occurs in deeper water. Such a difference in the life-histories of males and females of the species would neatly explain the relatively small number of individuals (9 of 36) returning to the shallow waters. In many modern cephalopods, the ratio of males to females approximates 4:1 (Boyle 1983, Hall and Hanlon 2002, Naud et al. 2004), lending some support to this hypothesis. The sedimentology and local tectonic setting of the Green Beds, as well as the abundance of terrestrial debris such as wood, are all consistent with proximity to a very shallow, near shore environment that may be required for spawning, given the evidence for the juvenile phase being spent in shallow water. However, the highlighted group of rostra share only 2 individuals with the previously cited group of rostra with depleted late life  $\delta^{13}\text{C}$  values. This requires further, higher resolution work, as fine scale variations may be lost with the current sampling technique. A great deal more work at higher resolutions of geochemical analysis would be required to determine whether any of these explanatory hypotheses are correct. Whether belemnites returned to deeper water after spawning, or died in shallow water with

the rostra transported to these sediments post mortem by wave action is unresolved.

To summarize,  $\delta^{18}\text{O}$  values and Mg concentrations may suggest that belemnites may have been migratory throughout ontogeny, with juveniles living in shallow, warmer water, preserving low  $\delta^{18}\text{O}$  values and high Mg concentration (Fig 9a), and with a movement to deeper, cooler waters further from shore with maturity, resulting in higher  $\delta^{18}\text{O}$  values and lower Mg concentration (Fig. 9b). As there is no obvious seasonal signal preserved in the analysed rostra, it is likely that these animals also undertook a latitudinal migration, following favourable water temperatures and therefore masking a seasonal temperature signal.  $\delta^{18}\text{O}$  values and Mg concentrations also indicate that a small number of females return to the shallow waters to spawn before expiring (Fig. 9c). While trends in  $\delta^{18}\text{O}$  values and Mg concentration have been identified, there is a large degree of geochemical variation within the sampled belemnite rostra. This is interpreted as variation in individual behaviour, local migration, local or short-term environmental fluctuations, etc. preserved in the geochemical signal of each rostra.

While the  $\delta^{18}\text{O}$  and Mg data from individual rostra often show covariance, the  $\delta^{18}\text{O}$  values and Mg concentrations obtained from the same sample are weakly, but significantly correlated ( $r^2_{\text{adj}} = 0.17$ ,  $p < 0.0005$ ,  $n=61$ ; Fig. 10a). Since the correlation is relatively weak, describing only 17% of the variance in the dataset, factors other than temperature must be independently influencing  $\delta^{18}\text{O}$  values and/or Mg concentrations. This low correlation may be due to environmental changes over geologic time effecting each proxy differently, for example the  $\delta_w$  value or ambient Mg level of ocean water may have varied independently. This seems likely as Fig 6 documents similar statistically significant trends in both  $\delta^{18}\text{O}$  and Mg over the lifetime of *Cylindroteuthis*. One factor that may cause a decoupling between  $\delta^{18}\text{O}$  values and Mg concentrations is meteoric water input, which could change the  $\delta_w$  of the basin, at least locally. Increased input of meteoric water into the basin would lower the  $\delta_w$  value, resulting in the calculation of higher temperatures and vice versa. However, Mg concentration varies little in comparison to  $\delta^{18}\text{O}$  values within the normal ocean to brackish salinity range (Klien et al. 1996). Thus, whereas the temperature record retrieved from Mg concentrations should be relatively unaffected by meteoric water input, palaeoenvironmental reconstructions based on  $\delta^{18}\text{O}$  values would document any fluctuation in the  $\delta_w$  value of the basin combined with changes in temperature. As such, a decoupling of the Mg and  $\delta^{18}\text{O}$  signals may be interpreted as a change in  $\delta_w$  value. Such a decoupling of  $\delta^{18}\text{O}$  values and Mg concentration

is observed in CRB1, CRB2, CRB3, CRB11, CRB26, CRB31, and CRB32 suggesting these individuals spent their early lives in slightly brackish waters (Fig. 5). Current data suggest that the relationship between  $\delta^{18}\text{O}$  and Mg is not simple; no reliable Mg temperature equation can be constructed using  $\delta^{18}\text{O}$  values for calibration at this time.

#### Reconstruction of the Palaeotemperature Record from $\delta^{18}\text{O}$ and Mg Geochemistry from Rostra from Different Layers in the Green Beds

As with  $\delta^{13}\text{C}$  records, aberrant data points identified in Fig. 6 and 7 will not be considered while interpreting changes over geologic time. Palaeotemperatures preserved in the rostra are likely influenced by migration between the rearing and spawning areas, which appear to be shallow near shore water conditions, and deeper waters further from shore. Based on this reconstruction, maximum palaeotemperatures are probably close to summer sea surface palaeotemperatures and minimum palaeotemperatures probably record palaeotemperatures from the deeper waters of the basin. To aid in the interpretation of the palaeotemperature record stored in belemnite rostra from different stratigraphic positions in the Green Bed, the range of values preserved in each rostrum is presented at its corresponding stratigraphic height and a three-point moving average of the maxima and minima values is presented across the section in order to assess the surface and deep-water temperatures respectively (Fig. 8). This approach not only allows the interpretation of the palaeotemperature record through time using belemnite rostra preserved in different strata, but also helps to minimise error associated with both inter-individual and intra-rostrum variability. The following sections summarise the interpretation of the  $\delta^{18}\text{O}$  and Mg values preserved in the analysed rostra in their stratigraphic position: This is an attempt to maximise the palaeoenvironmental information that may be extracted from the belemnite fossil record. Decoupling of the  $\delta^{18}\text{O}$  value and Mg concentration signals will be interpreted as changes in the  $\delta_w$  of the basin, probably controlled by the input meteoric water. However, as there are no firm data regarding quantifying the relationship between temperature and Mg incorporation, the interpreted changes described below are qualitative, and future work will likely alter their interpretation.

#### The Temporal Evolution of Near Sea Surface Palaeotemperatures and the Influence of Runoff

From the earliest part of the section, oxygen isotope values document a decline in palaeotemperature from  $\sim 21$  °C to  $\sim 13$  °C ( $-3.2$  ‰ to  $-1.0$  ‰) between the earliest sample and 1150cm. This is accompanied by a slight rise in Mg concentration from 900ppm to 1200ppm (Fig 8). The negative deviation of the  $\delta^{18}\text{O}$  signal from the Mg signal suggests that this represents a time of reduced meteoric water influence, with the initial  $\delta^{18}\text{O}$  values documenting a time of lower  $\delta_w$  values, not higher palaeotemperatures.

There is a rise in  $\delta^{18}\text{O}$  derived palaeotemperatures from  $\sim 13$  °C to  $\sim 23$  °C ( $-1.0$  ‰ to  $-3.5$  ‰) between 1150 and 1075cm, which is coincident with a slight fall in Mg concentration before a rise (1200ppm at 1150cm, to 900ppm at 1100cm, before rising to 2000ppm at 1075cm). Following this peak in temperature, oxygen isotope palaeotemperatures decline from 23 °C ( $-3.5$  ‰) at 1075cm to 15 °C ( $-1.3$  ‰) at 1000cm. This decline is also observed in Mg, falling from 2000 to 1050ppm, suggesting that this is a cooling trend, not an increase in the basin  $\delta_w$  value.

Between 1000cm and 800cm the oxygen isotope values of the few rostra that were collected indicate warming from  $\sim 15$  °C ( $-1.3$  ‰) at 1075cm to  $\sim 20$  °C at 750cm ( $-2.6$  ‰). However, over this same period, Mg concentration rose from 1050ppm to 1300ppm at 950cm, before falling to 1000ppm at 750cm. This indicates that the waters of this area cooled over this time, while the  $\delta_w$  value decreased.

At 750 cm, several rostra were collected, which record a sharp but intense period of warming, with  $\delta^{18}\text{O}$  temperatures approaching 30 °C ( $-5$  ‰), and Mg averaging 2500ppm. Following this horizon, there is more than 600cm of section where rostra were sparse. Those that are present record a long term slow increase in palaeotemperature recorded in both Mg and  $\delta^{18}\text{O}$ , from  $\sim 17$  °C at 650cm ( $-2.0$  ‰) to  $\sim 23$  °C at 50cm ( $-3.6$  ‰).

The remaining 50cm at the top of the section, immediately prior to the deposition of the Passage Beds contained many rostra. From 50cm to 40cm, there is a cooling of surface water palaeotemperature ( $\sim 25$  °C falling to  $\sim 17$  °C) recorded in both Mg and  $\delta^{18}\text{O}$  (1750ppm to 1000ppm, and  $-4.0$  to  $-2.0$  ‰ respectively). Between 40cm and the passage beds there is a rise in both  $\delta^{18}\text{O}$  water palaeotemperatures and Mg concentration, indicative of rising water palaeotemperatures.

#### Deeper Water Palaeotemperatures and the Influence of Meteoric Water

The deeper water palaeotemperatures for the Green Bed section contain less variability than the near surface waters, fluctuating between 5 and 14 °C (Fig.

8). It is possible that the temperature changes described here are the result of variations in water depth, with increases in depth resulting in lower temperatures and vice versa. However, there is no sedimentological evidence to support this, and so the trends identified will be reported solely in terms of temperature variation.

Oxygen isotope-derived palaeotemperatures decline from 12°C at the base of the section to 8 °C at 1180cm (-0.4 ‰ to +0.8 ‰), with a slight decline in Mg concentration (~600ppm to ~400ppm) confirming a cooling trend, not a change in  $\delta_w$ . This is followed by a rise in  $\delta^{18}\text{O}$  derived palaeotemperature, from 8 °C to 16 °C at 1060cm (+0.8 to 1.4 ‰). This trend is not observed in Mg concentrations, where values increase from 400ppm at the base of the section to 1000ppm at 1130cm before falling to 500ppm again at 1100cm. This suggests warming with an increasing  $\delta_w$  value.

Between 1100cm and 1050cm  $\delta^{18}\text{O}$  values and Mg concentrations rise to a peak (~17 °C and 1300ppm respectively) suggesting that the deeper waters of the basin warmed over this time period. Both  $\delta^{18}\text{O}$  derived palaeotemperatures and Mg concentration fall between 1050cm and 1000cm (falling to ~11 °C and ~600ppm) suggesting cooling, before rising to ~15 °C (-1.0 ‰  $\delta^{18}\text{O}$ , with Mg rising to 950ppm) at 950cm.  $\delta^{18}\text{O}$  value palaeotemperatures remain stable until 800cm where they decline to 10 °C (0.0 ‰) at 750cm. Between 900cm and 750cm, Mg values steadily fall from 950ppm to 500ppm at 750cm, implying a decline in water palaeotemperature not noted in  $\delta^{18}\text{O}$  values. This may be the result of slow freshening of the basin over this period, but given the paucity of data, no further comment is possible.

At ~750cm, many rostra were collected. The short period of warming observed in near surface water palaeotemperatures at this time is observed in deeper water Mg values, with moving averages peaking at 1200ppm, but not in  $\delta^{18}\text{O}$  values, where the cooling trend previously described continues smoothly until 650cm, reaching ~8 °C (0.8 ‰). Following the peak at 750cm, Mg values decline to 500ppm at 650cm. The interplay of the  $\delta^{18}\text{O}$  and Mg values suggests that palaeotemperatures rose before falling, which occurred while the basin  $\delta_w$  value was decreasing.

Between 650cm and 50cm, few belemnites were available for collection, but the deeper water temperature signal preserved in both  $\delta^{18}\text{O}$  and Mg values indicate a steady rise in palaeotemperature, from ~8 °C at 650cm to 13 °C at 50cm (+0.8 to -0.5 ‰  $\delta^{18}\text{O}$ , 500 to 800ppm Mg). Between this horizon and the top of the section, both  $\delta^{18}\text{O}$  and Mg indicate a short lived cooling to 9 °C, followed by warming of equal magnitude.

## Controls on Ba concentration

The Ba concentration profiles of these rostra (Fig. 5) are consistent with those observed in modern mussel shells, exhibiting low background values punctuated by sharp peaks (Gillikin et al. 2006b), indicating that these signals are reflecting the original environment. The quantity of Ba present in seawater is a function of both riverine input and upwelling (Putten et al. 1999, Putten et al. 2000, Hendry et al. 2001, Gillikin et al. 2006b). Since this basin was a shallow inland sea, particularly when and where this outcrop of the Green Beds was deposited, upwelling is probably not a major factor in Ba supply in these rostra. However, the presence of terrestrial plant matter, which is commonly observed in these sediments, supports the hypothesis that these samples accumulated in close proximity to a river system. Further support for the latter hypothesis would be found if the peaks in Ba are accompanied by lower  $\delta^{18}\text{O}$  values with no change concomitant change in Mg concentrations (assuming constant temperature), which is not observed.

However, removing samples containing in excess of 500 ppm Ba, which presumably would indicate an abundance of Ba seawater, also removes any significant correlation between  $\delta^{18}\text{O}$  and Mg ( $r^2_{\text{adj}} = 0.02$ ,  $p = 0.218$ ), implying the relationship between Ba, Mg and  $\delta^{18}\text{O}$  values is complicated (Fig. 10b). Similarly there is no correlation between Mg and Ba ( $r^2_{\text{adj}} = 0.02$ ,  $p = 0.735$ ; Fig. 10c) and  $\delta^{18}\text{O}$  value and Ba concentration ( $r^2_{\text{adj}} = 0.01$ ,  $p = 0.584$ ; Fig. 10d). The incorporation of Ba into belemnite calcite is complex and should be understood as it may become a useful proxy for palaeo-runoff or upwelling.

## Conclusions

1. Belemnite rostra from 2 genera display significant, increasing  $\delta^{13}\text{C}$  value trends with ontogeny, implying that belemnoida show a decrease in metabolic rate with ontogeny. The  $\delta^{13}\text{C}$  values of these rostra probably document metabolic changes superimposed on an environmental signal.
2. Examining the ranges in  $\delta^{13}\text{C}$  values within individual belemnites over time revealed a positive excursion at 1150cm.
3. There is a significant trend in both  $\delta^{18}\text{O}$  values and Mg concentration for *Cylindroteuthis*, indicating decreasing palaeotemperatures with ontogeny, with some individuals

- exhibiting late life increases in palaeotemperature. This trend is interpreted as a migration from warm shallow waters to deeper, cooler waters with maturity.
4. While trends in Mg concentration and  $\delta^{18}\text{O}$  value generally change at the same time within individual rostra, the correlation between them is too low to construct a robust palaeotemperature equation for Mg.
  5. Using a combination of oxygen isotope values and Mg concentration, it may be possible to distinguish times of warming from variance in  $\delta_w$  values.

#### Acknowledgements

The authors would like to thank NSERC for the NSERC Discovery Grant awarded to Dr Darren Gröcke for analysis and travel expenses. Also, we would like to thank the Albertan government for granting a fossil collection permit to Duncan Findlay for the summer of 2005. The authors would also like to thank Steven Farber for his informative statistical discussion, and Professor P. Doyle for assistance in indentifying these belemnite rostra.

## Figure Captions

Fig. 1. A simplified geologic map of southern Alberta showing the location of the Carbondale River collection site.

Fig. 2. The stratigraphy of the Fernie Formation. Depositional cycles indicate the 5 asymmetric shallowing up cycles identified by Stronach (1984).

Fig. 3. An idealised representation of the sampling strategy utilised for belemnite rostra in this study (after Findlay and Gröcke previous chapter).

Fig. 4. Cross plots of  $\delta^{13}\text{C}$  and  $\delta^{18}\text{O}$  values. a) Pre diagenetic screening b) post diagenetic screening

Fig. 5. The geochemistry of all rostra samples that survived diagenetic screening, including sample number, genus and stratigraphic position.

Fig. 6. Graphs of *Cylindroteuthis* geochemistry vs. normalised distance from the apical line to the outer edge of the rostrum. Geochemical data are presented as deviation from the medial value for each rostrum.

Fig. 7. Graphs of *Pachyteuthis* geochemistry vs. normalised distance from the apical line to the outer edge of the rostrum. Geochemical data are presented as deviation from the medial value for each rostrum.

Fig. 8. Stratigraphic profiles of the geochemistry of the Green Bed rostra. Stratigraphic positions is presented as centimetres below the contact between the overlying Passage Beds and the Green Beds. Each bold horizontal line represents the internal range in geochemistry of one belemnite at a particular stratigraphic position.

Fig. 9. Schematic summarising belemnite life history. a) Juvenile belemnites occupy shallow waters b) Migration to deeper waters with maturity before further migration following favourable water conditions c) Post mating migration of impregnated females back to shallow waters to spawn, followed by death.

Fig. 10. Cross plots of stable isotopes and trace elements analysed from the same sample. a) Bulk  $\delta^{18}\text{O}$  vs. Mg values b)  $\delta^{18}\text{O}$  vs. Mg values after removing samples containing in excess of 500ppm Ba c)  $\delta^{18}\text{O}$  vs. Ba values d) Ba vs. Mg values.

Findlay and Gröcke  
Fig. 1

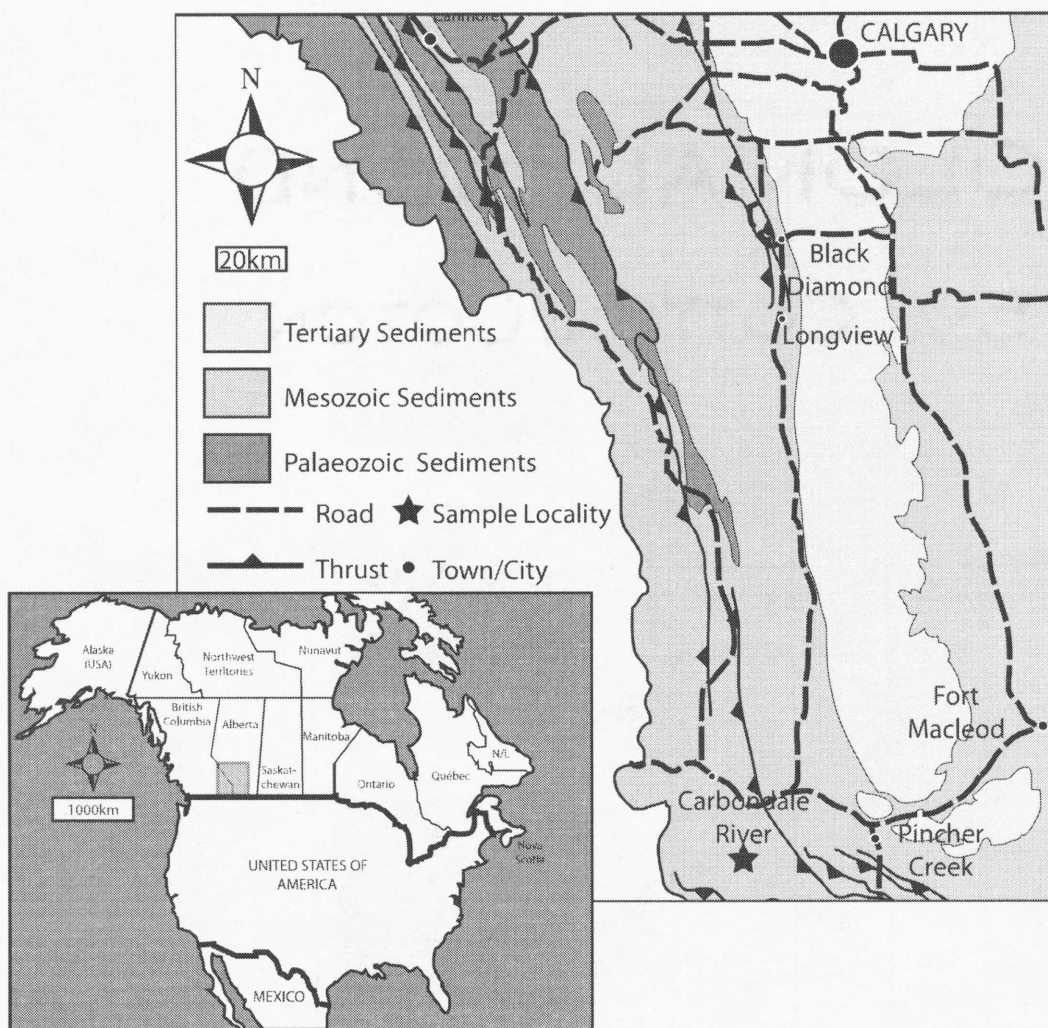


Fig. 1. A simplified geologic map of southern Alberta showing the location of the Carbondale River collection site.

Findlay and Gröcke  
Fig. 2

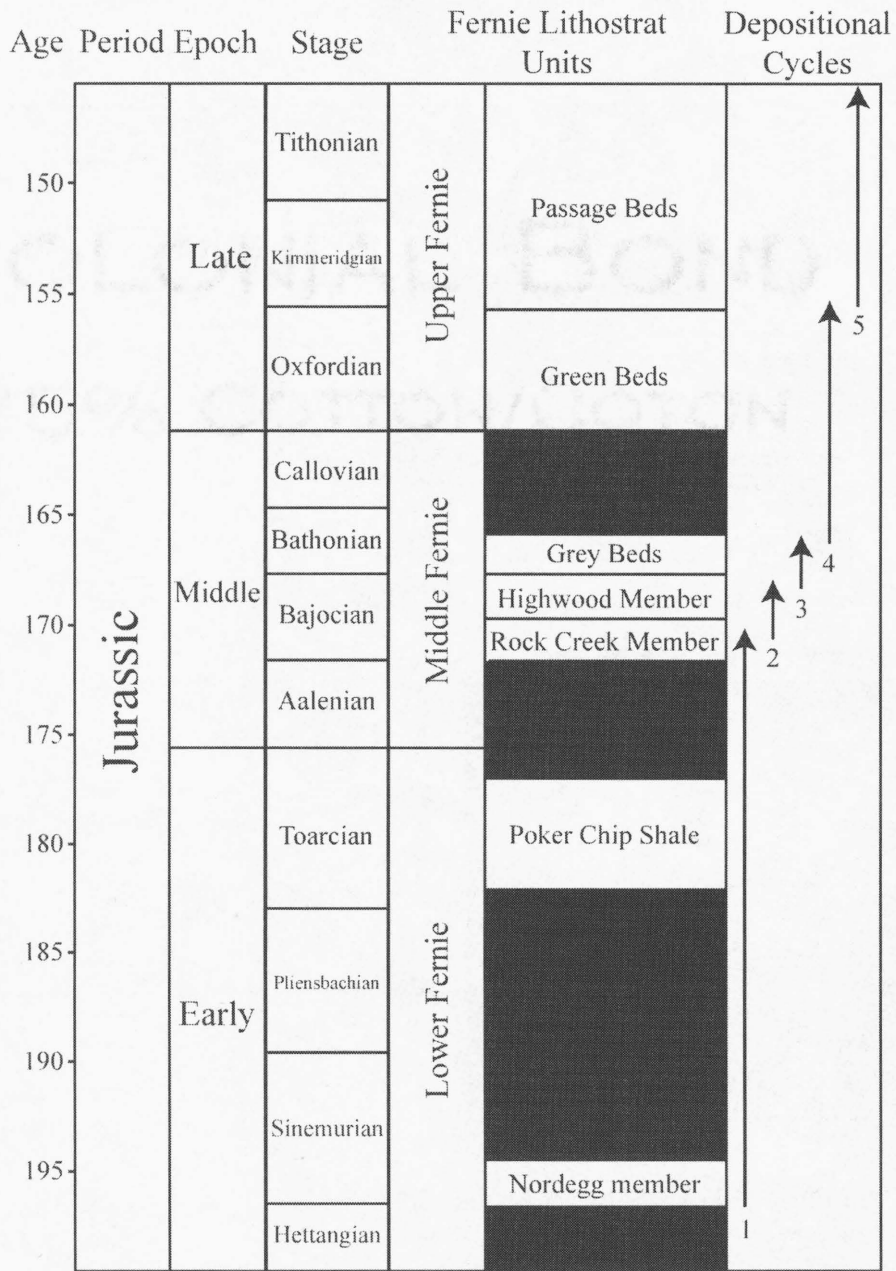


Fig.2. The stratigraphy of the Fernie Formation. Depositional cycles indicate the 5 asymmetric shallowing up cycles identified by Stronach (1984).

Findlay and Gröcke  
Fig 3

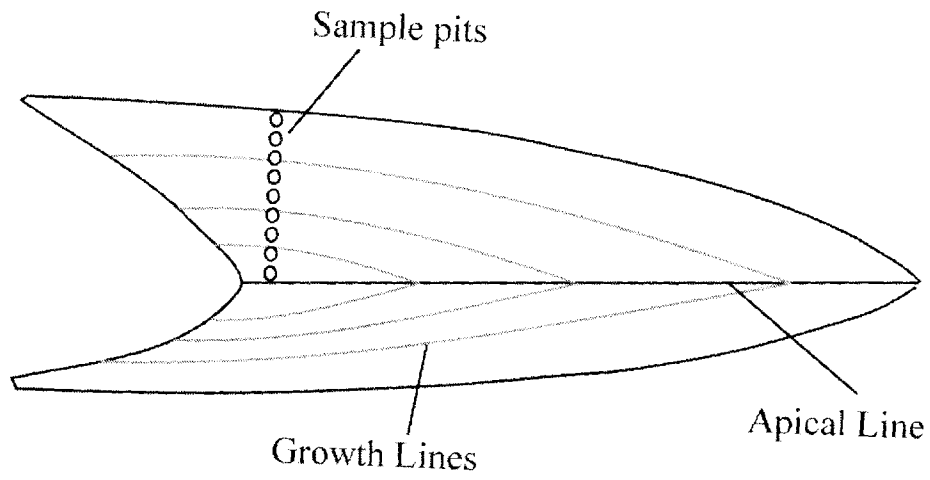


Fig. 3. An idealised representation of the sampling strategy utilised for belemnite rostra in this study (after Findlay and Gröcke previous chapter).

Findlay and Gröcke  
Fig 4

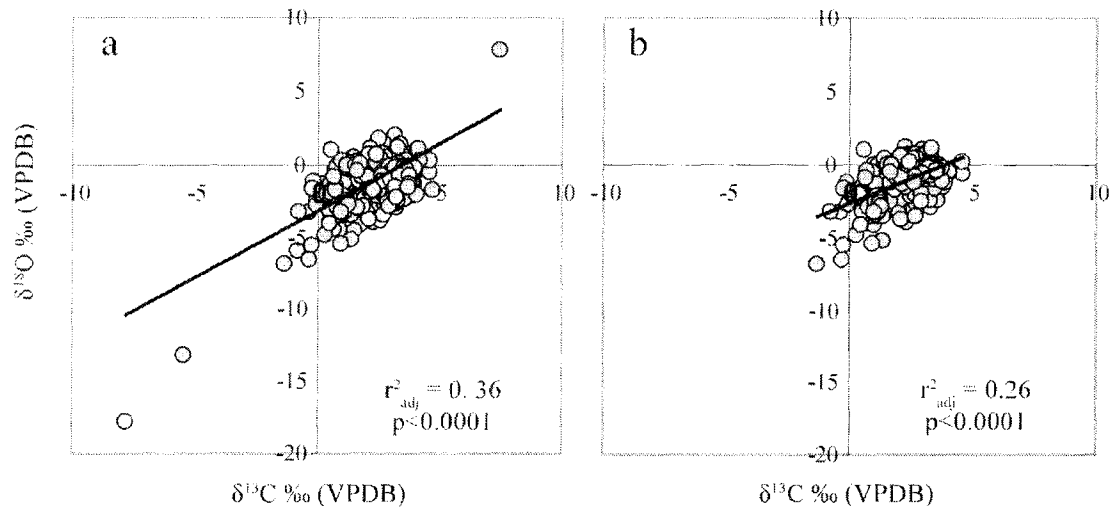


Fig. 4. Cross plots of  $\delta^{13}\text{C}$  and  $\delta^{18}\text{O}$  values. a) Pre diagenetic screening b) post diagenetic screening

Findlay and Gröcke  
Fig 5a

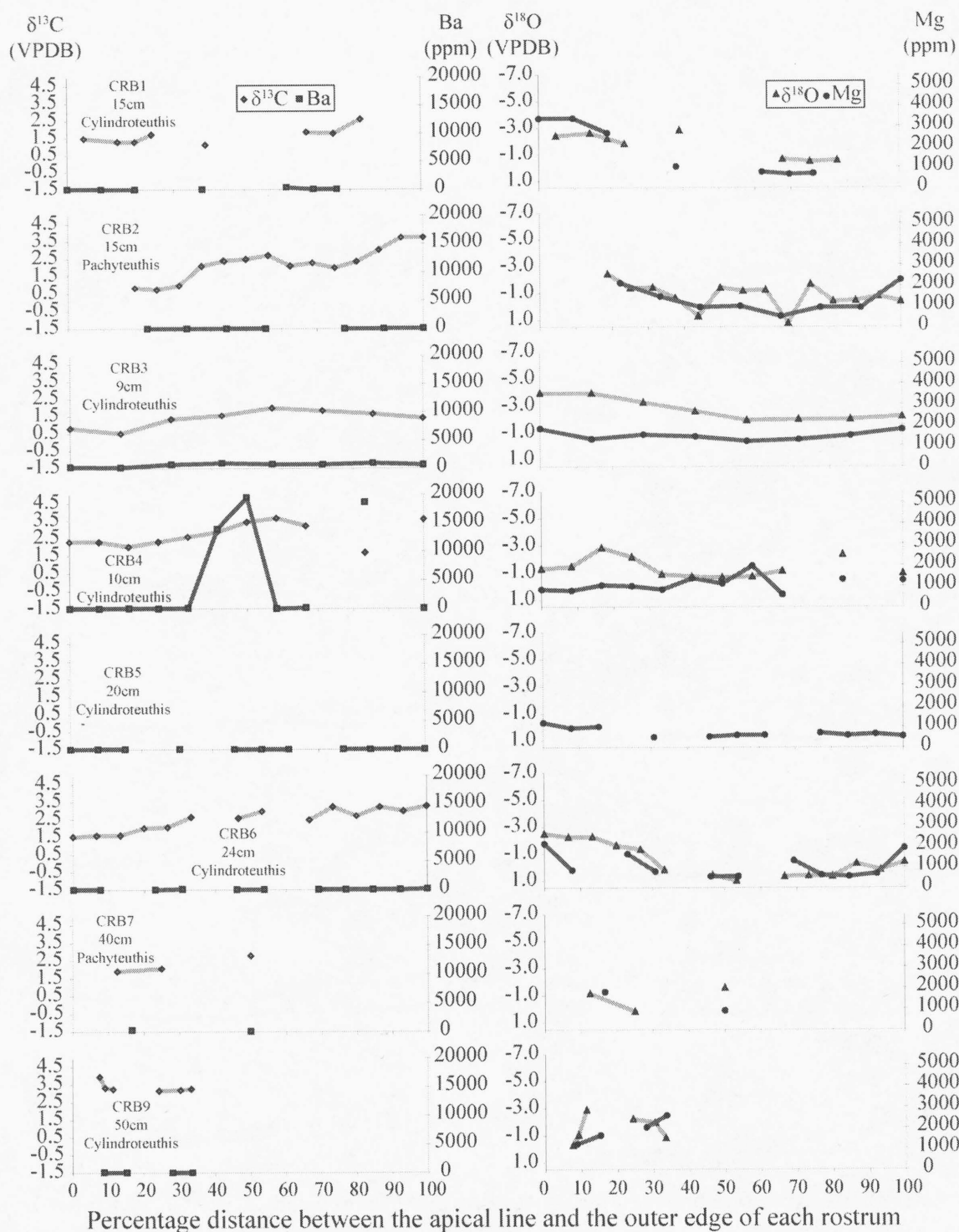


Fig. 5. The geochemistry of the belemnite samples that survived diagenetic screening, including sample number, genus and stratigraphic position.

Findlay and Gröcke  
Fig 5b

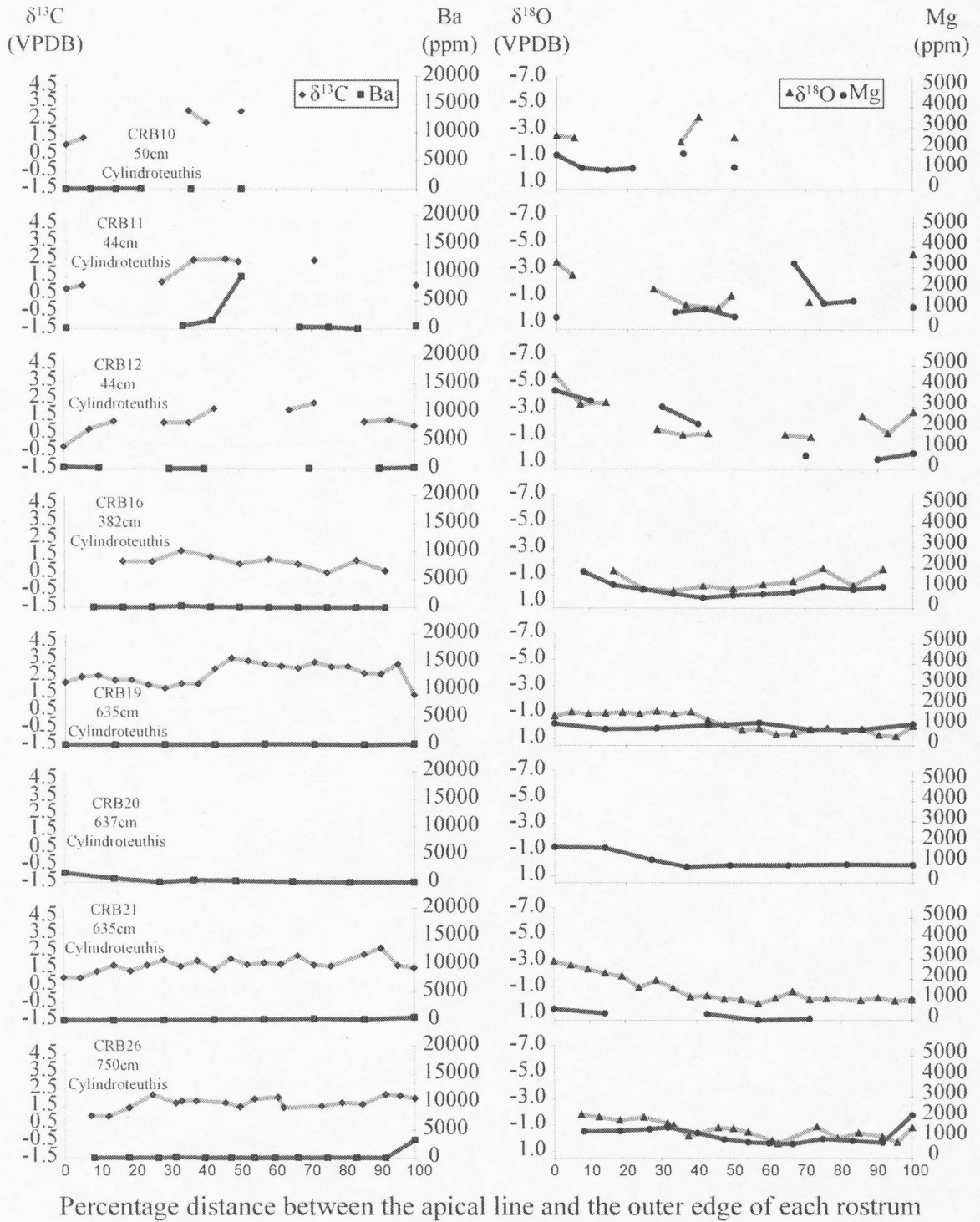


Fig. 5. The geochemistry of the belemnite samples that survived diagenetic screening, including sample number, genus and stratigraphic position.

Findlay and Gröcke  
Fig 5c

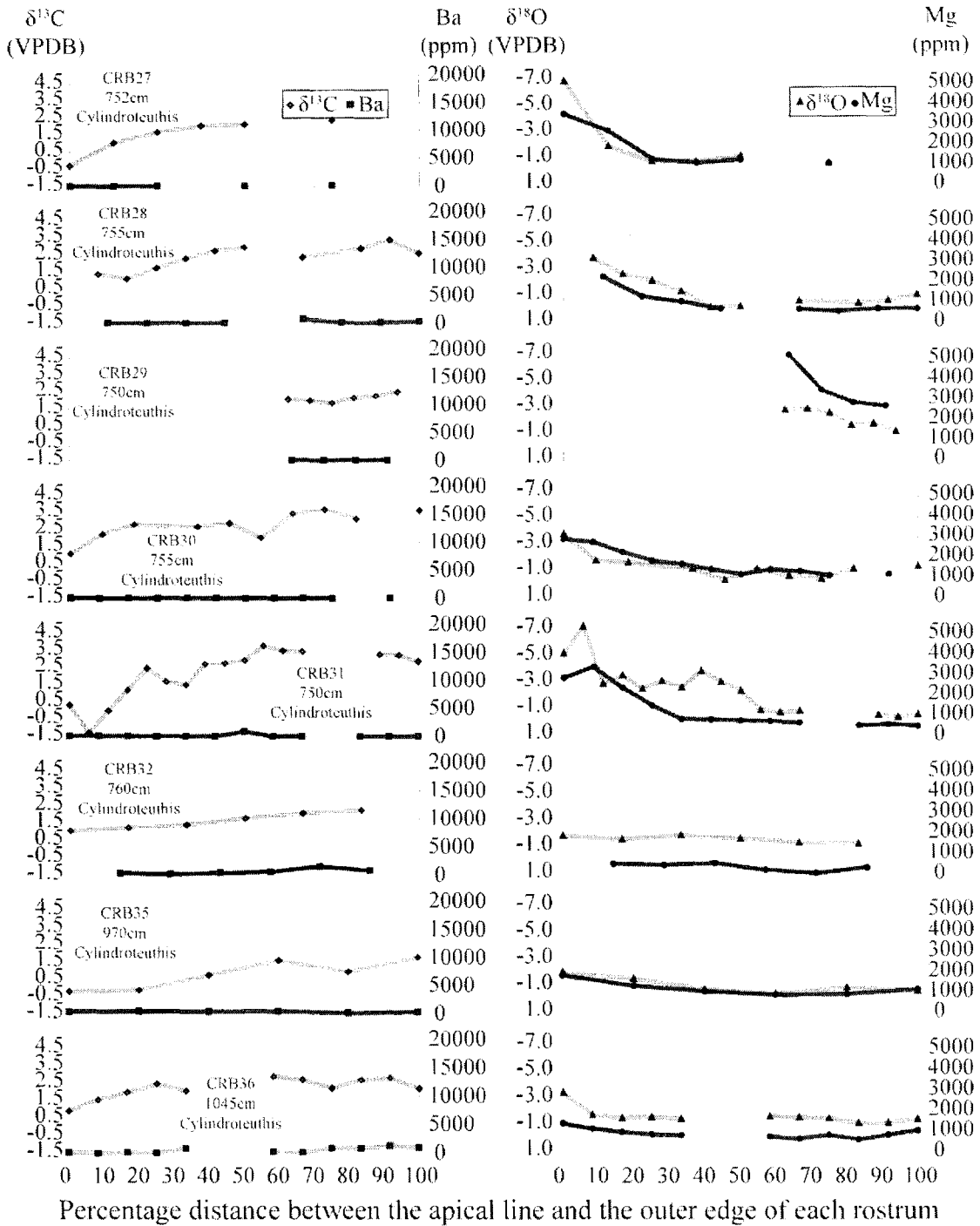


Fig. 5. The geochemistry of the belemnite samples that survived diagenetic screening, including sample number, genus and stratigraphic position.

Findlay and Gröcke  
Fig 5d

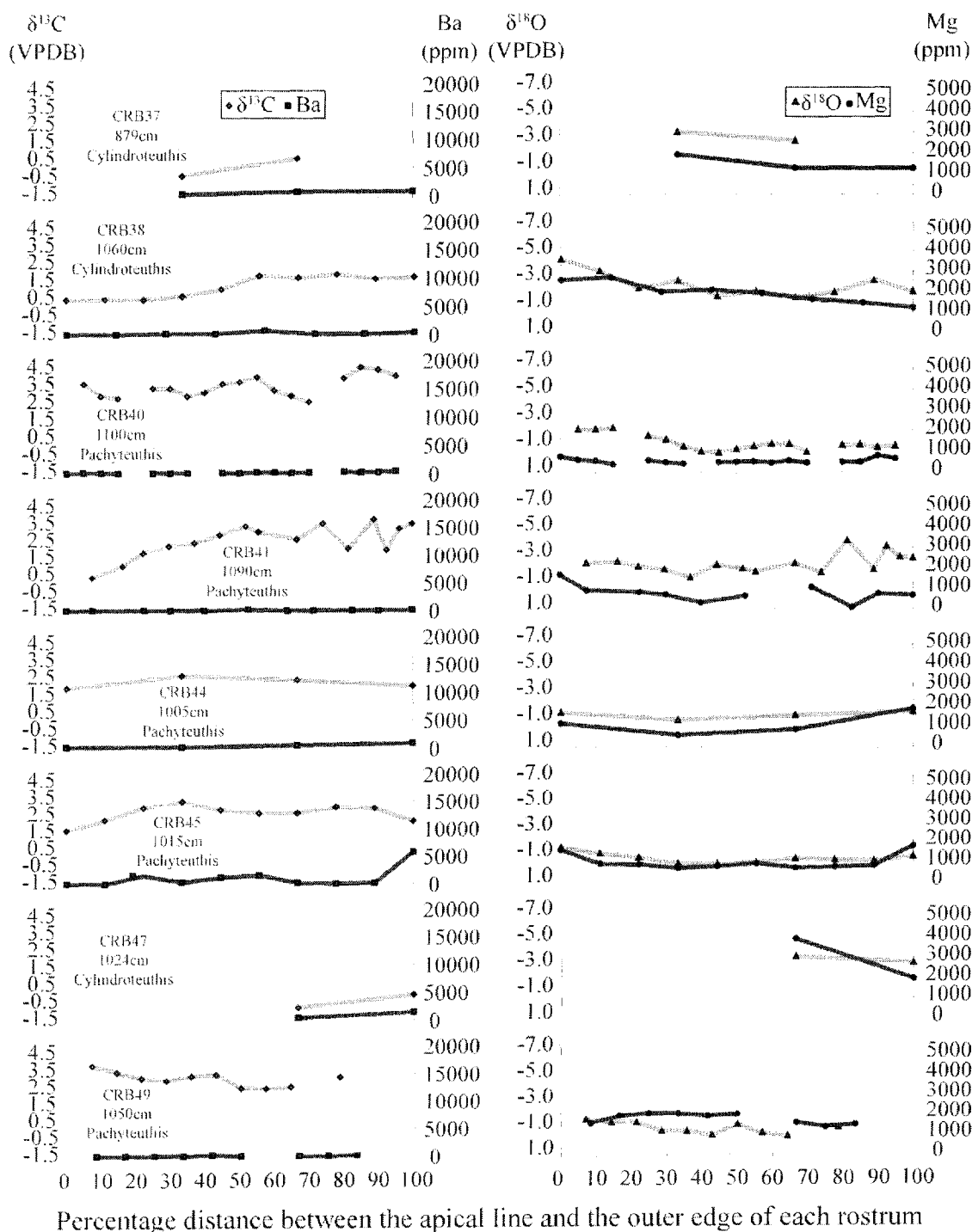


Fig. 5. The geochemistry of the belemnite samples that survived diagenetic screening, including sample number, genus and stratigraphic position.

Findlay and Gröcke  
Fig 5e

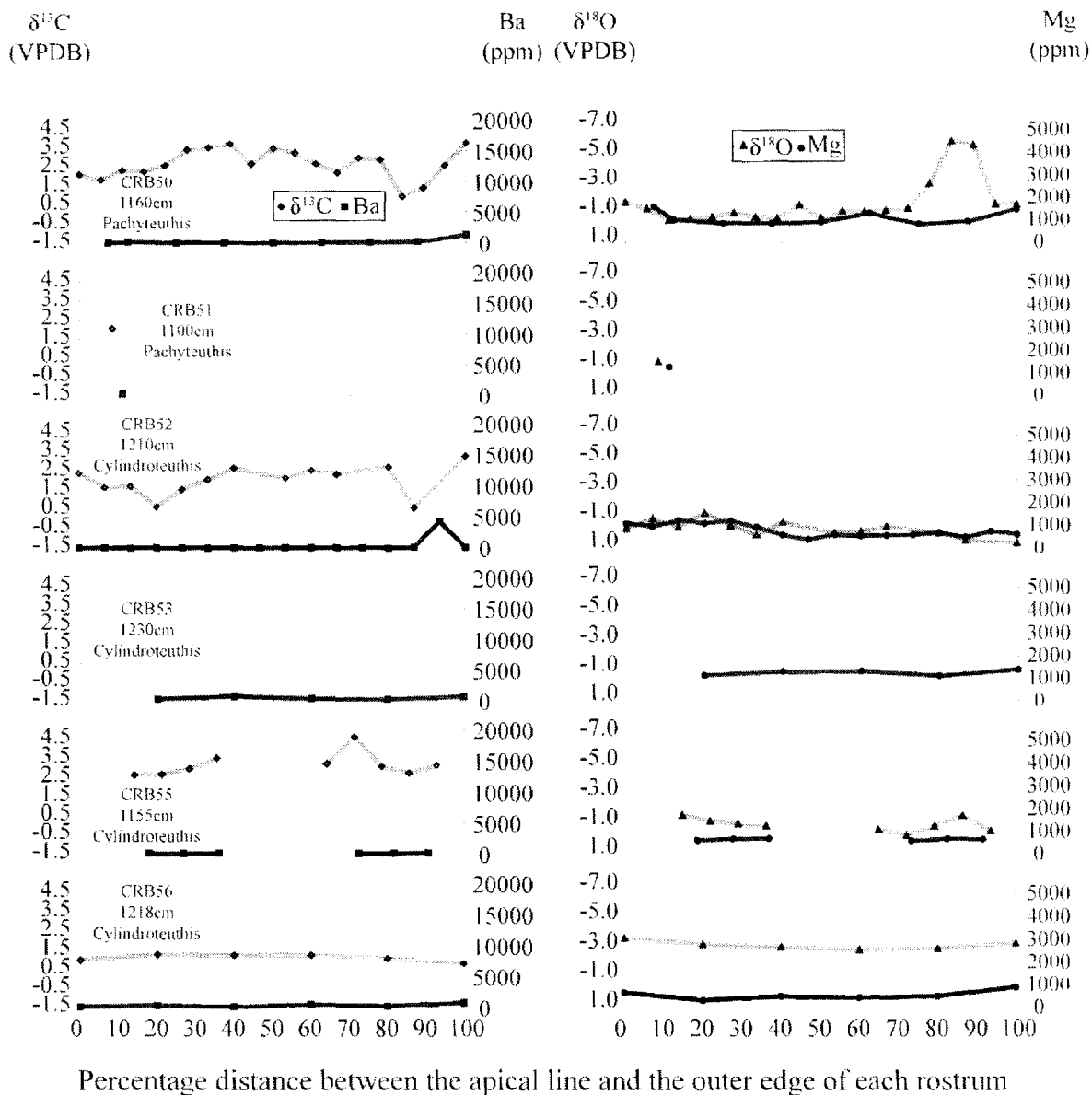


Fig. 5. The geochemistry of the belemnite samples that survived diagenetic screening, including sample number, genus and stratigraphic position.

Findlay and Gröcke  
Fig 6

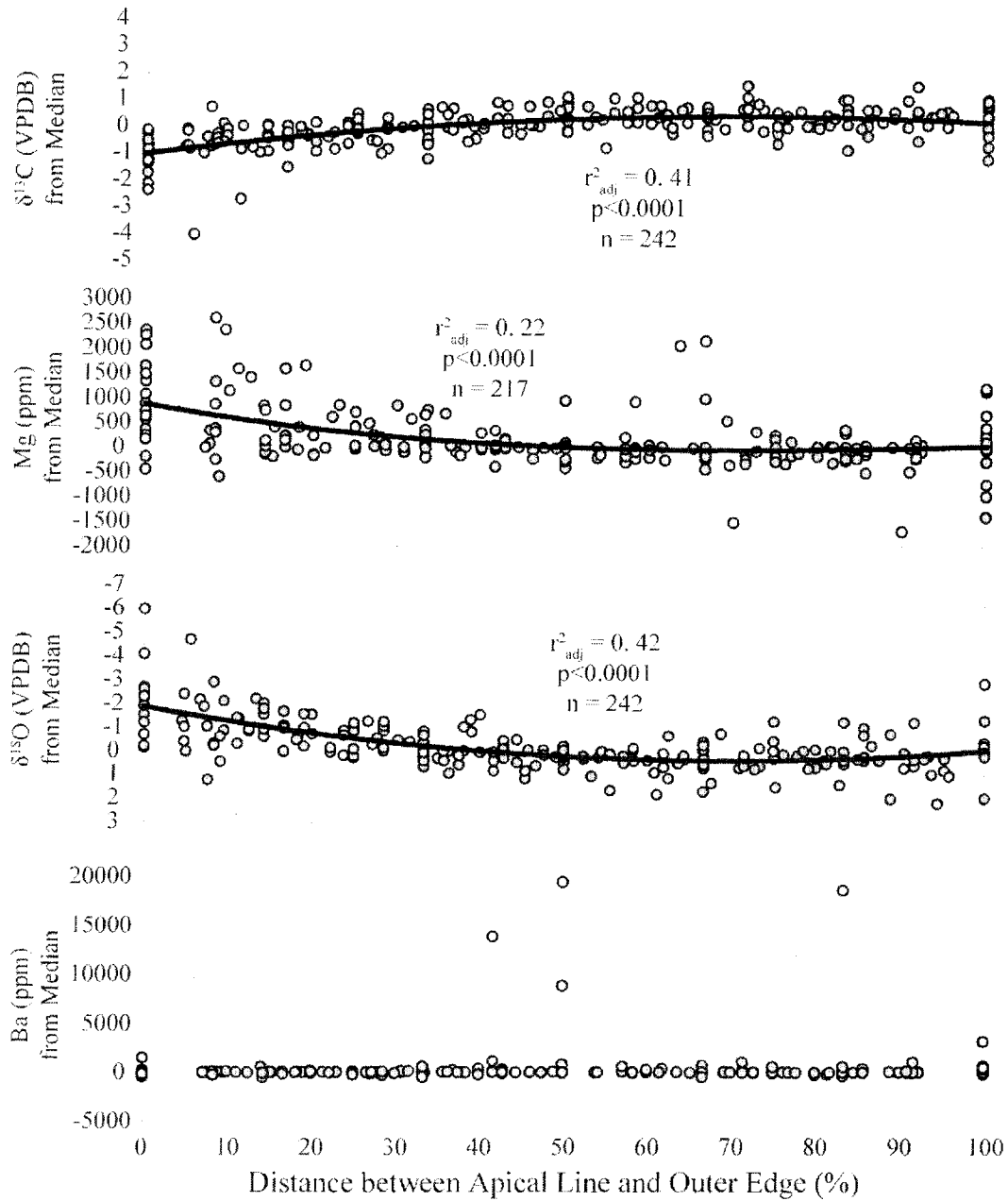


Fig. 6. Graphs of *Cylindroteuthis* geochemistry vs. normalised distance from the apical line to the outer edge of the rostrum. Geochemical data are presented as deviation from the medial value for each rostrum.

Findlay and Gröcke  
Fig 7

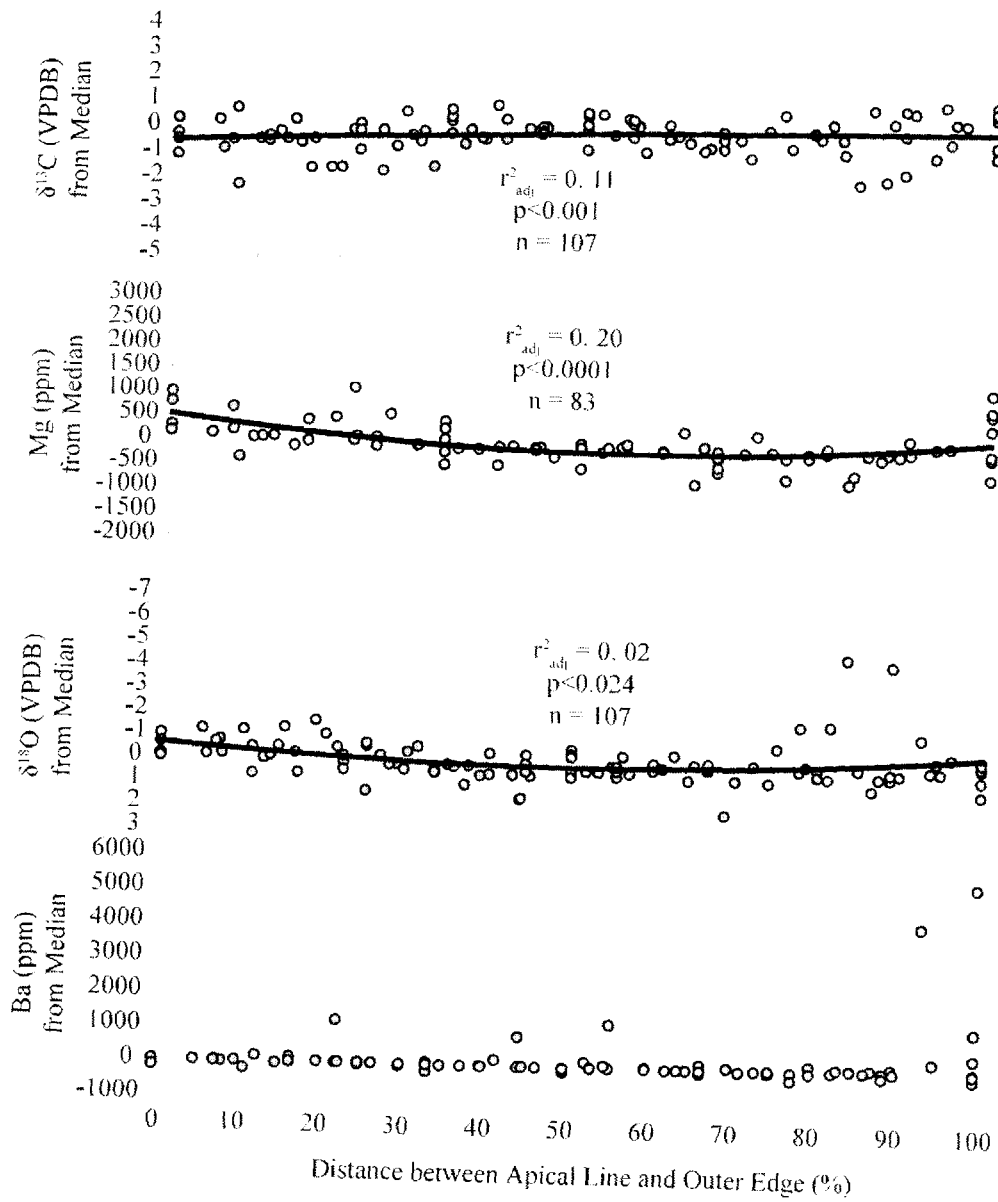


Fig. 7. Graphs of *Pachyteuthis* geochemistry vs. normalised distance from the apical line to the outer edge of the rostrum. Geochemical data are presented as deviation from the medial value for each rostrum.

Findlay and Gröcke  
Fig. 8

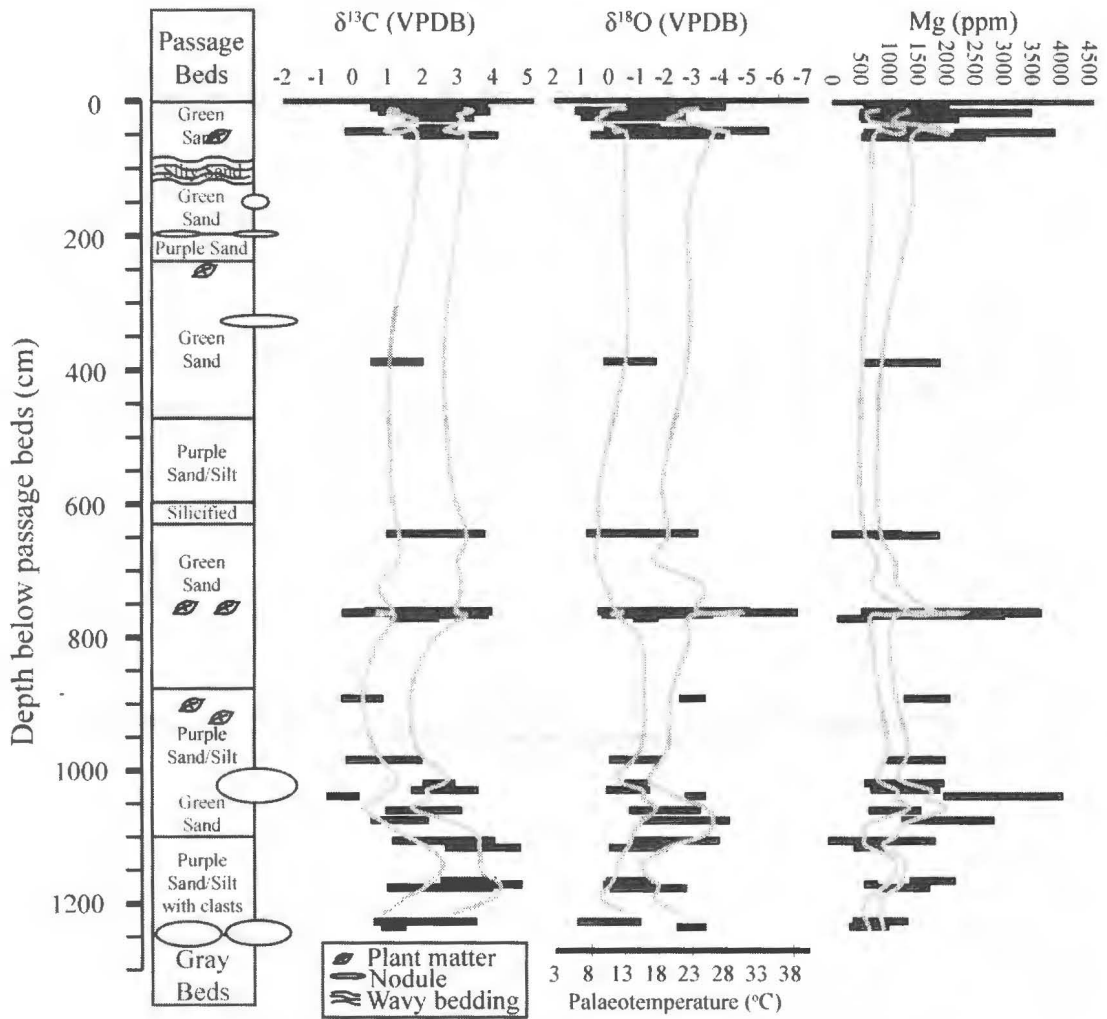


Fig. 8. Stratigraphic profiles of the geochemistry of the Green Bed belemnites. Stratigraphic positions are presented as centimetres from the contact between the overlying Passage Beds and the Green Beds. Each bold horizontal line represents the internal range in geochemistry of one belemnite at a particular stratigraphic position.

Findlay and Gröcke  
Fig 9

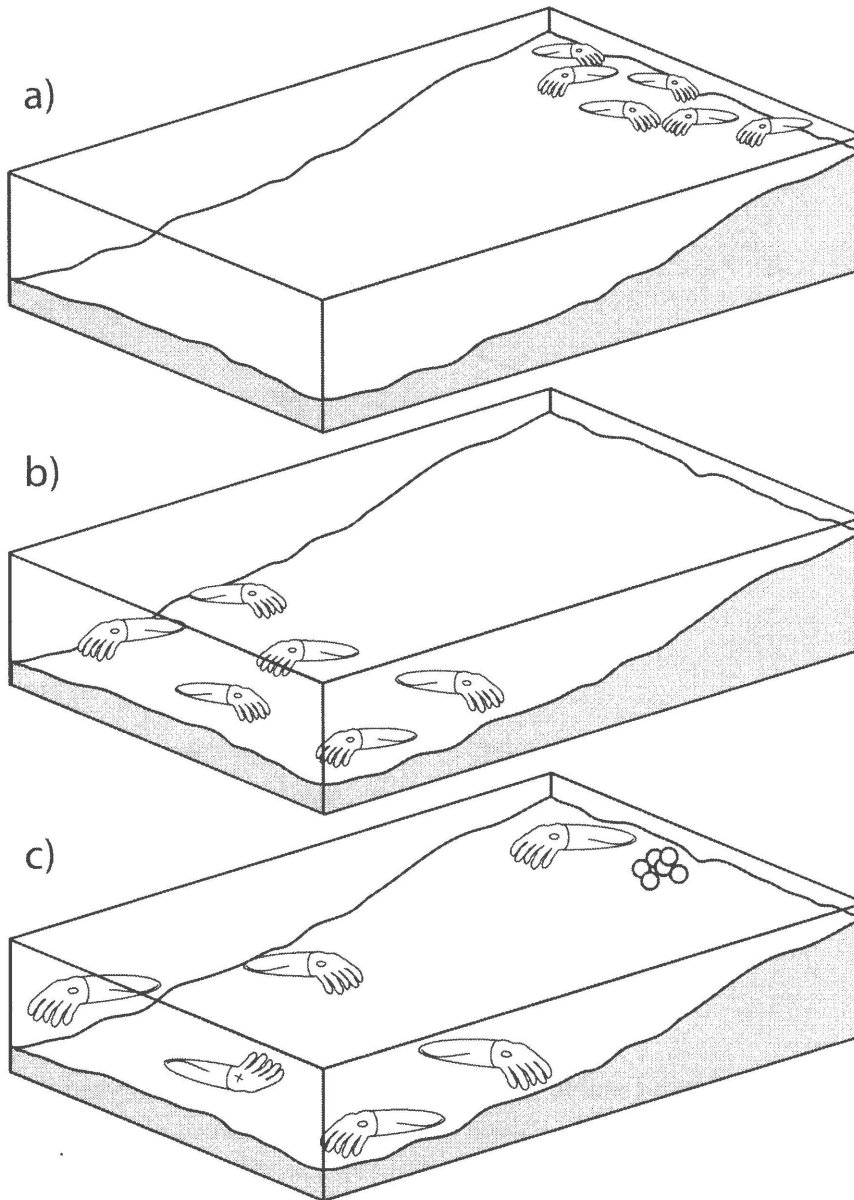


Fig. 9 . Schematic summarising belemnite life history. a) Juvenile belemnites occupying shallow waters b) Migration to deeper waters with maturity before further migration following favourable water conditions c) Post mating migration of successful females back to shallow waters to spawn, followed by death.

Findlay and Gröcke  
Fig 10

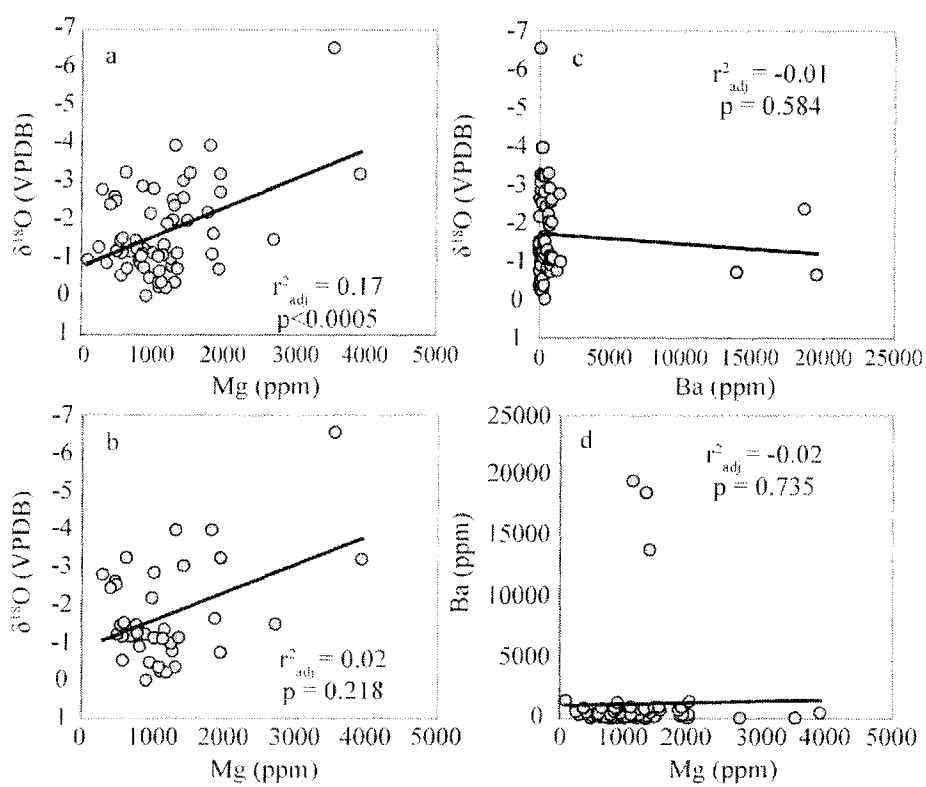


Fig. 10. Cross plots of stable isotopes and trace elements analysed from the same sample. a) Bulk  $\delta^{18}\text{O}$  vs. Mg values b)  $\delta^{18}\text{O}$  vs. Mg values after removing samples containing in excess of 500ppm Ba c)  $\delta^{18}\text{O}$  vs. Ba values d) Ba vs. Mg values.

Table 1

Stable Isotope Data					Trace Element Data (replicates where available)									
Sample	mm from Apical Line	Strat position from Passage Beds	$\delta^{13}\text{C}$ (VPDB)	$\delta^{18}\text{O}$ (VPDB)	Sample	mm from Apical Line	Ba	Mg	Mn	Sr				
crb-1-1	10.5	-15	1.3	-1.0	crb1-1	10.5	66	1184	108	556				
crb-1-2	9.7	-15	1.9	-1.2	crb1-2	10.0	22	709	38	745				
crb-1-3	8.9	-15	2.6	-1.1	crb1-3	9.0	20	506	27	665				
crb-1-4	8.1	-15	2.6	-0.6	crb1-4	8.0	25	689	29	842				
crb-1-5	7.3	-15	1.8	-0.5	crb1-5	7.3	22	660	17	801				
crb-1-6	6.5	-15	1.8	-0.7	crb1-6	6.5	371	763	7	874				
crb-1-7	5.7	-15	1.7	-0.8	crb1-7	5.5	21	734	8	798				
crb-1-8	4.8	-15	1.6	-1.4	crb1-8	5.0	19	763	5	775				
crb-1-9	4.0	-15	1.1	-2.8	crb1-9	4.0	21	1027	7	832				
crb-1-10	3.2	-15	1.8	-1.6	crb1-10	3.1	19	1000	34	681				
crb-1-11	2.4	-15	1.7	-1.8	crb1-11	2.0	21	2676	86	1101				
crb-1-12	1.6	-15	1.3	-2.2	crb1-12	1.0	29	3389	49	931				
crb-1-13	0.8	-15	1.3	-2.6	crb1-13	0.0	67	3380	80	994				
crb-1-14	0.0	-15	1.5	-2.4										
crb2-1	12.3	-15	3.7	-0.4	crb2-1	12.3	59	2267	61	1325				
crb2-2	11.6	-15	3.7	-0.8	crb2-2	10.9	48	925	8	1572				
crb2-3	10.9	-15	3.0	-0.5	crb2-3	9.6	4	935	7	1323				
crb2-5	9.6	-15	2.3	-0.4	crb2-4	8.2		508	7	1343				
crb2-6	8.9	-15	2.0	-1.7	crb2-5	6.8	2	994	10	1320				
crb2-7	8.2	-15	2.3	1.2	crb2-6	5.5	5	942	7	1380				
crb2-8	7.5	-15	2.1	-1.2	crb2-7	4.1	20	1448	11	1277				
crb2-9	6.8	-15	2.7	-1.2	crb2-8	2.7	5	2104	21	1345				
crb2-10	6.2	-15	2.5	-1.4	crb2-9	1.4	92	4463	191	1469				
crb2-11	5.5	-15	2.4	0.7	crb2-10	0.0	1130	4709	327	1358				
crb2-12	4.8	-15	2.4	0.7										
crb2-13	4.1	-15	2.1	-0.6										
crb2-14	3.4	-15	1.0	-1.4										
crb2-15	2.7	-15	0.7	-1.4										
crb2-16	2.1	-15	0.8	-2.4										
crb2-17	1.4	-15	0.6	-2.1										
crb2-18	0.7	-15	0.8	-2.5										
crb2-19	0.0	-15	1.5	-1.6										
crb3-1	8.2	-9	1.4	-2.2	crb3-1	8.2	634	629	1787	1518	49	42	1091	1050
crb3-2	7.0	-9	1.6	-2.0	crb3-2	7.0	903	880	1498	1329	35	29	1273	1217
crb3-3	5.9	-9	1.8	-2.0	crb3-3	5.9	654	648	1298	1093	22	16	1257	1104
crb3-4	4.7	-9	2.0	-1.9	crb3-4	4.7	712	701	1217	1029	23	19	1402	1347
crb3-5	3.5	-9	1.5	-2.6	crb3-5	3.5	898	880	1437	1218	20	15	1437	1371
crb3-6	2.3	-9	1.3	-3.3	crb3-6	2.3	671	651	1527	1352	13	9	1534	1453
crb3-7	1.2	-9	0.5	-4.0	crb3-7	1.2	148	154	1320	1176	15	12	1376	1330
crb3-8	0.0	-9	0.8	-3.9	crb3-8	0.0	222	224	1816	1706	29	26	1412	1393
crb4-1	10.0	-10	3.6	-1.0	crb4-1	10.0	75	220	1256	2359	59	134	1130	1911
crb4-2	9.2	-10	3.4	-0.8	crb4-2	9.2	17	21	700	631	26	28	741	819
crb4-3	8.3	-10	1.7	-2.4	crb4-3	8.3	18675	17223	1305	782	38	25	1498	972
crb4-4	7.5	-10	3.0	-1.2	crb4-4	7.5	871	1225	642	664	20	24	744	889
crb4-5	6.7	-10	3.2	-1.1	crb4-5	6.7	153	174	579	426	16	13	802	767
crb4-6	5.8	-10	3.7	-0.7	crb4-6	5.8	23	35	1947	3512	35	50	1022	1323
crb4-7	5.0	-10	3.4	-0.7	crb4-7	5.0	19527	41941	1101	1764	34	60	1359	2211
crb4-8	4.2	-10	2.9	-0.7	crb4-8	4.2	13933	22402	1352	2038	32	42	1143	1422
crb4-9	3.3	-10	2.6	-0.9	crb4-9	3.3	98	116	813	756	21	22	905	917
crb4-10	2.5	-10	2.3	-2.2	crb4-10	2.5	22	30	983	1148	9	10	1017	1228
crb4-11	1.7	-10	2.0	-2.8	crb4-11	1.7	65	69	1024	948	8	7	1021	1021
crb4-12	0.8	-10	2.3	-1.4	crb2-12	0.8	27	40	770	973	9	12	1017	1335
crb4-13	0.0	-10	2.3	-1.3	crb4-13	0.0	23	17	822	499	14	11	971	607
crb5-1	12.5	-20			crb5-1	12.5	37	58	541	697	138	110		
crb5-2	11.5	-20			crb5-2	11.5	24	35	649	806	138	104		

Table 1

Stable Isotope Data					Trace Element Data (replicates where available)									
Sample	mm from Apical Line	Strat position from Passage Beds	$\delta^{13}\text{C}$ (VPDB)	$\delta^{18}\text{O}$ (VPDB)	Sample	mm from Apical Line	Ba	Mg	Mn	Sr				
crb5-3	10.6	-20			crb5-3	10.6	17	28	581	729	139	104		
crb5-4	9.6	-20			crb5-4	9.6	38	49	703	874	139	106		
crb5-5	8.7	-20			crb5-5	8.7	30	49	848	1104	218	166		
crb5-6	7.7	-20			crb5-6	7.7	18	29	593	761	135	104		
crb5-7	6.7	-20			crb5-7	6.7	13	20	595	653	92	72		
crb5-8	5.8	-20			crb5-8	5.8	16	27	521	685	115	90		
crb5-9	4.8	-20			crb5-9	4.8	25	43	705	962	189	146		
crb5-10	3.8	-20			crb5-10	3.8	27	41	496	699	148	116		
crb5-11	2.9	-20			crb5-11	2.9	33	53	547	913	218	173		
crb5-12	1.9	-20			crb5-12	1.9	24	41	1000	1192	144	116		
crb5-13	1.0	-20			crb5-13	1.0	22	24	930	891	105	83		
crb5-14	0.0	-20			crb5-14	0.0	20	29	1190	1283	108	91		
crb6-1	12.5	-24	3.3	-0.4	crb6-1	12.5	156	106	1918	1300	52	44	1993	1239
crb6-2	11.7	-24	3.0	0.2	crb6-2	11.5	21	38	681	1092	4	5	1107	1785
crb6-3	10.8	-24	3.2	-0.3	crb6-3	10.6	15	22	548	640	4	5	959	1193
crb6-4	10.0	-24	2.7	0.6	crb6-4	9.6	18	20	611	590	5	3	901	879
crb6-5	9.2	-24	3.2	0.6	crb6-5	8.7	21	15	1307	903	12	9	963	564
crb6-6	8.3	-24	2.5	0.7	crb6-6	7.7	27	31	349	330	5	4	575	576
crb6-7	7.5	-24	3.1	0.7	crb6-7	6.7	20	32	559	781	21	31	1103	1593
crb6-8	6.7	-24	3.0	1.0	crb6-8	5.8	23	15	533	308	35	22	1033	602
crb6-9	5.8	-24	2.6	0.6	crb6-9	4.8	12	20	432	648	16	25	718	1059
crb6-10	5.0	-24	3.0	0.6	crb6-10	3.8	131	142	776	806	32	35	976	1012
crb6-11	4.2	-24	2.6	0.2	crb6-11	2.9	32	24	1624	1099	56	38	2022	1261
crb6-12	3.3	-24	2.1	-1.3	crb6-12	1.9	13	18	478	631	19	24	740	926
crb6-13	2.5	-24	2.0	-1.6	crb6-13	1.0	28	30	841	906	10	10	1196	1148
crb6-14	1.7	-24	1.6	-2.3	crb6-14	0.0	25	36	2108	2976	52	76	2261	3009
crb6-15	0.8	-24	1.6	-2.2										
crb6-16	0.0	-24	1.5	-2.5										
crb7-1	6.0	-40	3.7	-0.2	crb7-1	6.0	170		1141		55		598	
crb7-2	5.3	-40	3.9	-1.3	crb7-2	5.0	33		701		25		782	
crb7-3	4.5	-40	3.8	-0.1	crb7-3	4.0	43		902		27		753	
crb7-4	3.8	-40	3.3	-0.5	crb7-4	3.0	30		904		22		802	
crb7-5	3.0	-40	2.8	-1.6	crb7-5	2.0	18		1285		19		788	
crb7-6	2.3	-40	2.5	-0.1	crb7-6	1.0	274		1796		43		839	
crb7-7	1.5	-40	2.1	0.2	crb7-7	0.0	20		2072		41		794	
crb7-8	0.8	-40	1.9	-1.1										
crb7-9	0.0	-40	2.1	-1.3										
crb9-2	13.2	-50	3.0	0.6	crb9-1	12.5	658		1984		121		755	
crb9-3	12.7	-50	3.2	2.0	crb9-2	11.5	125		644		27		647	
crb9-4	12.0	-50	2.8	0.3	crb9-3	10.5	37		473		10		582	
crb9-5	11.3	-50	2.7	1.4	crb9-4	9.9	41		406		20		515	
crb9-6	10.5	-50	3.3	0.9	crb9-5	8.9	33		202		8		429	
crb9-7	10.0	-50	3.5	0.3	crb9-6	8.0	95		541		13		505	
crb9-9	9.0	-50	3.3	0.1	crb9-7	7.0	26		850		8		670	
crb9-10	8.5	-50	4.3	0.2	crb9-8	6.0	23		828		11		794	
crb9-11	8.0	-50	3.4	0.4	crb9-9	5.0	52		7327		661		3642	
crb9-12	7.8	-50	3.5	0.8	crb9-10	4.2	29		2581		128		1005	
crb9-13	7.5	-50	2.5	1.8	crb9-11	3.5	24		2022		124		1313	
crb9-14	7.0	-50	3.1	0.4	crb9-12	2.4	25		2472		176		1725	
crb9-16	6.8	-50	2.7	0.5	crb9-13	1.9	56		1638		82		1072	
crb9-17	5.5	-50	3.2	0.1	crb9-14	1.1	79		1226		37		912	
crb9-18	5.2	-50	3.1	-1.0	crb9-15	0.0	69		1332		51		697	
crb9-20	4.4	-50	3.3	-0.8										
crb9-23	4.0	-50	3.2	-2.0										
crb9-24	3.2	-50	3.2	-2.2										
crb9-25	2.5	-50	2.8	-2.6										

Table 1

Stable Isotope Data					Trace Element Data (replicates where available)									
Sample	mm from Apical Line	Strat position from Passage Beds	$\delta^{13}\text{C}$ (VPDB)	$\delta^{18}\text{O}$ (VPDB)	Sample	mm from Apical Line	Ba	Mg	Mn	Sr				
crb9-27	1.5	-50	3.2	-2.9										
crb9-28	1.2	-50	3.3	-1.1										
crb9-29	1.0	-50	4.0	-0.3										
crb9-30	0.0	-50	2.9	-0.2										
crb10-1	11.0	-50	3.3	0.5	crb10-1	11.0	128	1306	92	756				
crb10-2	10.5	-50	2.9	-1.0	crb10-2	10.2	23	499	13	582				
crb10-3	9.9	-50	2.4	0.1	crb10-3	9.4	19	506	10	674				
crb10-4	9.4	-50	1.7	-4.2	crb10-4	8.6	0	6	0	7				
crb10-5	8.8	-50	3.2	-2.6	crb10-5	7.9	25	808	86	658				
crb10-6	8.3	-50	3.4	1.4	crb10-6	7.1	15	808	119	688				
crb10-7	7.7	-50	3.4	-0.7	crb10-7	6.3	15	659	52	683				
crb10-8	7.2	-50	2.0	-0.7	crb10-8	5.5	20	1076	15	861				
crb10-9	6.6	-50	2.5	-2.6	crb10-9	4.7	20	778	6	734				
crb10-10	6.1	-50	3.9	-2.0	crb10-10	3.9	20	1744	15	1150				
crb10-11	5.5	-50	3.0	-2.4	crb10-11	3.1	12	814	8	730				
crb10-12	5.0	-50	2.6	-3.7	crb10-12	2.4	42	1038	16	991				
crb10-13	4.4	-50	2.3	-3.9	crb10-13	1.6	20	952	32	825				
crb10-14	3.9	-50	3.0	-2.1	crb10-14	0.8	18	1045	28	863				
crb10-15	3.3	-50	2.6	-3.9	crb10-15	0.0	17	1686	61	1300				
crb10-16	2.8	-50	-0.8	-5.9										
crb10-20	0.6	-50	1.5	-2.4										
crb10-21	0.0	-50	1.1	-2.5										
crb11-1	11.0	-44	1.0	-4.1	crb11-1	10.5	551	1088	62	1093				
crb11-4	9.0	-44	2.5	-0.2	crb11-2	9.0	1359	3373	239	1295				
crb11-5	7.8	-44	2.4	-0.5	crb11-3	7.5	58	1386	53	1525				
crb11-6	6.2	-44	1.2	-0.5	crb11-4	7.5	346	1276	53	1241				
crb11-7	5.4	-44	2.4	-1.0	crb11-5	6.5	340	3184	79	2836				
crb11-8	5.0	-44	2.5	-0.1	crb11-6	6.0	955	516	45	366				
crb11-9	4.0	-44	2.4	-0.3	crb11-7	5.0	9304	614	56	828				
crb11-11	3.0	-44	1.2	-1.5	crb11-8	4.0	1549	986	60	914				
crb11-12	2.2	-44	2.1	-1.0	crb11-9	3.2	523	841	55	823				
crb11-13	1.9	-44	2.0	-0.8	crb11-10	2.5	34	469	39	529				
crb11-14	1.5	-44	0.9	-4.5	crb11-11	2.0	40	549	33	688				
crb11-15	1.0	-44	0.7	-4.4	crb11-12	1.2	40	389	20	483				
crb11-16	0.5	-44	1.0	-2.5	crb11-13	0.0	185	581	25	856				
crb11-17	0.0	-44	0.8	-3.5										
crb12-1	9.0	-44	0.9	-2.7	crb12-1	9.0	234	227	766	705	140	1201	1137	
crb12-2	8.4	-44	1.3	-1.2	crb12-2	8.1	89	88	478	446	23	15	825	775
crb12-3	7.7	-44	1.2	-2.4	crb12-3	7.2	9	8	639	583	92	83	796	736
crb12-4	7.1	-44	1.7	-1.2	crb12-4	6.3	69	70	646	647	112	109	804	782
crb12-5	6.4	-44	2.3	-0.9	crb12-5	5.4	3	1	684	680	121	116	698	691
crb12-6	5.8	-44	1.9	-1.1	crb12-6	4.5	2	1	705	677	74	74	598	587
crb12-7	5.1	-44	2.0	-0.7	crb12-7	3.6	5	4	2169	2216	111	113	1126	1120
crb12-8	4.5	-44	1.3	-1.0	crb12-8	2.7	7	6	3013	3019	129	129	1138	1121
crb12-9	3.9	-44	1.9	-1.1	crb12-9	1.8	19	18	3496	3355	172	171	1165	1134
crb12-10	3.2	-44	1.1	-1.0	crb12-10	0.9	154	153	3305	3321	106	105	1153	1149
crb12-11	2.6	-44	1.1	-1.4	crb12-11	0.0	280	289	3801	3500	61	59	1072	1084
crb12-12	1.9	-44	1.1	-2.3										
crb12-13	1.3	-44	1.2	-3.5										
crb12-14	0.6	-44	0.8	-3.3										
crb12-15	0.0	-44	-0.2	-5.5										
crb13-1	8.5	-40	1.8	-1.0	crb13-1	8.5	193	1646	123	671				
crb13-2	7.9	-40	3.3	-0.9	crb13-2	7.3	24	1210	115	648				
crb13-3	7.4	-40	2.3	-0.7	crb13-3	6.0	18	931	111	586				
crb13-4	6.8	-40	1.9	-0.8	crb13-4	5.0	15	1063	88	616				

Table 1

Stable Isotope Data					Trace Element Data (replicates where available)									
Sample	mm from Apical Line	Strat position from Passage Beds	$\delta^{13}\text{C}$ (VPDB)	$\delta^{18}\text{O}$ (VPDB)	Sample	mm from Apical Line	Ba	Mg	Mn	Sr				
crb13-5	6.2	-40	2.2	-1.4	crb13-5	3.8	113	1202	86	548				
crb13-6	5.7	-40	1.9	-1.9	crb13-6	2.5	14	1588	76	668				
crb13-7	5.1	-40	1.2	-0.8	crb13-7	1.3	14	1749	95	656				
crb13-8	4.5	-40	1.6	-1.7	crb13-8	0.0	63	1899	73	715				
crb13-9	4.0	-40	0.9	-2.8										
crb13-10	3.4	-40	1.0	-1.4										
crb13-11	2.8	-40	1.7	-0.8										
crb13-12	2.3	-40	1.9	-1.0										
crb13-13	1.7	-40	1.7	-1.1										
crb13-14	1.0	-40	1.4	-1.8										
crb13-15	0.6	-40	1.3	-2.3										
crb13-16	0.0	-40	1.6	-2.1										
crb16-1	10.8	-382	0.3	-1.4	crb16-1	11.0	13	32	1127	400	85	197	786	783
crb16-2	9.9	-382	0.6	-1.4	crb16-2	10.1	7	7	1044	685	40	70	1229	1039
crb16-3	9.0	-382	1.2	-0.2	crb16-3	9.2	4	5	911	693	38	62	1058	996
crb16-4	8.1	-382	0.5	-1.5	crb16-4	8.3	7	8	1065	686	69	98	1168	992
crb16-5	7.2	-382	1.0	-0.5	crb16-5	7.3	4	5	783	577	36	50	1052	857
crb16-6	6.3	-382	1.3	-0.3	crb16-6	6.4	5	7	681	550	34	45	977	844
crb16-7	5.4	-382	1.0	0.1	crb16-7	5.5	36	39	627	507	44	54	892	733
crb16-8	4.5	-382	1.5	-0.2	crb16-8	4.6	102	111	506	337	62	66	801	654
crb16-9	3.6	-382	1.8	0.2	crb16-9	3.7	260	325	699	571	51	53	901	763
crb16-10	2.7	-382	1.2	0.1	crb16-10	2.8	75	84	914	805	88	101	905	765
crb16-11	1.8	-382	1.2	-1.3	crb16-11	1.8	8	9	1136	1038	89	90	905	768
					crb16-12	0.9	14	15	1780	1780	110	107	1016	870
					crb16-13	0.0	155	169	1401	1550	237	243	944	836
crb18-1	10.5	-650	1.9	0.0	crb18-1	10.5	1287		816		374		906	
crb18-2	9.2	-650	2.8	-0.6	crb18-2	9.6	521		794		338		832	
crb18-3	7.9	-650	2.9	-0.6	crb18-3	8.8	2073		808		291		825	
crb18-4	6.6	-650	2.4	-1.1	crb18-4	7.9	916		1009		267		740	
crb18-5	5.3	-650	7.5	7.8	crb18-5	7.0	2239		907		273		802	
crb18-6	3.9	-650	2.2	-0.7	crb18-6	6.1	528		982		205		790	
crb18-7	2.6	-650	2.8	-1.3	crb18-7	5.3	754		1117		181		665	
crb18-8	1.3	-650	2.8	-1.5	crb18-8	4.4	133		1053		201		723	
crb18-9	0.0	-650	2.1	-1.6	crb18-9	3.5	493		852		210		661	
					crb18-10	2.6	905		962		186		679	
					crb18-11	1.8	150		1028		105		631	
					crb18-12	0.9	51		1256		117		621	
					crb18-13	0.0	365		1491		112		731	
crb19-1	10.1	-635	1.4	0.0	crb19-1	9.2	178	166	1054	917	41	34	1162	1052
crb19-2	9.6	-635	3.2	0.8	crb19-2	7.9	37	43	781	680	13	9	1206	1112
crb19-4	9.1	-635	2.7	0.7	crb19-3	6.6	99	99	779	710	10	7	1191	1145
crb19-5	8.7	-635	2.7	0.3	crb19-4	5.3	124	125	1108	960	10	6	1149	1108
crb19-6	8.2	-635	3.1	0.4	crb19-5	3.9	25	32	988	864	8	5	1218	1172
crb19-7	7.7	-635	3.1	0.2	crb19-6	2.6	34	44	850	730	8	4	1450	1372
crb19-8	7.2	-635	3.3	0.3	crb19-7	1.3	5	11	804	725	6	4	1335	1282
crb19-9	6.7	-635	3.0	0.6	crb19-8	0.0	9	19	1074	952	8	5	1390	1336
crb19-10	6.3	-635	3.1	0.7										
crb19-11	5.8	-635	3.2	0.2										
crb19-12	5.3	-635	3.4	0.4										
crb19-13	4.8	-635	3.6	0.0										
crb19-14	4.3	-635	3.0	-0.4										
crb19-15	3.8	-635	2.1	-1.0										
crb19-16	3.4	-635	2.1	-0.8										
crb19-17	2.9	-635	1.8	-1.1										
crb19-18	2.4	-635	2.0	-0.9										
crb19-19	1.9	-635	2.3	-1.0										

Table 1

Stable Isotope Data					Trace Element Data (replicates where available)									
Sample	mm from Apical Line	Strat position from Passage Beds	$\delta^{13}\text{C}$ (VPDB)	$\delta^{18}\text{O}$ (VPDB)	Sample	mm from Apical Line	Ba	Mg	Mn	Sr				
crb19-20	1.4	-635	2.3	-0.9										
crb19-21	1.0	-635	2.6	-0.9										
crb19-22	0.5	-635	2.5	-1.0										
crb19-23	0.0	-635	2.2	-0.7										
crb20-1	9.2	-637			crb20-1	9.2	12	868	31	1128				
crb20-2	7.5	-637			crb20-2	7.5	6	893	93	919				
crb20-3	6.0	-637			crb20-3	6.0	114	853	22	1181				
crb20-4	4.5	-637			crb20-4	4.5	242	852	16	1217				
crb20-5	3.4	-637			crb20-5	3.4	374	777	6	1120				
crb20-6	2.5	-637			crb20-6	2.5	41	1118	9	1075				
crb20-7	1.3	-637			crb20-7	1.3	692	1713	12	1417				
crb20-8	0.0	-637			crb20-8	0.0	1672	1766	16	1319				
crb21-1	8.8	-635	1.5	0.0	crb21-1	8.8	503	976	36	1214				
crb21-2	8.4	-635	1.7	0.1	crb21-2	7.5	129		12	1439				
crb21-3	8.0	-635	2.7	-0.2	crb21-3	6.3	240	73	16	1323				
crb21-4	7.5	-635	2.3	0.0	crb21-4	5.0	148	13	9	1153				
crb21-6	6.7	-635	1.6	-0.1	crb21-5	3.8	101	312	12	1172				
crb21-7	6.3	-635	1.7	-0.1	crb21-6	2.5	10		5	1171				
crb21-8	5.9	-635	2.2	-0.6	crb21-7	1.3	2	336	2	1195				
crb21-9	5.4	-635	1.8	-0.1	crb21-8	0.0	4	557	5	1356				
crb21-10	5.0	-635	1.8	0.3										
crb21-11	4.6	-635	1.7	0.0										
crb21-12	4.2	-635	2.1	-0.1										
crb21-13	3.8	-635	1.4	-0.3										
crb21-14	3.4	-635	1.9	-0.3										
crb21-15	2.9	-635	1.6	-0.9										
crb21-16	2.5	-635	2.0	-1.5										
crb21-17	2.1	-635	1.7	-0.9										
crb21-18	1.7	-635	1.3	-1.8										
crb21-19	1.3	-635	1.7	-2.0										
crb21-20	0.8	-635	1.3	-2.4										
crb21-21	0.4	-635	1.0	-2.7										
crb21-22	0.0	-635	1.0	-2.9										
crb26-1	12.0	-750	2.0	-0.8	crb26-1	12.0	3210	2103	141	1762				
crb26-2	11.5	-750	2.1	0.3	crb26-2	11.0	31	752	41	1175				
crb26-3	11.0	-750	2.2	-0.1	crb26-3	10.0	29	842	63	1103				
crb26-4	10.2	-750	1.6	-0.4	crb26-4	9.0	17	935	86	1080				
crb26-5	9.5	-750	1.7	0.0	crb26-5	8.0	18	692	23	1151				
crb26-6	8.8	-750	1.5	-0.9	crb26-6	7.2	15	717	31	1105				
crb26-7	7.5	-750	1.4	0.4	crb26-7	6.5	17	777	33	979				
crb26-8	7.3	-750	2.0	0.2	crb26-8	5.7	15	913	40	998				
crb26-9	6.5	-750	1.9	-0.5	crb26-9	4.8	14	1224	43	1203				
crb26-10	6.0	-750	1.5	-0.7	crb26-10	3.8	136	1500	42	1273				
crb26-11	5.5	-750	1.7	-0.8	crb26-11	3.2	19	1415	32	1307				
crb26-12	4.5	-750	1.8	-0.2	crb26-12	2.2	68	1331	52	1153				
crb26-13	4.0	-750	1.8	-0.9	crb26-13	1.0	11	1307	69	1040				
crb26-14	3.8	-750	1.7	-1.1	crb26-14	0.0	10	1026	45	602				
crb26-15	3.0	-750	2.2	-1.6										
crb26-16	2.2	-750	1.4	-1.4										
crb26-17	1.5	-750	0.9	-1.6										
crb26-18	0.9	-750	1.0	-1.8										
crb26-19	0.0	-750	1.3	-1.0										
crb27-1	10.4	-752	3.0	0.2	crb27-1	10.4	192	197	1286	1139	314	292	1018	993
crb27-2	9.1	-752	2.5	-0.4	crb27-2	9.1	49	64	1200	1001	163	152	847	819
crb27-3	7.8	-752	2.4	-0.2	crb27-3	7.8	94	101	1111	997	45	42	1228	1192

Table 1

Stable Isotope Data					Trace Element Data (replicates where available)									
Sample	mm from Apical Line	Strat position from Passage Beds	$\delta^{13}\text{C}$ (VPDB)	$\delta^{18}\text{O}$ (VPDB)	Sample	mm from Apical Line	Ba	Mg	Mn	Sr				
crb27-4	6.5	-752	2.4	-0.4	crb27-4	6.5	114	123	1200	1084	308	284	1222	1172
crb27-5	5.2	-752	2.1	-0.8	crb27-5	5.2	16	23	1277	1140	43	39	1353	1317
crb27-6	3.9	-752	2.0	-0.4	crb27-6	3.9		8	1129	962	15	12	1250	1228
crb27-7	2.6	-752	1.7	-0.4	crb27-7	2.6	33	38	1324	1213	22	20	1205	1163
crb27-8	1.3	-752	1.0	-1.5	crb27-8	1.3	6	11	2716	2526	56	51	1376	1310
crb27-9	0.0	-752	-0.3	-6.5	crb27-9	0.0	5	11	3553	3339	51	47	1263	1236
crb28-2	9.6	-755	2.6	-0.7	crb28-1	10.4	305		710		12		1364	
crb28-3	8.8	-755	3.3	-0.2	crb28-2	9.2	142		715		11		1050	
crb28-4	8.0	-755	2.9	0.0	crb28-3	8.1	93		588		1		1330	
crb28-6	6.4	-755	2.4	-0.2	crb28-4	6.9	779		694		4		1503	
crb28-7	5.6	-755	3.0	-0.1	crb28-5	5.8	91		562		4		778	
crb28-8	4.8	-755	2.9	0.2	crb28-6	4.6	92		708		0		1398	
crb28-9	4.0	-755	2.7	0.3	crb28-7	3.5	68		1061		28		1297	
crb28-10	3.2	-755	2.3	-0.9	crb28-8	2.3	64		1319		11		1274	
crb28-11	2.4	-755	1.7	-1.8	crb28-9	1.2	100		2291		89		1354	
crb28-12	1.6	-755	1.1	-2.3	crb28-10	0.0	164		4552		69		692	
crb28-13	0.8	-755	1.4	-3.5										
crb28-14	0.0	-755	0.6	-3.7										
crb29-1	9.0	-750	1.8	-1.2	crb29-1	9.0	76		1925		445		851	
crb29-2	8.4	-750	2.5	-0.8	crb29-2	8.2	61		2700		83		3330	
crb29-3	7.9	-750	2.3	-1.3	crb29-3	7.4	30		2875		74		1915	
crb29-4	7.3	-750	2.2	-1.2	crb29-4	6.5	21		3505		58		1934	
crb29-5	6.8	-750	1.8	-2.2	crb29-5	5.7	67		5239		117		2161	
crb29-6	6.2	-750	2.0	-2.5	crb29-6	4.9	42		648		42		410	
crb29-7	5.6	-750	2.1	-2.4	crb29-7	4.1	224		530		33		621	
crb29-8	5.1	-750	2.3	-2.0	crb29-8	3.3	58		609		29		702	
crb29-9	4.5	-750	1.8	-2.0	crb29-9	2.5	10		213		13		236	
crb29-10	3.9	-750	1.8	-1.7	crb29-10	1.6	15		523		25		647	
crb29-11	3.4	-750	2.0	-1.5	crb29-11	0.8	86		454		20		474	
crb29-12	2.8	-750	1.5	-2.1	crb29-12	0.0	122		734		28		779	
crb29-13	2.3	-750	1.3	-2.3										
crb29-14	1.7	-750	1.4	-1.9										
crb29-15	1.1	-750	1.4	-2.1										
crb29-16	0.6	-750	1.3	-2.2										
crb29-17	0.0	-750	1.4	-2.5										
crb30-2	10.3	-755	3.6	-1.0	crb30-1	11.2	87		1352		40		517	
crb30-3	9.3	-755	3.2	-0.8	crb30-2	10.3	22		1199		14		959	
crb30-4	8.4	-755	3.1	-0.8	crb30-3	9.3	10		594		7		302	
crb30-5	7.5	-755	3.7	0.0	crb30-4	8.4	11		1140		10		932	
crb30-6	6.5	-755	3.4	-0.2	crb30-5	7.5	36		1338		12		1026	
crb30-7	5.6	-755	2.0	-0.7	crb30-6	6.5	18		1414		17		1182	
crb30-8	4.7	-755	2.9	0.1	crb30-7	5.6	12		1181		10		1129	
crb30-9	3.7	-755	2.7	-0.7	crb30-8	4.7	38		1431		13		1195	
crb30-11	1.9	-755	2.8	-1.2	crb30-9	3.7	114		1676		14		1074	
crb30-12	0.9	-755	2.2	-1.4	crb30-10	2.8	59		1848		17		1093	
crb30-13	0.0	-755	1.1	-3.4	crb30-11	1.9	44		2275		63		860	
					crb30-12	0.9	14		2756		25		1135	
					crb30-13	0.0	86		2905		21		1078	
crb31-1	8.3	-750	2.9	-0.2	crb31-1	8.3	16	19	518	598	114	128	905	787
crb31-2	7.8	-750	3.2	0.0	crb31-2	7.6	6	7	601	665	60	57	939	818
crb31-3	7.4	-750	3.3	-0.2	crb31-3	6.9	13	14	538	722	91	83	993	856
crb31-5	6.5	-750	3.4	0.7	crb31-4	6.2	3	4	405	557	64	60	717	648
crb31-6	6.0	-750	3.6	0.5	crb31-5	5.5	6	6	686	800	77	70	1051	904
crb31-7	5.5	-750	3.4	-0.5	crb31-6	4.8	4	4	750	890	66	60	948	830
crb31-8	5.1	-750	3.5	-0.3	crb31-7	4.2	832	905	785	993	85	76	1103	981

Table 1

Stable Isotope Data					Trace Element Data (replicates where available)									
Sample	mm from Apical Line	Strat position from Passage Beds	$\delta^{13}\text{C}$ (VPDB)	$\delta^{18}\text{O}$ (VPDB)	Sample	mm from Apical Line	Ba	Mg	Mn	Sr				
crb31-9	4.6	-750	3.8	-0.5	crb31-8	3.5	18	18	836	1054	80	73	979	868
crb31-10	4.2	-750	2.9	-2.0	crb31-9	2.8	62	60	852	1096	95	84	1000	820
crb31-11	3.7	-750	2.8	-2.7	crb31-10	2.1	17	17	1524	1603	79	72	1009	911
crb31-12	3.2	-750	2.7	-3.5	crb31-11	1.4	65	69	2394	2448	66	61	1045	940
crb31-13	2.8	-750	1.5	-2.2	crb31-12	0.7	102	112	3417	3328	59	55	1153	1193
crb31-14	2.3	-750	1.7	-2.7	crb31-13	0.0	74	70	2872	2846	126	113	1154	1095
crb31-15	1.8	-750	2.5	-2.1										
crb31-16	1.4	-750	1.2	-3.1										
crb31-17	0.9	-750	0.0	-2.5										
crb31-18	0.5	-750	-1.3	-6.9										
crb31-19	0.0	-750	0.3	-4.8										
crb32-1	7.5	-760	1.8	-0.6	crb32-1	7.0	392		875		400		1111	
crb32-2	6.3	-760	2.2	-0.9	crb32-2	6.0	806		370		41		1351	
crb32-3	5.0	-760	2.1	-1.0	crb32-3	5.0	1497		102		31		1405	
crb32-4	3.8	-760	1.8	-1.3	crb32-4	4.0	543		255		69		1339	
crb32-5	2.5	-760	1.4	-1.5	crb32-5	3.0	374		590		21		1355	
crb32-6	1.3	-760	1.2	-1.2	crb32-6	2.0	153		499		26		1359	
crb32-7	0.0	-760	1.1	-1.5	crb32-7	1.0	333		556		30		1291	
crb35-1	6.5	-970	1.8	-0.2	crb35-1	6.5	256	251	1191	891	35	22	1164	1068
crb35-2	5.2	-970	0.9	-0.5	crb35-2	5.2	76	77	955	758	21	14	1362	1315
crb35-3	3.9	-970	1.6	0.0	crb35-3	3.9	379	348	917	753	85	69	1563	1423
crb35-4	2.6	-970	0.7	-0.4	crb35-4	2.6	285	262	1086	938	19	15	1414	1314
crb35-5	1.3	-970	-0.1	-1.1	crb35-5	1.3	431	396	1364	1232	15	11	1566	1431
crb35-6	0.0	-970	-0.2	-1.6	crb35-6	0.0	321	293	1864	1703	18	14	1599	1502
crb36-1	14.0	-1045	2.2	-1.0	crb36-1	14.0	934	905	1088	982	77	72	1321	1271
crb36-2	12.8	-1045	2.8	-0.7	crb36-2	12.8	1270	1241	876	752	35	32	1312	1299
crb36-3	11.7	-1045	2.7	-0.7	crb36-3	11.7	797	780	648	550	18	16	1272	1246
crb36-4	10.5	-1045	2.2	-1.1	crb36-4	10.5	798	790	873	716	23	20	1279	1272
crb36-5	9.3	-1045	2.7	-1.2	crb36-5	9.3	131	137	688	508	15	12	1312	1294
crb36-6	8.2	-1045	2.9	-1.2	crb36-6	8.2	266	266	785	640	21	17	1211	1170
crb36-7	7.0	-1045	1.8	-1.5	crb36-7	7.0	205	205	793	780	45	43	705	735
crb36-8	5.8	-1045	1.7	-1.0	crb36-8	5.8	129	131	770	767	29	25	744	776
crb36-9	4.7	-1045	2.1	-1.0	crb36-9	4.7	829	844	853	846	18	14	878	884
crb36-10	3.5	-1045	2.5	-1.2	crb36-10	3.5	26	26	897	903	20	18	1110	1069
crb36-11	2.3	-1045	2.0	-1.1	crb36-11	2.3	112	112	1015	995	20	18	1022	1003
crb36-12	1.2	-1045	1.6	-1.3	crb36-12	1.2	22	22	1170	1159	25	23	1065	1040
crb36-13	0.0	-1045	0.9	-3.0	crb36-13	0.0	90	90	1434	1431	114	112	1113	1073
crb37-1	3.0	-879			crb37-1	3.0	781	712	1273	1171	123	114	1084	1019
crb37-2	2.0	-879	0.6	-2.5	crb37-2	2.0	759	695	1292	1093	27	17	1371	1190
crb37-3	1.0	-879	-0.4	-3.2	crb37-3	1.0	267	251	1949	1831	34	28	1285	1181
crb38-1	8.5	-1060	1.8	-1.6	crb38-1	8.5	360	335	1224	1310	24	25	947	893
crb38-2	7.6	-1060	1.7	-2.5	crb38-2	7.3	88	60	1460	1487	19	20	1246	1160
crb38-3	6.6	-1060	1.9	-1.6	crb38-3	6.1	92	71	1643	1465	44	43	1129	980
crb38-4	5.7	-1060	1.7	-1.2	crb38-4	4.9	687	672	1935	1717	24	25	1060	1041
crb38-5	4.7	-1060	1.9	-1.6	crb38-5	3.6	117	106	2102	2022	15	16	1028	1008
crb38-6	3.8	-1060	1.1	-1.3	crb38-6	2.4	166	161	2014	1976	11	12	887	915
crb38-7	2.8	-1060	0.7	-2.4	crb38-7	1.2	22	8	2714	2699	26	30	1030	1054
crb38-8	1.9	-1060	0.5	-1.9	crb38-8	0.0	20	13	2598	2542	33	35	896	916
crb38-9	0.9	-1060	0.5	-3.2										
crb38-10	0.0	-1060	0.5	-4.1										
crb40-1	17.3	-1100	3.2	-0.5	crb40-1	17.3	203		1771		162		1270	
crb40-2	16.4	-1100	4.1	-0.5	crb40-2	16.4	471		650		33		931	
crb40-3	15.6	-1100	4.5	-0.3	crb40-3	15.6	286		780		22		1110	

Table 1

Stable Isotope Data					Trace Element Data (replicates where available)									
Sample	mm from Apical Line	Strat position from Passage Beds	$\delta^{13}\text{C}$ (VPDB)	$\delta^{18}\text{O}$ (VPDB)	Sample	mm from Apical Line	Ba	Mg	Mn	Sr				
crb40-4	14.7	-1100	4.6	-0.5	crb40-4	14.7	225	462	9	897				
crb40-5	13.8	-1100	4.0	-0.5	crb40-5	13.8	322	479	19	924				
crb40-6	13.0	-1100	3.4	-0.1	crb40-6	13.0	138	1060	259	938				
crb40-7	12.1	-1100	2.6	0.0	crb40-7	12.1	232	445	8	869				
crb40-8	11.2	-1100	3.0	-0.6	crb40-8	11.2	130	542	14	1182				
crb40-9	10.4	-1100	3.3	-0.6	crb40-9	10.4	170	448	17	991				
crb40-10	9.5	-1100	4.0	-0.5	crb40-10	9.5	212	508	76	1002				
crb40-11	8.7	-1100	3.8	-0.2	crb40-11	8.7	101	488	11	1472				
crb40-12	7.8	-1100	3.6	0.0	crb40-12	7.8	128	476	6	940				
crb40-13	6.9	-1100	3.2	0.0	crb40-13	6.9								
crb40-14	6.1	-1100	2.9	-0.4	crb40-14	6.1	120	417	10	916				
crb40-15	5.2	-1100	3.4	-0.9	crb40-15	5.2	91	470	21	1046				
crb40-16	4.3	-1100	3.4	-1.2	crb40-16	4.3	91	567	19	1199				
crb40-17	3.5	-1100	2.9	-1.8	crb40-17	3.5	112	451	22	796				
crb40-18	2.6	-1100	2.8	-1.8	crb40-18	2.6	77	390	12	1007				
crb40-19	1.7	-1100	2.9	-1.7	crb40-19	1.7	132	549	35	820				
crb40-20	0.9	-1100	3.6	-1.7	crb40-20	0.9	137	614	17	866				
crb40-21	0.0	-1100			crb40-21	0.0	101	765	24	951				
crb41-1	13.5	-1090	3.6	-2.3	crb41-1	13.3	74	657	100	1232				
crb41-3	13.0	-1090	3.3	-2.4	crb41-2	12.0	34	730	107	1204				
crb41-4	12.5	-1090	2.0	-3.2	crb41-3	11.0	29	72	141	892				
crb41-5	12.0	-1090	3.8	-1.5	crb41-4	9.5	7	1047	91	1208				
crb41-6	11.0	-1090	2.1	-3.7	crb41-5	8.5	4		87	1283				
crb41-7	10.0	-1090	3.6	-1.2	crb41-6	7.0	181	631	59	1349				
crb41-8	9.0	-1090	2.7	-1.9	crb41-7	5.3	4	305	44	1420				
crb41-9	7.5	-1090	3.1	-1.4	crb41-8	4.0	4	701	32	1201				
crb41-10	7.0	-1090	3.4	-1.6	crb41-9	3.0	10	839	51	1108				
crb41-11	6.0	-1090	2.9	-1.8	crb41-10	1.0	8	926	88	1107				
crb41-12	5.0	-1090	2.5	-0.9	crb41-11	0.0	8	1691	90	1089				
crb41-13	4.0	-1090	2.3	-1.5										
crb41-14	3.0	-1090	1.9	-1.7										
crb41-15	2.2	-1090	1.1	-2.1										
crb41-16	1.0	-1090	0.4	-2.0										
crb44-1	5.0	-1005	2.1	-1.1	crb44-1	4.0	884	1840	136	894				
crb44-2	3.3	-1005	2.5	-0.8	crb44-2	3.0	571	833	43	1244				
crb44-3	1.7	-1005	2.7	-0.5	crb44-3	2.0	213	574	8	1464				
crb44-4	0.0	-1005	2.0	-1.1	crb44-4	1.0	236	1149	49	1387				
crb45-1	12.0	-1015	2.2	-0.4	crb45-1	12.0	5674	5773	1766	1750	94	91	1000	976
crb45-2	10.7	-1015	3.0	-0.1	crb45-2	10.7	161	160	793	786	15	12	955	927
crb45-3	9.3	-1015	3.0	-0.2	crb45-3	9.3	32	32	732	767	12	9	866	857
crb45-4	8.0	-1015	2.7	-0.3	crb45-4	8.0	182	189	692	723	8	6	1077	1050
crb45-5	6.7	-1015	2.7	0.0	crb45-5	6.7	1534	1571	917	940	32	31	1148	1108
crb45-6	5.3	-1015	2.9	0.1	crb45-6	5.3	1127	1178	772	800	15	14	1152	1145
crb45-7	4.0	-1015	3.4	0.1	crb45-7	4.0	329	338	686	690	9	6	932	934
crb45-8	2.7	-1015	3.0	-0.4	crb45-8	2.7	1483	1606	874	894	20	19	1198	1186
crb45-9	1.3	-1015	2.3	-0.7	crb45-9	1.3	31	32	911	937	13	11	1046	992
crb45-10	0.0	-1015	1.7	-1.2	crb45-10	0.0	72	47	1603	1260	40	30	1170	881
crb46-1	12.4	-1015	2.1	-0.7	crb46-1	13.9	312	531	623	975	372	257	430	430
crb46-2	11.7	-1015	3.8	0.1	crb46-2	13.1	610	782	440	751	285	172	748	740
crb46-3	10.9	-1015	3.3	0.1	crb46-3	12.3	76	39	243	492	203	122	519	530
crb46-4	10.2	-1015	4.1	1.1	crb46-4	11.4	81	70	367	590	175	117	574	549
crb46-5	9.5	-1015	3.0	0.4	crb46-5	10.6	378	531	261	531	190	128	484	492
crb46-6	8.8	-1015	2.9	0.3	crb46-6	9.8	129	79	996	1470	261	183	729	656
crb46-7	8.0	-1015	3.2	0.1	crb46-7	9.0	131	52	960	1413	339	260	992	898
crb46-8	7.3	-1015	4.2	0.3	crb46-8	8.2	139	80	316	758	345	251	741	674

Table 1

Stable Isotope Data					Trace Element Data (replicates where available)									
Sample	mm from Apical Line	Strat position from Passage Beds	$\delta^{13}\text{C}$ (VPDB)	$\delta^{18}\text{O}$ (VPDB)	Sample	mm from Apical Line	Ba	Mg	Mn	Sr				
crb46-9	6.6	-1015	3.7	0.3	crb46-9	7.4	43	24	549	733	119	93	655	608
crb46-10	5.8	-1015	2.9	0.0	crb46-10	6.5	56	18	515	789	161	141	774	731
crb46-11	5.1	-1015	3.1	0.3	crb46-11	5.7	597	586	366	684	206	184	636	580
crb46-12	4.4	-1015	3.1	0.0	crb46-12	4.9	69	42	482	736	254	267	469	451
crb46-13	3.6	-1015	2.6	-0.1	crb46-13	4.1	71		576	865	196	194	488	457
crb46-14	2.9	-1015	2.3	-0.4	crb46-14	3.3	53		410	726	183	236	570	513
crb46-15	2.2	-1015	2.1	-0.9	crb46-15	2.5	33		482	688	96	127	584	516
crb46-16	1.5	-1015	1.9	-0.8	crb46-16	1.6	57		703	1065	193	265	719	644
crb46-17	0.7	-1015	2.1	-0.9	crb46-17	0.8	94		543	1151	347	501	788	707
crb46-18	0.0	-1015	2.0	-2.4	crb46-18	0.0	38		536	771	160	233	645	572
crb47-1	23.7	-1024	0.0	-2.7	crb47-1	4.5	1390		1959		90		1417	
crb47-2	25.4	-1024	-0.8	-3.2	crb47-2	3.0	433		3925		129		1476	
crb47-3	48.1	-1024	-5.4	-13.2	crb47-3	1.5	637		4227		1493		1252	
crb47-4	49.8	-1024	-7.8	-17.8	crb47-4	0.0	127		2905		1484		1123	
crb48-1	10.0	-1100	2.9	0.4	crb48-1	10.0	113	78	527	518	161	106	627	547
crb48-2	9.2	-1100	2.1	1.1	crb48-2	9.1	84	43	797	813	162	100	777	685
crb48-3	8.5	-1100	1.5	0.0	crb48-3	8.2	74	39	508	513	166	101	661	581
crb48-4	7.7	-1100	1.4	0.1	crb48-4	7.3	61	24	484	501	152	88	633	563
crb48-5	6.9	-1100	1.6	0.2	crb48-5	6.4	70	33	496	519	155	88	634	551
crb48-6	6.2	-1100	0.7	-1.5	crb48-6	5.5	116	133	612	662	204	114	692	617
crb48-7	5.4	-1100	1.2	0.2	crb48-7	4.5	174	426	486	575	167	90	622	558
crb48-8	4.6	-1100	0.8	-0.2	crb48-8	3.6	74	107	693	786	152	82	674	607
crb48-9	3.8	-1100	1.0	0.3	crb48-9	2.7	89	44	761	913	210	115	688	617
crb48-10	3.1	-1100	1.5	-0.2	crb48-10	1.8	83	25	813	1015	247	138	646	600
crb48-11	2.3	-1100	1.2	-0.1	crb48-11	0.9	66	30	1671	1878	185	111	767	693
crb48-12	1.5	-1100	1.7	-1.1	crb48-12	0.0	50	14	1878	2139	155	90	694	644
crb48-13	0.8	-1100	0.6	-1.9										
crb48-14	0.0	-1100	2.1	-1.8										
crb49-1	12.5	-1150	2.5	-0.8	crb49-1	11.5	546		1852		171		1349	
crb49-3	10.7	-1150	3.2	-0.7	crb49-2	9.4	786		1654		179		1102	
crb49-4	9.8	-1150	3.2	-0.6	crb49-3	7.3	172		1463		129		1044	
crb49-5	8.9	-1150	3.2	0.2	crb49-4	5.2	31		1362		115		844	
crb49-6	8.0	-1150	2.6	0.1	crb49-5	3.1	53		1565		129		1029	
crb49-7	7.1	-1150	2.5	-0.1	crb49-6	1.0	115		1749		190		1151	
crb49-8	6.3	-1150	2.5	-0.8	crb49-7	-1.1	45		1999		97		1278	
crb49-9	5.4	-1150	3.3	0.0	crb49-8	-3.2	234		1929		69		1168	
crb49-10	4.5	-1150	3.2	-0.3	crb49-9	-5.3	69		2035		84		1016	
crb49-11	3.6	-1150	3.0	-0.3	crb49-10	-7.4	72		2037		91		867	
crb49-12	2.7	-1150	3.1	-1.0	crb49-11	-9.5	39		1937		128		883	
crb49-13	1.8	-1150	3.5	-1.0	crb49-12	-11.6	26		1566		82		951	
crb49-14	0.9	-1150	3.9	-1.2	crb49-13	0.0	42		1440		211		880	
crb49-15	0.0	-1150	1.5	-4.5										
crb50-1	14.5	-1160	3.8	-1.1	crb50-1	13.4	1265	1250	1454	1439	54	50	1134	1053
crb50-2	13.7	-1160	2.6	-1.1	crb50-2	11.7	150	149	904	899	41	35	1024	960
crb50-3	12.9	-1160	1.4	-5.2	crb50-3	10.1	64	65	784	769	29	26	1151	1064
crb50-4	12.1	-1160	1.0	-5.4	crb50-4	8.4	24	24	1267	1233	24	20	1046	961
crb50-5	11.3	-1160	2.9	-2.5	crb50-5	6.7	0	1	890	887	9	9	1190	1129
crb50-6	10.5	-1160	3.0	-0.8	crb50-6	5.0	17	17	834	837	6	4	1122	1129
crb50-7	9.7	-1160	2.2	-0.7	crb50-7	3.4	31	30	843	857	8	5	1000	956
crb50-8	8.9	-1160	2.7	-0.6	crb50-8	1.7	177	177	999	1006	17	15	1143	1080
crb50-9	8.1	-1160	3.3	-0.6	crb50-9	1.0	15	34	1585	1739	36	59	813	1053
crb50-10	7.3	-1160	3.5	-0.1										
crb50-11	6.4	-1160	2.7	-1.1										
crb50-12	5.6	-1160	3.7	-0.1										
crb50-13	4.8	-1160	3.6	-0.2										

Table 1

Stable Isotope Data					Trace Element Data (replicates where available)									
Sample	mm from Apical Line	Strat position from Passage Beds	$\delta^{13}\text{C}$ (VPDB)	$\delta^{18}\text{O}$ (VPDB)	Sample	mm from Apical Line	Ba	Mg	Mn	Sr				
crb50-14	4.0	-1160	3.4	-0.5										
crb50-15	3.2	-1160	2.6	-0.3										
crb50-16	2.4	-1160	2.3	-0.1										
crb50-17	1.6	-1160	2.4	0.0										
crb50-18	0.8	-1160	1.8	-0.8										
crb50-19	0.0	-1160	2.1	-1.3										
crb51-1	9.0	-1015	3.3	-1.9	crb51-1	8.2	697	1894	224	1290				
crb51-2	8.3	-1015	3.0	-1.7	crb51-2	7.3	291	1313	309	983				
crb51-3	7.5	-1015	1.9	-2.8	crb51-3	6.4	144	1388	394	949				
crb51-4	6.8	-1015	1.6	-2.9	crb51-4	5.5	191	1492	181	1208				
crb51-5	6.0	-1015	3.4	-0.4	crb51-5	4.6	370	1558	266	1068				
crb51-6	5.3	-1015	2.9	-1.0	crb51-6	3.6	104	1292	238	1010				
crb51-7	4.5	-1015	2.7	-1.6	crb51-7	2.7	72	1594	342	1200				
crb51-8	3.8	-1015	2.5	-1.8	crb51-8	1.8	756	1248	181	999				
crb51-9	3.0	-1015	2.9	-1.1	crb51-9	0.9	193	1254	139	978				
crb51-10	2.3	-1015	3.0	-0.7	crb51-10	0.0	51	1525	247	966				
crb51-11	1.5	-1015	2.2	-1.1										
crb51-12	0.8	-1015	2.1	-0.8										
crb51-13	0.0	-1015	0.7	-1.7										
crb52-2	14.0	-1210	3.3	1.2	crb52-1	14.9	55	154	593	660	93	80		
crb52-4	12.1	-1210	0.6	1.0	crb52-2	13.9	4276	4490	720	798	101	85		
crb52-5	11.2	-1210	2.7	0.5	crb52-3	12.9	71	81	464	581	114	98		
crb52-6	9.3	-1210	2.4	0.1	crb52-4	11.9	16	22	668	716	65	55		
crb52-8	8.4	-1210	2.6	0.4	crb52-5	10.9	57	84	564	619	53	44		
crb52-9	7.5	-1210	2.2	0.5	crb52-6	9.9	22	26	552	559	59	49		
crb52-10	5.6	-1210	2.7	-0.2	crb52-7	8.9	39	70	514	643	79	65		
crb52-11	4.7	-1210	2.1	0.6	crb52-8	7.9	22	35	578	652	63	52		
crb52-13	3.7	-1210	1.6	0.0	crb52-9	7.0	13	19	364	431	54	44		
crb52-14	2.8	-1210	0.7	-0.9	crb52-10	6.0	19	27	555	648	70	58		
crb52-15	1.9	-1210	1.7	0.1	crb52-11	5.0	26	34	910	979	70	59		
crb52-16	0.9	-1210	1.7	-0.5	crb52-12	4.0	22	43	1178	1210	62	52		
crb52-17	0.0	-1210	2.4	0.2	crb52-13	3.0	46	68	1082	1117	70	59		
					crb52-14	2.0	13	20	1201	1215	61	51		
					crb52-15	1.0	11	16	938	967	50	42		
					crb52-16	0.0	10	15	1071	1093	48	41		
					crb53-1	6.2	671		1375		57	1222		
					crb53-2	5.0	173		1092		22	1297		
					crb53-3	3.7	313		1303		18	1335		
					crb53-4	2.5	668		1274		16	1222		
					crb53-5	1.2	237		1121		11	1201		
crb54-1	4.0	-1218	2.8	-0.3	crb54-1	7.3	43		1106		255	640		
crb54-2	3.0	-1218	2.6	-0.6	crb54-2	6.3	33		798		279	632		
crb54-3	2.0	-1218	2.2	-1.7	crb54-3	5.2	34		1309		278	659		
crb54-4	1.0	-1218	3.3	-1.0	crb54-4	4.2	38		1082		254	612		
					crb54-5	3.1	32		1027		281	716		
					crb54-6	2.1	67		1085		358	678		
					crb54-7	1.0	136		970		257	572		
					crb54-8	0.0	1716		1156		220	393		
crb55-1	11.0	-1155	2.3	-1.7	crb55-1	10.5	244	436	1602	1431	192	72	2136	777
crb55-2	10.2	-1155	3.1	-0.1	crb55-2	9.5	137	49	642	715	78	20	1210	845
crb55-3	9.4	-1155	2.7	-1.1	crb55-3	8.6	29	68	660	784	93	31	1150	1036
crb55-4	8.6	-1155	3.1	-0.4	crb55-4	7.6	31	22	565	1240	69	30	1110	943
crb55-5	7.9	-1155	4.6	0.2	crb55-5	6.7	54	26	788	768	278	23	1033	1111
crb55-6	7.1	-1155	3.2	-0.2	crb55-6	5.7	38	12	1234	593	163	14	1204	1183

Table 1

Stable Isotope Data					Trace Element Data (replicates where available)									
Sample	mm from Apical Line	Strat position from Passage Beds	$\delta^{13}\text{C}$ (VPDB)	$\delta^{18}\text{O}$ (VPDB)	Sample	mm from Apical Line	Ba	Mg	Mn	Sr				
crb55-7	6.3	-1155	2.4	0.6	crb55-7	4.8	46	8	567	600	209	16	1141	1063
crb55-8	5.5	-1155	2.9	-0.2	crb55-8	3.8	42	49	670	754	92	44	1316	1002
crb55-9	4.7	-1155	3.6	-0.4	crb55-9	2.9	30	20	655	935	72	65	1303	846
crb55-10	3.9	-1155	3.5	-0.4	crb55-10	1.9	25		592		80		975	
crb55-11	3.1	-1155	3.0	-0.5	crb55-11	1.0	45		1282		294		1675	
crb55-12	2.4	-1155	2.7	-0.7	crb55-12	0.0	28		1358		200		1970	
crb55-13	1.6	-1155	2.6	-1.1										
crb55-15	0.0	-1155	2.3	-1.8										
crb56-1	5.4	-1218	0.8	-2.9	crb56-1	5.4	703		867		123		836	
crb56-2	4.3	-1218	1.1	-2.5	crb56-2	4.3	182		482		29		1077	
crb56-3	3.2	-1218	1.2	-2.4	crb56-3	3.2	457		413		28		1139	
crb56-4	2.2	-1218	1.2	-2.6	crb56-4	2.2	17		467		23		1222	
crb56-5	1.1	-1218	1.3	-2.8	crb56-5	1.1	288		302		30		1395	
crb56-6	0.0	-1218	1.0	-3.2	crb56-6	0.0	86		631		49		1334	
crb57-1	15.9	-1100	4.1	-2.0	crb57-1	15.9	362	385	901	1606	541	694	894	1510
crb57-2	15.1	-1100	4.7	-1.8	crb57-2	15.0	104	108	853	1146	218	275	495	516
crb57-3	14.3	-1100	3.9	-0.5	crb57-3	14.0	119	153	1307	1714	249	319	342	753
crb57-4	13.5	-1100	3.2	-0.2	crb57-4	13.1	48	66	1007	1369	288	367	617	649
crb57-5	12.7	-1100	3.5	-0.5	crb57-5	12.2	49	69	1509	1981	363	462	597	978
crb57-6	11.9	-1100	3.7	-0.5	crb57-6	11.2	38	51	745	1063	226	287	535	602
crb57-7	11.1	-1100	4.2	0.2	crb57-5	10.3	26	37	806	1032	189	236	293	366
crb57-8	10.3	-1100	3.9	-0.1	crb57-8	9.4	22	33	922	1214	174	217	272	384
crb57-9	9.5	-1100	4.0	-0.3	crb57-9	8.4	31	44	970	1234	216	268	303	358
crb57-10	8.7	-1100	3.5	-0.2	crb57-10	7.5	41	50	901	1124	161	197	254	328
crb57-11	8.0	-1100	3.6	-0.3	crb57-11	6.5	20	29	1317	1564	156	191	286	251
crb57-12	7.2	-1100	3.3	-1.1	crb57-12	5.6	28	37	936	1136	106	127	201	218
crb57-13	6.4	-1100	3.0	-1.0	crb57-13	4.7	16	24	931	992	131	156	173	266
crb57-14	5.6	-1100	3.4	-0.7	crb57-14	3.7	14	20	953	1015	116	137	265	188
crb57-15	4.8	-1100	3.8	-0.8	crb57-15	2.8	75	90	1062	1161	156	185	370	296
crb57-16	4.0	-1100	3.0	-2.7	crb57-16	1.9	18	26	1067	1020	148	172	311	300
crb57-17	3.2	-1100	3.2	-1.5	crb57-17	0.9	21	29	1271	1197	155	177	320	257
crb57-18	2.4	-1100	3.0	-2.8	crb57-18	0.0	99	95	1616	1403	197	207	360	308
crb57-19	1.6	-1100	3.8	-1.4										
crb57-20	0.8	-1100	3.7	-1.5										
crb57-21	0.0	-1100	3.2	-2.2										

## **Chapter 6**

### **General Conclusions and Future Research**

## **Chapter 6**

### **General Conclusions and Future Research**

This purpose of this thesis was to investigate the geochemistry of the internal skeletons of fossil and modern cephalopods in order to improve our understanding of ancient Belemnnoidea. Belemnite rostra are geologically important as they have the highest preservation potential of any common Mesozoic fossil and an improved understanding Belemnnoidea, both in terms of their physiology, behaviour, and life-history strategy and as palaeoenvironmental proxies, may allow future palaeoenvironmental studies to extract more information from the geochemical record. The development and application of a high resolution intra rostrum sampling technique through the course of the research presented here has proven valuable in investigating the geochemical evolution of the Logan Sea of western Canada during the Oxfordian. Some specific conclusions from this research follow.

#### **Specific Conclusions**

Although the geochemistry of modern cuttlebones shows significant variability, *Sepia officinalis* cuttlebones contain an excellent record of climatic and metabolic changes. Oxygen isotope values within the cuttlebone provide detailed records of water temperature change during the lifetime of the organism. Carbon isotope values are not secreted in isotopic equilibrium with seawater, but instead exhibit increasing values with ontogeny: This may reflect a decrease in metabolic rate with maturity. Two of the five cuttlebones document a large decrease in carbon isotope values late in life, which has been hypothesised to be the result of sex-specific spawning carbon reallocation or increases in metabolic rate. Profiles of both carbon and oxygen isotope values appear to record migration to deep water over winter. The concentrations of Sr and Mn exhibit a general inverse relationship with coeval oxygen isotope values, suggesting a possible relationship between Sr and Mn incorporation rate and temperature. However, the construction of a relevant temperature equation is not possible at the current time due insufficient correlation between Sr or Mn and  $\delta^{18}\text{O}$  values. Mg abundance tends to vary with coeval carbon isotope values in some specimens, suggesting a possible relationship between Mg precipitation rate and metabolism.

The oxygen and carbon isotope values of belemnnoidea rostra were shown to vary in a radial pattern around the apical line and spatial centre. Both diagenetically altered and better preserved specimens display some radial symmetry and a wide range in stable isotope values. As such, radial symmetry

should not be interpreted as an indicator of preservation, supporting Longinelli (1969). High resolution radial profiles from diagenetically screened rostra display a statistically significant ontogenetic increase in carbon isotope values in both of the identified genera. An analogous increase in carbon isotope values is observed in modern cuttlebones and may reflect a decrease in metabolic rate with ontogeny. Mg concentration generally changes with oxygen isotope values, suggesting that Mg precipitation rate may be temperature-dependent in some respect. Oxygen isotope values in *Cylindroteuthis* tend to increase while Mg concentrations decrease with ontogeny, which may reflect a life-history strategy involving hatching in shallow waters and migration to deeper waters with maturity. Based on the interpretation of the ontogenetic temperature signal, maximum temperatures within a rostrum are likely slightly below ancient sea surface temperatures, as these belemnites probably spent their early lives in shallow waters, much like modern *Sepia*. Minimum palaeotemperature values obtained from the rostra may, therefore, document the temperature of deeper waters in the basin. No seasonal signal was observed in the rostra, which may indicate that these individuals migrated with favourable water conditions, or lived for approximately 6 months.

When presented in stratigraphic order, the range in carbon isotope values per rostra is relatively constant at about 2 ‰, but the average value changes through time. Changes in the average value of carbon isotopes indicate a positive carbon isotope excursion in the Oxfordian that had not been previously identified in North America.

Future belemnite studies, like studies of the internal geochemistry of many other organisms, will benefit from the high-resolution sampling technique developed through the course of this research and elucidated in chapters 4 and 5. This technique allows the ontogenetic geochemical variation recorded in a rostrum to be sampled, which provides a great deal more information than the standard practice of obtaining a single sample per rostra. This technique may also allow a reduction in sample bias, since values obtained from a single sample may represent any value within the ontogenetic range, which may lead to inaccurate interpretations. Use of these methods in future studies of Belemnnoidea rostra may increase the amount of environmental information extracted from the fossil record, as similar methods have improved the information obtained from the study of other molluscs, fish otoliths, and the hard parts of many other organisms.

## **Future Research**

Several avenues of future research were identified while completing this thesis. The geochemistry of the cuttlebone is only understood on a basic level. One important step in understanding *Sepia* (and other organisms with internal skeletons) as an environmental proxy is to quantify the effects of DIC and food carbon isotope composition on the carbon isotope values preserved in the cuttlebone. To this end, an experiment could be devised where several tanks are maintained with different DIC isotopic signatures. The *Sepia* specimens therein should then be provided food of varying isotopic composition for set periods of time (for instance, three months with one carbon isotope signature, the following three months with a different isotopic composition, and so on). As cuttlebone carbon isotope values should change with the differing food sources, such an experiment should allow for the quantification of the influences of DIC, food composition, and metabolic slowdown on the isotope composition of the seawater in *Sepia* cuttlebones. An experiment like this would also allow a more accurate determination of cuttlebone growth rate. Such information would be valuable for comparison to belemnite carbon isotope values.

A second important avenue of research is quantifying a temperature equation for Sr abundance in the cuttlebone. This could be achieved by examining the geochemistry of wild specimens from different temperature regimes while running a series of controlled laboratory experiments that vary temperature through the life span of captive animals. This should improve our understanding of correlation between Sr concentration, growth rate and temperature, hopefully allowing the construction of a temperature equation. This may be important for evaluating the  $\delta_w$  value of ancient water bodies.

As the geochemistry of belemnite rostra from the Green Beds section hints that these organisms may have migrated seasonally (since no seasonal temperature signal was observed), it would be useful to examine the relationship between migration and seasonal geochemical temperature signatures in the modern world in order to investigate the migration hypothesis. The Logan Sea of the Green Beds had a shoreline oriented roughly north-south, so examining cuttlebones from a different species of *Sepia* from analogous areas in the modern world may help test this hypothesis. Two such areas that may be suitable for investigation are the west coast of Australia and the coast of Portugal, both of which have native *Sepia* populations (Boyle 1983, Norman, 2000). The orientation of the shoreline would facilitate the most efficient north-south migration with favourable water temperatures, which may suppress a seasonal temperature signal. The geochemistry of *Sepia* cuttlebones from these areas could be compared to the internal geochemistry of belemnite rostra, as the influence of large scale migration would be better understood.

Despite the improvements on sampling methodology presented in this thesis and used in the course the research presented herein, low sampling resolution remained a hindrance to the observation and interpretation of patterns in belemnite rostra. For example, higher resolution sampling of rostra would be required to more fully investigate the hypothesis that belemnites return to shallow water for spawning near the end of their life cycle. The best current solution to this problem would be to use a laser ablation unit combined with a multi collector inductively coupled plasma mass spectrometer (LA-ICP-MS). This would allow the investigation of the internal geochemistry of belemnite rostra on a level comparable to that which can already be achieved with the cuttlebone (McArthur et al. 2007). The multi collector device may also be sensitive enough to measure oxygen isotope values in addition to the usual array of trace elements, something that a quadrupole ICP-MS is not capable of. The use of this technology would reduce the time required for analysis and may lower the overall cost of the study. The laser sampling device also allows the measurement of iron levels in the carbonate, which would be an advantage in identifying diagenetic alteration, since diagenetic fluids are generally enriched with iron (Veizer 1983, Veizer et al. 1999, McArthur et al. 2007, Price and Mutterlose 2004 and many others). Combined with manganese and strontium, this would provide a more stringent diagenetic screening process, or allow Sr to be investigated as a metabolism proxy while maintaining the same level of diagenetic screening.

As the development of a salinity-independent palaeothermometer may have important uses, the calibration of a magnesium palaeotemperature equation should be pursued for belemnite calcite. A possible source of the poor correlation between the oxygen isotope values and Mg abundance observed in chapters 4 and 5 is rapidly fluctuating oxygen isotope values of restricted ancient seas. The investigation of belemnites from an open ocean setting or from a basin that is very well connected to the open ocean with limited freshwater input may improve this correlation. The equivalent of the Arabian Peninsula in the geologic record would be helpful, as this area is so arid that there would be limited runoff, and there is direct connection to the open ocean. If a MC-ICP-MS is available for analysis, it would also be worth while investigating the possibility of a Ca isotope palaeothermometer in belemnite calcite.

Finally, other North American Jurassic marine exposures should be investigated in order to confirm or refute the presence of an Oxfordian carbon isotope excursion in North America. Using the sampling strategies developed in this thesis in concert with bulk carbon and the analysis of other fossil species, belemnites from these sections may allow more precise dating of these horizons.

*I hope my careful investigation of the internal geochemical variation within the cuttlebone of modern Sepia officinalis and the rostrum of Mesozoic belemnoides will be considered a valuable contribution to the field: The internal geochemistry of belemnite rostra contains clues not only to the climate of past epochs, but also to the biology, ecology and behaviour of these interesting organisms. Analyses of these fossils would be beneficial to any investigation of Jurassic strata.*

## References

- Adkins, J.F., Cheng, H., Boyle, E.A., Druffel, E.R.M and Edwards, L. 1998. Deep-sea coral evidence for rapid change in ventilation of the deep North Atlantic 15,400 years ago, *Science*, **280**: 725-728.
- Anderson, T.F. and Arthur, M.A. 1983. Stable isotopes of oxygen and carbon and their applications to sedimentologic and paleoenvironmental problems. *In* *Stable Isotopes in Sedimentary Geology Edited by* M.A. Arthur, T.F. Anderson, I.R. Kaplan, J. Veizer and L.S. Land. Society of Economic Paleontologists and Mineralogists, Dallas, pp. 1-1-1-151.
- Bailey, T.R., Rosenthal, Y., McArthur, J.M., van de Schootbrugge, B., and Thirlwall, M.F. 2003. Paleoceanographic changes of the late Pliensbachian-early Toarcian interval: A possible link to the genesis of an oceanic anoxic event, *Earth and Planetary Science Letters*, **212**: 307-320.
- Bettencourt, V. and Guerra, A. 1999. Carbon- and oxygen-isotope composition of the cuttlebone of *Sepia officinalis*: A tool for predicting ecological information? *Marine Biology*, **133**: 651-657.
- Billups, K. and Schrag, D.P. 2002. Paleotemperatures and ice volume of the past 27 myr revisited with paired Mg/Ca and  $^{18}\text{O}/^{16}\text{O}$  measurements on benthic foraminifera, *Paleoceanography*, **17**: PA000567.
- Boucaud-Camou E, Boismery J. 1991. The migrations of the cuttlefish (*Sepia officinalis* L) in the English Channel IN *The Cuttlefish, 1<sup>st</sup> international symposium on the cuttlefish Sepia, Caen, June 1-3 1989. Centre de Publications de l'Universite de Caen*
- Bowen, R. 1961a. Oxygen isotope paleotemperature measurements on cretaceous Belemnoida from Europe, India and Japan, *Journal of Paleontology*, **35**: 1077-1084.
- Bowen, R. 1961b. Paleotemperature analysis of Mesozoic Belemnoida from Germany and Poland, *Journal of Geology*, **69**: 75-83.
- Boyle, P.R. 1983. *Cephalopod life cycles, vol. 1 species accounts*. Academic Press Inc., London.

- Boyle, P.R., Boletzky, S.V. 1996. Cephalopod populations: definition and dynamics. *Philosophical Transactions of the Royal Society, London* **351**:985-1002.
- Boyle, P.R. and Rodhouse, P. 2005. *Cephalopods : Ecology and fisheries*. Blackwell Pub., Oxford, UK ; Ames, Iowa.
- Brand, U., Logan, A., Hiller, N. & Richardson, J. 2003. Geochemistry of modern brachiopods: applications and implications for oceanography and paleoceanography. *Chemical Geology*, **198**, 305-334.
- Bruland, K.W. and Lohan, M.C. 2004. Controls of trace metals on seawater. *In* *Treatise on Geochemistry Volume 6, The Oceans and Marine Geochemistry Edited by H. Elderfield*. Elsevier-Pergamon, Oxford, pp. 23-48.
- Carpenter, S.J., Lohmann, K.C. 1995.  $\delta^{18}\text{O}$  and  $\delta^{13}\text{C}$  values of modern brachiopod shells. *Geochimica Et Cosmochimica Acta* **59**:3749-3764.
- Carre, M., Bentaleb, I., Bruguier, O., Ordinola, E., Barrett, N.T., Fontugne, M. (2006) Calcification rate influence on trace element concentrations in aragonitic bivalve shells: Evidences and mechanisms. *Geochimica et Cosmochimica Acta*, **70**, 4906-4920.
- Cherel, Y., Hobson, K.A. 2005. Stable isotopes, beaks and predators: a new tool to study the trophic ecology of cephalopods, including giant and colossal squids. *Proceedings of the Royal Society B* **272**:1601-1607.
- Curry, G.B., Fallick, A.E. 2002. Use of stable oxygen isotope determinations from brachiopod shells in palaeoenvironmental reconstruction. *Palaeogeography, Palaeoclimatology, Palaeoecology* **182**:133-143.
- Ditchfield, P.W. 1997. High northern palaeolatitude Jurassic-Cretaceous palaeotemperature variation: new data from Kong Karls Land, Svalbard. *Palaeogeography, Palaeoclimatology, Palaeoecology*, **130**, 163-175.
- Doyle, P., Donovan, D.T., Nixon, M. 1994. Phylogeny and systematics of the Coleoidea. *University of Kansas Paleontological Contributions* **5**: 1-15.
- Ellis, R. 2001. *Aquagenesis, the origin and evolution of life in the sea*. Viking Penguin, New York, USA.
- Emiliani, C. 1966. Isotopic Paleotemperatures. *Science*, **154**, 851-857.
- Epstein, S., Buchsbaum, H.A., Lowenstam, H., and Urey, H.C. 1953. Revised carbonate-water isotopic temperature scale, *Geological Society of America Bulletin*, **64**: 1315-1326.

Epstein, S., Buchsbaum, R., Lowenstam, H., and Urey, H.C. 1951. Carbonate-water isotopic temperature scale, *Bulletin of the Geological Society of America*, **62**: 417-426.

Freebold, H., Mountjoy, E., and Reed, R. 1959. The Oxfordian beds of the Jurassic Fernie group, Alberta and British Columbia. Department of Mines and Technical Surveys Canada, **53**.

Gabr, H.R., Hanlon, R.T., Hanafy, M.H., El-Etreby, S.G. 1998. Maturation, fecundity and seasonality of reproduction of two commercially valuable cuttlefish, *Sepia pharaonis* and *S. dollfusi*, in the Suez Canal. *Fisheries Research* **36**:99-115.

Gillikin, D.P., Lorrain, A., Bouillon, S., Willenz, P., and Dehairs, F. 2006a. Stable carbon isotopic composition of *Mytilus edulis* shells: Relation to metabolism, salinity,  $\delta^{13}\text{C}_{\text{DIC}}$  and phytoplankton, *Organic Geochemistry*, **37**: 1371-1382.

Gillikin, D.P., Dehairs, F., Lorrain, A., Steenmans, D., Baeyens, W., and Andre, L. 2006b. Barium uptake into the shells of the common mussel (*Mytilus edulis*) and the potential for estuarine paleo-chemistry reconstruction, *Geochimica et Cosmochimica Acta*, **70**: 395-407.

Glowniak, E. and Wierzbowski, H. 2007. Comment on "the mid-Oxfordian (late Jurassic) positive carbon-isotope excursion recognised from fossil wood in the British isles" by C.R. Pearce, S.P. Hesselbo, A.L. Coe, *Palaeogeography, Palaeoclimatology, Palaeoecology* **221**: 343-357, *Palaeogeography, Palaeoclimatology, Palaeoecology*, **248**: 247-251.

Goodwin, D.H., Flessa, K.W., Schöne, B.R., Dettman, D.L. 2001. Cross-calibration of daily growth increments, stable isotope variation, and temperature in the Gulf of California bivalve mollusk *Chione cortezi*: Implications for paleoenvironmental analysis. *Palaios* **16**:387-398.

Goodwin, D.H., Schöne, B.R., Dettman D.L. 2003. Resolution and fidelity of oxygen isotopes as palaeotemperature proxies in bivalve mollusc shells: models and observations. *Palaios* **18**:110-125.

Gomez, J.J., Goy, A., and Canales, M.L. 2008. Seawater temperature and carbon isotope variations in belemnites linked to mass extinction during the Toarcian (early Jurassic) in central and northern Spain. Comparison with other European sections, *Palaeogeography, Palaeoclimatology, Palaeoecology*, **258**: 28-58.

Gradstein, F.M., Ogg, J.G., Smith, A.G., Bleeker, W., and Lourens, L.J. 2004. A new geological timescale with special reference to Precambrian and Neogene, *Episodes*, **27**: 83-100.

- Grossman, E.L., Ku, T.L. 1986. Oxygen and carbon isotope fractionation in biogenic aragonite: Temperature effects. *Chemical Geology* 59:59-74.
- Guerra, A., Nixon, M., Castro, B.G. 1988. Initial stages of food ingestion by *Sepia officinalis* (Mollusca: Cephalopoda). *Journal of the Zoological Society, London* 214:189-197.
- Hall, R.L. 1984. Lithostratigraphy and biostratigraphy of the Fernie formation (Jurassic) in the southern Canadian rocky mountains. *In The Mesozoic of Middle North America Edited by D.F. Stott and D.J. Glass. Canadian Society of Petroleum Geologists*, pp. 233-247.
- Hall, K.C., Hanlon, R.T. 2002. Principal Features of the mating system of a large spawning aggregation of the giant Australian cuttlefish *Sepia apama* (Mollusca: Cephalopoda). *Marine Biology* 140:533-545.
- Hanlon, R.T., Messenger, J.B. 1996. *Cephalopod behaviour*. Cambridge University Press, Cambridge, England, p 1-248.
- Harwood, A.J.P., Dennis, P.F., Marca, A.D., Pilling, G.M., Millner, R.S. 2008. The oxygen isotope composition of water masses within the North Sea. *Estuarine Coastal and Shelf Science* 78: 353-359.
- Haq, B.U., Hardenbol, J., and Vail, P.R. 1987. Chronology of fluctuating sea levels since the Triassic (250 million years ago to present), *Science*, **235**: 1156-1167.
- Hendry, J.P., Perkins, W.T., and Bane, T. 2001. Short-term environmental change in a Jurassic lagoon deduced from geochemical trends in aragonite bivalve shells, *GSA Bulletin*, **113**: 790-798.
- Hewitt, R.A., Stait, B. 1988. Seasonal variation in septal spacing of *Sepia officinalis* and some Ordovician actinocerid nautiloids. *Lethaia* 21:383-394.
- Hobson, K.A., Sirois, J., Gloutney, M.L. 2000. Tracing nutrient allocation to reproduction with stable isotopes: a preliminary investigation using colonial waterbirds of Great Slave Lake. *The Auk* 117:760-774.
- Høie H, Otterlei M, Folkvord A. 2004. Temperature-dependent fractionation of stable oxygen isotopes in otoliths of juvenile cod (*Gadus morhua* L.). *ICES Journal of Marine Science* 61:243-251.
- Jarvis, I., Mabrouk, A., Moody, R.T.J., and de Cabrera, S. 2002. Late Cretaceous (Campanian) carbon isotope events, sea-level change and correlation of the

- Tethyan and boreal realms, *Palaeogeography, Palaeoclimatology, Palaeoecology*, **188**: 215-248.
- Jeletzki, J.A. 1966. Comparative morphology, phylogeny and classification of fossil Coleoidea, The University of Kansas Paleontological Contributions, Mollusca 7: 1-162
- Klein, R.T., Lohmann, K.C., and Thayer, C.W. 1996. Sr/Ca and  $\delta^{13}\text{C}$  and ratios in skeletal calcite of *Mytilus trossulus*: Covariation with metabolic rate, salinity, and carbon isotopic composition of seawater, *Geochimica et Cosmochimica Acta*, **60**: 4207-4221.
- Klein, R.T., Lohmann, K.C., and Thayer, C.W. 1996. Bivalve skeletons record sea-surface temperature and  $\delta^{18}\text{O}$  via Mg/Ca and  $^{18}\text{O}/^{16}\text{O}$  ratios, *Geology*, **24**: 415-418.
- Laane, R.W.P.M., Southward, A.J., Slinn, D.J., Allen, J., Groenenveld, G., and Vries, A. 1996. Changes and causes of variability in salinity and dissolved inorganic phosphate in the Irish Sea, English Channel and Dutch coastal zone. *Journal of Marine Science* 53: 933-944.
- Lea, D.W., Pak, D.K., Spero, H.J. 2000. Climate impact of late Quaternary Equatorial Pacific Sea Surface Temperature Variations, *Science*, **289**:1719-1724
- Lee, X., Hu, R., Brand, U., Zhou, H., Liu, X., Yuan, H., Yan, C. & Cheng, H. 2004. Ontogenetic trace element distribution in brachiopod shells: an indicator of original seawater chemistry. *Chemical Geology*, **209**, 49-65.
- Lécuyer C, Bucher H. 2006. Stable isotope compositions of a late Jurassic ammonite shell: a record of seasonal surface water temperatures in the southern hemisphere? *eEarth* 1:1-7.
- Leng, M.J., Heaton, T.H.E., Lamb, H.F., Naggs, F. 1998. Carbon and oxygen isotope variations within the shell of an African land snail (*Limicolaria kambeul chudeaui* Germain): a high resolution record of climate seasonality? *The Holocene* 8:407-412.
- Lissajous, M. 1925. Répertoire alphabétique des belemnites Jurassiques précède d'un essai de classification, Faculté des Sciences, Mémoire 7: 1-55.
- Longinelli, A. 1969. Oxygen-18 variations in belemnite guards. *Earth Planetary Science Letters* 7: 209-212

- Lorrain, A., Paulet, Y., Chauvaud, L., Dunbar, R., Mucciarone, D., Fontuge, M. 2004.  $\delta^{13}\text{C}$  variation in scallop shells: Increasing metabolic carbon contribution with body size? *Geochimica et Cosmochimica Acta* **68**:3509-3519.
- Louis-Schmid, B., Rais, P., Schaeffer, P., Bernasconi, S.M., and Weissert, H. 2007a. Plate tectonic trigger of changes in  $\text{pCO}_2$  and climate in the Oxfordian (late Jurassic): Carbon isotope and modelling evidence, *Earth and Planetary Science Letters*, **258**: 44-60.
- Louis-Schmid, B., Rais, P., Bernasconi, S.M., Pellenard, P., Collin, P.Y., and Weissert, H. 2007b. Detailed record of the mid-Oxfordian (late Jurassic) positive carbon-isotope excursion in two hemipelagic sections (France and Switzerland): A plate tectonic trigger? *Palaeogeography, Palaeoclimatology, Palaeoecology*, **248**: 459-472.
- Lowenstam, H. and Epstein, S. 1954. Paleotemperatures of the post-Aptian cretaceous as determined by the oxygen isotope method, *Journal of Geology*, **62**: 207-248.
- Marion, D.J. 1984. The middle Jurassic rock creek member and associated units in the subsurface of west-central Alberta. *In The Mesozoic of Middle North America Edited by D.F. Stott and D.J. Glass. Canadian Society of Petroleum Geologists*, pp. 319-343.
- McArthur, J.M., Donovan, D.T., Thirlwall, M.F., Fouke, B.W., and Matthey, D. 2000. Strontium isotope profile of the early Toarcian (Jurassic) oceanic anoxic event, the duration of ammonite biozones, and belemnite palaeotemperatures, *Earth and Planetary Science Letters*, **179**: 269-285.
- McArthur, J.M., Mutterlose, J., Price, G.D., Rawson, P.F., Ruffell, A., and Thirlwall, M.F. 2004. Belemnites of Valanginian, Hauterivian and Barremian age: Sr-isotope stratigraphy, composition ( $^{87}\text{Sr}/^{86}\text{Sr}$ ,  $\delta^{13}\text{C}$ ,  $\delta^{18}\text{O}$ , Na, Sr, Mg), and palaeo-oceanography, *Palaeogeography, Palaeoclimatology, Palaeoecology*, **202**: 253-272.
- McArthur, J.M., Doyle, P., Leng, M.J., Reeves, K., Williams, C.T., Garcia-Sanchez, R., and Howarth, R.J. 2007. Testing palaeo-environmental proxies in Jurassic belemnites: Mg/Ca, Sr/Ca, Na/Ca,  $\delta^{18}\text{O}$  and  $\delta^{13}\text{C}$ , *Palaeogeography, Palaeoclimatology, Palaeoecology*, **252**: 464-480.
- McArthur, J.M., Janssen, N.M.M., Reboulet, S., Leng, M.J., Thirlwall, M.F. & van de Schootbrugge, B. 2007. Palaeotemperatures, polar ice-volume, and isotope stratigraphy (Mg/Ca,  $\delta^{18}\text{O}$ ,  $\delta^{13}\text{C}$ ,  $^{87}\text{Sr}/^{86}\text{Sr}$ ): The Early Cretaceous (Berriasian, Valanginian, Hauterivian). *Palaeogeography, Palaeoclimatology, Palaeoecology*, **248**, 391-430.

- McLearn, F.H. 1927. Some Canadian Jurassic faunas, Transactions of the Royal Society of Canada 61-73.
- Minton, J.W. 2004. The pattern of growth in the early life cycle of individual *Sepia pharaonis*. Marine and Freshwater Research **55**:415-422.
- Minton, J.W., Walsh, L.S., Lee, P.G., Forsythe, J.W. 2001. First multi-generational culture of the tropical cuttlefish *Sepia pharaonis* Ehrenberg, 1831. Aquaculture International **9**:375-392.
- Mitsuguchi, T., Matsumoto, E., and Abe, O. 1997. Mg/Ca thermometry in coral skeletons, Oceanographic Literature Review, **44**: 431-431.
- Moore, R.C., Lalicker, C.G., and Fischer, A.G. 1952. Invertebrate Fossils, McGraw-Hill Book Company, New York, 388-393.
- Naud, M., Hanlon, R.T., Hall, K.C., Shaw, P.W., and Havenhand, J.N. 2004. Behavioural and genetic assessment of reproductive success in a spawning aggregation of the Australian giant cuttlefish, *Sepia apama*, Animal Behaviour, **67**: 1043-1050.
- Murray, J.W. 1985. Atlas of invertebrate macrofossils. John Wiley & Sons, New York.
- Mulitza, S., Wolff, T., Pätzold, J., Hale, W., Wefer, G. 1998. Temperature sensitivity of planktic foraminifera and its influence on the oxygen isotope record. Marine Micropaleontology **33**:223-240.
- Nixon, M., Mangold, K. 1998. The early life of *Sepia officinalis*, and the contrast with that of *Octopus vulgaris* (Cephalopoda). Journal of the Zoological Society, London, **245**:407-421.
- Norman M., 2000. Cephalopods a world guide, octopuses, argonauts, cuttlefish, squid, nautilus. ConchBooks, Hackenheim, Germany, p 1-320.
- Norman, M. & Reid, A. 2000. 'Guide to Squid, Cuttlefish and Octopuses of Australasia.' 1st Edn. (CSIRO Publishing: Melbourne, Australia.).
- Nurnberg, D. 2000. Taking the temperature of Past Ocean Surfaces, Science, **289**:1698-1699
- Palacios-Fest, M. and Dettman, D. 2001. Temperature controls monthly variation in ostracode valve Mg/Ca: *Cypridopsis vidua* from a small lake in Sonora, Mexico, Geochimica et Cosmochimica Acta, **65**: 2499-2507.

Pearce, C.R., Hesselbo, S.P., and Coe, A.L. 2005. The mid-Oxfordian (late Jurassic) positive carbon-isotope excursion recognised from fossil wood in the British Isles, *Palaeogeography, Palaeoclimatology, Palaeoecology*, **221**: 343-357.

Pirrie, D., Marshall, J.D., Doyle, P., and Riccardi, A.C. 2004. Cool early Albian climates; new data from Argentina, *Cretaceous Research*, **25**: 27-33.

Price, G.D. and Mutterlose, J. 2004. Isotope signals from late Jurassic-early Cretaceous (Volgian-Valanginian) sub-arctic belemnites, Yatrria River, western Siberia, *Journal of the Geological Society, London*, **161**: 959-968.

Putten, E.V., Dehairs, F., Andre, L. & Baeyens, W. 1999. Quantitative in situ microanalysis of minor and trace elements in biogenic calcite using infrared laser ablation - inductively coupled plasma mass spectrometry: a critical evaluation. *Analytica Chimica Acta*, **378**, 261-272.

Putten, E.V., Dehairs, F., Keppens, E., and Baeyens, W. 2000. High resolution distribution of trace elements in the calcite shell layer of modern *Mytilus edulis*: Environmental and biological controls, *Geochimica et Cosmochimica Acta*, **64**: 997-1011.

Rexfort, A. and Mutterlose, J. 2006. Stable isotope records from *Sepia officinalis*: a key to understanding the ecology of belemnites? *Earth and Planetary Science Letters*, **247**: 212-221.

Richard, A. 1969. The part played by temperature in the rhythm of formation of markings on the shell of cuttlefish (*Sepia officinalis* L.) (cephalopoda, mollusca), *Experientia*, **25**: 1051-1052.

Romanuk TN, Levings CD. 2005. Stable isotope analysis of trophic position and terrestrial vs. marine carbon sources for juvenile Pacific salmonids in nearshore marine habitats. *Fisheries Management and Ecology* 12:113-121.

Rosales, I., Robles, S., and Quesada, S. 2004a. Elemental and oxygen isotope composition of early Jurassic belemnites: Salinity vs. temperature signals, *Journal of Sedimentary Research*, **74**: 342-354.

Rosales, I., Quesada, S., and Robles, S. 2004b. Palaeotemperature variations of early Jurassic seawater recorded in geochemical trends of belemnites from the Basque-Cantabrian basin, northern Spain, *Palaeogeography, Palaeoclimatology, Palaeoecology*, **203**: 253-275.

Rosenberg, G.D. & Hughes, W.W. 1991. A metabolic model for the determination of shell composition in the bivalve mollusc, *Mytilus edulis*. *Lethaia*, **24**, 83-96.

- Rosenthal, Y. and Lohmann, G.P. 2002. Accurate estimation of sea surface temperatures using dissolution corrected calibrations for Mg/Ca paleothermometry, *Paleoceanography*, **17**: PA000749.
- Saelen, G. 1989. Diagenesis and construction of the belemnite rostrum, *Palaeontology*, **32**: 765-798.
- Schettino, A., and Scotese, C.R. 2005, Apparent polar wander paths for the major continents (200 Ma - Present Day): A paleomagnetic reference frame for global plate tectonic reconstructions, *Geophysical Journal International*, **163**, 727-759.
- Schrag, D.P. (1999). Rapid analysis of high-precision Sr/Ca ratios in corals and other marine carbonates. *Paleoceanography*, **14**, 97-102.
- Schrag, D.P., and DePaolo D.J. 1993. Determination of  $\delta^{18}\text{O}$  of seawater in the deep ocean during the Last Glacial Maximum, *Paleoceanography*, **8**: 1-6.
- Schwarcz, H.P., Gao, Y., Campana, S., Browne, D., Knyf, M., Brand, U. 1998. Stable carbon isotope variations in otoliths of Atlantic cod (*Gadus morhua*). *Canadian Journal of Fisheries and Aquatic Science* **55**:1798-1806.
- Scotese, C.R. 2003. PALEOMAP Project, [www.scotese.com](http://www.scotese.com).
- Shackleton, N.J. and Kennett, J.P. 1975. Late Cenozoic oxygen and carbon isotopic changes at DSDP Site 284: implications for glacial history of the Northern Hemisphere and Antarctica. In Kennett, J.P., Houtz, R.E., et al., *Init. Repts. DSDP, 29*: Washington (U.S. Govt. Printing Office), 801-807.
- Sharp, Z. 2007. Principles of stable isotope geochemistry. Pearson Educational, New Jersey.
- Shen, C.C., Chiu, H.Y., Chiang, H.W., Chu, M.F., Wei, K.Y., Steinke, S., Chen, M.T., Lin, Y.S., and Lo, L. 2007. High precision measurements of Mg/Ca and Sr/Ca ratios in carbonates by cold plasma inductively coupled plasma quadrupole mass spectrometry, *Chemical Geology*, **236**: 339-349.
- Sherrard, K.M. 2000. Cuttlebone morphology limits habitat depth in eleven species of *Sepia* (cephalopoda: Sepiidae), *Biological Bulletin*, **198**: 404-414.
- Sherwood, G.D., Rose, G.A. 2003. Influence of swimming form on otoliths  $\delta^{13}\text{C}$  in marine fish. *Marine Ecology Progress Series* **258**:258-289.
- Sinclair, D.J., Kinsley, L.P.J. & McCulloch, M.T. 1998. High resolution analysis of trace elements in corals by laser ablation ICP-MS. *Geochimica et Cosmochimica Acta*, **62**, 1889-1901.

- Spaeth, R., Hoefs, and Vetter. 1971. Some aspects of isotopic composition of belemnites and related paleotemperatures, *Geological Society of America Bulletin*, **82**: 3139-3150.
- Steuber, T. 1999. Isotopic and chemical intra-shell variations in low-mg calcite of rudist bivalves (mollusca-hippuritacea): Disequilibrium fractionations and late cretaceous seasonality, *International Journal of Earth Sciences*, **88**: 551-570.
- Stoll, H.M. and Schrag, D.P. 2001. Sr/Ca variations in Cretaceous carbonates: Relation to productivity and sea level changes, *Palaeogeography, Palaeoclimatology, Palaeoecology*, **168**: 311-336.
- Stronach, N.J. 1984. Depositional environments and cycles in the Jurassic Fernie formation, southern Canadian Rocky Mountains. *In* *The Mesozoic of Middle North America Edited by D.F. Stott and D.J. Glass*. Canadian Society of Petroleum Geologists, pp. 43-67.
- Tan, F.C. and Hudson, J.D. 1974. Isotopic studies on the palaeoecology and diagenesis of the great estuarine series (Jurassic) of Scotland, *Scottish Journal of Geology*, **10**: 91-128.
- Takai N, Onaka S, Ikeda Y, Yatsu A, Kidokoro H, Sakamoto W. 2000. Geographical variations in carbon and nitrogen stable isotope ratios in squid. *Journal of the Marine Biological Association of the United Kingdom* **80**:675-684.
- Urey, H.C., Lowenstam, H., Epstein, S., and McKinney, C.R. 1951. Measurement of paleotemperatures and temperatures of the upper cretaceous of England, Denmark, and the southeastern United States, *Bulletin of the Geological Society of America*, **62**: 399-416.
- van de Schootbrugge, B., McArthur, J.M., Bailey, T.R., Rosenthal, Y., Wright, J.D., and Miller, K.G. 2005. Toarcian ocean anoxic event: An assessment of global causes using belemnite C isotope records, *Paleoceanography*, **20**: PA3008.
- van de Schootbrugge, B., Föllmi, K.B., Bulot, L.G., and Burns, S.J. 2000. Paleoceanographic changes during the early Cretaceous (Valanginian-Hauterivian): Evidence from oxygen and carbon stable isotopes, *Earth and Planetary Science Letters*, **181**: 15-31.
- Vander Putten, E., Dehairs, F., Andre, L., and Baeyens, W. 1999. Quantitative in situ microanalysis of minor and trace elements in biogenic calcite using infrared laser ablation-inductively coupled plasma mass spectrometry: A critical evaluation, *Analytica Chimica Acta*, **378**: 261-272.

Veizer, J. 1983. Chemical diagenesis of carbonates: Theory and application of trace element technique. *In Stable Isotopes in Sedimentary Geology Edited by M.A. Arthur, T.F. Anderson, I.R. Kaplan, J. Veizer and L.S. Land. Society of Economic Paleontologists and Mineralogists, Dallas, pp. 3-1-3-100.*

Veizer, J., Ala, D., Azmy, K., Bruckschen, P., Buhl, D., Bruhn, F., Carden, G.A.F., Diener, A., Ebner, S., Godderis, Y., Jasper, T., Korte, C., Pawellek, F., Podlaha, O.G., and Strauss, H. 1999.  $^{87}\text{Sr}/^{86}\text{Sr}$ ,  $\delta^{13}\text{C}$  and  $\delta^{18}\text{O}$  evolution of Phanerozoic seawater, *Chemical Geology*, **161**: 59-88.

Voigt, S., Wilmsen, M., Mortimore, R.N., and Voigt, T. 2003. Cenomanian palaeotemperatures derived from the oxygen isotopic composition of brachiopods and belemnites: Evaluation of cretaceous palaeotemperature proxies, *International Journal of Earth Sciences*, **92**: 285-299.

Weissert, H. and Mohr, H. 1996. Late Jurassic climate and its impact on carbon cycling, *Palaeogeography, Palaeoclimatology, Palaeoecology*, **122**: 27-43.

Wierzbowski, H. and Joachimski, M. 2007. Reconstruction of late Bajocian-Bathonian marine palaeoenvironments using carbon and oxygen isotope ratios of calcareous fossils from the Polish Jura chain (central Poland), *Palaeogeography, Palaeoclimatology, Palaeoecology*, **254**: 523-540.

Wierzbowski, H. 2004. Carbon and oxygen isotope composition of Oxfordian-early Kimmeridgian belemnite rostra: Palaeoenvironmental implications for late Jurassic seas, *Palaeogeography, Palaeoclimatology, Palaeoecology*, **203**: 153-168.

Wierzbowski, H. 2002. Detailed oxygen and carbon isotope stratigraphy of the Oxfordian in central Poland, *International Journal of Earth Sciences*, **91**: 304-314.

Wurster, C.M., Patterson, W.P., Stewart, D.J., Bowlby, J.N. 2005. Thermal histories, stress, and metabolic rates of Chinook salmon in Lake Ontario: evidence from intra-otolith  $^{18}\text{O}$  and  $^{13}\text{C}$  values and energetics modelling. *Canadian Journal of Fisheries and Aquatic Sciences* **62**:700-713.

Zazzo, A., Smith, G.R., Patterson, W.P., Dufor, E. 2006) Life history reconstruction of modern and fossil sockeye salmon (*Oncorhynchus nerka*) by oxygen isotopic analysis of otoliths, vertebrae, and teeth: Implication for palaeoenvironmental reconstructions. *Earth and Planetary Science Letters* **249**:200-215.